NETWORK MODELING AND OPTIMIZATION FOR ENERGY AND SUSTAINABLE TRANSIT

by

Olufolajimi Oke

A dissertation submitted to Johns Hopkins University in conformity with the requirements for the degree of Doctor of Philosophy

Baltimore, Maryland

May 2016

Abstract

Energy and transportation systems are integral to our infrastructure. Along with other types of networks, critical challenges constantly arise, particularly with regard to accessibility, efficiency, optimality, and sustainability. In this dissertation, we use mixed integer programming, data mining and mixed complementarity techniques to address some of these challenges. We have developed an improved schematic mapping algorithm to facilitate the process of network representation for a variety of systems beyond transportation. We also discover fundamental patterns in bicycle ownership on a global scale with implications for sustainable urban planning and public health outcomes. Finally, we model the fast-growing crude oil market in North America, implementing scenarios that point to integrated approaches to exports, pipeline investments and targeted rail restrictions as most viable for addressing medium-term oil transportation concerns. The methods we employ are generalizable to other types of energy and transit systems, and beyond. Finally, we discuss the importance of these methods to newer applications.

Dr. Kavi Bhalla, Reader

Dr. James Guest, Reader

Dr. Sauleh Siddiqui, Advisor

Preface

The work described in this dissertation aims to highlight the importance of transportation and energy systems, and to unify them through the applications of optimization and equilibrium modeling methods in conjunction with those of knowledge and data discovery. It delves into the details of three major projects I have embarked upon in the course of my doctoral studies.

My interest in schematic mapping arose from a bike route optimization project I developed for my advisor, Sauleh Siddiqui's Equilibrium Problems in Systems Engineering course. In my efforts to visualize the solutions within the network in my model, I realized the importance of automated schematic mapping and began to investigate recent efforts in the field. Dr. Siddiqui motivated me to push this further, and our results are presented here.

The lack of integration of bicycling in many urban transit systems also captured my attention. I began to investigate models for bicycle traffic. Along the way, Dr. Siddiqui and Dr. Bhalla alerted me to an opportunity to investigate trends in bicycle ownership. Up to that point, there was a void in the academic literature regarding bicycle ownership patterns on a global scale, and it was clear that understanding ownership would be useful for researchers and planners alike. Dr. Bhalla was instrumental in guiding me through the data gathering process. Along with the invaluable collaboration of Dr. David Love, we spent the next two years developing a model to

unearth information from a sparse dataset. Our results received widespread domestic and international press coverage, and we hope others can build on this work.

With the oil boom in the U.S. and Canada garnering attention in the energy circles, especially with the high-profile crude-by-rail spills, we decided to contribute to solving this problem. Daniel Huppmann had earlier developed an equilibrium model for the global energy market. Using that as a basis, we built a model for the North American crude oil market (NACOM) that is able to track the flow of heavy and light oils along different modes of transportation with granularity at the U.S. state level. I worked for over a year under the guidance of Dr. Huppmann and Dr. Siddiqui in building this new model, while also assisted by my undergraduate advisees Max Marshall and Ricky Poulton. With NACOM, we test ran several scenarios to investigate how best to mitigate the crude-by-rail problem.

I have presented various portions of this work over the past three years at the Institute for Operations Research and Management Sciences Annual Meeting, Modeling and Optimization: Theory and Applications hosted at Lehigh University, the International Symposium on Mathematical Programming, among other internal and external speaking engagements.

Baltimore, April 2016

Acknowledgments

I am indebted to my mentor and advisor, Dr. Sauleh Siddiqui for guiding my academic path over the past three and a half years. I have grown immensely as a researcher in the Mathematical Optimization for Decisions Lab (MODL) under his supervision. Thank you for letting me explore, while instilling in me the fundamentals of academic pursuit and driving me toward excellence. I am also grateful for your unwavering support and your belief in my ideas and abilities, especially for the opportunities you afforded me to realize them.

My current and past MODL colleagues and affiliates have been a source of inspiration, constantly spurring me to produce better work: Dr. Daniel Huppmann, Dawud Ansari, Dr. Felipe Feijoo, Lissy Langer, Sriram Sankaranarayanan, Tom Brijs and Wei Jiang. It was also great to have Max Marshall, Molly Van Doren and Ricky Poulton on board as undergraduate research assistants. Thank you all for your hard work and enthusiasm, especially Max.

To my Thesis Committee and Graduate Board Oral Exam Committee members—Drs. Kavi Bhalla, James Guest, J. Hugh Ellis, Judith Mitrani-Reiser, Sauleh Siddiqui and Takeru Igusa: thank you for your time and critique of my work. I am deeply grateful to Dr. Ben Zaitchik of the Department of Earth and Planetary Sciences and Dr. Ben Hobbs of the Department of Geography and Environmental Engineering, both of whom have mentored me in various capacities during my time at Johns Hopkins

University. Your encouragement and belief went a long way in getting me to this point. I thank other faculty members who have advised, collaborated and showed interest in my work at various points, especially, Dr. Joel Gittelsohn (obesity modeling), Dr. David C. Love (bicycle transportation), and Dr. Tony Dalrymple (GPU computing). Your support is greatly appreciated.

The Civil Engineering department staff have been kind and supportive over the years. I appreciate Lisa Wetzelberger for going above and beyond in the months prior to my enrollment, and for her continued support for all my needs and requests. Deborah Lantry, Vess Clarke, Tanya Waith and Shamija Jackson were also encouraging and helpful at crucial points during my time in the department. Special thanks go to Dr. Khairul Bariah Abd Majid for being a source of motivation in the final months and for opening her home to me. I am also grateful to Jessica Ader for her interest in my progress and support of my various endeavors within the department.

My friends have been a huge support during this PhD journey. Thank you all for your support and care at various stages. In particular, I am grateful to cherished friends in the department, Anindya Bhaduri, Dave Fratamico, Gary Lin and Hwanpyo Kim, for their encouragement and companionship. I also thank Caitlin Jacques for her friendship and for serving as an accountability partner during the dissertation writing period. Running has kept me sane during these past four years, and I thank the folks at the Hopkin Harriers (notably Dr. Ben Schafer, Dr. Marc Ostermeier, Dr. Tom Haine and Dave Fratamico) and the Baltimore Pacemakers (led by the tireless Bob Hilson) for numerous hours of delightful pavement pounding. To my Graduate Christian Fellowship friends—thank you for continually challenging my thoughts and actions. Special thanks to Dr. Dwight Schwartz for his mentorship over the years. I am deeply grateful to my faith community at City Bible Church Baltimore, which has been a bedrock of growth and support during this period. I am grateful for the deep bonds of friendship that will last a lifetime. In particular, I would like to recognize

my pastor Ben Malmin and his wife Rebecca, for their love and encouragement, and the part they played in making this city truly home for me. To my spiritual grandparents—John and Aruna Desai of Princeton—thank you for your love, support and incredible hospitality.

The special support of my family (both here and abroad, immediate and extended) cannot go unrecognized. Thank you for everything, especially the sacrifices you have made on my behalf. To John and Janet Santmann: I am forever grateful for your generous investment toward my first-year expenses at Johns Hopkins. I could not have made it here without your extraordinary support. Finally, I thank God for making all this possible and providing all I have needed to accomplish this task from September 2012 up to this point.

Funding

My research was partially supported by the Gordon Croft Fellowship awarded for the 2015-16 academic year by the Energy, Environment, Sustainability and Health Institute (E^2SHI) at The Johns Hopkins University. An E^2SHI seed grant also supported my work in 2014-15. I received partial funding from the Global Obesity Prevention Center (formerly Johns Hopkins Global Center on Childhood Obesity) in 2013-14.

Dedication

To Jola, Joke, Jide, Mom and Dad.

Contents

List of Figures

List of Tables

CHAPTER 1

Introduction

Our world is a complex web of interacting systems, all of which impact our lives and our world in one way or the other. These systems or networks include structures, transportation networks, energy grids and markets. In order to track behavior and ensure better outcomes, models are often employed to describe system behavior. Data collection and analyses can be critical to model formulation. Representation is also important to handle user interactions. Rich bodies of work have been developed over the past 100 years to model and solve problems with a systems framework. In this dissertation, we describe research that focuses on network models in transportation and energy. The methods, however, have wide-ranging applications to other types of systems. In this century, governments, policymakers, scientists and engineers, are scrambling to tackle national issues with respect to population, health, climate and resource management. Efficient modeling techniques can contribute toward providing solutions to numerous problems that have existed or that continue to emerge. The systems surrounding transportation and energy, in particular, are of great interest, as they are more often than not subject to arbitrary policy decisions and influenced by various competing concerns.

In the next section, we detail the methods the author has studied and employed

in understanding and modeling systems. The section following highlights the areas where these have been applied, advances made and new knowledge created. The final section describes the layout of the dissertation.

1.1 Background and methods

1.1.1 Multiobjective mixed integer programming

Multiobjective mixed integer programs (MOMIPs) are a class of tools that apply the principles of multiobjective optimization (MOO) to models that involve integer variables (Mixed Integer Programs).

Multiobjective optimization

Multiobjective optimization is a broad field that historically developed from theoretic and applied work in the mathematical sciences, engineering and economics [107]. Engineers often have to solve problems in which a combination of objectives or criteria must be met with practical, logistical and fiscal considerations. Economists search for equilibria in markets, points at which demand is satisfied while utility or welfare and profits are maximized. The advancement of game theory is also considered influential in MOO development, as it is primarily concerned with finding optimal decision-making strategies in various situations.

In most MOO applications, there do not exist single globally optimal points for all objectives, and even if there were, they are often impractical to determine. Paradoxically, therefore, points of efficiency are of primary interest, wherein a palette of tradeoffs among preferences can be examined from the standpoint of the decision maker. The concept of maximum "ophelimity" first described by Pareto [147] in his 1906 treatise describes the point in a feasible space where a simultaneous improvement in the objective of interest for *all* entities in the system is impossible; as such

any variation from such a point to optimize utility for one particular entity would result in a worsening for another or more entities. Thus, according to Pareto, points of maximum ophelimity are "collectively" optimal for all the entities at the same point. Following Pareto, this concept has since developed to precisely and robustly describe "optimality" in multiobjective space [97, 100, 5, 207]. Such points are called *Pareto [optimal] points* and the set of such points make up a *Pareto set* and are formally defined thus [107]:

Definition 1. Given a set of objective functions $F_i \in \boldsymbol{F}$ and a set of points x in feasible region $\boldsymbol{X}$. A point $x^* \in \boldsymbol{X}$ is a Pareto point if it satisfies the following necessary and sufficient conditions:

i. $F_i(x) \leq F_i(x^*)$ for all $F_i \in \boldsymbol{F}$

ii. $F_i(x) < F_i(x^*)$ for some $F_i \in \boldsymbol{F}$

Other interchangeable terms for Pareto or efficient points include "admissible," "noninferior" and "nondominated," of which the latter is the prevailing alternative term in the modern literature [44].

Various approaches have been developed in solving multiobjective problems [107]. In the weighting or weighted-sum method [107, 207], the objective is formulated as the scalar product of a vector of objectives and a corresponding vector of scalars whose values may be chosen as a measure of the importance of each objective in the problem. However, the points obtained by this method are not always guaranteed to be Pareto optimal. The lexicographic method [107, 175] allows for a sequential optimization of each objective by order of importance. The bounded objective function finds the optimal point for the designated objective of greatest importance, while the bounds of the other objectives constrain the overall problem. Following this method, the ε-constraint method proposed by Haimes et al. [70], addresses the choice of upper bounds in the constraints in order to guarantee Pareto optimality. Goal programming,

initially developed by Charnes et al. [27], and its several variations, solves for efficient points by minimizing deviations from predefined objective function values or goals. Das and Dennis [35] introduced the normal boundary intersection (NBI) to produce an evenly spaced Pareto set. Siddiqui et al. [167] developed a modification to improve the efficiency of NBI.

Computing the Pareto set for a given MOO application can be an expensive task. Continuing developments therefore focus on improving efficiency. Among these, Mavrotas [109], Mavrotas and Florios [110] developed the augmented ε-constraint algorithm (AUGMECON2). In AUGMECON2, lexicographic optimization is first used to generate a payoff table for the objectives, whose gridded granularity is determined by the user. Following this, the ε-constraint method is then employed within a framework of heuristics to generate the Pareto set, the density determined by the number of grids afore-specified.

One of the advances demonstrated in this dissertation is the application of AUGMECON2 in an MOMIP for schematic mapping, as described in Chapter 2.

Mixed integer programs

A mixed integer program (MIP) is an optimization problem whose objective (linear, quadratic or otherwise) space is defined by a mixture of discrete and continuous variables. Discrete variables allow for the modeling of choice or the combination of specific actions as related to a given problem. A general definition is given below [104].

Definition 2. A mixed integer [linear] program is of the form:

$$\max \sum_{j \in C} c_j x_j + \sum_{j \in I} c_j x_j \tag{1.1}$$

$$\text{subject to} \sum_{j \in C} a_{ij} x_j + \sum_{j \in I} a_{ij} x_j \leq b_i \qquad i = 1, ..., m \tag{1.2}$$

$$l_j \leq x_j \leq u_j \qquad j \in C \cup I \tag{1.3}$$

$$x_j \in \mathbb{R} \qquad j \in C \tag{1.4}$$

$$x_j \in \mathbb{Z} \qquad j \in I, \tag{1.5}$$

where C is the index set of continuous variables and I the index set of integer variables.

MIP models are indispensable to tackling engineering and operations problems including those that deal with location, scheduling, and assignments. MIPs are NP-complete, but various algorithms have been developed to solve them. These methods have arisen from the subfields of set theory, cutting planes and enumeration. The branch and bound (B&B) approach, an enumeration method, has evolved as a robust solution technique for MIPs.

1.1.2 Mixed complementarity problems

The concept of complementarity is central to conditions for equilibria and optimality [49]. In various systems, be they structural, economic, social, among others, the existence of an equilibrium can be represented by the mathematical definition of complementarity, which in the geometric context is equivalent to orthogonality. Before giving the formal definition of a complementarity problem, we will illustrate it with the classic example of a Wardorp equilibrium.

Wardrop equilibrium

In 1952, traffic engineer John Wardrop postulated in his first principle that traffic a given network may ultimately attain an equilibrium in which the travel times on all the used paths for an origin-destination pair used are equal and the shortest possible. In other words, network users (drivers, for instance) will be unable to improve their travel times by choosing a different route in such a situation [202].

Thus, let $i \in I$ be the origin-destination (OD) node pairs in a given network $G(N, A)$, with nodes $n \in N$ and arcs $a \in A$. Also, we define P_i as the set of paths p for each OD pair i. For each path p, the flow is given by f_p while the travel time along the path is given by $T_p(f)$. The function T_p can be generalized to account for other costs and interferences and can therefore be considered a disutility, delay or latency function. For the sake of this example, we consider it a generalized travel time function of the flow in the entire network f (vector of the path flows f_p). Finally, the minimum time (also possibly generalized as a cost) to travel from one origin node to its respective destination nodes is t_i.

Now, according to Wardrop's first principle, f is an equilibrium for all OD pairs $i \in I$ and all paths $p \in P_i$ if $f_p > 0 \iff t_i = T_p(f)$ and $f_p = 0 \iff T_p(f) >= t_i$. These statements can be rewritten thus:

$$f \cdot (T(h) - t_i) = 0 \tag{1.6}$$

$$f \geq 0 \tag{1.7}$$

$$T(h) - t_i \geq 0 \tag{1.8}$$

if we consider $T(h)$ as the vector $\langle T_1(h), T_2(h), \ldots, T_p(h) \rangle$. The above relations concisely state that at equilibrium, the travel times on all used paths are the minimum for the OD pair they connect. Equation (1.6) expresses the orthogonality of f and $(T(h) - t_i)$, while (1.7) and (1.8) are their respective nonnegativity bounds. In fact, these relations can even more compactly given as

$$0 \leq f \perp T(h) - t_i \geq 0 \tag{1.9}$$

where $f \perp T(h) - t_i$ is simply a restatement of (1.6).

The Wardrop example has been shown to represent an instance of Nash Equilibrium: a

steady-state point at which no player can improve their current situation by selecting an alternate strategy. The problem of interest in a Wardrop user equilibrium is usually to find the flow distribution f that achieves this. Other extensions can be made to incorporate congestion, intermodal impedance, and thereby solve for related quantities.

Given this illustration, we can now define the nonlinear complementarity problem (NCP) as follows:

Definition 3. For a function $F : \mathbb{R}^n \to \mathbb{R}^n$, find $x \in \mathbb{R}^n$ such that

$$x \leq 0 \perp F(x) \geq 0 \tag{1.10}$$

where the operator $\perp$ indicates a zero dot product.

In NCP, the vector variable x is strictly nonnegative. The mixed complementarity problem (MCP) is a generalization that allows for the inclusion of both free variables and nonnegative variables, hence the term "mixed." According to Gabriel et al. [57], the prevalent form is given below.

Definition 4. Given a function $F : \mathbb{R}^n \to \mathbb{R}^n$, find $x \in \mathbb{R}^{n_1}$ and $y \in \mathbb{R}^{n_2}$ such that for each $i \in \{1, \ldots, n_1\}$ and $j \in \{1, \ldots, n_2\}$

$$x_i \leq 0 \perp F_i(x, y) \geq 0 \tag{1.11}$$

$$F_{j+n_1}(x, y) = 0, \quad y_j \text{ free} \tag{1.12}$$

Another instance that arises is having lower and upper bounds for the variables in question besides 0 or ∞.

The versatility of the MCP framework is multifold. We have established its utility in modeling equilibrium problems (e.g. Wardrop, Walrasian, Nash, market, structural, among others). Also of significance is the natural equivalence of the MCP and the

system of first-order optimality conditions for a constrained optimization problem, commonly referred to as Karush-Kuhn-Tucker (KKT) conditions. These were independently derived by William Karush, and Kuhn and Tucker [95].

Given a general constrained optimization problem [133]:

$$\min_{x\in\mathbb{R}^n} f(x) \quad \text{s.t.} \begin{cases} c_i(x) = 0, & i \in \mathcal{E} \\ c_i(x) \geq 0, & i \in \mathcal{I} \end{cases} \tag{1.13}$$

where $f : \mathbb{R}^n \to \mathbb{R}^n$, $c_i, i \in \mathcal{E}$ are equality constraints and $c_i, i \in \mathcal{I}$ are the inequality constraints.

The KKT conditions for (1.13) are as follows

$$\nabla_x \mathcal{L}(x^*, \lambda^*) = 0 \tag{1.14}$$

$$\lambda_i^* c_i(x^*) = 0 \qquad i \in \mathcal{E} \cup \mathcal{I} \tag{1.15}$$

$$\lambda_i^* \geq 0 \qquad i \in \mathcal{I} \tag{1.16}$$

$$c_i(x^*) \geq 0 \qquad i \in \mathcal{I} \tag{1.17}$$

$$c_i(x^*) = 0 \qquad i \in \mathcal{E} \tag{1.18}$$

where $\nabla_x \mathcal{L}(x^*, \lambda^*)$ is the Lagrangian defined as

$$\nabla_x \mathcal{L}(x^*, \lambda^*) = \nabla f(x^*) - \sum_{i\in\mathcal{A}(x^*)} \lambda_i^* \nabla c_i(x^*) \tag{1.19}$$

The set $\mathcal{A}$ indexes the active constraints. The vector λ_i^* is the Lagrange multiplier. We see the orthogonality in (1.15), which indicates that either the Lagrange multiplier is 0 or the respective constraint is active (i.e. $i \in \mathcal{A}$). As such, (1.15) are known as the complementarity conditions of the KKT system of equations and inequalities. The complementarity can be strict, i.e. $\lambda_i^* > 0$, ensuring that the possibilities are not inclusive for the inequality constraints (of importance in algorithm development).

The necessity of the KKT conditions can be proven by Farkas' lemma, which states that given a vector in $\mathbb{R}^n$, only one of the following alternatives hold: (i) the vector exists in a given convex cone K; (ii) there exists a separating hyperplane between the vector and the cone K.

Thus, we see that the KKT system of an optimization problem can be formulated as an MCP. The MCP can therefore be applied to an even broader suite of problems. This utility has especially been exploited in the modeling of energy markets. Gabriel et al. [57] detail these applications and their significance in recent years.

Various algorithms have been developed to solve MCPs. They are largely based on modifications to the Newton method. A widely used solver is PATH, developed by Ferris and Munson [50] in the late 1990s and now available across a variety of platforms.

1.1.3 Data mining and pattern discovery

Data mining refers to the body of work concerned with gathering and discovering useful information from datasets. These data are often multidimensional and may contain numerous bits. Various learning models have been developed to discover rules and patterns within otherwise inscrutable data, with applications ranging from healthcare to social networks. With respect to data mining, learning is divided into two broad categories: supervised and unsupervised. The category of interest here is unsupervised learning, in which "clustering" is a major technique. Clustering is the process of measuring the separation of elements in a dataset and then grouping those elements based on the collective closeness within defined groups [89]. Two examples of clustering methods are k-means clustering and hierarchical clustering.

Hierarchical methods are often desirable, as they produce the overall tree structure of the dataset. Within hierarchical clustering are a set of agglomerative methods, so-called as they employ a "bottom-up" approach. Examples of hierarchical agglom-

erative clustering (HAC) include: the weighted pair group method with arithmetic means (WPGMA), the unweighted pair group method with arithmetic means (UPGMA), the method of complete linkages, the method of single linkages and the Ward method.

1.2 Applications and contributions

In this section, we detail the systems applications of the methods described in Section 1.1. We also highlight the importance and contributions of the work the author has carried out, both under his advisor and in collaboration with other researchers. There are three major areas of application: network representation, bicycle transportation, and oil market modeling and transport. In each of these cases, a corresponding journal article has either been published or submitted for review.

1.2.1 Network maps

Every system with which users must interact on a regular basis must have as accessibility as its hallmark. Infrastructure systems, in particular, must be accessible and navigable in order to be user-friendly and thereby serve their purpose. Ease of navigability is even more critical in transportation systems, where users require information to utilize the network infrastructure. Historically, maps have served as a representation tool for networks of all kinds: electric, geographic, conceptual, among others. Schematic mapping arose from a need to provide the most effective representation within a set of practical constraints. As will be discussed in Chapter 2, the *Tabula Peutigeriana*, a schematic map of the Roman road network, is one of the earliest ones in recorded history [181].

With advancement in graph theory and computational methods, various algorithms were developed to tackle the schematic map drawing problem. An early effort

described by Hong et al. [75] employed a combination of algorithms based on field attraction principles to create schematic maps quickly. Others efforts have since followed. Notably, Nöllenburg and Wolff [134] developed a mixed integer program to solve this problem.

In furthering this work, we have enhanced the mixed integer formulation with a justified simplification of the objective framework. We also apply the augmented ε-constraint method in order to generate the complete Pareto set of mapping solutions for a given problem, which is a first in this field.

The importance of schematic mapping is growing beyond its historic origins in the urban rail transit domain. Hahn and Weinberg [69] showed that the same rules of representation could be used to visualize the progression of disease in the human body. Another exciting development is the recent multiyear iteration of the Edinburgh Inntertube Map, a schematic representation of the bikeways in the city. While this work has purely been from a design standpoint, there are promising applications of the same optimization for bicycle transit networks, which are of increasing interest as sustainability is gaining deserved attention in planning and policy spheres.

1.2.2 Sustainable transit: bicycles

As efforts are being renewed toward sustainable urban communities and safe and clean streets, a resurgence in bicycle ownership and usage would be a welcome development [87, 159, 117]. In keeping with this pattern, policymakers are promoting schemes to further improve cycling conditions in various locales [34]. Some of these include increasing the level of cycling infrastructure, investing in bike sharing programs and raising awareness toward bicycle safety. An important factor affecting the usage of bicycles is availability. For many, especially in places where sharing programs are inaccessible, household ownership becomes a determining factor of bicycle access and activity.

In the first undertaking of its kind on a global scale, we mined household ownership data, discovering patterns that shed more light on national bicycle ownership trends from 1989 to 2012. In particular, ownership could be broadly classified into four levels, while the overall trend indicated a decline which was more pronounced in the 150 countries studied, excluding India and China [140].

1.2.3 Crude oil

Crude oil production in the United States has experienced a major boom in recent years. With the proliferation of horizontal drilling technologies—of which hydraulic fracturing predominates—domestic production increased in North Dakota, Texas, Colorado and Montana. This boom also brought with it several problems. One of great economic and environmental concern is the increasing use of rail to transport crude from the oil fields to the refiners. Numerous accidents and their consequent oil spills and related damage have resulted from increased rail shipments. There have also been growing concerns that grain shipments are often displaced or relegated in favor of the more lucrative crude payload. The energy analysts have so far been unable to provide concrete explanations as to why rail has edged out pipeline as the mode of choice for the growing thousands of barrels being extracted. Some have hypothesized that rail is cheaper and more accessible, hence its excessive use. However, no in-depth policy solutions to the current problem have been proffered, although a thorough inquiry into the situation has been undertaken [54]. The initial research question this project therefore aims to explore is the market and distribution network for domestic crude oil in the United States. We have developed the very first crude oil model for the U.S. hope to provide answers and policy recommendations to maximize welfare among the prevailing players.

1.3 Outline

Chapter 2 describes the author's work in schematic mapping as an application of two multiobjective optimization tools: mixed integer programming and the augmented ε-constraint method. This was conducted under the supervision of Dr. Sauleh Siddiqui and the work has been published in *Computers & Operations Research* [139]. In Chapter 3, we describe a data mining approach toward identifying trends in bicycle ownership around world, making the case for its importance in policymaking in sustainable transit. The author conducted this project under the guidance of Drs. Bhalla, Love and Siddiqui, and their results have been published in *Journal of Transport & Health* [140]. A mixed complementarity program formulation applied to the North American crude oil market and its capability to predict impacts of possible mitigating interventions in the transportation network are detailed in Chapter 4. The author has written much of the content of this chapter as an article which is currently in review for publication [142]. The research was completed with Drs. Huppmann and Siddiqui, and with the assistance of Max Marshall and Ricky Poulton.

In closing, we reiterate the foundational importance of the research described in this dissertation and provide a few promising examples for future directions (Chapter 5).

CHAPTER 2

Optimal network representation via schematic mapping

2.1 History and impact

A schematic map is a linear cartogram of a given network, which simplifies complexity and facilitates orientation through symbolic representation. Schematization therefore increases visual impact and makes it easier to digest information. Distortion is regularly employed to make this possible. Figure 2.1 illustrates the influence of schematization on a network user. A well-designed map is readily accessible and, through regular interaction, a user is ultimately able to virtually recreate the image of the network through a process known as "mental mapping" [66] to hasten the process of navigation.

Schematic map drawing dates back centuries. A classic example is the *Tabula Peutingeriana* from the fifth century—a representation of the Roman road network across three continents [181] notable for its use of symbolism and distortion. In modern times, the power of schematization has been most visible in the representation of electric circuits and in the mapping of modern urban transit networks. Harry

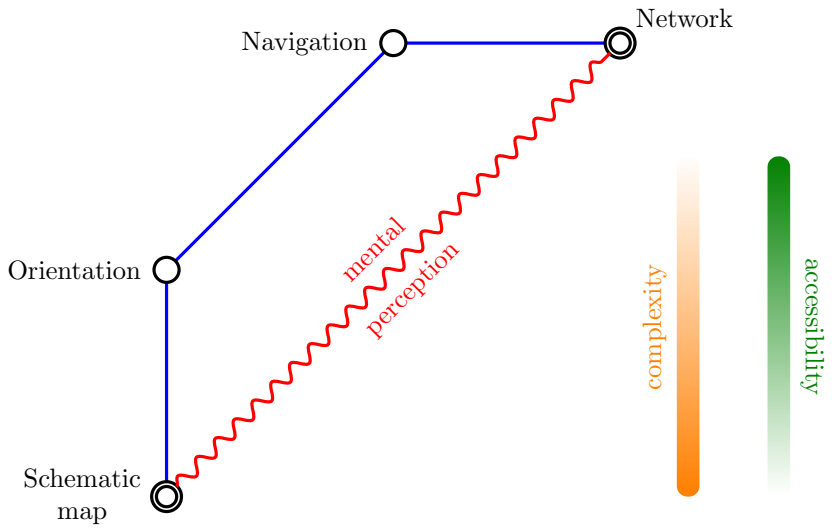

Figure 2.1 Impact of schematization

Beck's work in schematizing the London Underground map over a 30-year period beginning in the 1930s set standards that are still relevant today [60, 146]. Beck's representation did away with the curves of previous maps and replaced these with piecewise straight lines oriented in multiples of 45° (a scheme now termed *octilinear*). Beck also significantly enlarged the congested central portion of the map to make it more readable [60] (see Figure 2.2). Subsequent official revisions to the Underground map by Beck and others rarely departed from his original ideal. The majority of the metro maps created after Beck's effort also followed his design cues [146], and a comparative study of these maps reveals a consistent set of principles often referred to as "metro map rules." Beyond metro networks and transportation systems in general, schematic maps have been found to be effective in other areas. They have been successfully used to represent cancer pathways [69], as well as organizational structures and project plans [178]. Schematic maps have broad applications, as they are useful for visualizing pathways in networks of all kinds.

Producing a good schematic map can be an expensive and time-consuming process [10]. The best diagrams are usually created by professional designers with the aid of computer graphics software. Any represented network may undergo changes during

Figure 2.2 Central sections of the 1908 edition of the London Underground map and Beck's first schematic version published in 1933 [60]

its lifespan, and the needs and perceptions of its users will also vary with time. These usually require modifications to its schematic map. A procedure that can therefore automate the schematization process to give consistent results subject to specified requirements in real time would be ideal and efficient. (Efforts in this area of research are detailed in Section 2.2.) Of interest is Nöllenburg and Wolff's multiobjective mixed integer program implementation [134].

In this chapter, we describe improvements on Nöllenburg and Wolff's method—a reduction in the number of objective functions and a relaxation of integer constraints—for better performance. Essentially, we reduced a mixed integer program to a mixed binary linear program and implemented a method of finding the entire set of non-dominated (Pareto optimal) solutions, which is critical as not all Pareto optimal solutions can be obtained by the weighting method approach employed by Nöllenburg and Wolff. We also establish a framework for analysis and decision-making in the Pareto space of equally efficient solutions. Finally, we show through some examples how schematic maps can be automated for a variety of applications. This work has been published in the journal, Computers & Operations Research [139].

2.2 Background and related work

Over the past 60 years, important insights have been gained in the automation of schematic maps. Purchase et al. [154] conducted a study that underscored the importance of aesthetics in schematization. In particular, their work proved that minimal line crossings and bends make maps easier to use and remember. In their review, Avelar and Hurni [10] motivate the importance of good design in schematizing transportation networks, and they propose a standardization in representation.

Tamassia [182] developed an algorithm that utilized the network properties of graphs to solve the problem of embedding a graph in a rectilinear grid. The problem was modeled in terms of minimum cost flow and the solution preserved topology while minimizing the bend count. Tamassia's work [182] did much to characterize important graphical elements of schematic maps, and also generalized the implementation for k-gonal graphs. Avelar and Müller [11] proposed an iterative algorithm for schematic map generation that also preserved input topology. They showed that topological accuracy[1] could be maintained using relatively simple geometric analyses, as opposed to elaborate techniques. Their formulation also emphasized the role of the designer in setting constraints for aesthetics and legibility. Cabello et al. [23] describe a generalized procedure for schematizing transport maps using a path-endpoint framework. Their approach, which runs in linearithmic time, preserves the original layout but terminates if no correct solution can be found.

Metro maps are a subset of schematic maps. Much of the work done in automating metro map drawings is generally transferrable to schematic maps, which tend to follow similar rules. Hong et al. [75] were the first to completely automate metro map graph layouts, and they demonstrated this through the use of various force-directed

[1] "Topological accuracy" refers to the relative positioning of the nodes and edges in a schematic realization compared to the original layout of the network. A topologically accurate representation retains the face structure of the input. This concept is further described in Section 2.3.

algorithms. Hong et al.'s implementation neither preserved the topology of the input embedding nor produced octilinear solutions. Ribeiro et al. [157] also used a force-directed implementation to automatically draw schematic maps. Their results are efficiently produced and aesthetically pleasing, and they focus on using spider maps in representing transit networks. Stott et al. [179] later introduced a hill-climbing algorithm within a multiobjective optimization framework to solve the metro map automation problem. Their optimizer gave improved results, but octilinearity was not enforced and optimality could not be guaranteed. Wolff [203], Nöllenburg and Wolff [134] then developed a multiobjective mixed integer program to solve the metro map drawing problem. Like Stott et al. [179], Nöllenburg and Wolff [134] used the weighting method [107] to find optimal octilinear results.

While Nöllenburg and Wolff's multiobjective formulation is a significant improvement compared to previous efforts and is able to produce good unlabeled maps, there is room for further development. Nöllenburg and Wolff used the weighting method, which may ignore potentially desirable solutions [167]. Their triobjective model, while elegant, does not lend itself easily to analysis of the solution space. Finally, the coordinate integrality requirements unnecessarily slowed down their method. We sought to address these issues by simplifying their model, relaxing coordinate integer constraints, and implementing an augmented ε-constraint method developed by Mavrotas and Florios [110] to determine the set of efficient solutions and analyze the objective space.

Multiobjective mixed integer programs (MOMIPs) have been successfully used to model numerous real-life problems. For example, Scaparra and Church [162] developed a two-level approach to a mixed-integer program for infrastructure management. Much important work has been done in finding non-dominated solutions to optimization problems, and several algorithms have been tailored to their specific applications [47, 172]. In the area of visual representation, Cano et al. [25] introduced a

novel metaheuristic approach to solving the problem of proportionally symbolic cartograms. Martí and Estruch [108] also proposed a heuristic method for solving the edge-crossing minimization problem.

Various other research problems related to automated schematic map drawing have also been tackled, such as those dealing with bend minimization and path simplification [43, 14]. In a departure from convention, Fink et al. [52] have proposed a "curvilinear" drawing approach which has produced metro maps using a force-directed algorithm. Hurter et al. [81] have also created a schematic automation method specifically for air traffic control routes. They use simulated annealing to solve a cost minimization model that penalizes crossings, density and distortion.

2.2.1 Why automation is important

It has been amply demonstrated that distortion, when correctly applied, can greatly enhance the mental perception of a network [154, 179, 10]. The best diagrams still require significant manual effort to produce and usually at great expense [10]. For example, the London Underground network map took over three decades to attain the widely accepted form that has not changed much since the 1950s [60]. This is why computer automated drawings are crucial for modern applications. With the emergence of modern mobile technology, demand is ripe for dynamic maps that can toggle layered information. Here, we focus on static maps, but we keep in mind that advances in computing technology will mean that complex problems will be increasingly solvable in real time. The computer-automated process in schematic diagramming can save significant amounts of time and money in map making, with a potential for impact in transit network design [68], understanding disease progressions [69], and visualizing complex plans [178] and pathways.

Guo [68] has shown that schematic maps influence how passengers perceive and utilize a transit network. Taking the London Underground network as an example,

it can be argued that passengers' favorable disposition to a network is affected by how it is represented, a phenomenon Guo coins as the "map effect." In the case of bicycle networks, numerous efforts, both personal and official, have been made to schematize their maps in the hopes of boosting ridership. An automated solution to this can significantly increase the production of schematic maps. Bicycle networks are of particular interest [166], as urban sustainability through reduced automobile congestion and increased public health benefits [135] are critical outcomes of positive network perceptions.

2.2.2 Contributions and improvements

The work presented here is significant in that it shows we can generate schematic solutions much quicker by simplifying, reformulating, and tightening the multiobjective model presented by Nöllenburg and Wolff [134]. In particular, we relax the integrality constraints on the coordinate variables to achieve this efficiency. We still obtain proven optimal solutions, and we show this through three numerical examples and two applications.

An important characteristic of an automatic schematization tool is to provide a useful starting point for a designer to produce a final representation, as computers have limited decision-making ability. Beyond manually selecting weights to obtain tailored solutions, we show how the ε-constraint method of solving multiobjective programs can be used to efficiently generate a Pareto frontier of non-dominated solutions. Specifically, we adapt Mavrotas and Florios' augmented ε-constraint implementation [110]. Our results show how a framework can be developed for evaluating desirable schematic diagrams from a set of efficient (Pareto optimal) solutions. This is the first time this method has been used in solving the schematic map drawing problem, and we believe this is a critical development in that all Pareto points—which may not always be found by varying weights—can be obtained by the user or designer.

Automatic schematic map drawing has largely been presented within the sphere of metro map drawing. This is understandable, as much of the interest in this subject arose from efforts to automate metro maps. In this chapter, we implement our method on the Vienna Underground as a case study. However, we go further to illustrate how the automatic schematic method can also be applied to disease pathway representation. We hope that our efforts will spur further work in broadening the applications of automatic schematic mapping.

2.3 The schematic drawing problem

First, we provide a summary of important symbols and definitions (Table 2.1). The

Table 2.1 Important symbols and their definitions

$G(V, E)$	planar input graph, as a function of V and E
$(G, \mathcal{L})$	possible metro graph
Γ	drawing operator
$\Pi(v)$	geographic location of each vertex v in the plane
$\mathcal{L}$	set of lowest number of paths linking all vertices in G (line cover)
L	metro line (element in $\mathcal{L}$)
E	set of edges e in graph
V	set of vertices v in graph G
F	set of faces f in graph
l	number of lines in G
m	number of edges of G
n	number of vertices of G
r	number of faces of G

schematic map drawing problem is then formally defined as follows:

Definition 5. Find the best drawing Γ of the graph $(G, \mathcal{L})$ subject to schematic rules, where $G(V, E)$ is a planar input embedding $\Pi(v)$ of a set V of vertices and a set E of edges, with $\mathcal{L}$ the set of lines or line cover of G.

The vertices $v \in V$ and edges $e \in E$ constitute the topology of G. Together, these elements divide the graph into bounded zones known as faces, where each face f is an

element of F, the set of all faces. Trailing or circumferential edges collectively make up the unbounded external face [182]. A graph can thus be further described by a list of the edges, in circular order, occurring in each face—a planar representation [182]. The sets of vertices, edges and faces in a planar graph are related by Euler's formula:

$$|E| + 2 = |V| + |F| \tag{2.1}$$

The nature of the schematic rules enforced depend on the type of map being drawn. In this chapter, we restrict ourselves to the Beck-inspired diagram whose aesthetics are encapsulated within the following major guidelines:

(A) *Octilinearity*: all edges must originate at angles that are multiples of 45°. This necessitates that the output be on an octilinear grid with four axes: $x\,(0°)$, $y\,(90°)$, $z_1\,(45°)$ and $z_2\,(-45°)$.

(B) *Bend avoidance*: Along each line, bends must avoided as much as possible. Obtuse bends are favored over acute or right ones.

(C) *Topological correctness*: The relative positions of vertices and their connectivities must remain the same, for the sake of readability and mental mapping. In other words, the face structure of the solution is identical to that of the input.

(D) *Edge uniformity and spacing*: Edge lengths should be kept as even as possible. Nonadjacent edges must also keep a minimum distance to ensure clarity.

(E) *Edge shifting*: Imposing an optimal octilinear output necessitates linear distortion. Edges are allowed to be shifted in keeping with this geometry as long their relative positions to other adjacent edges are maintained.

A few of these guidelines are illustrated in Figure 2.3.

We do not address the labeling problem here. If labels were to be included, however, they would ideally not overlap and would be grouped into blocks with the

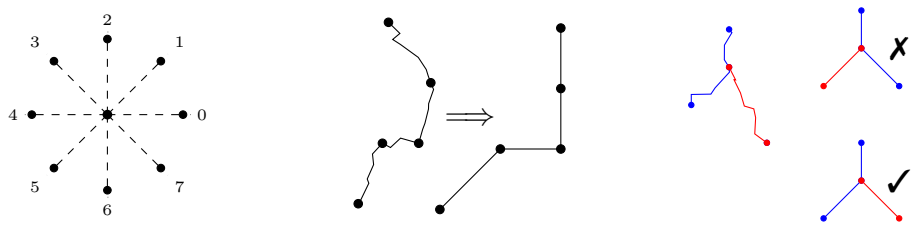

(a) Edge octlinearization **(b)** Line bend minimization **(c)** Topology preservation

Figure 2.3 Illustration of three guidelines under consideration for schematization

same orientations. Line colors should also be optimally distinguishable, but this component is not included in our implementation. In the mixed integer formulation that will be discussed in the following section, guidelines (A), (C) and (D) are modeled as hard constraints since they are strict requirements. Guidelines (B) and (E) are however modeled as objective cost functions or soft constraints, as they describe aesthetic preferences.

2.4 Mixed integer program formulation

The mixed integer program presented in this chapter develops the model introduced by Nöllenburg and Wolff [134] into a multiobjective mixed binary linear program. Unlike Nöllenburg and Wolff's formulation, which has three objective cost functions, ours utilizes only two, namely: shift and bend. We eliminate their "total edge length" cost function, replacing this with an upper bound on edge lengths $\ell_{\max}$. This can have the same value for all edges, or take on different values based on the edge or face properties (as we demonstrate in the Vienna Metro and cancer pathway examples). The conversion to a biobjective problem facilitates analyses, especially regarding tradeoffs on a two-dimensional Pareto frontier. Notably, we also find that it is not necessary to impose integer constraints on the vertex coordinates. The subsequent relaxation greatly speeds up solve times, as we will demonstrate. Numerical evidence indicates that Pareto optimal solutions will remain on the octilinear grid, and we obtain them

faster with integrality relaxation in place.

The bend and shift costs describe the objective functions that address the aesthetic considerations of schematic maps in the Beck style [60]. The objectives are subject to three sets of hard constraints that deal with the following properties: octilinearity and edge length, circular ordering and nonadjacent edge spacing. We describe each set of constraints in detail. Before this, we introduce the geometric and combinatorial framework for the input problem layout.

2.4.1 Coordinate space for octilinear grid

To facilitate constraint formulation, Nöllenburg and Wolff proposed two new axes in the $\pm 45°$ directions, namely z_1 and z_2. Each vertex v can thus be referenced by four coordinates: $x(v), y(v), z_1(v), z_2(v)$, although only the first two are sufficient to locate the vertex. The new axes are related to the conventional ones in the following manner:

$$\begin{aligned} z_1(v) &= \frac{x(v) + y(v)}{2} \\ z_2(v) &= \frac{x(v) - y(v)}{2} \end{aligned} \tag{2.2}$$

This definition reinforces the L^∞ metric used as the basis for the grid. Thus, all vertices at the corner of a unit square are equidistant from the origin as are those centered on each side of the square. The coordinate system is shown in Figure 2.4.

It is important to note that integer coordinates (on all four axes) will always guarantee grid placement. Our numerical results indicate that we can obtain Pareto optimal grid-based points without specifying integer constraints on the coordinates x, y, z_1 and z_2, in a departure from Nöllenburg and Wolff's implementation [134]. By relaxing the coordinate integer constraints

$$0 \leq x(v), y(v), z_1(v), z_2(v) \in \mathbb{R} \tag{2.3}$$

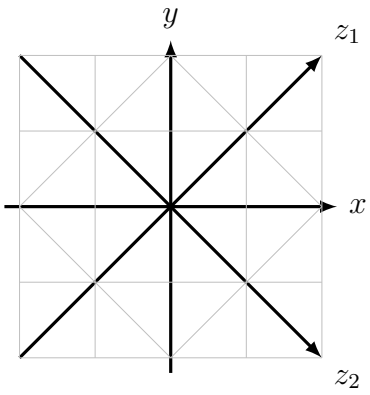

Figure 2.4 Quadraxial coordinate system and octilinear grid

we gain efficiency. There are still binary variables in the model that remain unchanged. In a few examples in Section 2.5, we compare our relaxation results against those of Nöllenburg and Wolff, highlighting significant improvements in execution time.

We hold that optimal solutions to the schematic drawing problem will always be found on the octilinear grid. We demonstrate this idea through a few examples. While some planar representations can have off-grid optimal solutions, as we will show, it appears that on-grid optimal solutions are the cheaper to compute. It is on this basis that we motivate the relaxation of the coordinate integer constraints Nöllenburg and Wolff imposed in their model. Our observation is that we still obtain integer solutions but in a shorter period of time, as fewer nodes have to be traversed during the branch-and-bound search.

Consider the graph in Figure 2.5A, which is the solution to a given input embedding, where $x(1) = 0$, $x(2) = 2$ and $x(3) = 4$. If we fixed $x(3) = 4.5$ before solving, then the solution would result in a shift of $x(1)$ and $x(2)$, as well (Figure 2.5B). This is essentially a translation of the grid in order to maintain octilinearity. If we decided, however, to keep $x(2)$ at 2, while $x(3)$ was also fixed at 4.5, the solution would result in a shift of $y(3)$ to maintain octilinearity (Figure 2.5C).

Also, moving any one of the y coordinates would result in a solution that translates

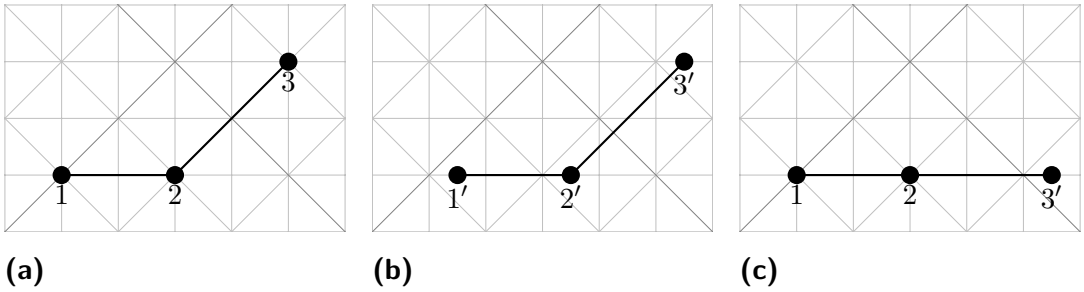

Figure 2.5 Non-integer and off-grid solutions are possible in a simple face structure such as this one, but they are typically more costly to find.

the entire graph by the same amount. If two y coordinates are forced to be in a position where the resulting edge cannot be octilinear, then the problem becomes infeasible.

Non-integer edge lengths can always be forced to appear, as long as octilinearity is not violated. Sometimes, this would result in scaling or translating the grid. In such cases, the solution would still be considered as on a grid. As will be seen in the next several subsections, the minimum integer edge lengths we set also encourage integer solutions. Also, solver architecture ensures we never encounter non-integer solutions. An optimal integer result is always favored, and even more so since we set integer edge lengths as starting points.

To bring this point further home, we consider a second example (Figure 2.6A). This graph has one bounded face. A possible outcome of fixing $y(1)$ at $v_{1'}$ is a translation of the entire graph (Figure 2.6B). The solution is still essentially on a grid. While y coordinates have non-integer values, the edges maintain integer lengths. Forcing both $x(1)$ and $y(1)$ to remain at $v_{1''}$ might result in a scalar expansion of the graph, a solution which still lies on a grid (Figure 2.6C). Scaling the grid accordingly would mean the edge lengths essentially have integer values on the new scale.

The examples in Figure 2.5 and Figure 2.6 are simple but atypical for most real-world applications. They both have only one unbounded face. For a graph with a more complicated structure (two or more faces), it becomes even more difficult to find

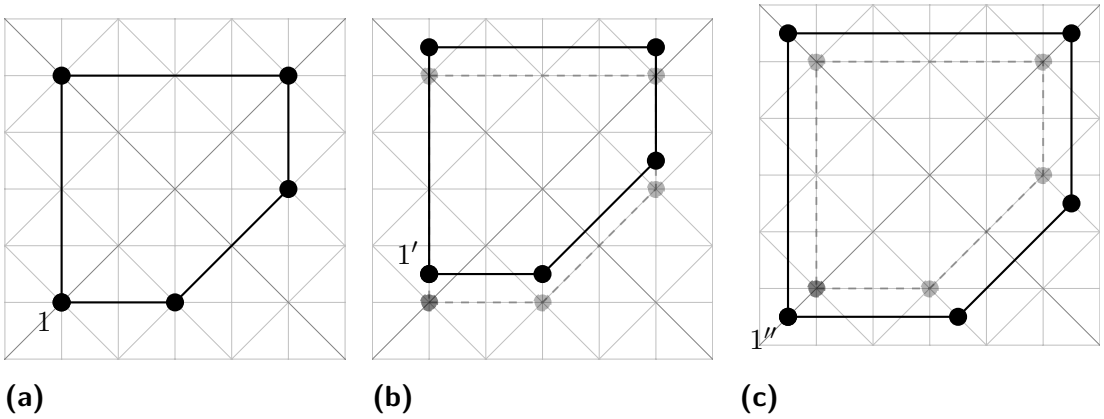

Figure 2.6 Fixing non-integer coordinates create solutions which retain integer edge lengths on a translated or scaled grid

an off-grid Pareto optimal point. We consider a four-face planar graph (Figure 2.7). A non-integer edge length may be impossible to have if adjacent edges cannot be adjusted accordingly to retain the face structure and maintain octilinearity. If edge $e(5,6)$ (in the z_2 direction), for example, were to have a non-integer edge length that was not proportional to that of $e(1,6)$ and $e(6,3)$, an octilinear structure would not be possible.

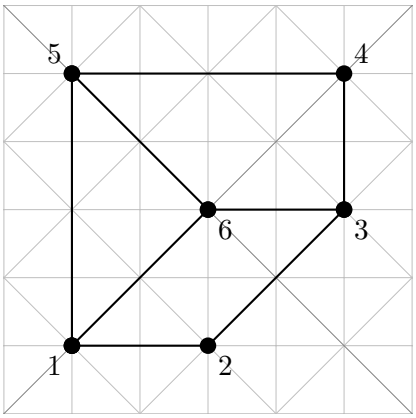

Figure 2.7 A more complex face structure makes it difficult or impossible to find completely off-grid solutions

We can further motivate the existence of a drawing with integer edge lengths for every octilinear graph of a given input embedding by assuming that all edge lengths in such a graph are rational numbers. It is then trivial to show that there is always

a number that can be multiplied by each edge length to produce an integer solution.

In summary, integer Pareto optimal points can be obtained without enforcing integer constraints. The major difference in our model, compared to Nöllenburg and Wolff's [134], is the reduction of a mixed integer program to a mixed binary linear program, which is demonstrably easier to solve, and the application of the augmented ε-constraint method to find efficient solutions.

2.4.2 Sector assignments

The key building block of this formulation, which Nöllenburg and Wolff introduced, is the sectorialization of edges. Based on the eight-direction octilinear grid, each edge $e(u, v)$ in the input embedding is assigned to a sector $\text{sec}_0(u, v)$ based on its angular orientation within the grid. Thus,

$$\text{sec}_0(u,v) = \begin{cases} 0 & 337.5^\circ \leq \angle uv < 22.5^\circ \\ 1 & 22.5^\circ \leq \angle uv < 67.5^\circ \\ 2 & 67.5^\circ \leq \angle uv < 112.5^\circ \\ \quad\vdots & \\ 6 & 247.5^\circ \leq \angle uv < 292.5^\circ \\ 7 & 292.5^\circ \leq \angle uv < 337.5^\circ \end{cases} \tag{2.4}$$

In pursuit of an optimal solution, each edge is allowed to either remain in its original sector (sec_0) or move one sector forward (sec_{+1}) or backward (sec_{-1}):

$$\text{sec}_{+1} = \text{sec}_0 + 1 \mod 8 \tag{2.5}$$

$$\text{sec}_{-1} = \text{sec}_0 - 1 \mod 8 \tag{2.6}$$

The modular arithmetic operator (mod) in the above equations ensures that the values of $\text{sec}_{\pm 1}$ always reamin within 0 and 7, i.e. in modulo 8. Thus, if $\text{sec}_0 = 7$, then by Equation (2.5), $\text{sec}_{+1} = 0$. Similarly, if $\text{sec}_0 = 0$, then (2.6) would give $\text{sec}_{-1} = 7$.

The variable $\text{dir}(u, v)$ holds the value of the sector each edge in the solution eventually takes. This disjunction sets up a combinatorial problem which necessitates the use of binary variables α_0, α_{+1} and α_{-1} for each edge, which can only take one of three possible sectors. These variables must satisfy the relation

$$\sum_{i \in \{-1,0,1\}} \alpha_i(u, v) = 1 \tag{2.7}$$

The directional variables are thus described as follows:

$$\text{dir}(u, v) = \sum_{i \in (-1,0,1)} \text{sec}_i(u, v) \cdot \alpha_i(u, v) \tag{2.8}$$

$$\text{dir}(v, u) = \sum_{i \in (-1,0,1)} \text{sec}_i(v, u) \cdot \alpha_i(u, v) \tag{2.9}$$

The direction and sector variables are directional, and all movements are represented in modulo 8. Thus,

$$\text{sec}_i(u, v) = \text{sec}_i(v, u) + 4 \mod 8 \tag{2.10}$$

$$\text{dir}(u, v) = \text{dir}(v, u) + 4 \mod 8 \tag{2.11}$$

2.4.3 Octilinearity and edge length constraints

Further disjunctive constraints are necessary for ensuring octilinearity. For each of the eight possible directions, they require the ordinates of the edge be equal, while the abscissae must differ by a minimum edge length $\ell_{\text{min}}(u, v)$. The constraints are shown below for sectors 0 and 1. Similarly constructed constraints hold for the six other sectors. They are disjunctive constraints [56], represented using a conjunction

of linear constraints in what is termed the "big-M formulation":

$$\mathrm{sec}_i(u,v) = 0 : \begin{cases} y(u) - y(v) & \leq & M(1 - \alpha_i(u,v)) \\ -y(u) + y(v) & \leq & M(1 - \alpha_i(u,v)) \\ -x(u) + x(v) & \geq & -M(1 - \alpha_i(u,v)) + \ell_{\min}(u,v) \end{cases} \tag{2.12}$$

$$\mathrm{sec}_i(u,v) = 1 : \begin{cases} z_2(u) - z_2(v) & \leq & M(1 - \alpha_i(u,v)) \\ -z_2(u) + z_2(v) & \leq & M(1 - \alpha_i(u,v)) \\ -z_1(u) + z_1(v) & \geq & -M(1 - \alpha_i(u,v)) + \ell_{\min}(u,v) \end{cases} \tag{2.13}$$

The coordinate values are bounded above by M:

$$x(v), y(v) \leq M \quad \forall v \in V \tag{2.14}$$

If M is too large, the model might become unstable or computation time may be lengthened. If M is not large enough, some otherwise optimal solutions may be rendered infeasible. In our implementation, we have chosen M as

$$M = \sum_{e \in E} e(u,v) \cdot \ell_{\max}(u,v) \tag{2.15}$$

which gives an upper bound with the assumption that all the edges are sequentially connected, thus spanning the map in any direction in L^∞. This value has proved large enough to accommodate all Pareto optimal points, while keeping the model stable.

In another departure from Nöllenburg and Wolff's implementation, we assume edge length maxima are user-defined. While Nöllenburg and Wolff minimize the sum

of all edge lengths, we argue for setting a hard constraint on these:

$$\begin{aligned} x(u) - x(v) &\leq \ell_{\max}(u, v) \\ -x(u) + x(v) &\leq \ell_{\max}(u, v) \\ y(u) - y(v) &\leq \ell_{\max}(u, v) \\ -y(u) + y(v) &\leq \ell_{\max}(u, v) \end{aligned} \tag{2.16}$$

We not only gain time in computation, but more critically, our formulation is now biobjective, making it easier to analyze (two-dimensional Pareto frontier) and quicker to solve (fewer variables).

2.4.4 Circular order constraints

An important set of constraints that preserve topology (input face structure) and guarantee readability are the circular order constraints. They ensure that spanning edges from a vertex retain their relative position and do not overlap. This set of constraints is expressed as

$$\mathrm{dir}(u, v_j) \leq \mathrm{dir}(u, v_{j++1}) - 1 + 8\beta(u, v_j), \quad \forall u : \deg(u) \geq 2, j = \{1, 2, ..., \deg(u)\} \tag{2.17}$$

where

$$\sum_{j=1}^{\deg(v)} \beta(u, v_j) = 1 \quad \forall u : \deg(u) \geq 2 \tag{2.18}$$

The order constraints only hold for vertices whose degree (number of spanning edges) is greater than or equal to 2. We can further control the number of variables required by restricting the application of these constraints to vertices of degree 3 or greater and only to degree-2 vertices for which the edges are 2 or fewer sectors apart.

2.4.5 Edge spacing constraints

Edge spacing constraints ensure a specified minimum distance $d_{\min}$ between nonadjacent edges on the same face. The binary variable γ_i, indexed over the 8 cardinal (or axial) directions, ensures this minimum distance is kept in at least one direction (or the relevant direction) for each nonadjacent same-face edge pairing. Hence,

$$\sum_{i \in \{\text{N, NW, ... , E, NE}\}} \gamma(e_1(u,v), e_2(u,v), f) \geq 1 \tag{2.19}$$

The big-M formulation is again employed to model disjunction. The two sets for the north (N) and the northwest (NW) directions are given below.

$$\begin{aligned}
y(u_2) - y(u_1) &\leq M(1 - \gamma_{\text{N}}(e_1, e_2, f)) - d_{\min} \\
y(u_2) - y(v_1) &\leq M(1 - \gamma_{\text{N}}(e_1, e_2, f)) - d_{\min} \\
y(v_2) - y(u_1) &\leq M(1 - \gamma_{\text{N}}(e_1, e_2, f)) - d_{\min} \\
y(v_2) - y(v_1) &\leq M(1 - \gamma_{\text{N}}(e_1, e_2, f)) - d_{\min}
\end{aligned} \tag{2.20}$$

$$\begin{aligned}
-z2(u_2) + z2(u_1) &\leq M(1 - \gamma_{\text{NW}}(e_1, e_2, f)) - d_{\min} \\
-z2(u_2) + z2(v_1) &\leq M(1 - \gamma_{\text{NW}}(e_1, e_2, f)) - d_{\min} \\
-z2(v_2) + z2(u_1) &\leq M(1 - \gamma_{\text{NW}}(e_1, e_2, f)) - d_{\min} \\
-z2(v_2) + z2(v_1) &\leq M(1 - \gamma_{\text{NW}}(e_1, e_2, f)) - d_{\min}
\end{aligned} \tag{2.21}$$

The minimum spacing requirement also ensures that edge crossings are avoided. (Please see Appendix A for a full list of the inequalities.)

2.4.6 Cost functions and soft constraints

The optimal solution must maximize the obtuseness of all bends in each line. The bend cost, to thus be minimized, is defined as

$$C_{\text{bend}} = \sum_{L \in \mathcal{L}} \sum_{uv,vw \in L} \text{bend}(u, v, w) \tag{2.22}$$

This cost can be described as the sum of all the bend costs for adjacent edge pairings in each line. Constraints are designed to assign costs of 1, 2, and 3 to bends of $135°, 90°$ and $45°$, respectively [134]:

$$\Delta\text{dir}(u, v, w) = \text{dir}(u, v) - \text{dir}(v, w) \tag{2.23}$$

$$\text{bend}(u, v, w) = \min\{|\Delta\text{dir}(u, v, w)|, 8 - |\Delta\text{dir}(u, v, w)|\} \tag{2.24}$$

We recall that $\text{dir}(u, v) \in \{0, 1, ..., 7\}$ denotes the sector assigned to the edge $e(u, v)$ in the solution. The difference $\Delta\text{dir}(u, v, w)$ between the directional variables of adjacent edges $e(u, v)$ and $e(v, w)$ gives a measure of the bend angle. Since there is a wrap-around at the modulus 8, we find the minimum of the absolute value of Δdir and its difference from 8 (Equation (2.25)). Linearizing this equation requires the use of two more binary variables, $\delta_1(u, v, w)$ and $\delta_2(u, v, w)$, thus:

$$\begin{aligned} -\text{bend}(u, v, w) &\leq \Delta\text{dir}(u, v, w) - 8\delta_1(u, v, w) + 8\delta_2(u, v, w) \\ \text{bend}(u, v, w) &\geq \Delta\text{dir}(u, v, w) - 8\delta_1(u, v, w) + 8\delta_2(u, v, w) \end{aligned} \tag{2.25}$$

Equations (2.25) simply represent the inequality

$$\text{bend}(u, v, w) \geq |\Delta\text{dir}(u, v, w) - 8\delta_1(u, v, w) + 8\delta_2(u, v, w)| \tag{2.26}$$

As the bend cost is minimized, δ_1, δ_2 or both are switched on or off in order to correctly calculate the bend cost for each edge, which will have a value of 0, 1, 2, or 3. For instance, if two adjacent edges have $\mathrm{dir}(u,v) = 1$ and $\mathrm{dir}(v,w) = 7$, respectively, then $\Delta\mathrm{dir}(u,v,w) = 1 - 7 = -6$. The cost of this bend would be $\mathrm{bend}(u,v,w) = 2$, where $\delta_1(u,v,w) = 0$ and $\delta_2(u,v,w) = 1$.

Each edge also incurs a cost of 1 for shifting forward or backward from its original sector. The total shift cost of the octilinear drawing is given by

$$C_{\text{shift}} = \sum_{uv \in E} \mathrm{shift}(u,v), \tag{2.27}$$

where

$$-M \cdot \mathrm{shift}(u,v) \leq \mathrm{dir}(u,v) - \mathrm{sec}_{\text{orig}}(u,v) \leq M \cdot \mathrm{shift}(u,v) \tag{2.28}$$

For each edge $e(u,v)$, $\mathrm{shift}(u,v)$ is thus a binary variable. For example, consider $\mathrm{sec}_0(u,v) = 3$ for a given edge in an input embedding. If $\mathrm{dir}(u,v) = \mathrm{sec}_0(u,v) = 3$, then $\mathrm{shift}(u,v) = 0$. However, if $\mathrm{dir}(u,v) = \mathrm{sec}_{-1}(u,v) = 2$ or $\mathrm{dir}(u,v) = \mathrm{sec}_{+1}(u,v) = 4$, then $\mathrm{shift}(u,v) = 1$. The total shift cost is the sum of all $\mathrm{shift}(u,v)$ for every edge $e(u,v)$ in the graph.

2.4.7 Implementing the augmented ε-constraint method

An important question in schematic map automation is how the decision on the final solution is made. For any given input embedding, a number of acceptable solutions may exist. In previous multiobjective formulations, particularly the one developed by Nöllenburg and Wolff [203, 134], the weighting method has been used to find these points. In our modified biobjective case, this would be written as

$$\min : \quad \lambda_{\text{bend}} C_{\text{bend}} + \lambda_{\text{shift}} C_{\text{shift}} \tag{2.29}$$

s.t.

$$\text{octilinearity and edge length constraints} \tag{2.30}$$

$$\text{circular order constraints} \tag{2.31}$$

$$\text{edge spacing constraints} \tag{2.32}$$

where λ_{bend} and λ_{shift} are appropriately chosen weights for bend and shift, respectively. This method is useful for generating a single result based on the desired weighting combination. However, the weighting method may fail to generate the complete set of Pareto optimal solutions, regardless of the choice of weighting combinations [167]. These supported solutions are obtained by optimizing a convex combination of the objectives. However, unsupported Pareto optimal solutions may also exist. The ε-constraint method is therefore necessary to fill any such gaps in finding efficient solutions. Scaling can also be an issue in the weighting method, and one might need to adjust the objective functions to reduce the effects of uneven matching. This is a non-issue in the ε-constraint method [109].

We thus implement an efficient version of the ε-constraint method to (i) counter the influence of weight scaling, (ii) relieve the user of the burden of deciding on weighting combinations, and (iii) produce both nonextreme and, importantly, unsupported Pareto optimal solutions. Our algorithm of choice is the augmented ϵ-constraint method (AUGMECON2) developed by Mavrotas and Florios [110] and implemented in GAMS[2]

The basic augmented ε-constraint method for a multiobjective problem optimizes the first objective and successively uses the other objectives as constraints bounded by

[2]Earlier, Mavrotas [109] introduced the AUGMECON method, which has since been superseded by AUGMECON2 in terms of performance.

the values generated in a payoff table partitioned into grid intervals. AUGMECON2 is preferred over the basic ε-constraint method for a number of reasons. First, it employs lexicographic optimization to calculate the payoff table, thus avoiding dominated solutions. Second, it ensures that only efficient (and not weakly efficient) solutions are produced. This is implemented by replacing the inequalities for the constrained objective functions with equalities and corresponding slack variables; the main objective is modified accordingly. Finally, AUGMECON2 [110] uses a "jump" procedure, in which bypass coefficients are calculated from the innermost slack variables to skip over grid locations that do not produce Pareto optimal solutions. This bypass feature improves performance, as does the "early exit loop" feature (first introduced in AUGMECON [109]) that skips to the next row of grid points once an infeasibility is detected. Overall, these features make Mavrotas and Florios' augmented ε-constraint method attractive for solving multiobjective mixed integer programs such as ours.

Our formulation is given below. The second term in Equation (2.33) is the "augmentation."

$$\min : \quad C_{\text{bend}} - \varepsilon \frac{s_{\text{shift}}}{r_{\text{shift}}} \tag{2.33}$$

s.t.

$$C_{\text{shift}} + s_{\text{shift}} = e_{\text{shift}} \tag{2.34}$$

$$e_{\text{shift}} = \text{ub}_{\text{shift}} - \frac{i_{\text{shift}} r_{\text{shift}}}{g_{\text{shift}}} \tag{2.35}$$

where $\varepsilon = 10^{-3}$ (a small scalar quantity), s_{shift} is the slack (or surplus) variable for the shift function, r_{shift} is the range of the payoff table for the shift cost function (used as a scaling factor), and e_{shift} is the RHS of the constrained shift function, whose value depends on the grid location in the payoff table. ub_{shift} is the upper bound of the shift function C_{shift}, and $i_{\text{shift}} \in \{0, 1, ..., g_{\text{shift}}\}$, where g_{shift} is the number of grid intervals determined by the user. The complete Pareto frontier is obtained when $g_{\text{shift}} := r_{\text{shift}}$.

Fewer grid points would result in shorter computation times but would give a sparser Pareto frontier [110]. The user, therefore, may want to carefully consider the selection of grid intervals, especially when solving large problems.

Using AUGMECON2, we obtain a Pareto frontier that enables us to visually and quantitatively evaluate the tradeoff between shift and bend across all the noninferior solutions.

2.5 Preliminary evaluation

We present three working examples to evaluate the performance of our implementation, compared to the earlier work of Nöllenburg and Wolff. The three examples are introduced in order of increasing complexity.

2.5.1 Minimal example

This first minimal example consists of four vertices and two lines (red and green). Figure 2.8 shows the input embedding and the original sectors to which each edge belongs. For ease of reference, we have assigned numerical labels to the vertices. From

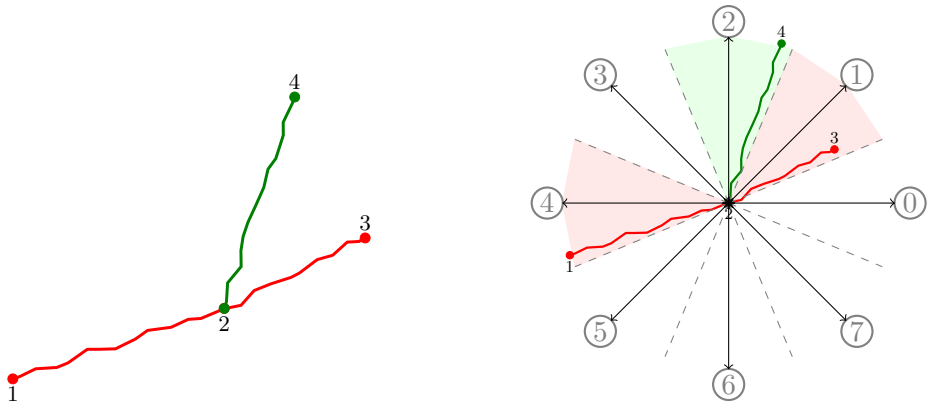

(a) Input embedding **(b)** Initial sectors of the edges

Figure 2.8 Minimal example: 2 lines, 3 edges, 4 vertices, 1 face; $\{l, m, n, f\} = \{2, 3, 4, 1\}$

Figure 2.8b, we see that edge $e(2, 3)$ is originally positioned at an angle slightly greater

than 22.5° to the horizontal. It is thus assigned to sector 1, that is $\text{sec}_0(2,3) = 1$. The circled numbers in Figure 2.8b denote the sector numbers from 0 to 7. Similarly, edge $e(2,4)$ lies within ±22.5° of 90°, hence it is assigned to sector 2: $\text{sec}_0(2,4) = 2$. Table 2.2 shows the sector assignments for each edge. In each case, sec_{-1} and sec_{+1} is also shown. In the solution(s), each edge can be assigned to any of the three sectors through the directional variable $\text{dir}(u,v)$, as long as none of the hard constraints are violated.

Table 2.2 Sector parameters for each edge

edge uv	$\text{sec}_{-1}(u,v)$	$\text{sec}_0(u,v)$	$\text{sec}_{+1}(u,v)$
1-2	7	0	1
2-3	0	1	2
2-4	1	2	3

Vertex 2 has three spanning edges, thus:

$$\deg(2) = 3 \tag{2.36}$$

It is clear that in this model, edges $e(1,2)$ and $e(2,3)$ will not overlap under any circumstances (see Equation (5.9)). The circular order constraints, (2.17) and (5.7), however, ensure that other edge pairs $e(2,3)$ and $e(2,4)$ or $e(1,2)$ and $e(2,4)$ never overlap. The edge spacing constraints are not under consideration here, as there are no nonadjacent edge pairs.

The optimal solutions to this input embedding are trivial (Figure 2.9). In the first solution (Figure 2.9A), $\{C_{\text{bend}}, C_{\text{shift}}\} = \{0,1\}$, while in the second (Figure 2.9B), $\{C_{\text{bend}}, C_{\text{shift}}\} = \{1,0\}$, since all three edges retain their original sector positions.

These two figures show that while mathematical models can produce Pareto optimal solutions, humans remain the best equipped to decide which solutions are desirable. Pareto point (A) has zero line bends but it sacrifices relative accuracy in

(a) $\{C_{\text{bend}}, C_{\text{shift}}\} = \{0, 1\}$ **(b)** $\{C_{\text{bend}}, C_{\text{shift}}\} = \{1, 0\}$

Figure 2.9 Pareto optimal solutions to minimal example

the positioning of edge $e(2, 3)$. For the decision-maker who does not consider a 135° bend a problem but prioritizes accuracy in representation, then the preferred solution would be (B).

2.5.2 Dual-line network

We present a second example that still has only 2 lines but with a more complex structure. This dual-line network has 2 faces, 7 edges and 7 vertices (Figure 2.10). The internal face is bounded by the edges $(2, 3), (3, 5), (2, 4)$ and $(4, 5)$. There are several nonadjacent same-face edge pairings in this example, thus making the edge spacing constraints (Equations (2.19), (2.20)) relevant.

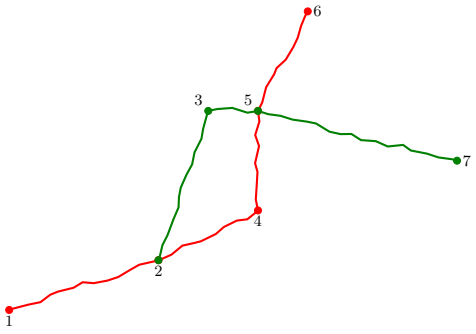

Figure 2.10 Dual-line network: 2 lines, 7 edges, 7 vertices, 2 faces; $\{l, m, n, r\} = \{2, 7, 7, 2\}$

Table 2.3 shows the sector assignments for all seven edges. We recall that the angle between two vertices u and v is measured counterclockwise from the horizontal. From Figure 2.10, it is clear that $\text{sec}_0(3, 5) = 0$. For this and the other edges, Equation (2.4) is used to determine the sector assignments.

Table 2.3 Sector parameters for each edge in the dual-line network

edge uv	$\text{sec}_{-1}(u,v)$	$\text{sec}_0(u,v)$	$\text{sec}_{+1}(u,v)$
1-2	7	0	1
2-3	1	2	3
2-4	0	1	2
3-5	7	0	1
4-5	1	2	3
5-6	0	1	2
5-7	7	0	1

Our augmented ε-constraint implementation generates three Pareto optimal solutions (Figure 2.11). Solution (A) has the lowest bend cost but it also has the highest shift cost, illustrating why solutions with smoother lines may appear increasing dissimilar to the original map. Solution (C) has no shifted edges, but it has the costliest bends. A designer, for instance, might be dissatisfied with the amount of geometric distortion in Solution (B), especially those of edges $e(1,2)$ and $e(5,7)$, in which case they may decide to increase their lengths. Other factors, such as the placement of geographic features or label positioning, can influence the choice of a solution.

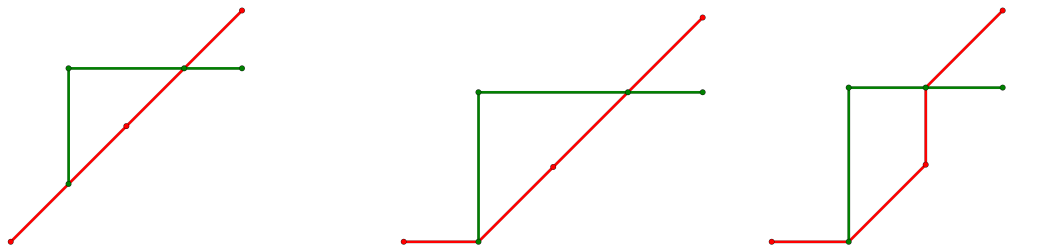

(a) $\{C_{\text{bend}}, C_{\text{shift}}\} = \{2,2\}$ **(b)** $\{C_{\text{bend}}, C_{\text{shift}}\} = \{3,1\}$ **(c)** $\{C_{\text{bend}}, C_{\text{shift}}\} = \{5,0\}$

Figure 2.11 Solutions to dual-line network

The graph of the Pareto frontier in Figure 2.12 visualizes the tradeoff between shift and bend for the three solutions. A graphic such as this one would be useful in evaluating the merits of each representation relative to the others. Since this example is still relatively simple, the solutions may seem obvious, not necessarily

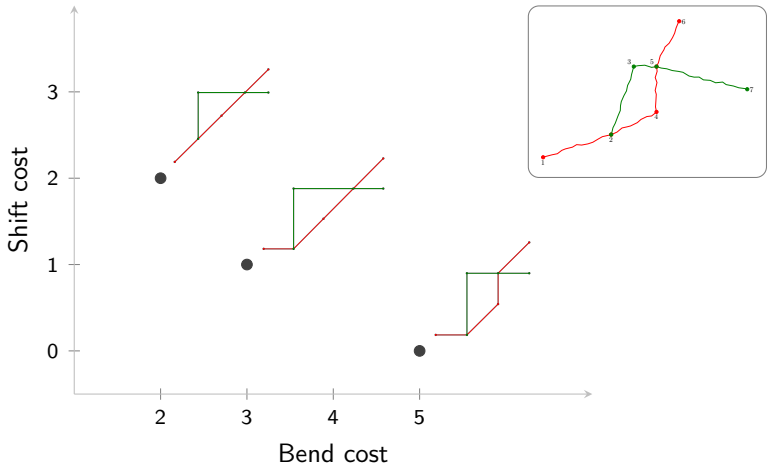

Figure 2.12 Pareto frontier for dual-line network solutions

requiring automated assistance to generate. The Pareto frontier, however, enables human involvement in the decision-making process.

2.5.3 Four-line network

This four-line example is more robust with a structure likely to be found in an actual network. It has 13 edges, 11 vertices and 4 faces (Figure 2.13).

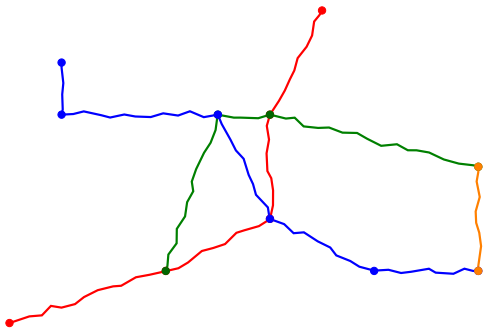

Figure 2.13 Four-line network: 4 lines, 13 edges, 11 vertices, 4 faces; $\{l, m, n, r\} = \{4, 13, 11, 4\}$

Five Pareto optimal points exist (Figure 2.14), and our method enables us to visually compare them alongside one another (Figure 2.15). Solution (E) has zero shift, and while it may be more appealing due to its similarity to the input embedding, the other solutions are equally valid and worthy of consideration. For instance,

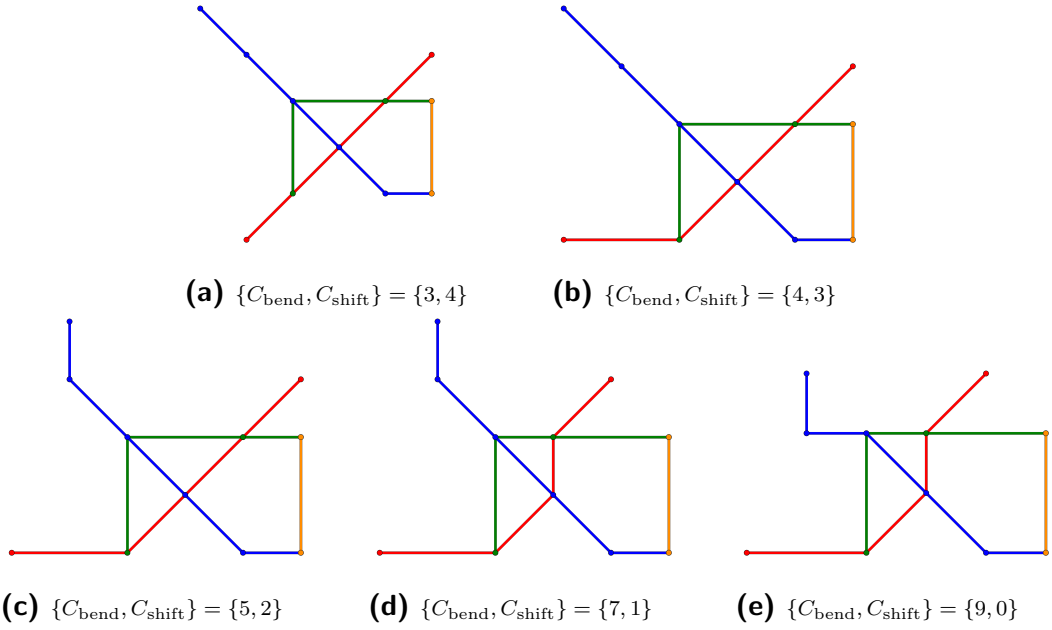

Figure 2.14 Pareto optimal solutions to four-line network

solution (A) has the lowest bend objective value and may be regarded by some as easiest to navigate. We checked with the weighting method and found that of the five Pareto points, solution (D) is unsupported, and may not have been found without the augmented ε-constraint method.

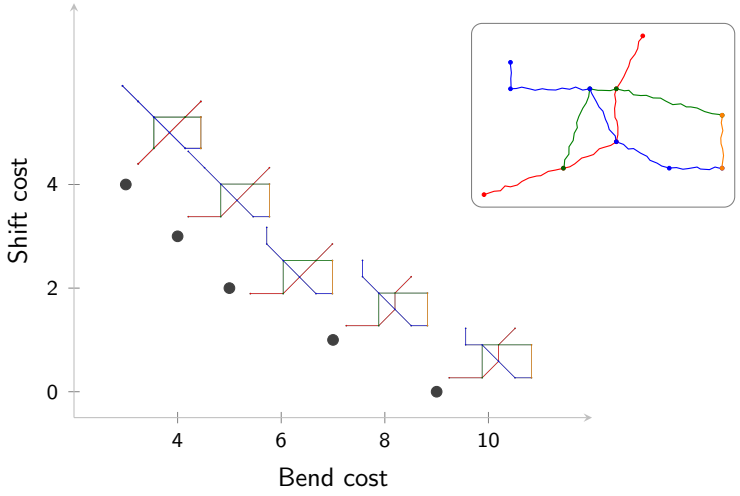

Figure 2.15 Pareto frontier for four-line network

2.5.4 Preliminary evaluation

We solved the examples described above on a 2.3GHz Intel i7 machine (16 GB RAM). The examples were programmed in GAMS and Python and solved with the CPLEX 12.6 solver. Our tests show that relaxing the integer constraints on the coordinates and simplifying the model to a biobjective one produces identical optimal results to Nöllenburg and Wolff's method [134] but in much less computational time. Using the AUGMECON2 [110] method also has the added benefit of generating multiple efficient solutions, including those unsupported, in a single run. In the augmented ε-constraint formulation, we chose unit-spaced grid intervals spanning the range of the shift objective. For the minimal example, we used only 2 grid points. In the dual-line and four-line networks, we used 3 and 5 grid points, respectively. The performance benefit of using fewer grid points is not readily apparent for these examples, since they are small. However, using the maximum possible number of grid points (equal to the range of the shift objective plus 1) will always produce the complete Pareto set for a given problem in our formulation.

In order to highlight our improvements, we compare the performance of three methods (Table 2.4). The first, N&W–WM$_3$, is Nöllenburg and Wolff's model—triobjective with coordinate integer constraints—implemented using the weighting method. The second, O&S–WM$_2$, is our improved model—biobjective with integer coordinates relaxed—also implemented using the weighting method only for the sake of direct comparison to Nöllenburg and Wolff's method. The third, O&S–AUGMECON2, is the augmented ε-constraint implementation of our improved model. We note again that the integer relaxation only affects the coordinate variables. The binary variables (α, β, δ_1, δ_2, γ, shift) remain intact, as they are essential in formulating the disjunctive constraints. Relaxing the integrality constraints reduces the number of nodes visited in the branch-and-bound algorithm used by the CPLEX MIP solver.

Table 2.4 Description of methods compared for performance (N&W – Nöllenburg and Wolff; O&S – Oke & Siddiqui)

Method	Objective functions	Integer constraints	Optimization approach
N&W–WM$_3$	3	Yes	weighting method
O&S–WM$_2$	2	No	weighting method
O&S–AUGMECON2	2	No	augmented ε-constraint method

Generally, both our implementations demonstrate better performance than that of Nöllenburg and Wolff, as shown in Table 2.5. Comparing the weighting approaches, ours (O&S–WM$_2$) solves to optimality in 15% less time for both the minimal and dual-line network examples. For the four-line network, there is a 30% decrease in execution time between N&W–WM$_3$ and O&S–WM$_2$. With O&S–AUGMECON2, we obtain multiple unique solutions in each single run. Considering the average execution time per solution, we observe a decrease in performance for the minimal example. This is not the case for the dual- and four-line networks, where we record a performance gain of 24% and 61%, respectively, in comparison to N&W–WM$_3$. The efficiency of AUGMECON2 increases substantially as the problem grows in size, and this is more telling for large networks, as our case studies will show.

Table 2.5 Average execution time per unique solution for three numerical examples, using three implementations; N&W – Nöllenburg and Wolff (3 objectives); O&S – Oke & Siddiqui (2 objectives)

Method	Minimal Example		Dual-line Network		Four-line Network	
	Solutions generated per run	Execution time per solution (s)	Solutions generated per run	Execution time per solution (s)	Solutions generated per run	Execution time per solution (s)
N&W–WM$_3$	1	0.778	1	1.069	1	1.767
O&S–WM$_2$	1	0.661	1	0.913	1	1.188
O&S–AUGMECON2	2	1.145	3	0.810	5	0.682

2.6 Evaluation on existing networks: two case studies

Our goal for improving the performance of this model is to increase its accessibility and scalability, such that it can be effectively applied over a broad range of situations. We therefore apply our method to the Vienna Underground network in Vienna, Austria, and to a cancer pathway map [69].

2.6.1 Vienna Metro

The Vienna Metro network has 5 lines, 90 edges, 84 vertices and 8 faces. Figure 2.16 shows the geographic layout and the official schematic version of the metro.

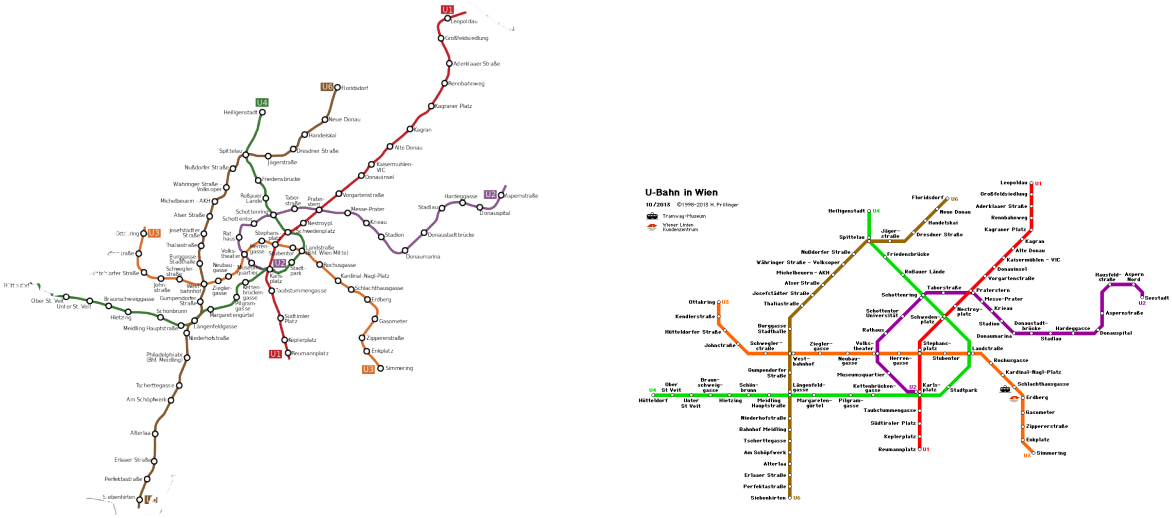

(a) Vienna Metro (geographic layout) **(b)** Vienna Metro (official layout) [153]

Figure 2.16 Geographic and official layouts of the Vienna Metro network

First, we used the weighting method based on our improvements (biobjective mixed binary) to find a single solution to the network. We compared our results to those obtained via Nöllenburg and Wolff's triobjective mixed integer model, also implemented within our framework. One set of constraints that generates the most variables in this model is the edge spacing constraint group. Especially in metro networks, these constraints are mostly relevant when there are pendant (trailing)

edges on the external face of a graph. They are also important for preventing interior faces from being too small in a final solution. In this example, we are able to solve the network using the weighting method without even calling upon the edge spacing constraints. In this case, Nöllenburg and Wolff's model execution time is 1.7 times as long as ours. When we enforce the edge spacing constraints, however, Nöllenburg and Wolff's model takes 14 times as long as ours to solve to optimality (Table 2.6).

Table 2.6 Execution times for the Vienna Metro problem, with $\lambda_{\text{bend}} : \lambda_{\text{shift}} = 7 : 3$; N&W – Nöllenburg and Wolff (3 objectives); O&S – Oke & Siddiqui (2 objectives)

Method	Vienna (no edge spacing constraints)		Vienna (with edge spacing constraints)	
	Objective cost $\{C_{\text{bend}}, C_{\text{shift}}\}$	Execution time per solution (s)	Objective cost $\{C_{\text{bend}}, C_{\text{shift}}\}$	Execution time per solution (m:s)
N&W–WM$_3$	$\{16, 25\}$	10.7	$\{16, 25\}$	28:41
O&S–WM$_2$	$\{13, 28\}$	6.2	$\{13, 28\}$	2:39

For these tests, we used the weighting ratio $\lambda_{\text{bend}} : \lambda_{\text{shift}} = 7 : 3$. In every case, the weights add up to 1. Thus, in O&S–WM$_2$, $\lambda_{\text{bend}} = 0.7$ and $\lambda_{\text{shift}} = 0.3$. We point out that in the N&W–WM$_3$ case, we have an additional objective function—total edge length—to consider. So, in order to maintain the same bend-shift weighting ratio for the sake of comparison, we use $\lambda_{\text{length}} = 0.2$, while $\lambda_{\text{bend}} = 0.56$ and $\lambda_{\text{shift}} = 0.24$. The solutions obtained via the implementations O&S–WM$_2$ and N&W–WM$_3$ are fairly identical, but that of O&S–WM$_2$ (Figure 2.17a) appears to be more spatially optimized, since we do not minimize the sum of edge lengths. The triobjective Nöllenburg and Wolff implementation, N&W–WM$_3$, generates solutions that lie on a three-dimensional Pareto frontier, which explains why its solution $\{16, 25\}$ is not optimal in O&S–WM$_2$ or O&S–AUGMECON2. With this particular weighting ratio, dispensing with the edge spacing constraints does not affect the solutions for both O&S–WM$_2$ and N&W–WM$_3$ (Figure 2.17). This implies that edge spacing constraints may not always be required. However, if they are not enforced, certain solutions may feature crossing violations

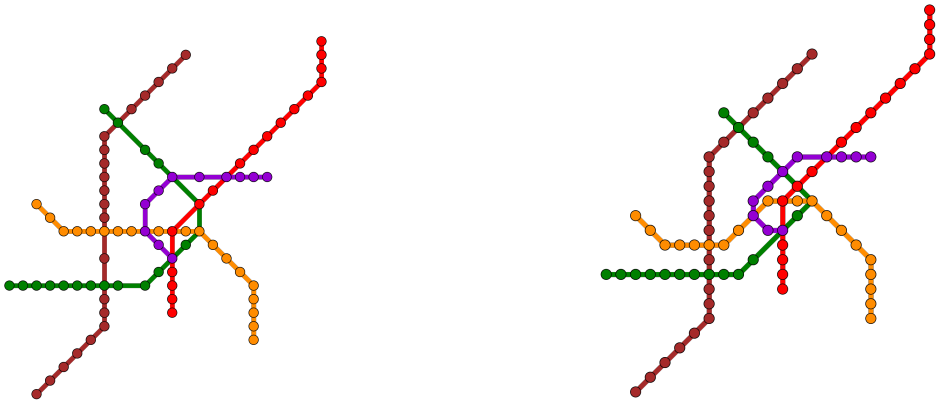

(a) O&S–WM$_2$; $\{C_{\text{bend}}, C_{\text{shift}}\} = \{13, 28\}$ **(b)** N&W–WM$_3$; $\{C_{\text{bend}}, C_{\text{shift}}, C_{\text{length}}\} = \{16, 25, 186\}$

Figure 2.17 Vienna solutions computed via the weighting approach; $\lambda_{\text{bend}} : \lambda_{\text{shift}} = 7 : 3$. N&W – Nöllenburg and Wolff (3 objectives); O&S – Oke & Siddiqui (2 objectives)

that alter the face structure of the graph. We observe this for a bend-shift weighting ratio of $1 : 1$ in O&S–WM$_2$. There is a clear edge violation between pendant edges on the green and orange lines in the solution generated (Figure 2.18). The edge spacing

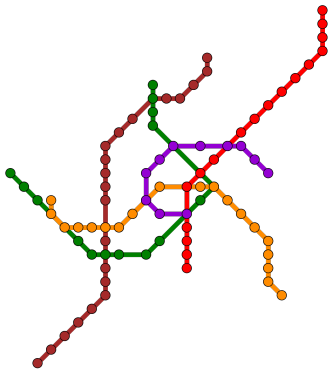

Figure 2.18 Edge crossing violation (O&S–WM$_2$). $\lambda_{\text{bend}} : \lambda_{\text{shift}} = 1 : 1$ and $\{C_{\text{bend}}, C_{\text{shift}}\} = \{24, 13\}$

constraints must therefore be consistently enforced, especially for O&S–AUGMECON2, as we cannot always predict where they will be redundant. For the Vienna network,

however, the edge spacing constraints can be restricted to pairs of nonadjacent pendant edges on the external face.

We then solve the Vienna network via O&S–AUGMECON2. The Pareto frontier obtained is shown in Figure 2.20. To generate the complete Pareto set, we use integer-spaced grid points spanning the range of the shift objective. In this case, the number of grid points is given by

$$n_g = \max\{C_{\text{shift}}\} - \min\{C_{\text{shift}}\} + 1 = 38 - 1 + 1 = 38 \tag{2.37}$$

There are 27 Pareto points in the complete set, five of which are displayed in Figure 2.19. A single run took 70 minutes to execute (an average of 2:36 minutes per solution), using four threads in CPLEX. Eight of these solutions were found to be supported, that is, they could be found using the weighting method. We checked this first by manually varying the weights in steps of 0.1. We then used the Gather-Update-Solve-Scatter (GUSS) extension in GAMS [91] to solve 39 scenarios generated from sequential weighting combinations. The augmented ε-constraint method was therefore indispensable in obtaining the other 19 unsupported Pareto optimal solutions.

In this case of the Vienna network, the decision-maker might determine that any existing pool of efficient solutions intermediate between (D) and (F) are likely to be very similar, but if such solutions (high number of bends but similar to original layout) are of interest, then more grid points could then be chosen. Furthermore, the AUGMECON2 algorithm can be modified to have unequal grid intervals, so that more solutions can be generated within the area of interest. The initial layout of the Pareto set and the corresponding solutions enable the decision-maker to be more acquainted with the solution space, and further steps can be taken from there regarding the choice or discovery of a final satisfactory solution.

An important innovation Harry Beck introduced in his creation of the London

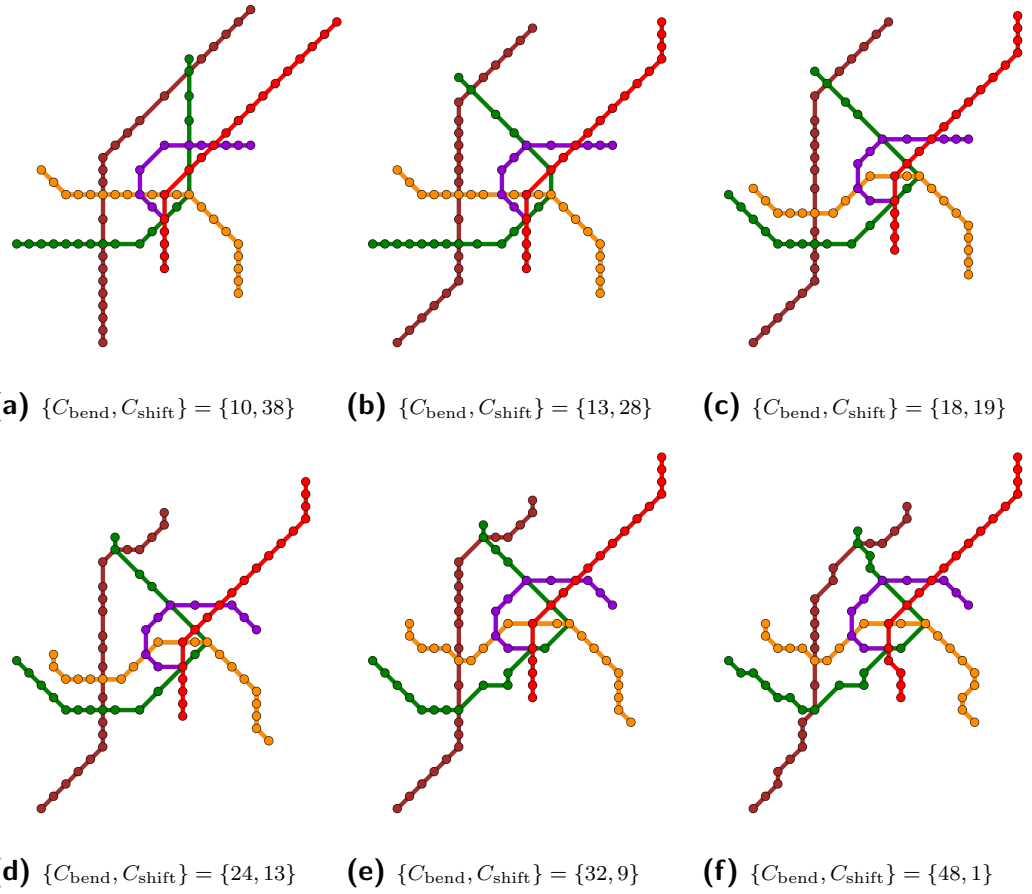

(a) $\{C_{\text{bend}}, C_{\text{shift}}\} = \{10, 38\}$ **(b)** $\{C_{\text{bend}}, C_{\text{shift}}\} = \{13, 28\}$ **(c)** $\{C_{\text{bend}}, C_{\text{shift}}\} = \{18, 19\}$

(d) $\{C_{\text{bend}}, C_{\text{shift}}\} = \{24, 13\}$ **(e)** $\{C_{\text{bend}}, C_{\text{shift}}\} = \{32, 9\}$ **(f)** $\{C_{\text{bend}}, C_{\text{shift}}\} = \{48, 1\}$

Figure 2.19 Pareto optimal points for the Vienna Underground network

Underground map [60] was the magnification of the central portion of a transit map, which tended to be denser with a higher concentration of tracks and lines. This central clustering is clearly visible in the geographically accurate map of the Vienna system (Figure 2.16a). Beck not only evened out distances between stations on his map but also increased the relative distances of central stations, creating the iconic "vacuum flask" shape that is a highlight of the London map (Figure 2.2). This type of distortion is perhaps more critical for transit networks, where interchanges tend to cluster at one or more central locations. We can correct for this in the Vienna implementation by doubling the minimum edge length $\ell_{\text{min}}(u, v)$ for those edges found in the smaller interior faces. At the same time, we decrease the maximum edge length $\ell_{\text{max}}(u, v)$

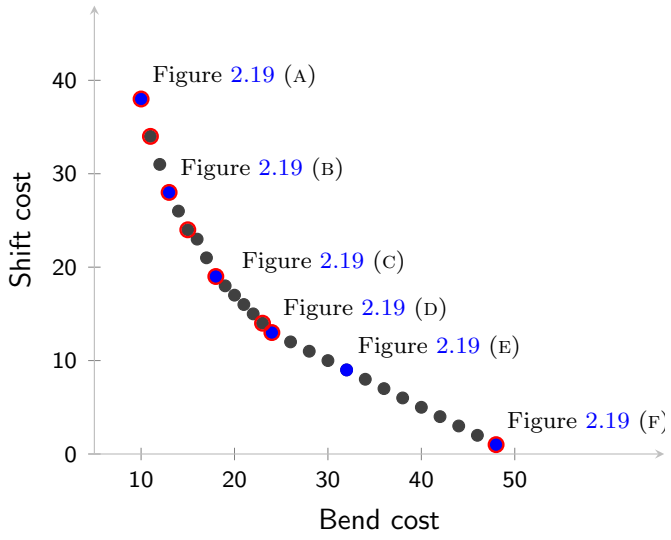

Figure 2.20 Pareto frontier for Vienna metro network (obtained via O&S–AUGMECON2). Points encircled in red are the supported solutions. Points in blue are shown in Figure 2.19.

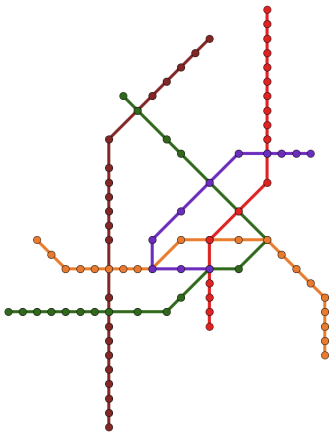

Figure 2.21 Vienna Pareto optimal point with central magnification emphasized; $\{C_{\text{bend}}, C_{\text{shift}}\} = \{17, 37\}$

constraint for the pendant (trailing) edges on the exterior face. These refinements ensure that the solution is spatially balanced with no visual overcrowding. They can be consistently applied in solving similar transit networks. The effects of this in our solution (Figure 2.19) may not be too evident, but we could always increase the bounds of these constraints for more desirable results, thereby creating other classes of solutions (Pareto frontiers). Figure 2.21 illustrates a solution we obtained

by properly addressing this issue. The edges in the four smallest faces have greater edge lengths than those on the external face.

2.6.2 Cancer pathway

Our second example is the "subway map of cancer pathways" developed by Hahn and Weinberg, and designed by Bentley [69] (Figure 2.22). While it is already a schematic map, we apply our method here to see if we can obtain comparable or better Pareto optimal points within our framework of requirements. Our implementation has 9 lines, 51 vertices, 56 edges and 6 faces.

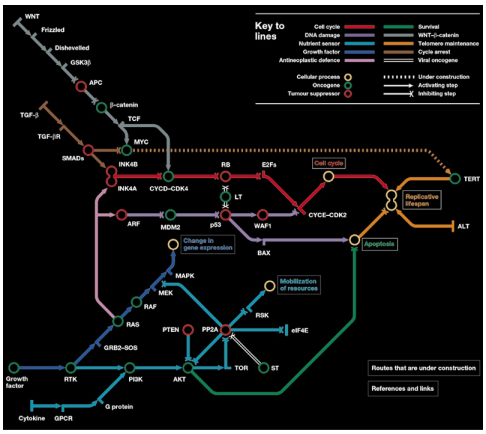

Figure 2.22 Subway map of cancer pathways Hahn and Weinberg [69]

Pathways, such as this one, may be challenging to model, as they tend to have more vertices with spanning edges than typical metro networks. The edge spacing constraints are essential here, as these also prevent edge crossings. In solving the Vienna metro network, we restricted the edge spacing constraints to the pendant edges on the external face. In this example, however, there are pendant edges on the internal faces, as well. Thus, we extend the application of the constraints to non-incident pairs of pendant and non-pendant edges in the same faces.

Using the AUGMECON2 implementation, we obtain the complete Pareto set in 165 minutes. A few selected solutions are shown in Figure 2.23. Unsurprisingly,

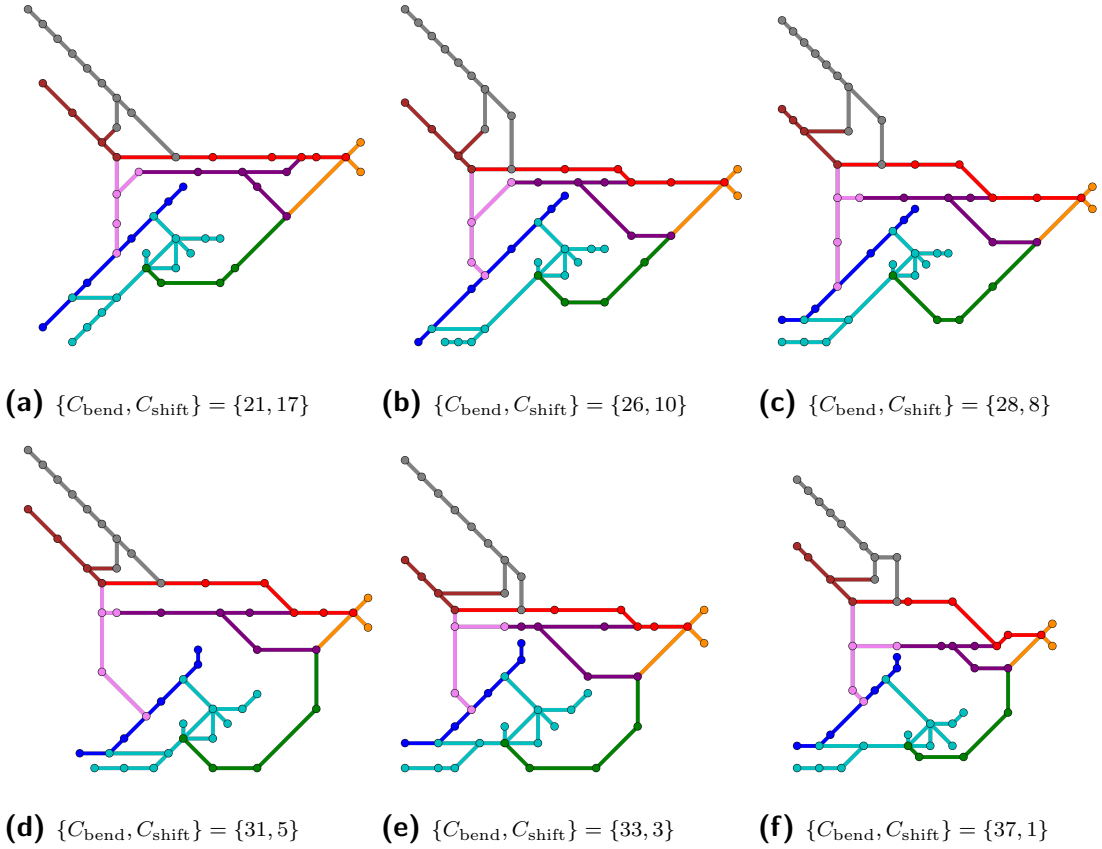

(a) $\{C_{\text{bend}}, C_{\text{shift}}\} = \{21, 17\}$ **(b)** $\{C_{\text{bend}}, C_{\text{shift}}\} = \{26, 10\}$ **(c)** $\{C_{\text{bend}}, C_{\text{shift}}\} = \{28, 8\}$

(d) $\{C_{\text{bend}}, C_{\text{shift}}\} = \{31, 5\}$ **(e)** $\{C_{\text{bend}}, C_{\text{shift}}\} = \{33, 3\}$ **(f)** $\{C_{\text{bend}}, C_{\text{shift}}\} = \{37, 1\}$

Figure 2.23 Selected Pareto optimal points for the cancer pathway

one of the Pareto points (solution (D) in Figure 2.23) is nearly identical to the input embedding (Figure 2.22), which indicates how well-designed the cancer map is. However, we now have a range of elegant solutions from which to choose. The complete Pareto frontier is shown in Figure 2.24, and it consists of 15 points. We note that all the pendant edges have an upper bound of length 4, while all other edges have a maximum length of 8 imposed. Changing any of these bounds would produce a Pareto set with a different range of solutions, which could also be explored.

As we have seen from the examples of the Vienna Underground and the Hahn and Weinberg cancer pathway, metro maps do not always share similar properties with other pathway or network representations. Depending on the nature of the application, certain considerations (for instance, edge length or edge spacing restrictions)

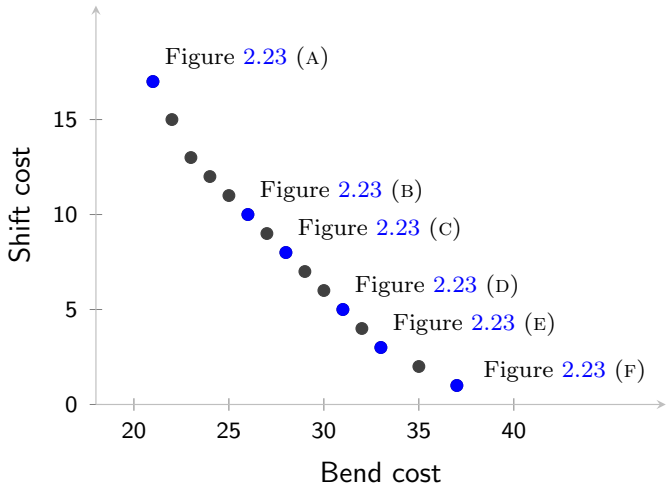

Figure 2.24 Pareto frontier for Hahn and Weinberg cancer pathway (obtained via O&S–AUGMECON2). Solutions corresponding to the points in blue are shown in Figure 2.23.

may be more relevant. To facilitate the versatile deployment of this model, a framework must be developed for standardizing constraints to accommodate all possible design specifications. We can fine-tune our implementation to eliminate or reduce programming inefficiencies and lower execution times.

2.7 Summary and avenues for further research

We have shown in this chapter that relaxing integrality constraints, simplifying the problem to two objective functions, and reformulating certain equations leads to obtaining more Pareto optimal solutions to the schematic map drawing problem than current methods. Moreover, the computational time to obtain solutions is greatly reduced. We built on Nöllenburg and Wolff's implementation and simplified their model to a biobjective mixed binary linear problem and obtained Pareto optimal solutions much quicker. We developed three hypothetical examples to demonstrate our results. We were also able to test our implementation on two real-world examples. A new development we have shown is the ability to compute a complete Pareto set for

a schematic drawing problem, using Mavrotas and Florios' augmented ε-constraint method (AUGMECON2). This implementation allows for multiple supported and unsupported efficient solutions to be generated in a single run, enabling decision-makers to quickly evaluate potential candidates for schematic mapping solutions. We have also demonstrated that AUGMECON2 is preferred to the weighting method used by Nöllenburg and Wolff, as it guarantees finding all Pareto optimal solutions, including those that are nonextreme and unsupported.

A problem that remains open is a formal theoretical proof in support of the conjecture that integer optimal solutions can be found without enforcing coordinate integer constraints in this framework. Also up for future consideration is the exploration of alternatives to the big-M formulation. Various methods have been developed to model disjunctivity, which features in the octilinearity and edge spacing constraints of this model. Care must be taken in determining the size of M, and in our implementation, it is equivalent to the maximum total edge length (Equation (5.8)). Thus far, this has worked well, but we would like to implement and test the merits of the Reformulation Linearization Technique (RLT). Khurana et al. [93] have demonstrated success in applying RLT to mixed 0-1 programs. We expect that implementing this would significantly increase performance in our case. Also in consideration is an attempt to reformulate this problem as a mathematical program with equilibrium constraints (MPEC). Siddiqui and Gabriel [169] developed a method that employs Schur's decomposition using type-1 special-ordered set (SOS1) variables to provide global optima for MPECs. The challenge in this case, would be devising ways to remodel the schematic requirements as complementarity constraints. If we succeed in doing this, we will then compare the performance of Siddiqui and Gabriel's method with the numerical relaxation approach for MPECs formulated by Steffensen and Ulbrich [176]. Also, Vincent et al. [199] have recently refined a branch-and-bound algorithm (initially developed by Mavrotas and Diakoulaki [111]) for solving our spe-

cific program class (mixed binary linear programs). We hope to adapt this to the map drawing problem as well. We note that we have not addressed the issue of non-uniqueness in this implementation. Alternate solutions for a given objective value could be found by initializing the program from different starting points. Also, we could explore the fixing of one or more nodes to tighten the feasible space. Further investigation would be necessary for a proper resolution and characterization of the impact of non-uniqueness on our solutions.

We hope to continue efforts to improve the performance of this algorithm and expand the applications of automatic schematic mapping. A few new rules may have to be developed along the way depending on the network in question. For example, bicycle and bus networks have slightly different specifications compared to those of urban rail. (We highlight the Edinburgh bicycle network example in Subsection 2.7.1). Ultimately, we are interested in creating a dynamic user-friendly optimization tool that would be accessible for professional and public use in a wide variety of situations, and also able to produce solutions that address relevant considerations to facilitate the decision-making process. In order to fully realize this, we could leverage the existing body of research in human and social interactions with maps to design experiments that would seek to measure the effectiveness of a schematic map in various contexts. Nöllenburg and Wolff [134] described their approach to including the human element in their schematic map solutions. They created a survey tool to test the satisfaction of human subjects on various maps in order to determine which factors were of importance in a schematic solution. This experimental concept could be further expanded and then integrated into our algorithm. We could thereby develop a method for determining the relevant portions of the Pareto space to discover not only the best efficient solutions, but also those that would be of the greatest benefit to the users.

2.7.1 The Edinburgh Innertube Map

In 2006, Edinburgh based journalist Tom Allan got lost on bike ride through some of the city's forgotten pathways. Over the next few years, he conceived a plan for a system through which ridership could be encouraged by highlighting the network of cycle paths around the city, especially the lesser known ones created from defunct railway lines and towpaths. A schematic map would be the key to this. Allan, however, realized that user feedback would be critical to its success. An interactive website would therefore be an integral part of this project.

With the help of Mark Sydenham, a bicycle charity manager, and Martin Baillie, a graphic designer, the Innertube Map was born [2]. The design framework is based on the metro map metaphor as described in this chapter. The current version of the map is shown in Figure 2.25. Sydenham is credited for creating the layout and rules for the map, whileBaillie designed the final output. The nodes represent entry or departure points in each of the paths. The website [180] allows users to obtain more information about the various points on the map. Users can also share their stories and experiences. A blog provides news on events along various stops on the map. The feedback also informs updates to the Innertube. The entire system is a vibrant interface that further establishes the map's purpose as an accessibility tool to a network that might otherwise have remained underutilized. 70,000 print copies of the Innertube Map have also been reportedly distributed since 2011 [180], and the project appears to have been a success on all fronts.

With an automated design tool developed from the program described in this chapter, the Edinburgh experience could perhaps be replicated faster in other cities. Schematic mapping for bicycle networks will likely grow in demand as bicycles become increasingly popular for sustainable transit. As communities across the globe grapple with environmental issues, emission-free transport must receive greater consideration

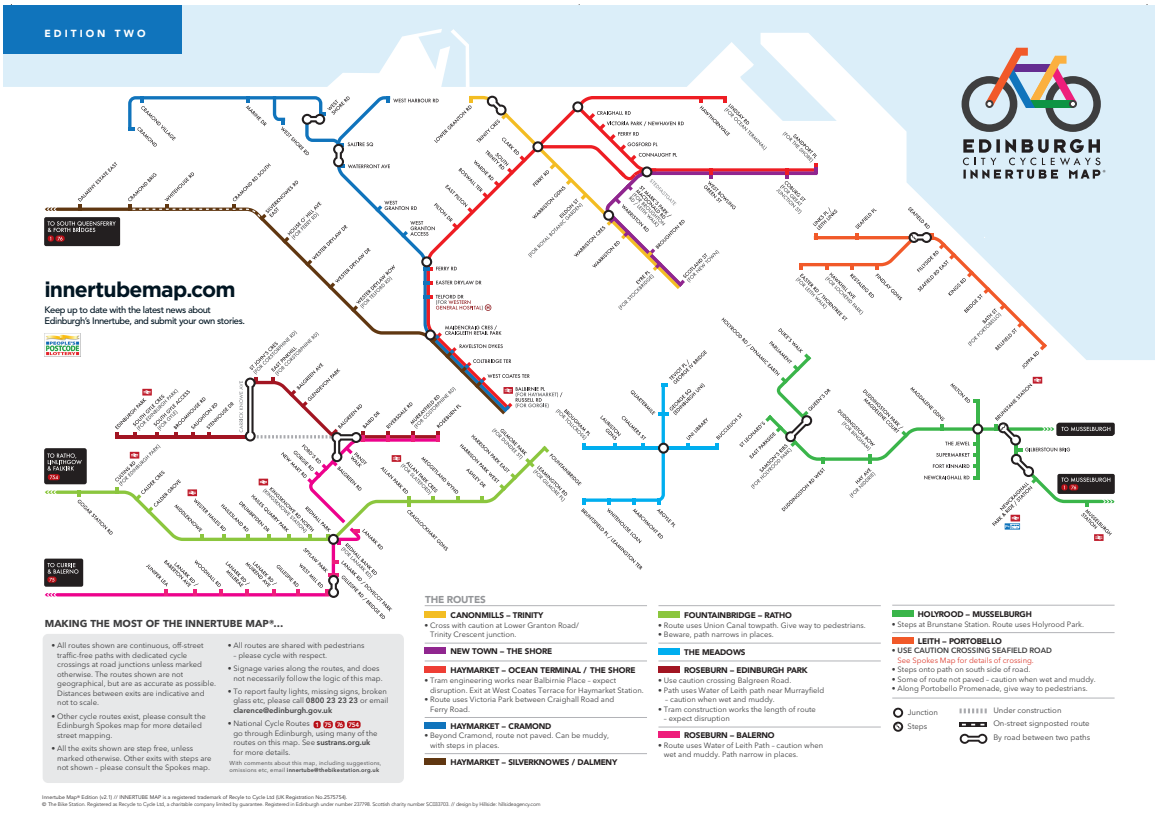

Figure 2.25 The Edinburgh Innertube Map of cycle paths. Each line (differentiated by color) represents a connected path. The vertices denote entry/exit points in the paths. [180]

in the planning of integrated transport systems. The next chapter describes the application of data mining methods in the discovery of patterns that will be fundamental to current and future efforts to improve the availability and usage of bicycles across the world, which could be an important element in the development emission-free transportation systems.

CHAPTER 3

Data mining for sustainable transit: bicycle ownership

3.1 Motivation

Bicycles have persisted as an accessible means of human-powered travel for more than 125 years, taking root in various parts of the world. Since the late 19th century, bicycles have also been regarded as a vehicle for social change, for instance, empowering women's emancipation [73]. The advent of paved roads in the United States is attributed in large part to the activism of cyclists who formed the Good Roads movement in the 1880s [156, 73].

In the past century, however, both developed and developing countries have undergone rapid transitions towards motorization, many of which have placed cycling at a disadvantage [163, 96]. At the same time, major shifts in population health trends have occurred. Infectious disease in infants are now less important than non-communicable diseases (NCDs) and adult injuries [123, 106]. NCDs and injuries now comprise 94% of all deaths in China, 65% in India, and 34% in sub-Saharan Africa [106]. The growth of motorization has led to a rise in injuries from road traffic crashes,

increasing vehicular air pollution, and declining physical activity [17]. Moreover, those living in densely populated and rapidly urbanizing areas receive far more exposure to vehicular air pollution. Given these circumstances, there is an urgent need to tackle the growth of NCDs and injuries globally. Collaborations between transportation scientists and engineers, urban planners, and public health researchers will be crucial in this regard, and these are already taking place [188, 152].

The adoption of bicycle-friendly policies by Denmark in the 1970s was effective in reducing traffic fatalities and managing energy-environment issues [51]. In the next several decades, as other areas followed suit, these measures were investigated and proven by researchers. The usage of bicycles was thus established as a virtuous cycle initiator with a number of positive feedback loops [99]. Notably, cycling as a mode of transportation both reduces vehicular atmospheric pollution and road traffic congestion [46]. Furthermore, cycling is important to the concept of a "livable city" [61], as it integrates easily with other modes of transit and can stimulate local businesses via the addition of new cycling routes [105]. From a public health perspective, cycling promotes wellness [138], and its benefits outweigh its risks [38, 158]. The more cyclists are present, the safer the roads become, in accordance with the "safety in numbers" hypothesis [87]. On a global scale, cycling as a form of zero-emissions transportation can help fight climate change [204, 13, 165].

Globally, there is ample information about motor vehicles, as nearly every country tracks vehicle registration—some for tax purposes—and global data are gathered by various agencies, including the International Road Federation, the World Bank (via World Development Indicators), the World Health Organization (Global Status Reports on Road Safety), among others. Bicycles, however, have never been systematically counted and presented in the peer-reviewed literature. We not only compile data on household bicycle availability, but we also apply statistical and data mining techniques to discover patterns and obtain new information regarding bicycle owner-

ship. The work described in the following sections of this chapter has been published in the Journal of Transport & Health [140]. An extension of this work is also currently under review in the Annals of Operations Research [141].

3.2 Methods

3.2.1 Data collection

We obtained data on percentage bicycle ownership (PBO) from national and international surveys conducted at various times from 1971–2012 in 150 countries. However, we only consider for analysis the years 1989–2012, as only four countries have data available prior to 1989. Our sources for household bicycle ownership data include the World Health Surveys [145], Demographic and Health Surveys [40], Malaria Indicator Surveys [39], Integrated Public Use Microdata Services [119], International Crime Victim Surveys [67], Multiple Indicator Cluster Surveys [86, 85], and the India National Census [82]. We also had data available from the Southern and Eastern Africa Consortium for Monitoring Educational Quality [173, 174], but we did not include these in our analyses, as the respondents were schoolchildren and not representative of the national populations. Table B.1 lists the surveys mined for our analyses, indicating the contribution of each source to the dataset. Figure 3.1 shows the number of datapoints obtained from each country, showing the density and geographical distribution of the survey data obtained. (Table B.1 contains a list of all the countries for which data were collected.) Table 3.2 summarizes the objectives and sampling methodologies of the contributing surveys, most of which were global in scope. All were nationally representative, employing probability sampling of census enumeration areas (EAs) or otherwise determined zones, except for the INC, which involved an actual count. The household bicycle ownership questions vary little. Based on these, the survey data are fairly comparable.

Table 3.1 Survey sources for bicycle ownership data and the number of countries and country-years available from each.

Survey source	Acronym	Years	Countries	Country-years
Demographic and Health Surveys [40]	DHS	1990-2011	68	169
Enquête Démographique et de Santé et à Indicateurs Multiples [83]	EDSM	2006	1	1
India National Census [82]	INC	2001, 2011	1	2
Integrated Public Use Microdata Services [119]	IPUMS	1990-2006, 08, 09	21	26
Integrated Survey on the Welfare of the Population [84]	IBEP	2008-2009	1	1
International Crime Victim Surveys [67]	ICVS	1989-2002	62	130
Malaria Indicator Surveys [39]	MIS	2006-2009	3	3
Multiple Indicator Cluster Surveys 4 [86]	MICS4	2010-2011	17	17
Multiple Indicator Cluster Surveys 3 [85]	MICS3	2005-2009	39	39
Study on Global Ageing and Adult Health [144]	SAGE	2007-2011	5	12
World Health Surveys [145]	WHS	2002	65	65

We also collected household population numbers for the country-years in our dataset where available. Our sources primarily included [119] and the United Nations [189, 191]. In cases where direct household numbers were unavailable for certain country-years, we used a simple heuristic to find an approximation from nearest values or multiply average household sizes and corresponding national population [206] totals. (Please refer to Section B.1 for more details on this process.)

3.2.2 Cluster analysis

The bicycle ownership data obtained[1] were sparse and time series varied considerably in length from one country to another. To find similarities in ownership across geographical regions, clustering presented itself as an effective pattern recognition tool [89]. Hierarchical or agglomerative clustering relies on a matrix of pairwise distances between vectors in the dataset, which were nontrivial to compute in our case due to their nonalignment. The number of clusters must also be specified.

First, we used the dynamic time warping algorithm [160, 62] to obtain distance alignments between countries. Using the goodness-of-fit test proposed by [116], we then found the best agglomerative clustering method, which produced the minimum

[1]The data and supporting code are available at ce.jhu.edu/sauleh/obls-gbu

Table 3.2 Comparison of survey methodologies. Data collection methods include: paper and pen interviews (PAPI), computer-assisted person interviews (CAPI), computer-assisted field editing (CAFE) and face-to-face interviews (F2F). Responses choices include: "yes" (Y), "no" (N), "do not know" (DNK), "unknown" (U) and "not in universe" (NIU). For SAGE and WHS, 50+ and 18+ indicate that only household members at those respective ages and above were sought as respondents.

Survey	**Purpose**	**Scope**	**Interview methods**	**Question**	**Response Choices**	**Question Type**	**Sampling**
DHS	Monitor or evaluate population, health, nutrition indicators	Global	PAPI, CAPI, CAFE	Does any member of this household own: A bicycle?	Y/N	Household Characteristics	Clusters/ census enumeration areas; respondents: women 15-49 yrs, men 15-59 yrs
ICVS	Crime and victimization analysis; perceptions of safety and security	EU, Global	CATI, F2F	bicycle ownership	Y/N/ DNK	Screening	Random sampling and selection
INC	Census	India	F2F	Bicycle	N/A	Household asset availability	None
IPUMS	National censuses	Global	Various	Various	Y/N/ U/NIU	N/A	Probability sampling
MICS3, MICS4	MDG monitoring; wellbeing of women, children	Africa, Asia, South America	F2F	Does any member of your household own: A bicycle?	Y/N	Household Characteristics	Probability sampling of EAs
MIS	Track malaria intervention impact	At-risk malaria populations	F2F	Does any member of this household own: A bicycle?	Y/N	Household Characteristics	Probability sampling of EAs
SAGE	Older adult population health	Global	CAPI, CATI, F2F, PAPI	Does your household or anyone in your household have...? A bicycle?	Y/N	Permanent Income Indicators (Assets)	Used existing national framework; 50+ households targeted
WHS	Monitor critical national health outcomes	Global	F2F, PAPI	Does anyone in your household have: A bicycle?	Y/N	Permanent Income Indicators	Probability sampling by strata; 18+ private households

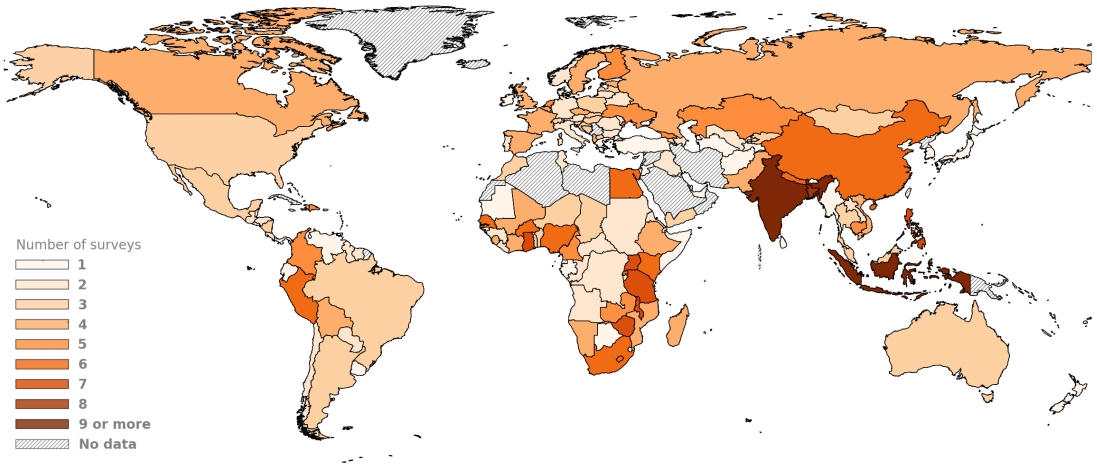

Figure 3.1 World map indicating the number of surveys (datapoints) obtained in each of the 150 countries for which household bicycle ownership data were available. (Only one datapoint was available for South Sudan, and that is accounted for by Sudan's tally of 2 datapoints for the purposes of this map.)

separation between the original distance matrix and that obtained from the tree. Of four possibilities, the unweighted pair-group method with arithmetic means (UPGMA) emerged as the best fit. The gap statistic and test [185] determined the optimal number of clusters for the data. We performed ordinary least squares regression on the PBO in each cluster but found no significant temporal dependencies on bicycle ownership. Thus, we used the rolling mean with five-year windows to observe possible ownership trends. From household estimates for all the country-years, we were able to determine a lower bound on the number of available bicycles in the world.

3.2.3 Dynamic time warping alignment

The dynamic time warping (DTW) algorithm was first introduced by [15]. Sakoe and Chiba [160] notably used it as a tool for aligning speech patterns for recognition. In this case, it provides a means of calculating the separation between our nonaligned points for each country, as the years do not all coincide. We use the package developed by Giorgino [62] to execute the DTW algorithm in our program. A brief explanation

is provided below.

Consider two time series A and B (a test and a reference) with P and Q observations, respectively. Elements a_i and b_j reside in series A and B, respectively. DTW computes a warping curve $\phi(k)$ with M elements, each mapped from A and B. Thus,

$$\phi(k) = (\phi_a(k), \phi_b(k)) \tag{3.1}$$

$$\phi_a(k) \in \{1, ..., P\} \tag{3.2}$$

$$\phi_b(k) \in \{1, ..., Q\} \tag{3.3}$$

The optimal deformation (alignment) minimizes the "average accumulated distortion" d_ϕ between the warped series.[2] The deformation D is given as

$$D(A, B) = \min_{\phi} d_\phi(A, B) \tag{3.4}$$

where the distortion d_ϕ is

$$d_\phi(A, B) = \frac{1}{C_\phi} \sum_{k=1}^{M} d(\phi_a(k), \phi_b(k)) c_\phi(k), \tag{3.5}$$

with $c_\phi(k)$ the weighting coefficient in each step and C_ϕ the normalization constant. The warping functions ϕ_a and ϕ_b are constrained for monotonicity, continuity and endpoint matching.

The output of DTW is robust, but we are only interested in obtaining the minimum cumulative distance for each possible pair of time series in our data. The result, which we call the dissimilarity matrix DM, is of size 150×150. However, since it is symmetric, there are only 11 325 unique entries, including a zero diagonal. We normalize the dissimilarity matrix D by dividing all its elements by the maximum

[2]The function d_ϕ may not be strictly convex and, as such, this would give rise to the possibility of multiple solutions to the optimal deformation. However, the since the value of the deformation is the only item of interest, the impact of non-uniqueness in this instance has not been further explored.

value element.

3.2.4 Finding the clustering method of best fit

There are several well-defined hierarchical or agglomerative clustering methods, each using a different distance algorithm to determine how new clusters are added to the forest. We perform the clustering procedure using four methods, namely: method of complete linkages, method of single linkages, unweighted pair group method with arithmetic means (UPGMA), weighted pair-group method with arithmetic means (WPGMA).

Using the fitness measure defined by [116] (who showed that their measure was superior to the established cophenetic correlation coefficient measure), we find that the UPGMA method gives the best fit clustering. The measure in question is the greatest singular value of difference between the original distance matrix D and the ultrametric matrix U (reordered distance matrix based on the clustering method).

A threshold for λ can also be estimated [116]:

$$\lambda = ||D - U||_2 \leq \theta = 2\sigma\sqrt{N}, \tag{3.6}$$

where σ^2 is the sum of the variances of D and U. A λ value less than the threshold indicates U is reasonably close to D. For all four methods, $\lambda > \theta$ (Table 3.3). This

Table 3.3 Goodness-of-fit test for hierarchical/agglomerative clustering methods

Method	λ	θ	λ/θ
Single linkage	2723.7	347.8	7.83
Complete linkage	4551.8	759.7	5.99
UPGMA	**883.2**	**423.1**	**2.09**
WPGMA	966.1	434.7	2.22

is not surprising considering the sparsity of our data. However, we observe that the method that also minimizes the λ/θ ratio is the best fit, which in this case is UPGMA.

Table 3.4 lists the countries in each of the four clusters found using the unweighted pair-group method. The corresponding dendrogram is shown in Figure 3.2.

Table 3.4 Countries in the four groups determined by clustering with UPGMA.

Group 1

ISO	Country
AUT	Austria
BFA	Burkina Faso
DNK	Denmark
FIN	Finland
DEU	Germany
NLD	Netherlands
NOR	Norway
SVN	Slovenia
SWE	Sweden

Group 2

ISO	Country
ARG	Argentina
AUS	Australia
BEL	Belgium
BLZ	Belize
BRA	Brazil
KHM	Cambodia
CAN	Canada
CHN	China
CRI	Costa Rica
CZE	Czech Republic
ECU	Ecuador
EST	Estonia
FRA	France
GUY	Guyana
IDN	Indonesia
IRL	Ireland
ITA	Italy
JPN	Japan
LAO	Laos
LUX	Luxembourg
MKD	Macedonia
MUS	Mauritius
MMR	Myanmar
NZL	New Zealand
POL	Poland
ZZZX	Serbia
SVK	Slovakia
CHE	Switzerland
THA	Thailand
TTO	Trinidad and Tobago
ARE	United Arab Emirates
USA	United States
URY	Uruguay
VNM	Vietnam

Group 3

ISO	Country
AFG	Afghanistan
ALB	Albania
BLR	Belarus
BEN	Benin
BOL	Bolivia
BIH	Bosnia and Herzegovina
CHL	Chile
COL	Colombia
CIV	Cote d'Ivoire
HRV	Croatia
GMB	Gambia
GRC	Greece
GNB	Guinea-Bissau
HND	Honduras
HUN	Hungary
IND	India
ISR	Israel
LVA	Latvia
LTU	Lithuania
MWI	Malawi
MYS	Malaysia
MDV	Maldives
MLI	Mali
MLT	Malta
MEX	Mexico
MNE	Montenegro
PAK	Pakistan
PAN	Panama
PRY	Paraguay
PRT	Portugal
KOR	Republic of Korea
MDA	Republic of Moldova
RUS	Russia
ESP	Spain
LKA	Sri Lanka
SUR	Suriname
TZA	Tanzania
TGO	Togo
TUN	Tunisia
TUR	Turkey
UGA	Uganda
UKR	Ukraine
GBR	United Kingdom
VEN	Venezuela
ZMB	Zambia

Group 4

ISO	Country
AGO	Angola
ARM	Armenia
AZE	Azerbaijan
BGD	Bangladesh
BTN	Bhutan
BWA	Botswana
BGR	Bulgaria
BDI	Burundi
CMR	Cameroon
CAF	Central African Republic
TCD	Chad
COM	Comoros
COG	Congo
COD	Congo DRC
DJI	Djibouti
DOM	Dominican Republic
EGY	Egypt
ERI	Eritrea
ETH	Ethiopia
GAB	Gabon
GEO	Georgia
GHA	Ghana
GTM	Guatemala
GIN	Guinea
HTI	Haiti
IRQ	Iraq
JOR	Jordan
KAZ	Kazakhstan
KEN	Kenya
KGZ	Kyrgyzstan
LBN	Lebanon
LSO	Lesotho
LBR	Liberia
MDG	Madagascar
MRT	Mauritania
MNG	Mongolia
MAR	Morocco
MOZ	Mozambique
NAM	Namibia
NPL	Nepal
NIC	Nicaragua
NER	Niger
NGA	Nigeria
PER	Peru
PHL	Philippines
ROM	Romania
RWA	Rwanda
STP	Sao Tome and Principe
SEN	Senegal
SLE	Sierra Leone
SOM	Somalia
ZAF	South Africa
SSD	South Sudan
SDN	Sudan
SWZ	Swaziland
TJK	Tajikistan
TLS	Timor-Leste
TKM	Turkmenistan
UZB	Uzbekistan
VUT	Vanuatu
YEM	Yemen
ZWE	Zimbabwe

3.2.5 The gap test

While there are rules of thumb (involving root functions) for finding the number of clusters in a dataset, various methods have been developed to find the optimal group

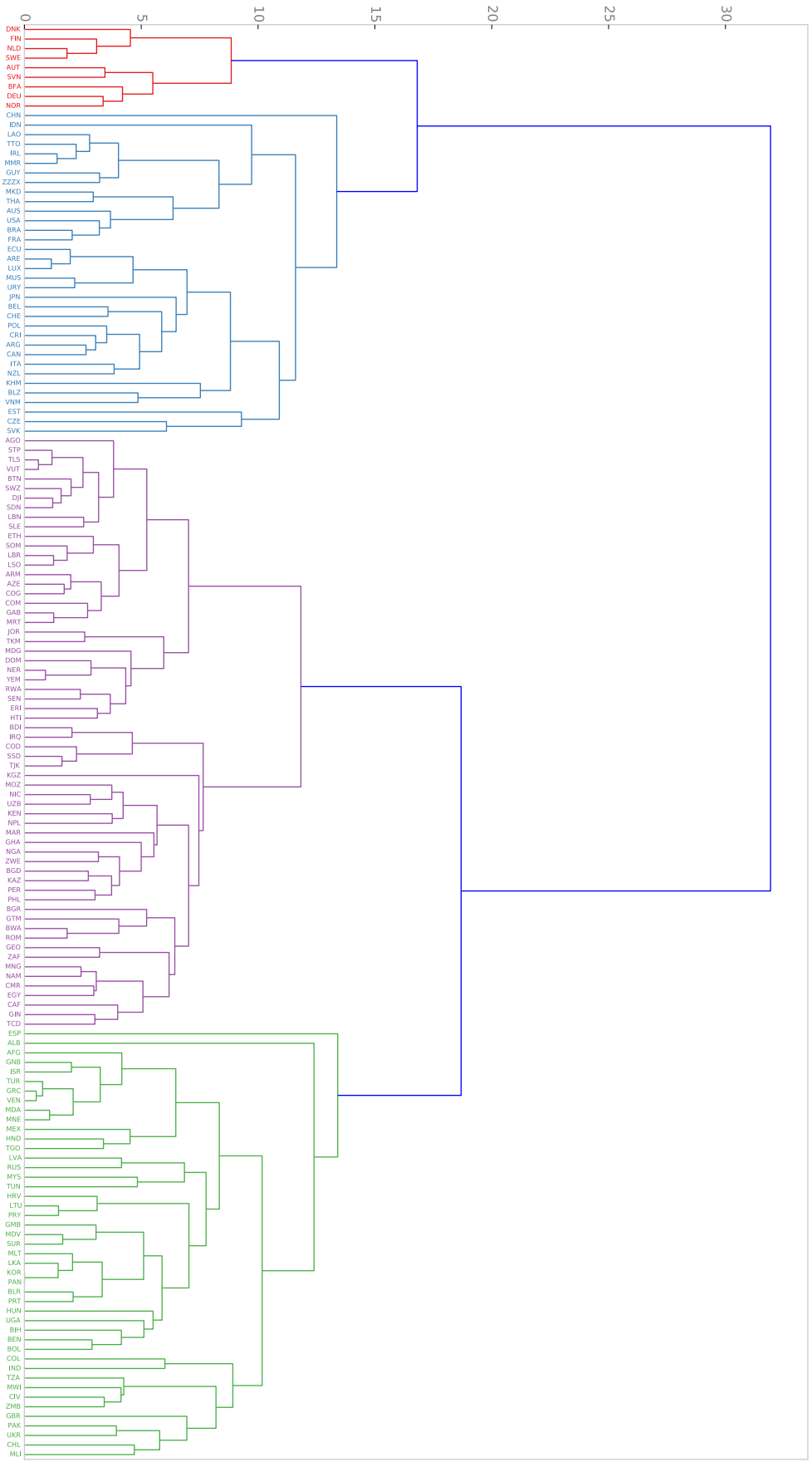

Figure 3.2 Dendrogram of UPGMA clustering

number based on the structure of the dataset. We use a quantity referred to as the gap statistic [185] to find the optimal number of clusters. The gap statistic is defined as

$$\text{Gap}_n(k) = E_n^*\{\log(W_k)\} - \log(W_k), \tag{3.7}$$

where W_k is the within-cluster sum of pair-wise distances. The expected value $E_n^*\{\log(W_k)\}$ is determined by a Monte Carlo simulation of several samples of the dissimilarity matrix (obtained using a uniform distribution), from which $\log(W_k^*)$ is the calculated. If we let B be the number of Monte Carlo samples generated, then the gap statistic can be redefined as

$$\text{Gap}_n(k) = \frac{1}{B}\sum_b \log(W_{kb}^*) - \log(W_k) \tag{3.8}$$

We define a simulation error term ε_k such that

$$\varepsilon_k = \text{sd}_k\sqrt{\left(1 + \frac{1}{B}\right)}, \tag{3.9}$$

where sd_k is the standard deviation of the reference datasets.

$$\text{sd}_k = \sqrt{\frac{1}{B}\sum_b \left\{\log(W_{kb}^*) - \frac{1}{B}\sum_b \log(W_{kb}^*)\right\}^2} \tag{3.10}$$

The optimal number of clusters $\hat{k}$ is chosen as the smallest k such that

$$\text{Gap}(k) \geq \text{Gap}(k+1) - \varepsilon_{k+1} \tag{3.11}$$

The gap statistic algorithm can be briefly described as follows:

(1) Using any given clustering method (in our case, the best-fit agglomerative method) and varying the number of clusters k from 1 through K, find within-

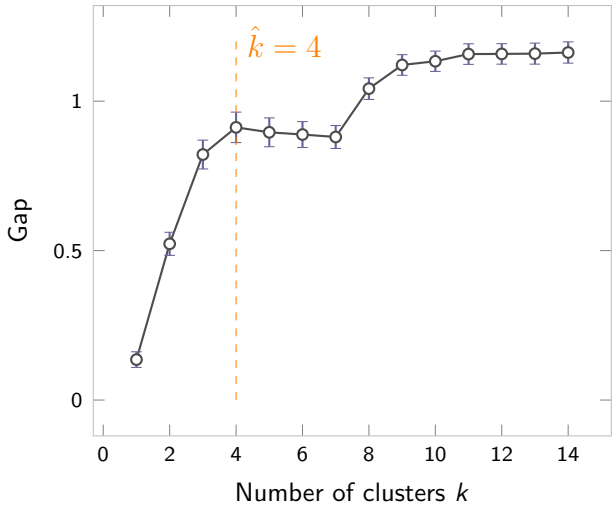

Figure 3.3 Gap curve; optimal cluster number $\hat{k} = 4$, chosen as smallest local maximum

cluster sum of squares W_k for the dissimilarity matrix

(2) Assume a uniform distribution and produce B instances of the dissimilarity matrix. Again, using the method of choice, we cluster each of these datasets, in each case finding W_{kb} for $b = 1, ..., B$ and $k = 1, ..., K$.

(3) Compute the gap estimate

$$\text{Gap}_n(k) = \frac{1}{B}\sum_b \log(W^*_{kb}) - \log(W_k) \tag{3.12}$$

(4) Find the simulation error term

$$\varepsilon_k = \sqrt{\frac{1}{B}\sum_b \left\{\log(W^*_{kb}) - \frac{1}{B}\sum_b \log(W^*_{kb})\right\}^2 \left(1 + \frac{1}{B}\right)}, \tag{3.13}$$

(5) Choose the number of clusters $\hat{k}$ such that

$$\hat{k} = \arg\min_k \text{Gap}(k) \quad \text{subject to} \quad \text{Gap}(k) \geq \text{Gap}(k+1) - \varepsilon_{k+1} \tag{3.14}$$

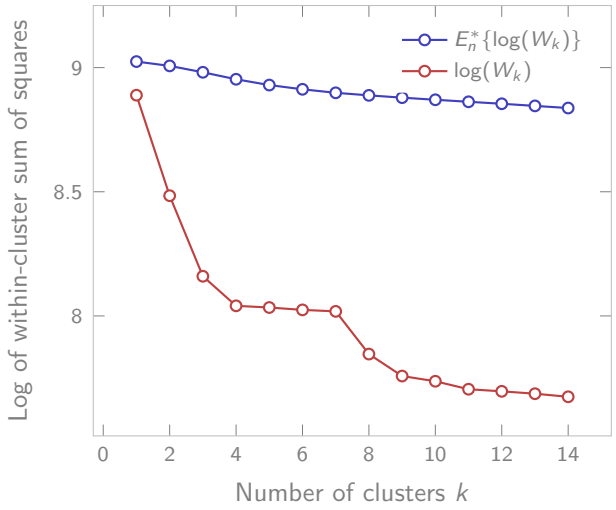

Figure 3.4 The observed and expected values $E_n^*(\,)$ of $\log(W_k)$, where W_k is the within-cluster sum of squares for k clusters. $\log(W_k)$ falls rapidly for $k < \hat{k}$ and less so for $k > \hat{k}$. Given the gap statistic $\text{Gap}(k)$ and the test value $\text{Gap}(k+1) - \varepsilon_{k+1}$, we consider cluster numbers at which the gap statistic is greater than the test value. Then we choose the smallest value of k at which this happens. In this case, the k value of interest is 4.

We choose $B = 1000$ for our dataset and obtain the gap curve shown in Figure 3.3. An "elbow heuristic" suggests $\hat{k} = 4$. But the final step in the algorithm formalizes this choice, as shown in Figure 3.4.

Further detail on data collection and a table of the post-processed data (Table B.3) are provided in Appendix B, which also includes percentage bicycle ownership trend plots for each of the 150 countries analyzed (Figure B.1).

3.3 Results

Household bicycle ownership rates were compiled for 150 countries from survey data. There were wide variations in bicycle ownership across different countries. In 2010, for example, Burkina Faso had a high household percentage bike ownership (PBO) of 84.2%, while Armenia had a low value of 4%. Even within the same region, there can be wide disparities. For instance, Ethiopia had a PBO of 2.3% in 2011, while

Uganda (also in East Africa) had a PBO of 37.1%, about 12 times greater. Temporal variations at the country level can also be substantial. China, perhaps, exhibits the most dramatic variation here. In 1992, China had a PBO of 97.2%, indicating that there was at least one bicycle available in almost every household. This statistic had dropped (by nearly half) to 48.7% by the year 2007 but then rose to 63.2% (an increase of about 30%) in 2009. Figure B.1 shows bicycle ownership trends for each of the countries in this study.

Figure 3.5 Bicycle ownership trends (1989–2012) for the four groups determined by clustering analyses. In each plot, the thick line represents the rolling mean (in a five-year window) of the population-weighted annual median bicycle ownership (gray points; the thin lines are the individual time series for the member countries).

In spite of this variation in bicycle ownership among the 150 countries, we were able to identify four distinct ownership levels using cluster analysis methods. Groups

1, 2, 3, and 4 had an average weighted PBO of 81%, 60%, 40%, and 20%, respectively. Group 1 comprises the countries with the highest PBO values (Figure 3.5A). There are only 9 in this group: the Scandinavian countries, the Netherlands, Germany, Austria, Slovenia (all in Europe), and Burkina Faso in West Africa. There are 34 countries in Group 2 (Figure 3.5B). They include, notably, USA, Canada, Brazil, Argentina, Uruguay, China, Australia, New Zealand and several European nations (e.g. France, Ireland, Italy, Luxembourg and Poland). Group 3 includes Russia and parts of Eastern Europe, the United Kingdom, four nations in the African Rift Valley system (Malawi, Tanzania, Uganda and Zambia) and five in West Africa (four of which are border states to Burkina Faso), the Indian subcontinent, Maritime Southeast Asia, Mexico, Chile and other South American countries, and Panama and Nicaragua in Central America (Figure 3.5C). The lowest PBOs are to be found in most West, Central, and North African nations, as well as the Middle East and Central Asia. These make up Group 4, (Figure 3.5D). There are 45 countries in Group 3 and 62 in Group 4.

The world map (Figure 3.6) enables us to visually compare countries within their geographical region. We clearly see that Burkina Faso is an outlier in the entire African continent. Peru and the Philippines also stand out as the only Group 4 countries in South America and Southeast Asia, respectively.

From 1989 through 2012, the global household-weighted PBO averaged 42% (Figure 3.7A). The median PBO was weighted by the number of households available for each year analyzed. India and China together account for over a third of the world's population [20], and on average, they make up close to a quarter of the household population analyzed in this study. We therefore plot the household-weighted median PBO for these two nations separately (Figure 3.7B). The rest of the world accounts for an average PBO of 37% (Figure 3.7C).

Finally, we determine a conservative lower bound on the number of bicycles cur-

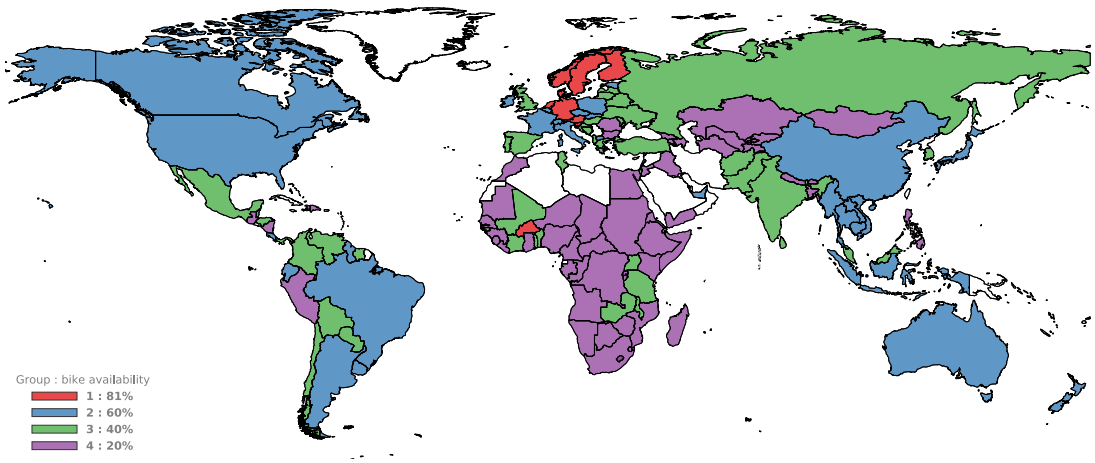

Figure 3.6 World map showing countries color-coded by cluster. The weighted mean percentage household bicycle ownership is shown next to each group label. The red countries have the highest ownership numbers. Data were unavailable for the white portions of the map (notably in North Africa and the Middle East). South Sudan is not shown on the map, but it is also in Group 4, as is Sudan.

rently available for use globally. An estimated 1.25 billion households (averaged over the years 1989 to 2012) make up the 150 countries we studied. These account for 80% of the estimated number of households in the world. [190] Using the mean weighted PBO values for each cluster (multiplied by the corresponding household population of each), we estimate that there are at least 580 million bicycles currently in the possession of the world's households.

3.4 Discussion

In each of the clusters we discovered, the availability of bicycles by household has remained largely unchanged since 1990. Forty percent of the 150 countries considered occupy the group with the lowest PBO. Only 6% of the countries are in the top-ranked group. Household ownership is understandably low in places generally geographically inhospitable to bicycles, such as deserts and mountainous regions, i.e., Central Asia, the Sahara, and so forth. Interestingly, wealth is not always an indicator of bicycle

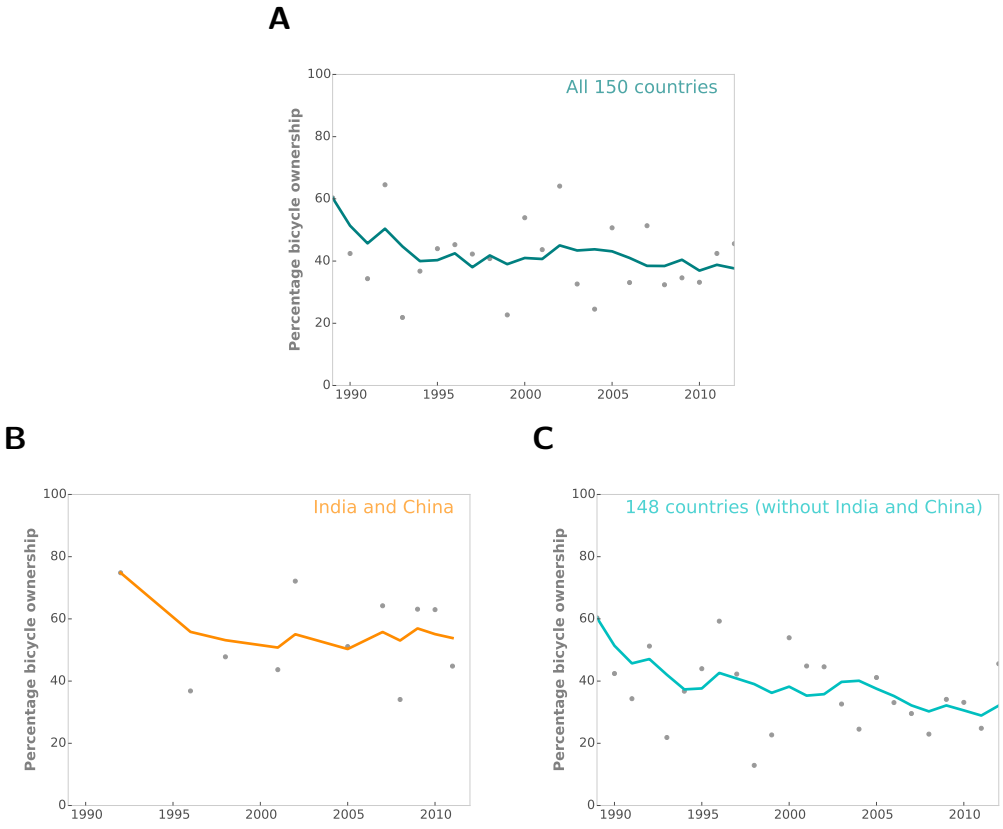

Figure 3.7 Global trends in bicycle ownership from 1989 to 2012 for (A) all 150 countries analyzed, (B) India and China, and (C) all countries excluding India and China. The points in gray are median ownership levels weighted by the number of households surveyed in each year. The lines are the rolling means within a 5-year window.

availability. Notably, the United Kingdom with one of the world's highest per capita GDP [205] sits in Group 3, which collectively has a PBO of 40%. Attitudes, safety and poor infrastructure may have contributed to the relatively low level of ownership in the UK [201], compared to its neighbors (see Figure 3.6).

Beyond ownership levels, each cluster shows characteristic behavior (Figure 3.5). Group 1 has the most stable trend, and its member nations have had long-existing bicycle prioritization policies. Of note, 8 of the 9 Group 1 countries (those in Europe) are proximate. Group 2 also has a largely static trend. The mean number of households in this group is half a billion, which is about 40% of the households in

the dataset. The Group 3 PBO trend has a trough of 30% in 1994 and a peak of 48% in 2006. Similarly, Group 4 pits at 14% in 1998 before rising to a maximum of 25% in 2004. Group 3, however, has a more pronounced post-peak decline (by 10 percentage points in 2011) compared to Group 4 (3 percentage points in 2011). The overall outlook in all four clusters is therefore flat or declining. We note, however, that no statistically significant trend can be observed for any of the ownership plots.

Worldwide, bicycle availability at the household level did not experience any significant increases or decreases (Figure 3.7A), as it hovered around a weighted average of 42%. We see from Figure 3.7B that China and India together also exhibit a flat trend in ownership, excepting the initial decline in the early 1990s. However, their mean weighted PBO of 54% is 12 percentage points greater than the global average. For the other 148 countries, the mean weighted PBO is 5 percentage points less than the global average. We note, however, that in these countries bicycle availability declined by a half during the period under consideration, from an average PBO of 60% in 1989 to 32% in 2012 (Figure 3.7C).

Since India and China are the most influential nations (with regard to household population) in Groups 3 and 2, respectively, it may be instructive to observe their respective outcomes for bicycle ownership. We can also examine the success story of Burkina Faso in West Africa, which has an average PBO of 78%, over three times the unweighted regional average of 26%. Although one of the poorest nations in the world, Burkina Faso has invested substantially in cycling infrastructure (on a scale perhaps not seen in other African nations), and its positive attitudes toward cycling have been well documented [200]. Cycling is also popular in Burkina Faso as a sport (for example, Tour du Faso since 1987 [9]) and as a tourist activity—further evidence for the widespread acceptance of bicycles in the country. However, the popularity of cycling does not always indicate household bicycle availability, as exemplified by Peru in Group 4. Cycling and mountain biking have been growing as a sport in Peru, and it

remains a highly-desired destination for bicycle tourists [90], due in part to its sights and scenic routes. Yet, only 20% of Peruvian households own bicycles, compared to the much higher South American average of 52%. Similarly, in Southeast Asia, where the mean ownership is 49%, the Philippines stands out with a low 23% mean ownership level. Congestion, poor roads and inadequate planning have all contributed toward making bicycling unpopular [65]. However, like in Peru, mountain biking has gained popularity in recent years both among residents and visitors, and investments are now being made to improve cycling infrastructure in certain areas.

3.5 Summary and future work

While our study was not able to assess bicycle usage, we have found that about four-tenths of households around the world have within arm's reach a powerful tool for low-carbon transportation and healthy physical activity. Governments, with the help of public health experts, health and transport geographers [37], and other stakeholders, can harness and mobilize cyclists as change agents by developing policies that support bicycle education, infrastructure, and a culture of safety for all road users. Socio-spatial factors, which have been shown to be of significance in characterizing bicycle usage patterns [71], must also be taken into consideration in understanding ownership trends. We do acknowledge, however, that ownership does not necessarily imply usage, and herein lies a limitation of the survey data we have currently compiled. Nevertheless, tracking bicycle ownership and usage should be a priority for countries and cities wanting to increase exercise and urban livability, thus reducing NCDs and the carbon footprint of their populations.

National health surveys are robust multi-year data sources that could have many unintended applications. Here, we have used them to develop global estimates of household bicycle ownership. Through data alignment and clustering techniques, we

identified four characteristic ownership groups and trends. It would be useful to investigate how broader ownership patterns might depend on variations in climate, development and economic prosperity across the clusters. Further collaboration between the public health and transportation fields on the analyses of nationally-available datasets is possible and can be mutually beneficial for advancing priorities within both fields. For example, further research could be undertaken to identify the determining factors of bicycle ownership, motor vehicle ownership, and their interdependencies. These national surveys will also help to identify countries or regions on new in-depth case studies of bicycle usage can be conducted.

More households will purchase bicycles for regular use with the availability of good supporting infrastructure and systemic attitudes. The findings detailed in this chapter are encouraging, as they also highlight the importance of attitudes and values to improving the adoption of cycling, as changes to these can be achieved at a lower cost than large-scale infrastructural advancements. As efforts are turning toward renewable energy systems and sustainable transit however, challenging problems still need to be addressed in our current systems, especially those for non-renewable energy sources. In the next chapter, we discuss a model that analyses crude oil movements and can serve as a tool for reducing the environmental impact of the industry over the next two decades.

CHAPTER 4

A North American crude oil market model: NACOM

4.1 Motivation

The United States experienced a major upsurge in the production of crude oil beginning in 2009. This has been largely attributed to the advancement in drilling technologies (namely hydraulic fracturing, or "fracking") that has made it commercially viable to exploit tight shale oil in the Bakken formation (North Dakota) and in the Permian Basin (Texas, New Mexico). The impact of this technology on the U.S. and global natural gas markets has been extensively studied [114, 115] but economic-engineering modeling of the crude oil sector has received less attention in the academic literature. Kilian [94] provides a comprehensive background on the effects of this "shale revolution" on prices and infrastructure in the U.S. Heavy oil production has also been expanding across North America, particularly in Canada [21, 74]. Investments in transport infrastructure, especially pipelines, have not kept up with the ramped up pace of production. The rail network has thus filled this void. It has also come under increased pressure as production in the oil sands of Western Canada has been

on the rise, and Canadian exports to the United States via rail nearly quadrupled from 46 kbpd (kilobarrels per day) in 2012 to 161 kbpd in 2014 [127]. A major consequence of the increased demand on rail infrastructure has been the rise of crude oil accidents. While pipelines do spill more gallons per incident, crude-by-rail spills have had more devastating impacts, as the rail lines often run next to rivers or through densely populated areas.

In order to better understand the United States crude oil market and provide policy recommendations toward mitigating the crude-by-rail problem, we have developed NACOM (North American crude oil market model), via which we simulate the resulting market equilibria under a range of different policy measures over the medium term, and the detailed engineering-economic model allows us to track crude oil movements by mode and at a spatial disaggregation level of U.S. states. The scenarios we have designed to aid the investigation are: restricting rail loading and flows, pipeline investments, the lifting of the U.S. export ban on crude oil, and a combination of these three policies. The producers and consumers (refiners) are Eastern and Western Canada, Mexico, and the states that make up 95% of the United States supply-demand crude oil market. The time periods considered in NACOM are 2012, 2015 and 2018. In an attempt to account for differences in crude oil qualities, we consider light-sweet and heavy-crude oil types. The implications of this differentiation are significant as demand and transportation are constrained by the quality of the crude.

4.2 Review of related work

Over the past several decades, several models have been built to study the global crude market, often with a view to understanding price movements and impacts. In 1974, Kennedy [92] published a global oil model incorporating all sectors from the

producers to the end-users, but with a focus on prices and tax effects. Krichene [98] developed a crude oil and natural gas model (2002) that served as a historical analysis of the global market from 1918 to 1999. More recently, a Global Oil Trade Model was constructed by Alkathiri et al. [1], which they used to explore the impact of supplier diversification on oil importer profits. Huppmann and Holz [80] presented a numerical Stackelberg Nash-Cournot partial-equilibrium numerical model to investigate the global crude oil market. Their one-period model was structured as a mixed complementarity problem, and it accounted for pool market behavior by ensuring price equivalence within specified demand hubs. Kilian [94] provides a detailed assessment of the current production boom in the U.S. crude oil industry, particularly with regard to prices and infrastructure. Most recently, Langer et al. [101] have developed a partial-equilibrium model that details refining technologies and explores the global impact of lifting the U.S. crude oil export ban.

Notably, Uri and Boyd [192] developed a linear model for the U.S. oil market in order to examine the effects of price on imports. However, no modeling attempt with multimodal flow granularity and distinction by crude quality in the North American oil market currently exists in the academic literature. The development of NACOM is a step toward filling this void, especially as it allows us to track equilibrium crude oil movements in detail within the medium term and thereby compare scenario outcomes at the U.S. state level. The transportation modes we consider are the waterways, railways and the pipeline network. A major effort in the development of NACOM, besides data gathering, went into calibrating the parameters, including costs of production, investments and transportation, in order to obtain valid results.

As new crude-by-rail regulation and pipeline projects are being proposed to improve the infrastructure level of service as well as reduce the environmental impact of the crude oil industry from production to refining or export, NACOM can serve as a viable testing ground for a counterfactual scenario assessment of the impacts of these

measures. The model development, methods, scenarios and results are described in the following sections. This work is currently under review for publication as at the time of writing [142].

4.3 Model description

The model presented here has been built on a partial-equilibrium framework, *Multi-mod*, developed by Huppmann and Egging [79] to analyze the global energy market. It incorporates endogenous investments and fuel substitution, Nash-Cournot market power, storage operations, and seasonal variability.

In this adaptation, we are concerned with granularity within the United States and interactions within the North American market. The players therein are restricted to the suppliers, which are synonymous with the producing nodes, and independent arc operators. We do not consider storage operators and transformation operators, as we limit consumption to the refining industry and do not include a further representation along the downstream value chain. We have also assumed perfect competition and, as such, the suppliers always exhibit profit-taking behavior. There are 14 supply nodes in the model, 10 of which are U.S. states. Eastern Canada, Western Canada, Mexico and "Rest of the World" are the remaining four. All the aforementioned states are also included as consumers, with the addition of 14 other states within the U.S.

The following sections describe the general execution of the model and relevant parameters in the data initialization process.

4.3.1 Model implementation

Complementarity modeling has grown in importance owing to its ability to capture the complex interactions in energy markets [57]. Mixed complementarity problems (MCPs) generalize equilibria and nonlinear programs, and they can be solved by a

variety of Newton-based methods. In a competitive marketplace, each player's optimization problem can be expressed as a set of Karush Kuhn Tucker (KKT) equations. The concatenation of the KKT conditions yields an MCP, and the solution to this system of equations is a market equilibrium of the underlying non-cooperative game.

We consider the North American crude oil market within an MCP framework, with the KKT conditions formulated from the optimization problems of the suppliers, the arc operators and the demand sector. The program is in GAMS, a high-level modeling language [59]. Data initialization, variable declarations and parameter assignments make up the first step. An algorithm is then called to reduce the size of the problem by excluding extraneous variables. As a feasibility check (to ensure total demand can be met), the program solves an overall cost minimization problem. Initial points for the supply prices are assigned from the solution. An automated iterative calibration algorithm is then run in order to match consumption at all nodes to reference levels, manipulating the end-use cost parameters in the process.

The program utilizes the PATH solver [50] to obtain an equilibrium to the non-cooperative game between market participants. We manually calibrate the model parameters such that the results coincide with reference production and regional transportation quantities for the base year (2012) and subsequent projected years (2015, in part, and 2018). This process is nontrivial, as it requires the adjustment of costs, both for production and transportation.

We provide a complete formulation of the equilibrium model, as pertaining to this dataset. There are three sets of optimization problems relating to the supply side, transportation and the demand sector, each with their own sets of constraints. These are detailed in the following three subsections (Subsection 4.3.2, Subsection 4.3.3, Subsection 4.3.4). The MCP is formulated as a set of KKT conditions (not enumerated) solved simultaneously. The relevant set descriptions are given in Table 4.1. We have limited the notation only to those essential in the current model. For further

discussion and detail on the basic model framework, please refer to Huppmann and Egging [79].

Table 4.1 Selected sets and mappings

$y \in Y$	Years
$s \in S$	Suppliers
$n, k \in N$	Nodes
$a \in A$	Arcs
$a \in A^+_{ne} \subseteq A$	Arcs ending at node n transporting fuel e
$a \in A^-_{ne} \subseteq A$	Arcs starting at node n transporting fuel e
$d \in D$	Demand sector
$e, f \in E$	Crude oil qualities

4.3.2 Supply side profit maximization

The supplier maximizes profit from the quantity of product q^D sold at market price p^D, taking into account costs of production, transportation, emissions and future investment in production capacity (4.1). The term $\text{cost}^P_{yse}(\cdot)$ represents the production cost function, while p^A and p^G are the unit equilibrium prices of fuel transported via the arcs and production-based emissions, respectively. The variables q^A and q^P are the quantities produced and transported, respectively, ems^P is the emission intensity, and inv^P and z^P are the unit investment costs and the size of the investment (expansion of capacity), respectively.

$$\max_{\substack{q^P, q^A \\ q^D, z^P}} \sum_{\substack{y \in Y \\ n \in N \\ e \in E}} \text{df}_y \left(p^D_{yne} q^D_{ysne} - \text{cost}^P_{yse}(\cdot) - \sum_{a \in A^+_{ne}} p^A_{yae} q^A_{ysae} - p^G_{yn} \text{ems}^P_{yse} q^P_{yse} - \text{inv}^P_{yse} z^P_{yse} \right) \tag{4.1}$$

The production cost function (4.3.2) is logarithmic [63, 78] in order to better model the behavior of the marginal cost (4.3), which becomes prohibitive as production

approaches capacity, and the decreasing effect the investment has on future costs of production (4.4).

$$\begin{aligned}\text{cost}^P_{yse}(\cdot) = &\left(\text{lin}^P_{yse} + \text{gol}^P_{yse}\right) q^P_{yse} + \text{qud}^P_{yse}(q^P_{yse})^2 \\ &+ \text{gol}^P_{yse}\left(\widehat{\text{cap}}^P_{yse} - q^P_{yse}\right) \ln\left(1 - \frac{q^P_{yse}}{\widehat{\text{cap}}^P_{yse}}\right)\end{aligned} \tag{4.2}$$

$$\frac{\partial \text{cost}^P_{yse}(\cdot)}{\partial q^P_{ysne}} = \text{lin}^P_{yse} + 2\text{qud}^P_{yse} q^P_{yse} - \text{gol}^P_{yse} \ln\left(1 - \frac{q^P_{yse}}{\widehat{\text{cap}}^P_{yse}}\right) \tag{4.3}$$

$$\frac{\partial \text{cost}^P_{yse}(\cdot)}{\partial z^P_{\hat{y}se}} = \text{gol}^P_{yse}\text{avl}^P_{yse}\text{dep}^P_{\hat{y}yse}\left[\ln\left(1 - \frac{q^P_{ysne}}{\widehat{\text{cap}}^P_{yse}}\right) + \frac{q^P_{ysne}}{\widehat{\text{cap}}^P_{yse}}\right], \hat{y} < y \tag{4.4}$$

$$\widehat{\text{cap}}^P_{yse} = \text{avl}^P_{yse}\left(\text{cap}^P_{yse} + \sum_{y'<y} \text{dep}^P_{y'yse} z^P_{y'sne}\right) \tag{4.5}$$

The supplier profit maximization problem is subject to the following constraints:

$$q^P_{yne} \leq \text{avl}^P_{yne}\left(\text{cap}^P_{yne} + \sum_{y'<y} \text{dep}^P_{y'yne} z^P_{y'ne}\right) \qquad (\alpha^P_{yne}) \tag{4.6}$$

$$q^D_{yne} = (1 - \text{loss}^P_{ne}) q^P_{yne} + \sum_{a \in A^+_{ne}} (1 - \text{loss}^A_a) q^A_{ysae} - \sum_{a \in A^-_{ne}} q^A_{ysae} \qquad (\phi_{yne}) \tag{4.7}$$

$$z^P_{yne} \leq \text{exp}^P_{yne} \qquad (\zeta^P_{yne}) \tag{4.8}$$

$$\sum_{y \in Y} q^P_{yne} \leq \text{hor}^P_{ne} \qquad (\gamma^P_{ne}) \tag{4.9}$$

(4.6) and (4.9) are both production capacity constraints. The first constraint bounds production to the availability of combined capacity (initial and expanded). The second simply ensures that total production over all time periods considered does not exceed proven reserves. Constraint (4.7) ensures nodal mass balance, while also accounting for fuel transport losses. (4.8) sets a maximum for invested capacity expansion.

4.3.3 Fuel transport profit maximization

The independent arc operators seek to maximize profit by transporting fuel through their respective arcs, which are multifuel. The model allows for multiple crude oil types to be transported on any arc simultaneously. In computing the profit for each arc, the price p^A, less the cost of operating the arc trf^A, is multiplied by the flow f^A, while taking investment costs into account (4.10). Emissions and related costs are not considered.

$$\max_{f^A, z^A} \sum_{y \in Y} \text{df}_\text{y} \left[\left(p^A_{ya} - \text{trf}^A_{ya} \right) f^A_{ya} - \text{inv}^A_{ya} z^A_{ya} \right] \tag{4.10}$$

s.t.

$$f^A_{ya} \leq \text{cap}^A_{ya} + \sum_{y' < y} \text{dep}^A_{y'ya} z^A_{ya} \quad (\tau^A_{ya}) \tag{4.11}$$

$$z^A_{ya} \leq \text{exp}^A_{ya} \quad (\zeta^A_{ya}) \tag{4.12}$$

$$\sum_{s \in S, e \in E} q^A_{ysae} = f^A_{ya} \quad (p^A_{yae}) \tag{4.13}$$

The constraints provide bounds for flow (4.11) and capacity expansion (4.12) in each arc. The decision to invest in expanding arc capacity is undertaken if the cost inv^A of doing so is less than the dual τ^A of the flow constraint. The arc usage price p^A is determined by the market clearing constraint equation (4.13).

4.3.4 Demand sector welfare maximization

On the demand side, the goal is utility maximization from energy use in the demand sector, which in our case is represented solely by the refining industry. This produces

a quadratic problem (4.14), which can be linearized using first order conditions.

$$\begin{aligned}\max_{Q^D} \quad & \sum_{\substack{y\in Y\\ n\in N\\ e\in E}} \left[\mathrm{int}^D_n - \tfrac{1}{2}\mathrm{slp}^D_{nd}\left(\sum_{f\in E}\mathrm{eff}^D_{ynf}Q^D_{ynf}\right)\right]\mathrm{eff}^D_{yne}Q^D_{yne} - p^D_{yne}Q^D_{yne} \\ & - \mathrm{eucc}^D_{yne}Q^D_{yne} - \tfrac{1}{2}\mathrm{eucl}^D_{yne}(Q^D_{yne})^2 - p^G_{yn}\mathrm{ems}^D_{ye}Q^D_{yne}\end{aligned} \tag{4.14}$$

The derivation gives an inverse demand price function:

$$\begin{aligned}p^D_{yne} = \mathrm{eff}^D_{yne}\left[\mathrm{int}^D_{yn} - \mathrm{slp}^D_{nd}\left(\sum_{s\in S, f\in E}\mathrm{eff}^D_{yne}q^D_{ysf}\right)\right] \\ - \mathrm{eucc}^D_{yne} - \mathrm{eucl}^D_{yne}\left(\sum_{s\in S}q^D_{yse}\right) - p^G_{yn}\mathrm{ems}^D_{ye}\end{aligned} \tag{4.15}$$

The final price p^D consists of the efficiency weighted composite price of the energy supply (the first term in (4.15)), where slp^D and int^D are the slope and intercept, respectively, of the energy supply demand function. End-use costs for each fuel are also taken into account by a linear function parametrized by eucl^D (linear term) and eucc^D (constant term)[1]. The final term in (4.15) represents the emission costs of refining (or, in general, fuel consumption).

4.3.5 A note on multiplicity of equilibria

While the functions defined in this model are convex, they are not all strictly so. Thus, the equilibrium point obtained in any instance of solving the model is not guaranteed to be unique. Alternate equilibria may be found by initializing the program from different points. Owing to the nature of the capacity constraints and other network constraints, we hypothesize that the differences that might exist among multiple equilibria may only be found in the arcs that are used and these may not be significant

[1] See Appendix C. in Huppmann and Egging [79] for a robust discussion on how the end use costs are calculated in the model.

enough to produce marked changes in the outcome of interest. However, more work will be required to characterize and address the issue of non-uniqueness in NACOM.

4.3.6 Data initialization

We set 2012 as the base year for NACOM, which proceeds for two subsequent periods in steps of 3 years, i.e. 2015 and 2018. All quantities are expressed in kilobarrel per day (kbpd) units. An annual discount factor of 91% and 95% is applied to investment decisions for producers and arc operators, respectively. Initial prices and all other monetary values are in 2012 U.S. dollar terms. 100% capacity availability is assumed for all producers (thus $\text{avl}^P = 1$ in all cases). An energy service efficiency of 98% is assumed for all consumption nodes. We do not consider seasonal variations in either production or consumption patterns. Details on our data are provided in the following section.

4.4 Data collection and methods

Data on U.S. crude oil production and consumption (refining) were obtained from the U.S. Energy Information Administration (EIA) [196]. Domestic supply and demand projections are given by the EIA's Annual Energy Outlook 2015 [194]. Similar data for Canada are obtained both from the National Energy Board [126] and the Canadian Association of Petroleum Producers (CAPP) [24]. Global supply and demand quantities (including projections), including those for Mexico, are obtained from the International Energy Statistics on petroleum compiled by the EIA [195]. The EIA also annually tracks regional crude movements across the country (and to and from Canada) by barge, rail and pipeline. However, further information on pipeline and rail loading capacities are only available from private sources. A list of all the nodes and arcs in model are given in Table C.4 and Table C.5 in the Appendix. We se-

lected 2012 as the base year, as this was when rail movements of crude oil across the continent first rose to prominence after the oil boom.

4.4.1 Crude oil production

The U.S. has been a dominant player in the global crude oil market. Production peaked in the 1970s, and the subsequent decline persisted until 2009. The decline was a result of various factors: the institution of the crude oil export ban in 1978, the availability of cheaper oil from external suppliers and the increasing costs of domestic production. Canada also historically relied on the U.S. to export its oil to other markets [103]. Over time the industry in the U.S. converged to a market equilibrium under these conditions. Major refineries invested in technologies to improve capacity for the medium-heavy oil being imported from the Gulf States. The shale oil boom has again repositioned the United States as a major oil producer, but challenges have arisen in terms of refining and transporting this additional volume, which is of the light-sweet variety [94]. The trend in U.S. crude oil production is shown in Figure 4.1.

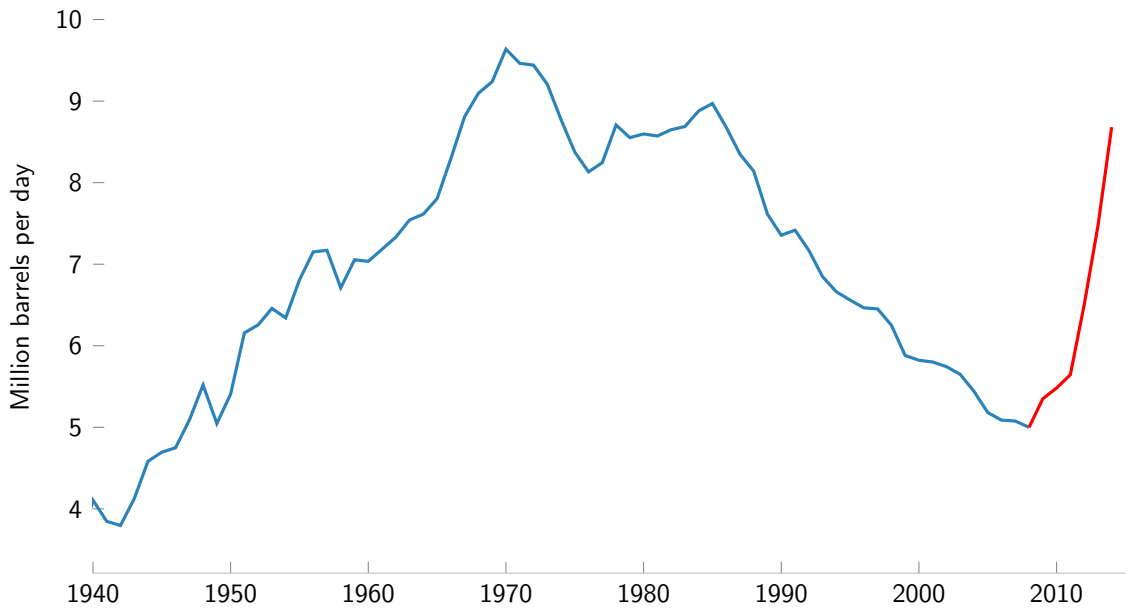

Figure 4.1 U.S. crude oil field production (Source: EIA)

Western Canada is also an influential player, its growth primarily driven by heavy oil exploited from the sands of Alberta. Much of this oil finds its way down to the Gulf of Mexico for refining or exportex. Eastern Canada predominantly produces light crude. It also supplies some refiners along the East Coast of the United States, while receiving shipments from Western Canada as well.

Mexico's crude oil production industry is run by the state-owned Petróleos Mexicanos (Pemex) [164]. Mexico is a net exporter of crude, producing close to 3 mbpd (million barrels per day) in 2012, and consuming only about half (for refining). However, it has to import refined gasoline to satisfy domestic demand. The United States is the top destination for Mexican crude, of which over 50% is of the heavy-sour grade [164, 155].

We considered the states that account for 95% of total U.S. output. Estimates of light-to-heavy yield ratios were made based on industry reports and other surveys. Offshore production in the Gulf of Mexico was attributed to Texas, and California also includes offshore production off the southwestern coast of the United States. In 2012, North Dakota and Texas were the fastest growing crude oil suppliers in the country [112]. Figure 4.2 shows the 2012 quantities for the suppliers. Production for the rest of the world was excluded from this diagram for clarity.

4.4.2 Refining and demand

The United States currently must refine or store all its domestically produced crude oil. Many of the U.S. refineries are situated next to waterways or in close proximity to the production field. Canada refines some of its oil and exports to the U.S. much of the remainder. Mexico is a net exporter of crude, shipping heavy oil to the U.S. and to the rest of the world. The U.S. therefore has the largest refining capacity on the continent.

We consider demand as crude oil refining for the purposes of this implementation of

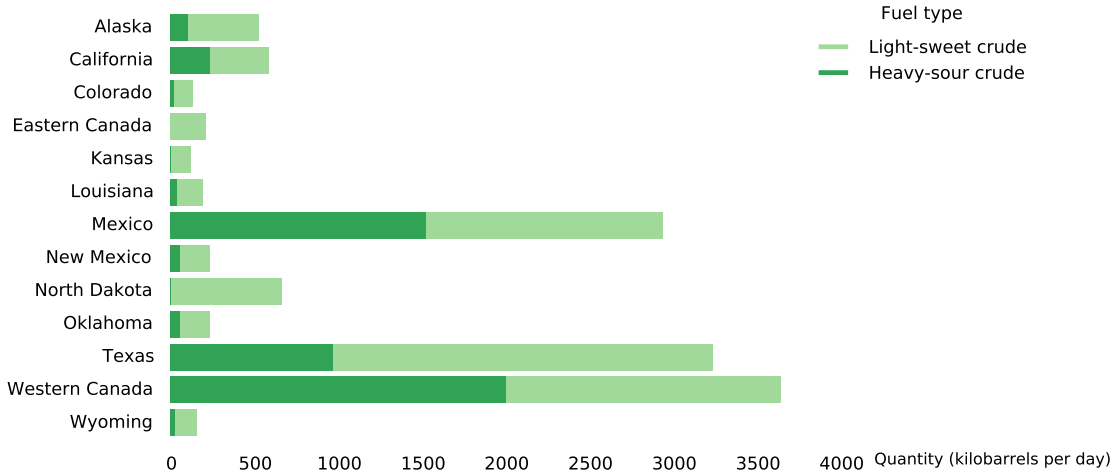

Figure 4.2 Production (supply) nodes, showing split between light-sweet and heavy-sour crudes

NACOM. Refining capacities for the U.S. are available from the EIA, as are estimated utility rates. From these, we can obtain the quantities of crude oil consumed at the nodes of interest. Data on API gravity averages of crude oil inputs to refineries enable us to calculate yield rates for light and, consequently, heavy crudes. For Canada, the relevant data were obtained from the Canadian Fuels Association [6].

The demand quantities at each node are show in Figure 4.3 for the base year 2012. The quantity for the rest of the world is again excluded here for clarity.

4.4.3 Transportation

The transfer of crude oil from the oil fields and production sites to and from refiners both within and outside North America occurs via land and water bodies. On land, pipelines, trains and trucks are used to transport crude. We do not consider the share of truckage, as it is insignificant compared to the other two. On water, tankers ply the sea routes while barges transport crude along the river system, of which the Mississippi is the most important. Intermodal exchanges also occur at certain nodes, e.g. rail to barge, tanker to pipeline, and so forth. In the following subsections,

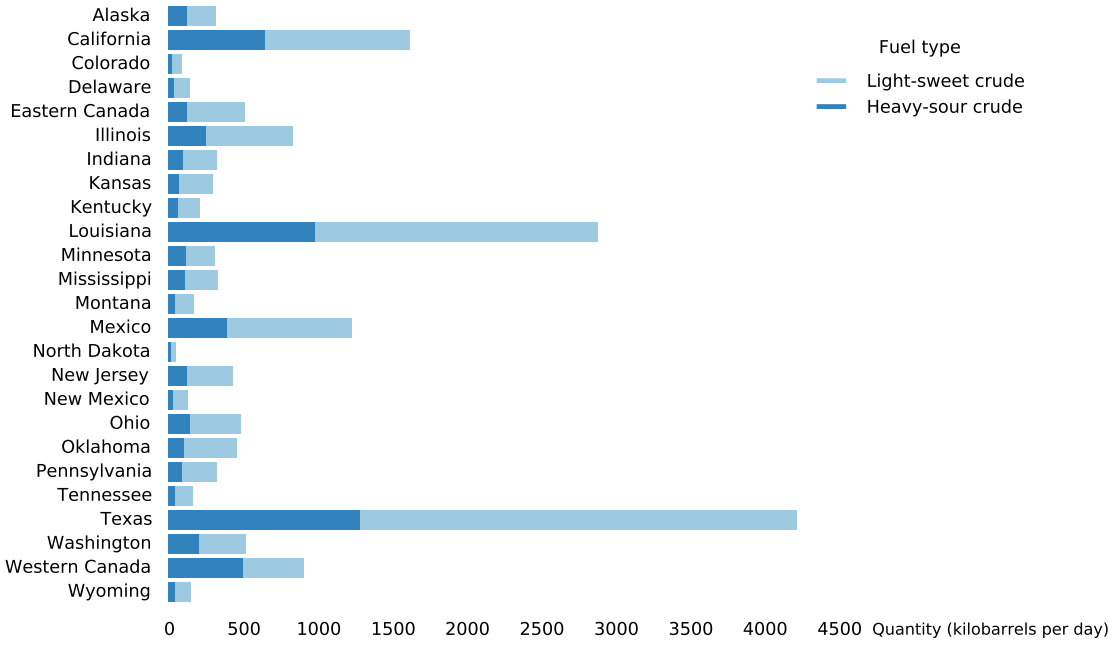

Figure 4.3 Refining (demand) nodes, indicating yield of light-sweet crude to heavy-sour crude

we outline the data collection process for the arcs in each mode, while providing a context for their importance in the market.

Railway

As discussed earlier, crude oil producers both in Canada and the United States have become increasingly reliant on trains to move oil to the refineries (Figure 4.4). All the production and consumption nodes, except for Alaska and Mexico, were considered as loading and unloading points for rail crude oil loads. Auxiliary rail nodes were then modeled at these points and in the intervening U.S. states. Initially, all arcs connecting auxiliary rail nodes were assigned unconstrained capacities, while the loading and unloading arcs were constrained. During calibration, some auxiliary arcs were constrained in order to obtain base-case flows matching closely to observed reference values.

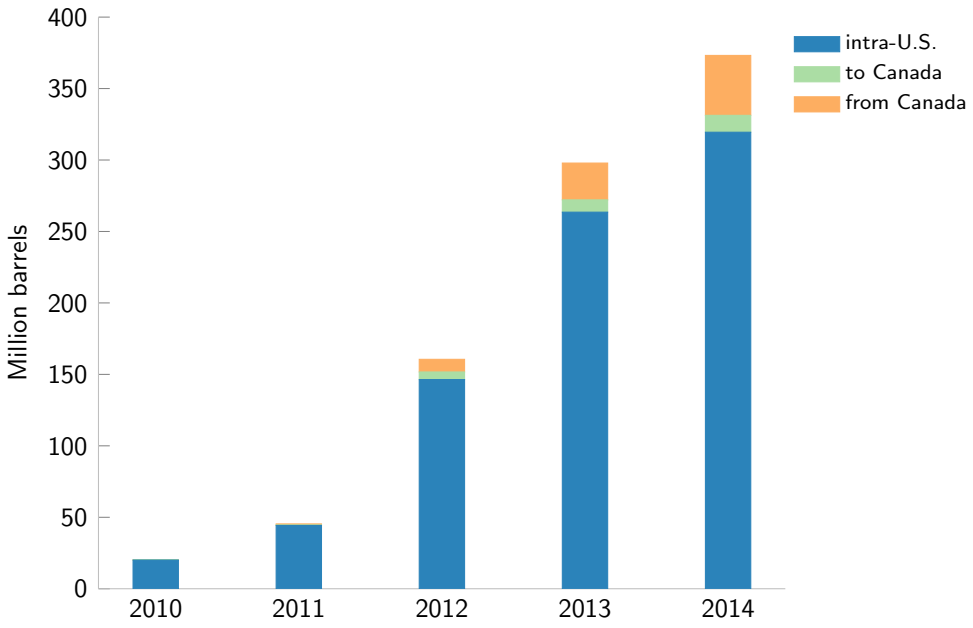

Figure 4.4 Rail movements of U.S. crude (Source: EIA)

The rail capacity data were obtained from a myriad of industry publications[2], as compiled by Oil Change International [137] and providing the unloading and loading capacities of crude oil facilities in the United States and Canada. We aggregated the loading and unloading capacities for each of the regions under consideration. Some of the facilities were operational but had no listed capacities. The missing data were filled using average capacities of the facility type. The scope of the rail network considered for the model is shown in Figure 4.5.

Pipelines

Historically, the crude oil pipeline network in the U.S. and Canada developed to transport oil from Canada toward the Gulf of Mexico, while capacity was increased within the Gulf region itself to facilitate movement between storage and refining facilities. Cushing, Oklahoma, became established as a trading and storage hub for both Canada and the U.S. In 2012, operators delivered over 20 mbpd of crude oil

[2]These include: RBN Energy, Hart Energy, Genscape, BNSF, Canadian Pacific, Canadian National, Meritage Midstream, Howard Energy Partners, and Rangeland Energy

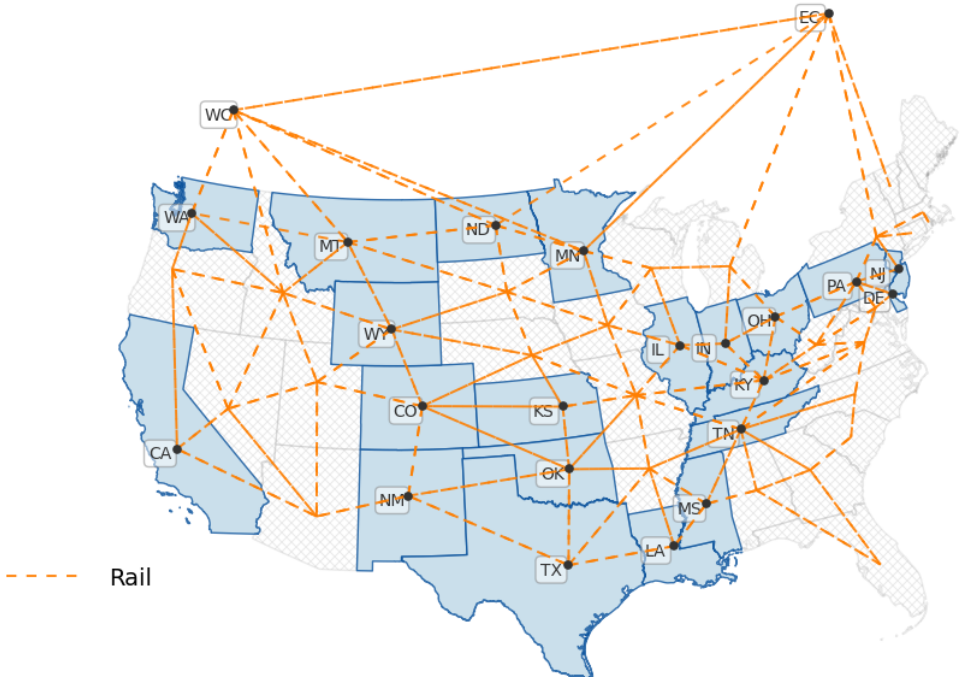

Figure 4.5 Map of internodal rail arcs in the model. The nodes AK (Alaska), MX (Mexico) and RW (Rest of World) are not shown, as they do not currently have any rail links with the other nodes. The U.S. states labeled are producing and demand nodes. Directionality is not indicated in this diagram but the solid lines indicate that the represented arc is bidirectional.

via pipeline in the United States. This value increased by 11.3% in 2013 [7]. The rate of increase in pipeline delivery in 2014 was also identical at 11.6% [8]. On average, pipelines have consistently accounted for 80% of the modeshare in crude oil transportation in the United States since 2000 [55]. They are therefore a vital part of the U.S. crude oil infrastructure.

The process for gathering pipeline data began by consulting maps of established and functioning pipelines [24, 33] Most of the major pipelines in the U.S. and Canada are owned by various private corporations.[3] Capacities were obtained from available databases of the oil corporations operating the respective pipelines. Intranodal pipelines were not considered. A scheme of the pipeline network for the model is

[3]Some of the major systems and pipeline operators include: Colonial, Enbridge/Lakehead, Keystone, Marathon, Mid-Valley, Pony Express, Seaway, Spearhead, and TransCanada.

shown in Figure 4.6.

On average, transporting crude oil via pipeline costs $5 per barrel [54]. Initial operational costs for each arc were then varied as a function of pipeline mileage. The mileage values were taken from individual corporation websites when available and estimated from digital maps otherwise. Some pipelines only provided capacity values at the terminals, and further investigation was required to ascertain the presence of major refineries between the terminals in order to properly account for changes in capacity. The pipelines were disaggregated to include separate arcs connecting refineries in different US states. The total capacity value of each pipeline was used as the initial capacity for the individual arcs thus created. In cases where multiple pipelines connected two nodes, capacities were aggregated into a single arc. As with the costs, pipeline capacities were modified during calibration to match baseline flows.

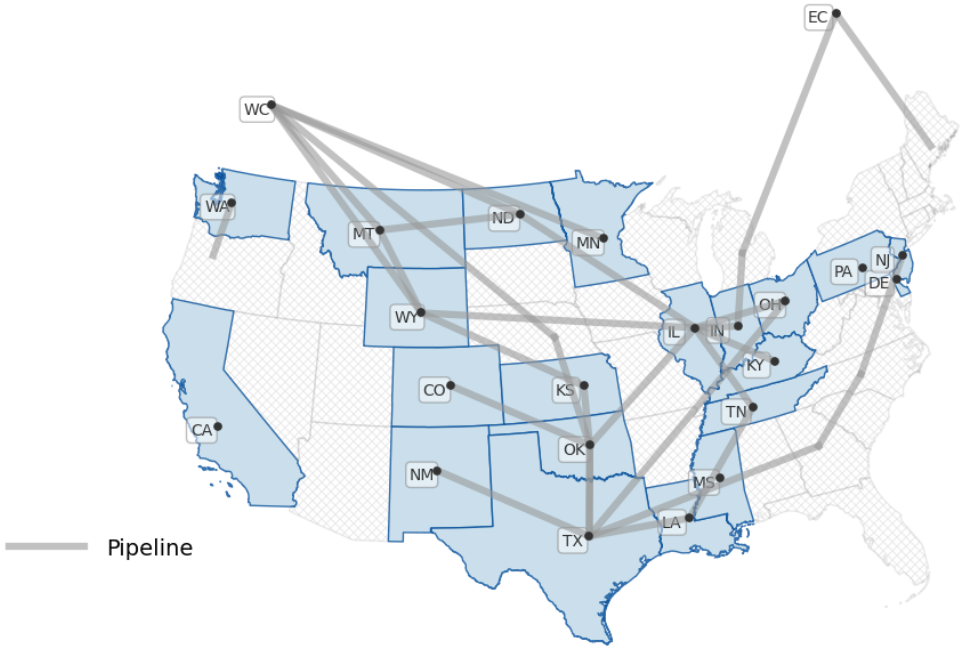

Figure 4.6 Map of internodal pipeline arcs in the model. Directionality is not indicated. The nodes AK (Alaska), MX (Mexico) and RW (Rest of World) are not shown, as they do not currently have any pipeline links with the other nodes. The U.S. states labeled are the supply or demand nodes included in the model.

Waterways

Domestic transportation of crude oil through inland waterways (chiefly via the Mississippi and Ohio river systems) occurs via river-going barges, which typically have a capacity of 30 barrels. Coastal transport of crude oil, for instance, from Washington to California, is undertaken by tank barges or seagoing barges, which have a larger capacity of 90 barrels [53]. Imports and exports are undertaken by tankers, which have a greater capacity. Some refineries in Eastern Canada obtain shipments from the Gulf of Mexico, while some pipeline and rail movements bound for Canada originate from the northern U.S. states.

Due to the Jones Act, vessels shipping domestic crude oil must be built and owned by U.S. interests [53]. This severely restricts the domestic waterway shipping of crude oil and increases the costs by as much as three times that of using a foreign-owned vessel carrying foreign oil. Thus, in some situations, some refiners find it cheaper to import crude oil than to buy it from other regional suppliers who would have to ship it by barge to them [53].

Data on major inland routes were obtained from Ref. [53]. These routes connect states along the Mississippi and Ohio river systems. From the same source, we obtained initial shipping costs as well. We differentiated between tankers, river-going barges and seagoing barges, the key factor being the operational cost. Alaska, California and Washington were assigned incoming arcs from the Rest of the World, as were nodes in the Gulf and on the East Coast (New Jersey, Texas, and others). Eastern Canada also has outgoing arcs to the U.S. eastern refineries, while Mexico has outgoing arcs to the Gulf states and the Rest of the World. Mexico and the Rest of the World are the only nodes in the model with a single mode of transport (ship) available to them.

4.4.4 Model calibration

Significant effort went into calibrating the model to produce results that matched observed quantities and prices for the base year of 2012. As production, transport and consumption figures for individual states (nodes) were not always readily available, regional data (by the Petroleum Administration Defense District system) were used as reference (see Section C.5 for further background on the PADD system). In addition, it was useful to describe a region (Canada) including both the Eastern Canada and Western Canada nodes for the purpose of flow calibration. The classification of the producing and refining nodes by region is given in Table 4.2.

Table 4.2 Regions designated in the model

Region	Supply and demand nodes
CAN	Eastern Canada, Western Canada
MEX	Mexico
ONA	Rest of World
PADD1	Delaware, New Jersey, Pennsylvania
PADD2	Kentucky, Minnesota, North Dakota, Ohio, Tennessee
PADD3	Kansas, Louisiana, Mississippi, Oklahoma, Texas
PADD4	Colorado, Montana, New Mexico, Wyoming
PADD5	Alaska, California, Washington

For the base year 2012, NACOM captured 82%, 85% and 91% of overall interregional rail, pipeline and waterway movements, respectively. The details are given in Section C.6. We have calibrated the model to EIA forecasts that are still based on an assumption of a crude oil export ban, and our scenarios therefore compare two futures: one with a ban (based on official projections), and the new status quo given our own results.

4.5 Results

Our results show that NACOM can be a useful tool for analyzing the the domestic crude oil market in the United States, and in particular, providing solutions to transit problems in the network. In the following subsections, we discuss the base case and four scenarios that investigate potential pathways for containing crude-by-rail flows while highlighting the capabilities of the model. The scenarios are as follows:

(i) Restricting rail flows from the Bakken region/North Dakota

(ii) Investing in pipeline capacity from the U.S. Midwest

(iii) Lifting the U.S. crude oil export ban

(iv) A concurrent implementation of the policies in (i), (ii) and (iii)

In each of the scenarios, all investment variables remained unchanged from the base case throughout the entire time horizon under investigation. Further, all the base year variables were fixed at base case levels in the scenarios. These steps allowed for consistent comparisons among all the cases.

4.5.1 The base case

Base case flows via rail and pipeline, according to the model, are depicted in Figure 4.7 and Figure 4.8. Intrastate activity is not accounted for in either of these figures. Furthermore, the arcs are drawn from centroid to centroid in each state and may therefore not reflect the geographical reality of the route represented.

Much of the rail movement in the U.S. originated from the Northern Plains/Bakken region, which includes Montana and North Dakota. From the Midwest, trains were used to deliver crude oil to East Coast refineries. Rail also helped to lift both heavy and light crude to the Gulf of Mexico for refining or exporting. Along the West Coast, trains from Western Canada delivered crude oil to the Washington refineries and traversed California to deliver oil to neighboring states. Canada also depended

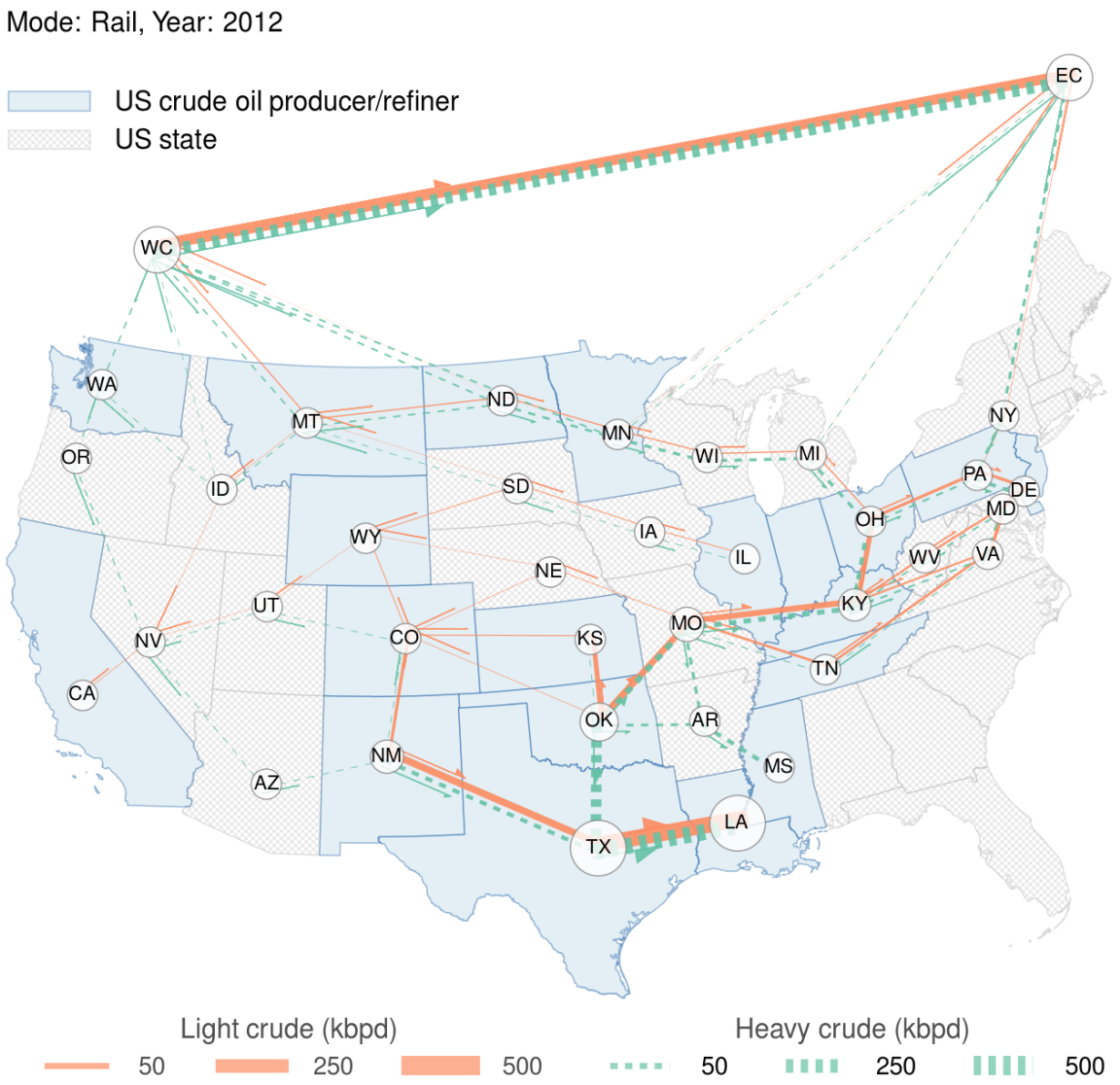

Figure 4.7 Rail movements of crude oil in the base year 2012. The size of the node labels indicate the larger of the quantities of crude leaving or entering the respective node.

on rail to move crude from west to east. While heavy oil production has surged in Western Canada, the absence of cross-country crude oil pipeline system has paved the way for the rise in crude-by-rail shipments across the country. Eastern Canada also sent crude by rail to New York refineries.

The pipeline system in 2012 primarily conveyed oil from Western Canada to the Midwest, and some ultimately to the Gulf Coast. Pipelines also moved oil through the

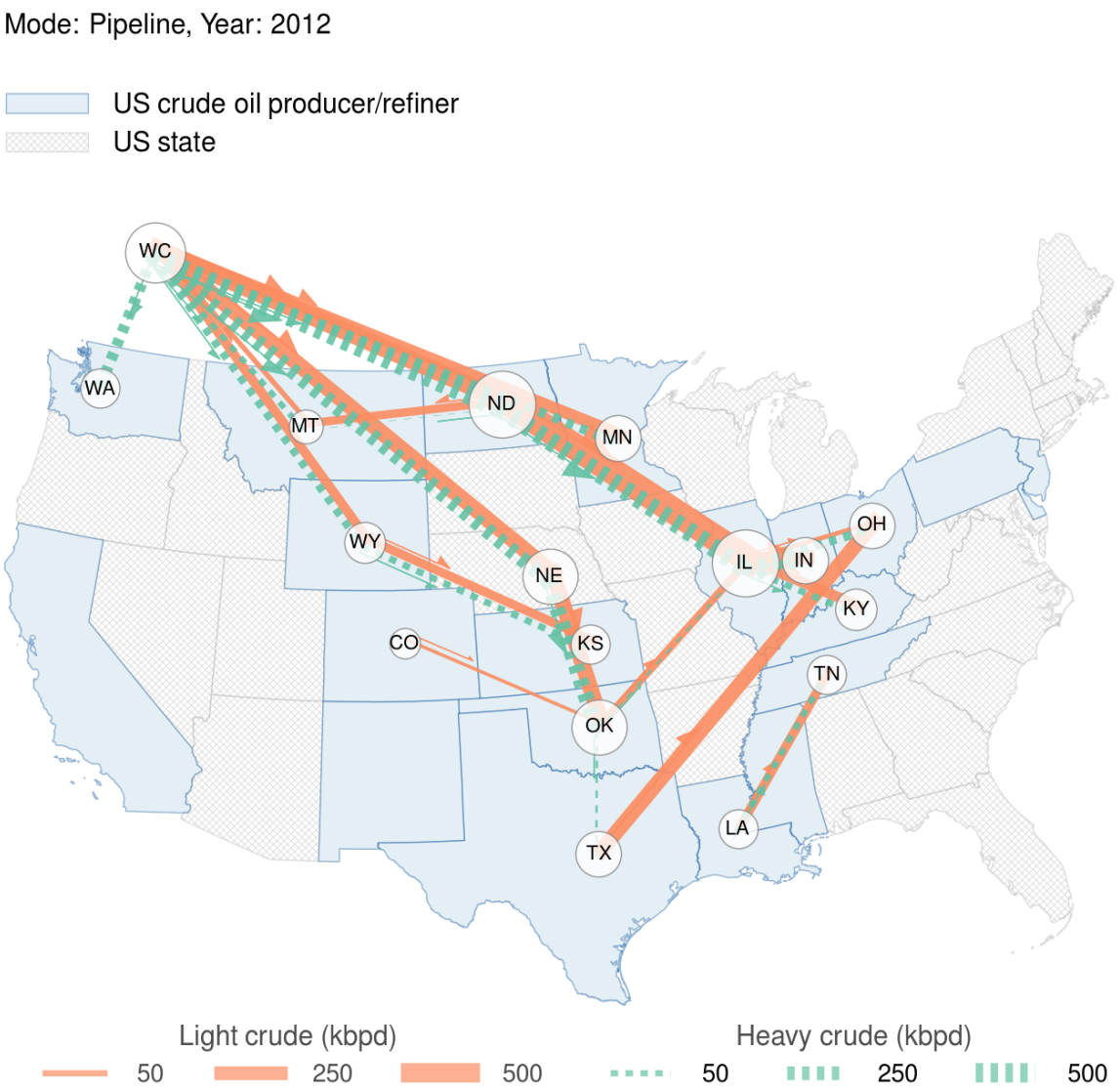

Figure 4.8 Pipeline movements of crude oil in the base year 2012. The size of the node labels indicate the larger of the quantities of crude leaving or entering the respective node.

Rockies (Montana, Wyoming, Colorado) toward Kansas and Oklahoma. Waterway movements are not shown. However, 3000 kbpd was imported into the Gulf of Mexico from the rest of the world in 2012, according to the model, while 800 kbpd and 900 kbpd were shipped into PADD1 (U.S. East Coast) and PADD3 (U.S. Gulf of Mexico) refineries, respectively. Mexico exported 240 kbpd to the rest of the world and 975 to PADD3. Canada sent 20 kbpd from its eastern shores to the rest of the world,

while 75 kbpd left for U.S. East Coast refineries. Other smaller barge movements were captured, notably the 58 kbpd from PADD2 to PADD3, which represents traffic along the Mississippi river system. These quantities compared to reference values are visualized in C.6, Figure C.4.

4.5.2 Restricting crude-by-rail flows

In this scenario, we investigate the effects of directly capping rail flows from the Bakken region of North Dakota. The motivation behind this design was the growing concern over the rise of crude-by-rail transportation across the heart of the country. In many instances, issues have been raised regarding the displacement of grain shipments by increasing crude oil loads. Also, the movement of crude-by-rail through California has been one of great concern, due to the fact that the rail lines pass through densely populated areas and close to water resources [32]. Most importantly, the rising number of crude-by-rail accidents have spurred the authorities to take action.

In August 2015, the U.S. Department of Transportation and Transport Canada jointly announced a "Final Rule" to govern the transit of crude oil via rail [150]. The stipulations provided by the Rule were adopted by the the Pipeline and Hazardous Materials Safety Administration (PHMSA) and the Federal Railroad Administration (FRA), with input from the National Transportation Safety Board (NTSB). The Rule aims to improve rail shipping standards by imposing speed reductions, tank car upgrades, enhanced braking requirements, routing regulations and stricter product classification. It has however been met with criticism from both industry and public administration representatives, who argue that the regulations are inadequate or too costly and disruptive to implement [122, 121].

A thorough implementation of this Rule will likely reduce crude-by-rail movements, especially from the Bakken region, and may encourage more pipeline deployment. To simulate the impact of these restrictions, we set rail arc capacities originat-

ing from the North Dakota area to half the equilibrium rail transportation quantities in the base case. We choose North Dakota as it is a key driver of the growth in crude-by-rail shipments.

This scenario results in a disappearance of all westward U.S. rail movements and those between the PADD5 nodes in 2015 (Figure 4.9A, B). While rail transportation in PADD5 is not completely eliminated in 2018, activity is limited only to California, Nevada and Washington, as compared to the base case in which all the nodes are involved in rail movements of crude oil (Figure 4.9C, D). Yet, in 2015, total U.S. internodal rail flows in this scenario are only 5 kbpd less than in the base case (∼1% decrease). One reason for this is the utilization of an alternate rail pathway for the crude oil from North Dakota to meet the demand in the Eastern U.S. in the absence of sufficient pipeline capacity. By 2018, however, the impact of this restriction is seen in a 21% reduction in overall U.S. rail movements from 9620 to 7554 kbpd. Meanwhile, pipeline throughput increases by nearly 1600 kbpd.

4.5.3 Pipeline investments in the U.S. Midwest

The pressure on U.S. oil transport infrastructure stemming from the Northern Plains has not only been due to increased oil production from the Bakken formation. Western Canada's flourishing industry (driven by oil sands exploration in Alberta) has also contributed to rising demand for transfer to refineries and export terminals. As there is yet no pipeline connection from Alberta to Canada's eastern shores and little capacity to Canada's west coast, unrefined crude from the oil sands is transported to the gulf via pipeline through the Northern Plains, ultimately to the Gulf of Mexico. However, pipeline investments have not kept up with the rising production [103]. Where feasible, barge and rail flows have grown accordingly. The Keystone XL pipeline was proposed by TransCanada to boost capacity for throughput to the Gulf but this was rejected in 2015 [36]. A major player in the North American oil transit industry,

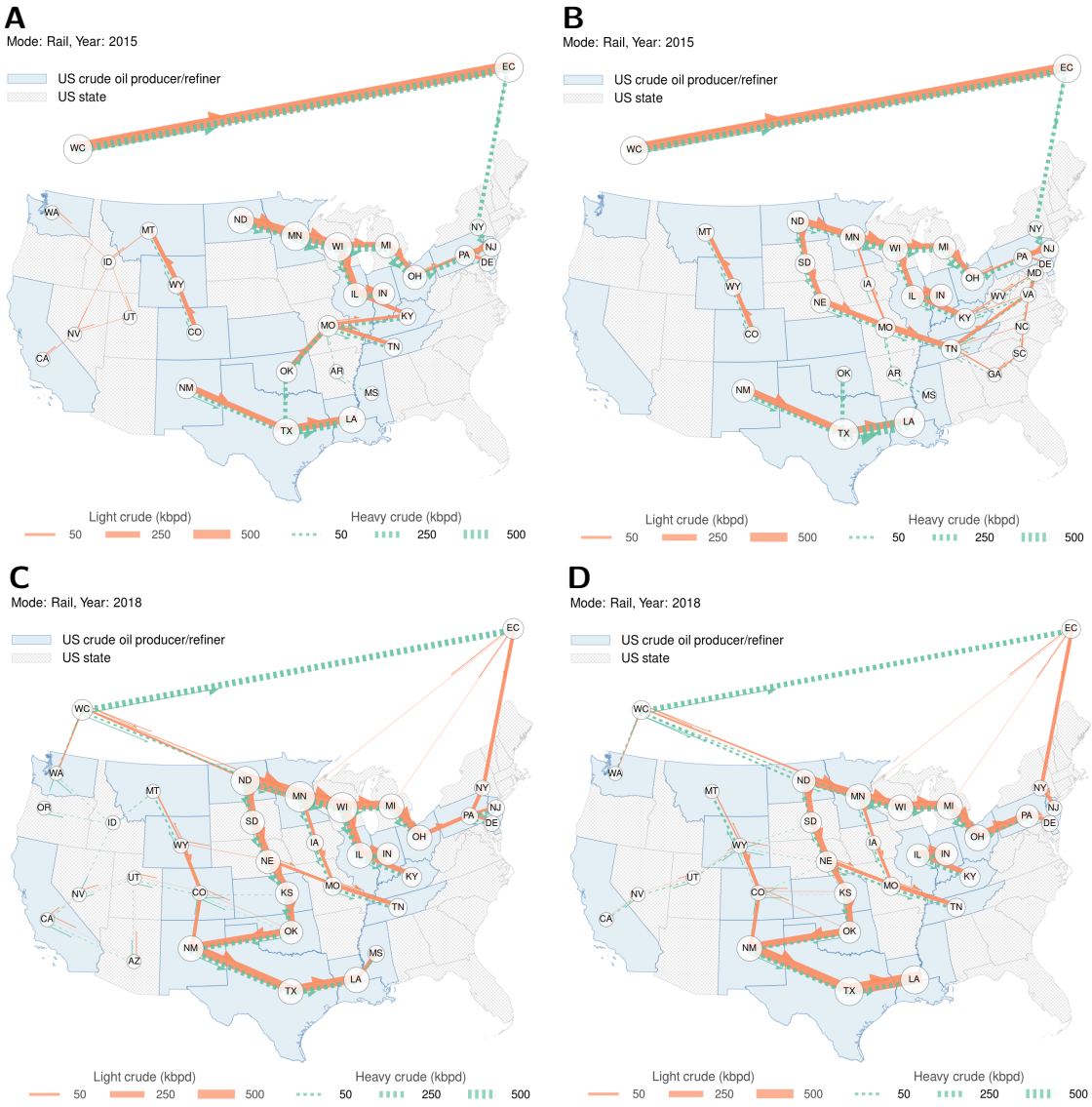

Figure 4.9 (A) Rail flows in the base case, 2015 (B) 2015 rail flows in the scenario "Capping Rail Flows From Bakken Region" in which surrounding rail capacities are set to half of the base case flows through those arcs. (C) Rail flows in the base case, 2018 (D) Rail flows of crude oil in 2018 under the scenario "Capping Rail Flows From Bakken Region."

TransCanada has also proposed the Energy East pipeline, with a maximum capacity of 1100 kbpd [18], to convey heavy crude from Alberta to Quebec. A decision on this project will be made by 2016. Like that of Keystone XL, the Energy East proposal has been met with mixed views amid concerns on possible impacts on communities and the environment vis-à-vis potential safety benefits over crude-by-rail transport

[131, 143].

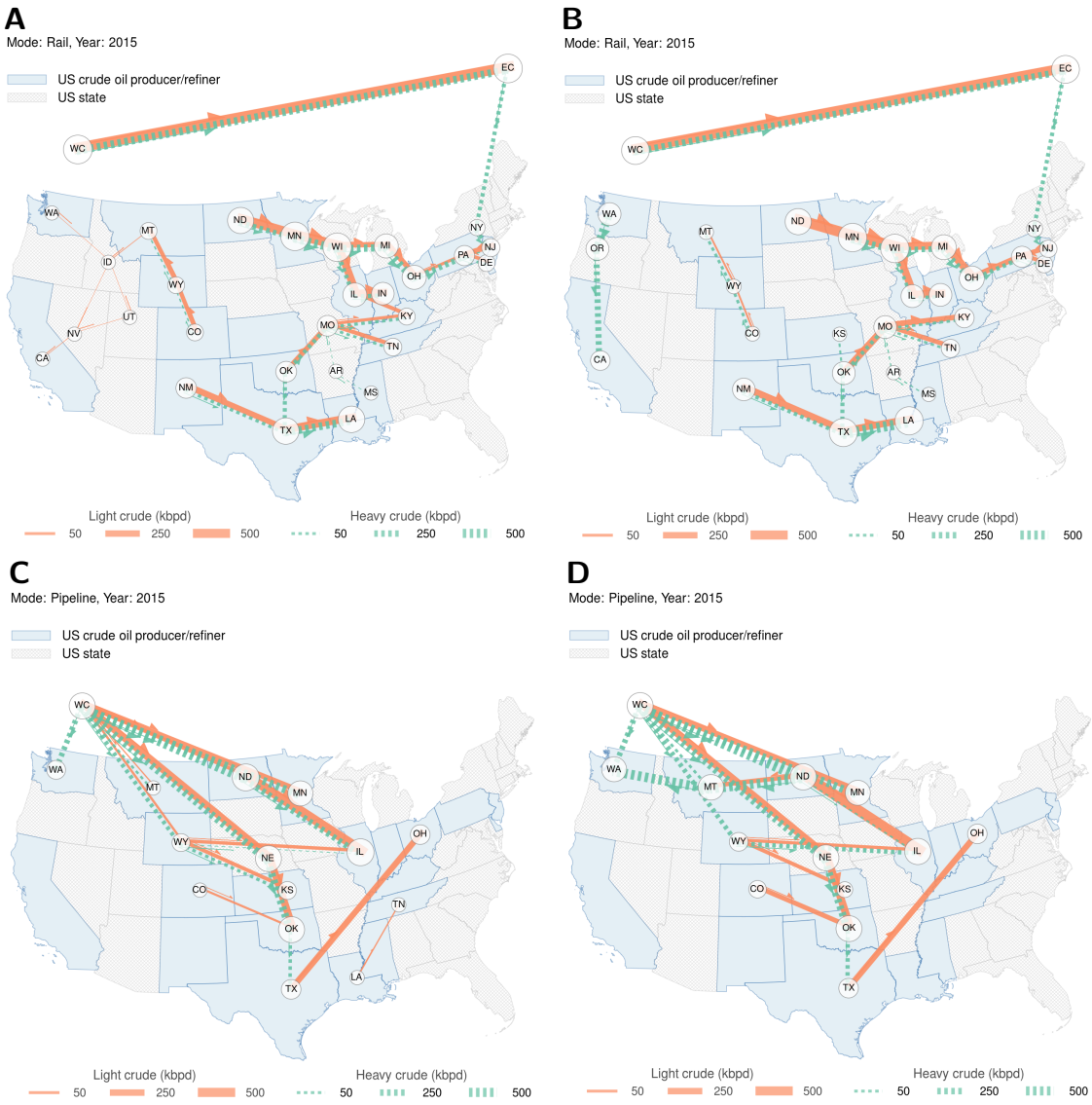

Figure 4.10 (A) Rail flows in the base case, 2015 (B) 2015 rail flows in the scenario "U.S. Midwest Pipeline Investments" in which new pipelines are built to convey oil from North Dakota both to the east and west. (C) Pipeline flows in the base case, 2015 (D) Pipeline flows of crude oil in 2015 under the scenario "U.S. Midwest Pipeline Investments."

While we closely follow ongoing pipeline developments in Canada, we shall initially focus on examining the situation in North Dakota, which has been the epicenter of outflows largely responsible for the growth in crude-by-rail shipments. North Dakota has approved the 12-inch 100 kbpd NST Express pipeline, scheduled to be in service

by late 2016, to transport Bakken crude to Montana [171]. The massive 30-inch 570 kbpd Dakota Access Pipeline (DAP) is also on track to come online toward the end of 2016 [184]. The DAP will provide access to terminals in Illinois. Notably, TransCanada has also proposed the Upland Pipeline to carry up to 300 kbpd from North Dakota to Saskatchewan, but the Upland is not expected to join the pipeline network until 2020 if the project obtains the requisite approval [132, 186].

Given this outlook, we develop a scenario in which pipeline capacity in the U.S. Midwest is expanded in both the eastern and western directions. Specifically, we add new pipeline connections from Michigan to New Jersey (eastward), and from Montana to Washington (westward). We also double pipeline capacity from North Dakota to Montana. The impact of these investments is seen in a transfer of 548 kbpd of heavy-sour crude to the new Montana-Washington pipeline in 2015. In 2018, this pipeline carries 60 kbpd of heavy-sour crude and 131 kbpd of light-sweet crude. These in turn result in a reduction of crude-by-rail flows originating from the Bakken region (i.e. North Dakota). Yet, overall rail flows increase by 13% in 2015. These are due to the movements of about 200 kbpd heavy-sour crude between Texas and Louisiana and also of 400 kbpd heavy-sour crude between Washington and Oregon, with half of this volume going on to California. However, we see that there are fewer rail movements within PADD5 and between PADD4 and PADD5. In 2018, reductions in the total interregional rail flows are realized—a 9% decrease from 9620 kbpd to 7123 kbpd.

The newly added pipeline from Michigan to New Jersey, however, is left unused both in 2015 and 2018, indicating that it may not be a viable investment due to the relative cost of transfer. The rail and pipeline flows in 2015 compared to the base case are shown in Figure 4.10.

4.5.4 Lifting the U.S. crude oil export ban

The United States effectively banned domestic crude oil exports when President Gerald Ford signed the Energy Policy and Conservation Act into law in 1975 [198, 102]. At the time, the country was experiencing a decline in oil production. Moreover, it had recently endured an economic crisis when OPEC imposed a retaliatory oil export embargo on the U.S. National sentiment was therefore understandably in favor of shoring up reserves and increasing domestic supply. Canada was exempt from this ban [19]. Thus, any unrefined oil from the U.S. invariably finds its way to Canada. Alaska had also been exempt from the ban since 1995, but its export volumes began to dwindle in the late 1990s [41]. Only in 2014, after a decade-long hiatus, did it send its first export shipment—784 kilobarrels to South Korea [125] (about 2 kbpd).

Considering the recent boom in U.S. domestic production, the ban had been increasingly perceived to be more of a hindrance than a boon [31]. A large portion of new crude oil supplies is of the light-sweet variety, for which refining capacity is not readily available at the source. Thus, producers have had to incur expensive transportation costs to deliver crude oil to refineries. Experts argued that an end to this export restriction could only benefit the economy [42] and increase the competitiveness of the U.S. oil industry. More crucially, authorizing crude oil exports could also relieve demand on strained transit infrastructure, especially rail. Notably, the U.S. Congress supported a motion to lift the ban in December 2015 [76]. The spending bill including a provision authorizing exports of domestically produced oil was finally passed and signed into law before the end of the year, thus ending the 40-year prohibition [149].

We investigate the impact of lifting this decades-long ban by implementing a scenario in which shipping capacity is added from U.S. coasts to the rest of the world. These shipping arcs are incident from California, Washington (West Coast),

Louisiana, Texas (Gulf of Mexico) and New Jersey (East Coast) in the model scenario.

Under this scenario, Texas (which also represents the Gulf of Mexico in this model) exports 405 kbpd in 2015 and 324 kbpd in 2018. (Alaska also exports 5 kbpd in both years, but it was exempt from the ban and its exports are therefore present in the base case, as well.) More significant, however, is the reduction in imports into these regions. The net imports via waterways can thus be seen as an indicator of the new export volumes (Table 4.3). These movements, however, do not reduce the pressure

Table 4.3 Net imports of crude oil into the U.S. via ship (tankers) in the base case [BC] compared to those in the "U.S. crude oil export ban lifted" scenario [EBL], for the years 2015 and 2018.

Incoming Region	**2015**			**2018**		
	BC (kbpd)	EBL (kbpd)	% drop	BC (kbpd)	EBL (kbpd)	% drop
PADD1	630	630	0	860	675	22
PADD3	4050	2395	41	4350	2585	41
PADD5	1245	1160	7	1364	516	62

on the rail network as intra-U.S. flows increase by 12% from 7122 kbpd in 2015 (base case) to 7945 kbpd. In 2018, a similar trend is observed with a 22% rise from 9620 kbpd to 11750 kbpd in U.S. crude oil movements. The quantity transported via pipeline also increases accordingly while the volume of waterway transportation decreases. This result indicates that the opening of the global market to U.S. would lead to increased land transport in order to satisfy demand.

4.5.5 U.S. exports, Midwest pipeline investments and Bakken rail caps

This scenario is a simultaneous implementation of the three policies already considered: capping rail flows from the Bakken region, building two pipelines—one from North Dakota and the other from Michigan, and lifting the U.S. crude oil export ban.

In 2015, the new Michigan-New Jersey pipeline is utilized to supply 164 kbpd

of heavy-sour crude to the East Coast, which replaces oil tanker movements from Eastern Canada. Meanwhile, the other new pipeline from Montana to Washington transports 367 kbpd of the same quality of crude. Accordingly, net imports in PADD5 fall to 805 kbpd, a 35% decrease compared to the base case. With the Bakken rail cap in effect, intra-U.S. rail movements drop by 2% to 6995 kbpd, as intra-U.S. pipeline movements increase by 37% to 5279 kbpd.

In 2018, the capacity of the newly added Montana-Washington pipeline is fully utilized. Exports to the Rest of the World from PADD5 are registered at a value of 336 kbpd. About two-thirds of this volume is light-sweet oil from the Bakken region. Meanwhile, actual imports fall to 356 kbpd, reducing net crude imports at PADD5 to 20 kbpd.

Net imports at PADD3 in both years are slightly higher than in the "U.S. Crude Oil Export Ban Lifted" scenario but still considerably lower than in the base case (less 31% and 33%, respectively). A similar situation can be seen for PADD1 in 2018. In terms of intra-U.S. rail flows, however, the key result is a 26% reduction relative to the base case. With no restrictions on exports, the new pipelines and the rail caps result in more oil being transported to PADD5, making the region more important as an exporter of crude. Thus, less crude oil moves to PADD3 and thereby reducing the crude-by-rail impact in the U.S.

4.6 Discussion

Crude-by-rail flows within the U.S. are reduced under the "Capping Bakken Rail Flows" and "U.S. Midwest Pipeline Investments" scenarios, but these improvements are not realized until 2018, with decreases of 21% and 9% respectively. In the counterfactual scenario analysis for the year 2015, restricting the rail capacities from the Bakken Region results in only a 1% reduction. We note that while the pipeline in-

vestments result in a 13% increase in rail flows in 2015, the impact is only limited to two pairs of neighboring states: Texas-Louisiana and Washington-Oregon. Thus, the ability to analyze flows at the U.S. state level will be important for more accurate determinations of the environmental effects of crude oil transportation.

In the "U.S. Oil Export Ban Lifted" scenario, rail flows increase in both years, indicating that simply lifting the crude oil export ban in the U.S. will not solve the crude-by-rail problem in the medium term. However, when this is done in conjunction with pipeline investments and Bakken rail caps, maximum reductions in overall U.S. rail flows are realized, both in 2015 and 2018. Table 4.4 shows the relative rail

Table 4.4 Changes in crude-by-rail [CBR] scenario flows relative to the base case among the U.S. nodes (states) in 2015 and 2018.

Scenario	**2015 CBR flow**		**2018 CBR flow**	
	(kbpd)	% change	(kbpd)	% change
Base Case	7123	0	9620	0
Capping Bakken Rail Flows	7128	−1	7554	−21
U.S. Midwest Pipeline Investments	8077	+13	8771	−9
U.S. Oil Export Ban Lifted	7945	+12	11750	+22
U.S. Exports+Midwest Pipelines+Bakken Rail Caps	6992	−2	6147	−26

flow changes across the scenarios. The modal shares in each scenario are compared in Figure 4.11. In all the scenarios considered, there is no significant difference in consumer welfare with respect to the base case. This indicates that no one scenario has a particular advantage for the benefit of the refining sector.

Generally, these results show that in the near-to-medium term, restricting loading capacities from the Bakken region (North Dakota) is a consistently effective means of containing crude-by-rail flows. Investing in pipeline capacity from the same region will also eventually contribute to reducing crude-by-rail movements. A joint implementation of these strategies, however, provides the best mitigation of crude-by-rail.

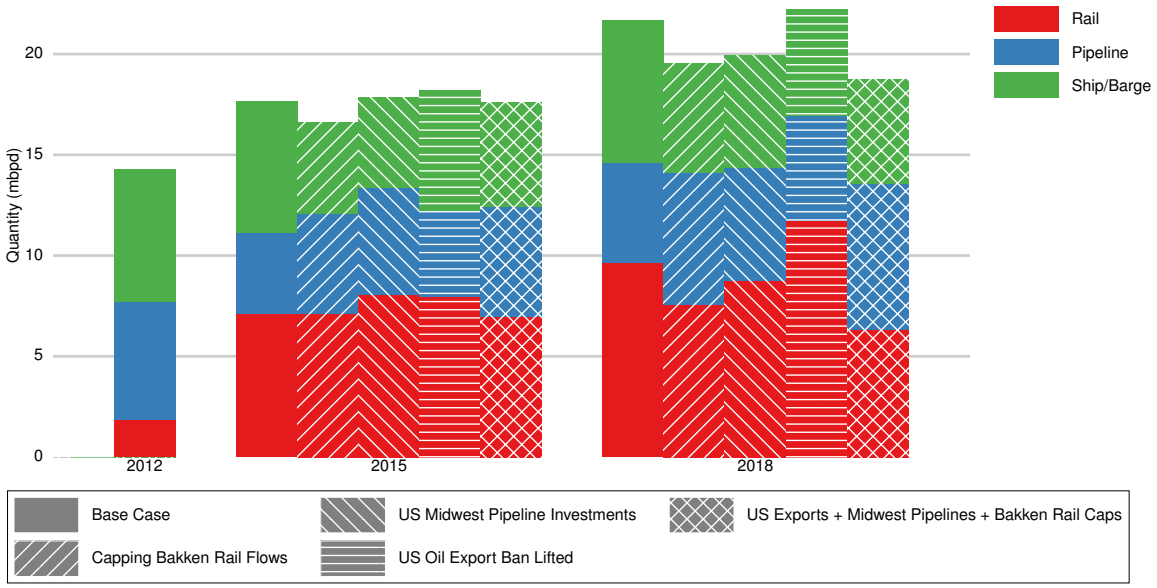

Figure 4.11 Multimodal interstate (U.S.) crude oil flows by scenario

4.7 Summary

We have presented a medium-term model of the North American crude oil market with U.S. state level granularity, which is a first in the literature to capture distinct crude oil qualities and the different modes of transportation across the continent. A key aspect of this effort was the investigation of the reduction of crude by rail with a focus on flows originating from the Bakken region in North Dakota. Two scenarios were implemented in this regard. We also considered the lifting of the U.S. crude oil export ban. Finally, we investigated a fourth scenario in which the policies of the first three scenarios are jointly implemented. Our results show that capping the rail flows from North Dakota or investing in pipeline capacity from the same area can help reduce the rail throughput in the United States. While only lifting the export ban results in increased rail flows, combining the export ban lifting with pipeline investments and rail caps provides the lowest crude-by-rail flows in the medium term up to 2018. All scenarios were similarly beneficial to the refining sector. These outcomes suggest that

integrated approaches are more likely to be successful in tackling the crude-by-rail problem.

We have not fully treated the issue of emissions and quantifying the environmental impact of crude oil transportation. This is certainly a growing concern that deserves a considerable amount of thought, and NACOM remains relevant in addressing this issue. In our subsequent effort, we can then consider the environmental factors in each of the scenarios we design. An important development in the last year was the creation of the Oil Climate Index (OCI) [64]. This would be valuable in future work to quantify the environmental impact of crude oil production in North America, particularly with regard to climate. To further address the environmental risks of moving crude oil, an important enhancement of this model would be the inclusion of a mechanism to determine the monetary cost of transporting crude oil with regard to oil spill incidents. These incident costs could be further linked to various metrics, such as public health, quality of life and economic activity. This undertaking would involve additional data collection and statistical analyses. However, through this work, NACOM could be adapted as an even more powerful tool for robust scenario analyses toward improving infrastructure resilience and public health outcomes at various scales, up to the national level in the United States and eventually for the North American continent.

With regard to crude oil types, we differentiated between the heavy and light qualities. On the production side, the heavy-to-light ratios were obtained from various industry reports and estimated otherwise. U.S. refining capacities for both qualities were calculated from average API gravity values of refined crude in each state as reported by the EIA. A report recently released by the American Fuel & Petroleum Manufacturers provides details on U.S. regional crude oil refining capacites and output by quality [3]. Future work could incorporate these results along with the data also collected by Langer et al. [101] in their study.

At this stage of development, the model does not account for storage. Along with Cushing, Oklahoma, which serves as a major hub of crude oil movements originating both in Canada and the U.S., there are other major holding facilities, notably the Louisiana Offshore Oil Port system (LOOP) that influence market dynamics [124]. In recent years, storage has become a major concern in the industry as capacity is being stretched [94, 197]. Obtaining data on storage capacities and modeling the hub activity at Cushing is an improvement we hope to make in the subsequent iteration of this modeling effort. This will also enable us to better capture the complex movements between the U.S. Midwest and the Gulf of Mexico.

One other promising avenue for future work is the combination of NACOM with other models currently being developed for natural gas [48] and biofuels [30, 168] in North America. We can then consider the effects of fuel substitution and obtain a better picture of the oil and gas market in the United States. Further, in light of the complex unfolding of all these developments in the industry, we can develop more robust scenarios to provide more insight and detail, not only in the United States, but also in Canada and Mexico.

Critical advances have been made in U.S. energy policy, and the viability of renewables, such as biofuels, is rising. Yet, crude oil will remain a major component of the U.S. energy landscape for the next several decades [161]. In Canada, crude oil is still considered a mainstay of the nation's economy, as investments in production capacity and transportation continue to grow [136, 74]. With proper reform, Mexico's oil industry can overcome current inefficiencies to transform its energy sector and economy [164, 45]. The recently approved crude oil swap between the U.S. and Mexico is also expected to be mutually beneficial to U.S. exporters and Mexico refiners [22]. Given all these trends, there will exist a need in the near-to-medium term to find the best intersections for policy and market decisions to minimize the environmental impact of crude oil production and transportation on the continent.

CHAPTER 5

Conclusion and outlook

In the preceding three chapters, we have described approaches to solve systems problems using optimization, data mining and modeling methods. We have seen the importance of schematic mapping and the promise it holds for increasing user access to transportation networks of increasing complexity, and even to other non-transit pathways. Bicycling has been proven to be a key element of sustainable development, urban transport, and safe and healthy lifestyles. Our work has shown that globally, household ownership is on the decline, yet the results also provide answers to the nature of the patterns that currently exist, while indicating avenues for discovering how to replicate successes across various locations. As concerns over the climate grow, various nations are looking to diversify their energy sources with greater attention and investments being made in renewable energy, especially biofuels. However, crude oil may remain an important piece of the global energy industry for the next quarter century, as production has surged in North America in the last six years, notwithstanding the decline in prices. To provide solutions to one of the pressing issues in the industry today—crude-by-rail—we developed the first oil market model for North America that incorporates multiquality and multimodal movements, implementing scenarios to find the best strategy for sustainably reducing the volume of

crude transported via rail in the medium term. Further directions for even more robust policy decisions will involve an integrated modeling approach to include natural gas and biofuels, in combination environmental and climate impact assessment tools.

Transportation and energy are invariably linked. Transportation systems require energy to operate. Energy systems cannot exist without supporting transportation networks. As with all physical systems, the consumers or users play a key role in energy and transit. With the proliferation of technology and modern means of communication, consumers can now interact with markets and networks in a variety of ways and for a motley of applications. As a result, social network analysis is becoming increasingly important as we seek to understand and tackle new challenges in the systems of the present and the near future. Bicycle sharing systems have been growing in popularity in the past decade, while the prospect of a major shift to autonomous electric vehicles is likely to become reality in next two decades. Integer programming models naturally lend themselves to solving problems associated with systems incorporating these two modes of travel, as they are poised to become fixtures in sustainable transit and energy programs.

In Section 5.1, we describe recent trends in bicycle sharing and autonomous vehicle systems research. We further illustrate a realistic application of the methods described in this dissertation to the partial development of a hypothetical autonomous electric vehicle taxi network (Section 5.2). Finally, in Section 5.3, we motivate social network modeling through the example of the "small-world problem."

5.1 Modeling the next generation of transit systems

Bicycle sharing programs have become of staple of major urban centers across the world. In the United States, the growth of bikesharing has been remarkable. In 2010, there were only 7 cities or areas with active programs, notably Washington D.C.,

Minneapolis, Denver and Chicago. With 114 stations, Washington D.C. boasted the largest system. In 2012, the number of U.S. urban areas with bikeshare programs grew to 27. In 2013, this number grew by nearly 50% to 40 areas, with New York narrowly edging out the D.C. area in terms of size, with 330 stations. The most recent data (from 2014) shows there are 44 active systems in the country. San Diego, Seattle and Miami are the major latest additions. Chicago, New York and D.C. remain the largest networks with 300, 328 and 347 stations, respectively. [16]

Sustained efforts in realizing the feasibility of autonomous (self-driving) [electric] vehicles has increased the anticipation of environmentally friendly driving systems. In particular, a taxi system of AVs servicing a network is one such realization. As with bikeshare, issues of charging station location and fleet management would have to be considered. Gacias and Meunier [58] have demonstrated an MIP and simulation approach in the development of such a system. Chen et al. [29] used an agent-based modeling (ABM) approach to investigate the operations of a shared autonomous electric vehicle fleet (SAEV). They have also explored issues of fleet reallocation and pricing through a similar approach [28]. Beyond these, there is a growing body of work regarding AV-based transportation systems as they certainly will be key to the future sustainable transit.

The rapid expansion of these systems have given rise to problems of design, location, fleet size and management, among others. Integer programming and other optimization methods remain highly relevant to providing solutions to these issues. Moreover, data mining and machine learning will be increasingly important in providing information on user preferences to better customize services. Schematic maps will be useful for efficient visualizations of the rapidly growing bicycle sharing networks. New paradigms will have to be developed for dynamic and customized situations, as users will require solutions for navigation and connectivity.

To illustrate these potential applications, we describe the development of a data

mining process and optimization model for an autonomous vehicle fleet network in the following section.

5.2 Development of an autonomous vehicle taxi network

Consider a city planning to phase out its existing taxi system in favor of an autonomous fleet of electric vehicles that can be summoned by passengers within the city. This new fleet would contribute to reduced carbon emissions and improve the quality of life of the city's inhabitants. It would also complement existing urban transit systems serving city, which might include a bike network and a subway. For efficiency and cost minimization, the city would need to obtain data to establish demand patterns to inform the design of the new network. Models would also need to be implemented to solve problems for station and fleet allocation. As a general rule for the quality of service of this network, the city would like to ensure that passenger wait times never exceed 7 minutes.

5.2.1 Data for network design

One approach for data collection would be to install GPS tracking devices in a sample of taxis servicing the city. This number may be chosen to reflect the percentage of taxi demand the government hopes to satisfy with automated vehicles (AVs). These devices would also be able to record entry points and exit points for passengers. It would appear that taxis typically have devices that already do this, so the necessary information could be tracked and obtained from the taxis in the sample.

The data collection can be performed over a period of several months (6–10, for instance) or even a year or two, depending on time constraints. Afterwards, a predictive model can be developed to estimate the origin-destination pairs and the

respective trip demand in the network. Density-based clustering can be performed to aggregate node locations in the network. Choices for the predictive model could be ARIMA (autoregressive integrated moving average) [120] or an artificial neural network model [88]. The model would provide forecasts for the specified time periods. Based on the nature of the demand, the length of the time periods can be adjusted in order to best capture ground truth.

5.2.2 Charging station location

Here we want to find the minimum number of charging stations to be located in the network in order to satisfy demand and to meet the required level of customer satisfaction (at most 7 minutes wait time for vehicle to reach the origin).

First, we define the following sets:

$i, j, k \in N$ demand points (origin, destination and possible charging station location)

$v \in V$ vehicles

We assume, for now, that the number of vehicles is unconstrained. We also assume that all vehicles are at charging stations when not executing a trip.

Further, we define x_i as the decision variable that a given node i in the network will be selected as the location for a charging station. The decision variable governing whether a vehicle v is summoned from node i to service a trip at j is given as z_{vij}. Thus, we have the mixed integer program:

$$\min \sum_{i \in N} x_i \tag{5.1}$$

s.t.

$$x_i, z_{vij} \in \{0, 1\} \tag{5.2}$$

$$z_{vij} T(i, j) \leq 7 + M(1 - x_i) \tag{5.3}$$

$$\sum_{v \in V} \sum_{i \in N} z_{vij} = \sum_{k \in N} d_{jk} \tag{5.4}$$

where M is chosen as large constant (a good choice would be: $M = \max T(i,j)$) and d_{jk} is the number of trips demanded from origin j to destination k.

Constraint (5.2) ensures x and z are binary, thus dictating that only one charging station can be placed at a node and that only one vehicle is used per trip. The maximum wait time constraint (5.3) applies when a vehicle is chosen from a node that in the solution is selected as a charging station. The final constraint (5.4) guarantees that demand is met at each node.

This model is formulated for a given time period in the network. It does not consider the temporal differences (with respect to the demand) within the period, which is a limitation. Another observation is this: even though demand is satisfied, the number of stations that results from this formulation, while optimal, may not be efficient. For the sake of simplicity, we have not considered maximizing demand or utilizing the concept of covering to maximize demand (service) at the nodes surrounding each charging station.

Since the model is defined for only one time period, it could be run for all the time periods (since demand will vary) and then the superset of charging stations (determined in all the executions) chosen as the operating minimum, if feasible. Otherwise, the largest minimum can be elected.

5.2.3 Fleet size optimization

Assuming that the charging stations have been located, we can now define two new subsets $S^b, S^e \subset N$, which contain the nodes that serve as charging stations. S^b and S^e both consist of the same nodes, but having them in different sets enables us to track vehicles leaving a charging station at the *beginning* of an upcoming trip and those entering a charging station at the *end* of a just completed trip. In similar fashion, we define the sets O and D, which consists of the same nodes but grouped into *origin* and *destination*.

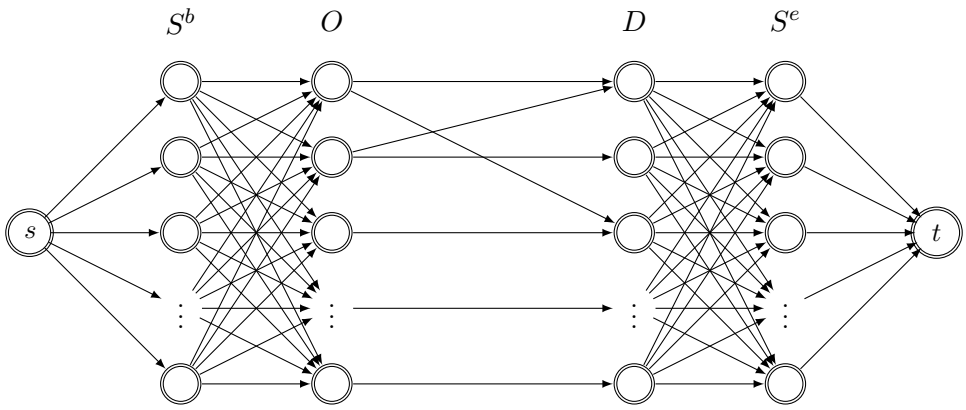

Figure 5.1 Diagram of flow model for fleet size minimization in an autonomous taxi network. The capacity of each edge is 1, and the flow along each edge is binary.

To solve for the minimum fleet size, we employ a network flow model in a directed acyclic graph $G(W, E)$. The vertices $w \in W$ are in S^b, O, D and S^e, with the addition of a source node s and a sink node t. (See Figure 5.1.) The directed arcs $e \in E$ connect:

(i) all the nodes in S^b to those in O, based on the assumption that in this network, an AV can reach any demand point from a charging station;

(ii) nodes in O to those in D, as determined by the OD pairs in the trip demand information;

(iii) all nodes in D to every possible node in S^e, also assuming that an AV can be recharged at any station after it completes its trip;

(iv) the source node s to all the nodes in S^b;

(v) all the nodes in S^e to the sink t.

Only outflows are allowed from s, and only inflows are allowed into t. We do not need a decision variable for vehicle selection in this formulation, as each flow value represents the vehicles moving from one node to another. The model formulation is shown below.

$$\min \ v \tag{5.5}$$

s.t.

$$\sum_{i \in S^b} x_{si} = v \tag{5.6}$$

$$\sum_{i \in S^e} x_{it} = v \tag{5.7}$$

$$\sum_{j \in O,D} x_{ij} - \sum_{j \in O,D} x_{ji} = 0 \tag{5.8}$$

$$\sum_{i \in S^b} x_{si} - \sum_{i \in S^b} x_{ij} \geq 0 \tag{5.9}$$

$$x_{ij} T(i,j) \leq 7 \quad \forall i \in S^b, j \in O \tag{5.10}$$

$$x_{ij} = d_i \quad \forall j \in O \tag{5.11}$$

$$x_{ij} \geq 0 \tag{5.12}$$

$$x_{ij} \in \mathbb{Z} \tag{5.13}$$

Constraints (5.6) and (5.7) ensure that the entire AV fleet is available for circulation in the network. The balance equation (5.8) ensures that the number of outgoing vehicles from from an origin or destination node is equal to the number of incoming vehicles at that same node. This ensures that no vehicle is left idling at any node in O or D. For the nodes in S^b (charging stations), the balance constraint is relaxed. Instead the net outflow is bounded below by zero, which allows for some AVs to remain in the charging stations. Constraint (5.10) guarantees that the customer satisfaction requirement is met (wait times for vehicle arrival do not exceed 10 minutes). Meanwhile, (5.11) imposes demand fulfillment at each origin node. Finally, (5.12) and (5.13) are integrality and positivity constraints on the flow variables.

This model has been assumed for the specified time period. Since overall network and nodal demand might vary in each period, it should be run for all the time periods

with the average minimum fleet [integer] value computed and compared to the greatest possible minimum value produced in all the runs. The final choice can then be chosen as the greater of the two, for a robust determination.

One limitation of this framework is that temporal differences within the period have not been accounted for. Thus, total trip times (which include wait time and charging time) are not considered, nor is the prospect of reusing a vehicle for another trip if its prior trip time is considerably shorter compared to the length of the period and with regard to the start times of other trips demanded within the period. Total trips demanded within each period are therefore assumed to be satisfied at the same time.

5.2.4 Dealing with congestion

The traffic conditions can be used to activate a new set of congestion constraints in the optimization program. Each time new estimates are generated, the model can be executed to provide an updated fleet size.

One idea on how to accomplish this would be to calculate the change in travel times between the affected origin and destination times. These in turn can be used to estimate a reduction (for instance, using a friction factor) in the number of trips demanded from affected points in each time period. In reality, demand may not decline with congestion, but it is likely that not all requested trips may be resolved, especially if the AVs cannot get to the origin nodes in time and still holding the assumption of maintaining customer satisfaction through the 7-minute wait time maximum. Thus, it makes sense to account for this effect by reducing the trips demanded at the affected points accordingly. Running the optimization routine would then result in a lower minimum fleet size. The excess vehicles can also be taken out at the most congested nodes. Each time a rerun produces a greater fleet minimum than the previous run, more vehicles must be added to the fleet to make up the difference.

It may also be necessary to account for the cost of removing and adding vehicles to the fleet. This must be minimized—placing this minimization problem as a constraint (or sub-problem) may help govern the nodes chosen for de-allocation or re-allocation. Furthermore, a threshold can be designed at which these actions are ultimately triggered. This can be in the form of a minimum number of traffic updates required for a removal or addition, or it could be based on the rate of change of traffic conditions.

5.3 Social network analytics

A host of network models have been developed to study social interactions in various contexts. These models have been borne out of the growing complexity of modern networks in which scientists and engineers have been able to draw behavioral parallels with more fundamental systems.

5.3.1 The small-world problem

One of the earliest investigations into the structure of social connections was performed by Milgram [118] in the famous small-world problem. The experiment was conducted by selecting a random sample of participants in Wichita, Kansas, to send a package to the same target in Cambridge, Massachusetts, simply by passing it on to someone most likely to know (or know someone who knew) the target. The only condition was that each immediate link in the chain had to know each other on a first-name basis.

Travers and Milgram [187] conducted a similar study with a more technical experimental design using a sample population from Omaha, Nebraska, and to a different target also in Cambridge, Mass. The empirical results established the historical "six degrees of separation" rule, as the median number of links in all completed chains in

the Nebraska study was 5.

While these studies did not provide detailed information on the structure of these social associations, they sparked decades of further work in unearthing these patterns—the how, why, what, when and where.

5.3.2 Applications and potential for systems research

Various properties can be of interest when a system is modeled as a social network. Some of these include patterns of growth and resilience, which are relevant within the contexts of academia [170, 130], infrastructure and population [183, 26, 177, 12]. Measures of influence of the nodes in a network are also consequential [4]. If the nodes already belong to certain groups, another property of interest is mixing, which is concerned with nature of the connectedness of nodes by their groupings [129]. Mixing patterns can provide insight into the associational behaviors of entities in a network [128, 72, 151].

In the last few decades, social network models have enabled us to understand and harness these pattern discoveries in order to strengthen and improve our systems beyond energy and transportation. As we seek robust and sustainable solutions for the systems that gird our infrastructure and ultimately support our survival, deeper integrations of these various modeling and representation approaches will be critical to addressing the challenges we face today and those of a rapidly approaching future.

APPENDIX A

Schematic mapping program formulation

We provide a summary of the variables and equations that make up the mixed binary linear program described in Chapter 2. For further background, the reader is referred to [134] and [110].

Table A.1 Parameters, variables and sets in schematic mapping program

Symbol	Description
$x(u), y(u), z_1(u), z_2(u)$	coordinate variables
$\delta_k(u, v, w), \quad i \in \{1, 2\}$	binary variables for bend cost
$\gamma_c(e_1, e_2, f), \quad c \in \{N, NE, ..., NW\}$	binary variables for edge spacing in each cardinal (axial) direction
$i \in \{-1, 0, 1\}$	positional index: original position or one sector back or forward
$\alpha_i(u, v)$	binary variable that switches position for sector and direction
$\text{sec}_i(u, v) \quad i \in \{-1, 0, 1\}$	sector assignment for edge

$\text{dir}(u, v)$	directional variable indicating sector chosen in solution
$\text{bend}(u, v, w)$	bend cost for edges uv and vw
$\text{shift}(u, v)$	shift cost per edge
M	large constant used in modeling disjunctivity
$\ell_{\max}(u, v), \ell_{\min}(u, v)$	upper and lower bounds on length of edge uv
$d_{\min}$	minimum spacing between vertices on nonadjacent edge pairs
$\beta(u, v_j), \quad j \in \{1, ..., \deg(u)\}$	set of vertices of specified lower bound of degree
$\varepsilon = 10^{-3}$	augmentation factor in AUGMECON2 ε-constraint method
s_{shift}	slack variable for shift function in AUGMECON2
r_{shift}	range of shift payoff table values in AUGMECON2
e_{shift}	RHS of equality constraint computed from payoff table
ub_{shift}	upper bound of shift function in payoff table
$i_{\text{shift}} \in \{0, 1, ..., g_{\text{shift}}\}$	steps for grid points in AUGMECON2
g_{shift}	number of desired grid intervals for AUGMECON2
λ_{bend}	weighting factor for bend function

λ_{shift}	weighting factor for shift function

Objective functions:

$$C_{\text{bend}} = \sum_{L \in \mathcal{L}} \sum_{uv,vw \in L} \text{bend}(u, v, w) \tag{A.1}$$

$$C_{\text{shift}} = \sum_{uv \in E} \text{shift}(u, v) \tag{A.2}$$

Augmented ε-constraint formulation (O&S–AUGMECON2):

$$\min : \quad C_{\text{bend}} - \varepsilon \frac{s_{\text{shift}}}{r_{\text{shift}}} \tag{A.3}$$

s.t.

$$C_{\text{shift}} + s_{\text{shift}} = e_{\text{shift}} \tag{A.4}$$

$$e_{\text{shift}} = \text{ub}_{\text{shift}} - \frac{i_{\text{shift}} r_{\text{shift}}}{g_{\text{shift}}} \tag{A.5}$$

General constraints (*)

Weighting method formulation (O&S–WM$_3$):

$$\min : \quad \lambda_{\text{bend}} C_{\text{bend}} + \lambda_{\text{shift}} C_{\text{shift}} \tag{A.6}$$

s.t.

General constraints (*)

General constraints (*):

$$\Delta\text{dir}(u, v, w) = \text{dir}(u, v) - \text{dir}(v, w) \tag{A.7}$$

$$\text{bend}(u, v, w) = \min\{|\Delta\text{dir}(u, v, w)|, 8 - |\Delta\text{dir}(u, v, w)|\} \tag{A.8}$$

$$\begin{aligned} -\text{bend}(u,v,w) &\leq \Delta\text{dir}(u,v,w) - 8\delta_1(u,v,w) + 8\delta_2(u,v,w) \\ \text{bend}(u,v,w) &\geq \Delta\text{dir}(u,v,w) - 8\delta_1(u,v,w) + 8\delta_2(u,v,w) \end{aligned} \tag{A.9}$$

$$-M \cdot \text{shift}(u,v) \leq \text{dir}(u,v) - \text{sec}_{\text{orig}}(u,v) \leq M \cdot \text{shift}(u,v) \tag{A.10}$$

$$M = \sum_{e \in E} e(u,v) \cdot \ell_{\max}(u,v) \tag{A.11}$$

$$\text{sec}_0(u,v) = \begin{cases} 0 & 337.5° \leq \angle uv < 22.5° \\ 1 & 22.5° \leq \angle uv < 67.5° \\ 2 & 67.5° \leq \angle uv < 112.5° \\ 3 & 112.5° \leq \angle uv < 157.5° \\ 4 & 157.5° \leq \angle uv < 202.5° \\ 5 & 202.5° \leq \angle uv < 247.5° \\ 6 & 247.5° \leq \angle uv < 292.5° \\ 7 & 292.5° \leq \angle uv < 337.5° \end{cases} \tag{A.12}$$

$$\text{sec}_{+1} = \text{sec}_0 + 1 \mod 8 \tag{A.13}$$

$$\text{sec}_{-1} = \text{sec}_0 - 1 \mod 8 \tag{A.14}$$

$$\text{sec}_i(u,v) = \text{sec}_i(v,u) + 4 \mod 8 \tag{A.15}$$

$$\sum_{i \in \{-1,0,1\}} \alpha_i(u,v) = 1 \tag{A.16}$$

Octilinearity and edge length constraints

$$\text{dir}(u,v) = \sum_{i \in \{-1,0,1\}} \text{sec}_i(u,v) \cdot \alpha_i(u,v) \tag{A.17}$$

$$\text{dir}(v,u) = \sum_{i \in \{-1,0,1\}} \text{sec}_i(v,u) \cdot \alpha_i(u,v) \tag{A.18}$$

$$\text{dir}(u,v) = \text{dir}(v,u) + 4 \mod 8 \tag{A.19}$$

$$\mathrm{sec}_i(u,v)=0:\begin{cases} y(u)-y(v) & \leq & M(1-\alpha_i(u,v)) \\ -y(u)+y(v) & \leq & M(1-\alpha_i(u,v)) \\ -x(u)+x(v) & \geq & -M(1-\alpha_i(u,v))+\ell_{\min}(u,v) \end{cases} \tag{A.20}$$

$$\mathrm{sec}_i(u,v)=1:\begin{cases} z_2(u)-z_2(v) & \leq & M(1-\alpha_i(u,v)) \\ -z_2(u)+z_2(v) & \leq & M(1-\alpha_i(u,v)) \\ -z_1(u)+z_1(v) & \geq & -M(1-\alpha_i(u,v))+\ell_{\min}(u,v) \end{cases} \tag{A.21}$$

$$\mathrm{sec}_i(u,v)=2:\begin{cases} x(u)-x(v) & \leq & M(1-\alpha_i(u,v)) \\ -x(u)+x(v) & \leq & M(1-\alpha_i(u,v)) \\ -y(u)+y(v) & \geq & -M(1-\alpha_i(u,v))+\ell_{\min}(u,v) \end{cases} \tag{A.22}$$

$$\mathrm{sec}_i(u,v)=3:\begin{cases} z_1(u)-z_1(v) & \leq & M(1-\alpha_i(u,v)) \\ -z_1(u)+z_1(v) & \leq & M(1-\alpha_i(u,v)) \\ z_2(u)-z_2(v) & \geq & -M(1-\alpha_i(u,v))+\ell_{\min}(u,v) \end{cases} \tag{A.23}$$

$$\mathrm{sec}_i(u,v)=4:\begin{cases} y(u)-y(v) & \leq & M(1-\alpha_i(u,v)) \\ -y(u)+y(v) & \leq & M(1-\alpha_i(u,v)) \\ x(u)-x(v) & \geq & -M(1-\alpha_i(u,v))+\ell_{\min}(u,v) \end{cases} \tag{A.24}$$

$$\mathrm{sec}_i(u,v)=5:\begin{cases} z_2(u)-z_2(v) & \leq & M(1-\alpha_i(u,v)) \\ -z_2(u)+z_2(v) & \leq & M(1-\alpha_i(u,v)) \\ z_1(u)-z_1(v) & \geq & -M(1-\alpha_i(u,v))+\ell_{\min}(u,v) \end{cases} \tag{A.25}$$

$$\mathrm{sec}_i(u,v)=6:\begin{cases} x(u)-x(v) & \leq & M(1-\alpha_i(u,v)) \\ -x(u)+x(v) & \leq & M(1-\alpha_i(u,v)) \\ y(u)-y(v) & \geq & -M(1-\alpha_i(u,v))+\ell_{\min}(u,v) \end{cases} \tag{A.26}$$

$$\mathrm{sec}_i(u,v) = 7 : \begin{cases} z_1(u) - z_1(v) & \leq & M(1-\alpha_i(u,v)) \\ -z_1(u) + z_1(v) & \leq & M(1-\alpha_i(u,v)) \\ -z_2(u) + z_2(v) & \geq & -M(1-\alpha_i(u,v)) + \ell_{\min}(u,v) \end{cases} \tag{A.27}$$

$$x(v), y(v) \leq M \quad \forall v \in V \tag{A.28}$$

$$\begin{aligned} x(u) - x(v) &\leq \ell_{\max}(u,v) \\ -x(u) + x(v) &\leq \ell_{\max}(u,v) \\ y(u) - y(v) &\leq \ell_{\max}(u,v) \\ -y(u) + y(v) &\leq \ell_{\max}(u,v) \end{aligned} \tag{A.29}$$

Circular order constraints

$$\mathrm{dir}(u,v_j) \leq \mathrm{dir}(u,v_{j++1}) - 1 + 8\beta(u,v_j), \quad j = \{1,2,...,\deg(u)\} \tag{A.30}$$

$$\sum_{j=1}^{\deg(v)} \beta(u,v_j) = 1 \quad \forall u : \deg(u) \geq 2 \tag{A.31}$$

Edge spacing and crossing constraints

$$\sum_{c \in \{\mathrm{N},...,\ \mathrm{NE}\}} \gamma(e_1,e_2,f) \geq 1 \tag{A.32}$$

$$\begin{aligned} x(u_2) - x(u_1) &\leq M(1-\gamma_{\mathrm{E}}(e_1,e_2,f)) - d_{\min} \\ x(u_2) - x(v_1) &\leq M(1-\gamma_{\mathrm{E}}(e_1,e_2,f)) - d_{\min} \\ x(v_2) - x(u_1) &\leq M(1-\gamma_{\mathrm{E}}(e_1,e_2,f)) - d_{\min} \\ x(v_2) - x(v_1) &\leq M(1-\gamma_{\mathrm{E}}(e_1,e_2,f)) - d_{\min} \end{aligned} \tag{A.33}$$

$$
\begin{aligned}
z_1(u_2) - z_1(u_1) &\leq M(1 - \gamma_{\mathrm{NE}}(e_1, e_2, f)) - d_{\min} \\
z_1(u_2) - z_1(v_1) &\leq M(1 - \gamma_{\mathrm{NE}}(e_1, e_2, f)) - d_{\min} \\
z_1(v_2) - z_1(u_1) &\leq M(1 - \gamma_{\mathrm{NE}}(e_1, e_2, f)) - d_{\min} \\
z_1(v_2) - z_1(v_1) &\leq M(1 - \gamma_{\mathrm{NE}}(e_1, e_2, f)) - d_{\min}
\end{aligned} \tag{A.34}
$$

$$
\begin{aligned}
y(u_2) - y(u_1) &\leq M(1 - \gamma_{\mathrm{N}}(e_1, e_2, f)) - d_{\min} \\
y(u_2) - y(v_1) &\leq M(1 - \gamma_{\mathrm{N}}(e_1, e_2, f)) - d_{\min} \\
y(v_2) - y(u_1) &\leq M(1 - \gamma_{\mathrm{N}}(e_1, e_2, f)) - d_{\min} \\
y(v_2) - y(v_1) &\leq M(1 - \gamma_{\mathrm{N}}(e_1, e_2, f)) - d_{\min}
\end{aligned} \tag{A.35}
$$

$$
\begin{aligned}
-z_2(u_2) + z_2(u_1) &\leq M(1 - \gamma_{\mathrm{NW}}(e_1, e_2, f)) - d_{\min} \\
-z_2(u_2) + z_2(v_1) &\leq M(1 - \gamma_{\mathrm{NW}}(e_1, e_2, f)) - d_{\min} \\
-z_2(v_2) + z_2(u_1) &\leq M(1 - \gamma_{\mathrm{NW}}(e_1, e_2, f)) - d_{\min} \\
-z_2(v_2) + z_2(v_1) &\leq M(1 - \gamma_{\mathrm{NW}}(e_1, e_2, f)) - d_{\min}
\end{aligned} \tag{A.36}
$$

$$
\begin{aligned}
-x(u_2) + x(u_1) &\leq M(1 - \gamma_{\mathrm{W}}(e_1, e_2, f)) - d_{\min} \\
-x(u_2) + x(v_1) &\leq M(1 - \gamma_{\mathrm{W}}(e_1, e_2, f)) - d_{\min} \\
-x(v_2) + x(u_1) &\leq M(1 - \gamma_{\mathrm{W}}(e_1, e_2, f)) - d_{\min} \\
-x(v_2) + x(v_1) &\leq M(1 - \gamma_{\mathrm{W}}(e_1, e_2, f)) - d_{\min}
\end{aligned} \tag{A.37}
$$

$$
\begin{aligned}
-z_1(u_2) + z_1(u_1) &\leq M(1 - \gamma_{\mathrm{SW}}(e_1, e_2, f)) - d_{\min} \\
-z_1(u_2) + z_1(v_1) &\leq M(1 - \gamma_{\mathrm{SW}}(e_1, e_2, f)) - d_{\min} \\
-z_1(v_2) + z_1(u_1) &\leq M(1 - \gamma_{\mathrm{SW}}(e_1, e_2, f)) - d_{\min} \\
-z_1(v_2) + z_1(v_1) &\leq M(1 - \gamma_{\mathrm{SW}}(e_1, e_2, f)) - d_{\min}
\end{aligned} \tag{A.38}
$$

$$
\begin{aligned}
-y(u_2) + y(u_1) &\leq M(1 - \gamma_{\mathrm{S}}(e_1, e_2, f)) - d_{\min} \\
-y(u_2) + y(v_1) &\leq M(1 - \gamma_{\mathrm{S}}(e_1, e_2, f)) - d_{\min} \\
-y(v_2) + y(u_1) &\leq M(1 - \gamma_{\mathrm{S}}(e_1, e_2, f)) - d_{\min} \\
-y(v_2) + y(v_1) &\leq M(1 - \gamma_{\mathrm{S}}(e_1, e_2, f)) - d_{\min}
\end{aligned}
\tag{A.39}
$$

$$
\begin{aligned}
z_2(u_2) - z_2(u_1) &\leq M(1 - \gamma_{\mathrm{SE}}(e_1, e_2, f)) - d_{\min} \\
z_2(u_2) - z_2(v_1) &\leq M(1 - \gamma_{\mathrm{SE}}(e_1, e_2, f)) - d_{\min} \\
z_2(v_2) - z_2(u_1) &\leq M(1 - \gamma_{\mathrm{SE}}(e_1, e_2, f)) - d_{\min} \\
z_2(v_2) - z_2(v_1) &\leq M(1 - \gamma_{\mathrm{SE}}(e_1, e_2, f)) - d_{\min}
\end{aligned}
\tag{A.40}
$$

APPENDIX B

Further information on methods, data and code for bicycle ownership study

I clarify aspects of our extraction and processing of survey data in Section B.1. Section B.2 contains plots of the bicycle ownership values for all the 150 countries analyzed, while Section B.3 includes the complete reference dataset. All the scripts (written in Python and R) and resources can be found at `ce.jhu.edu/sauleh/obls-gbu`, and the organizational structure of the code is provided in Section B.4.

B.1 Data collection from household surveys

In this section, we describe how household bicycle availability and household population data was collected and processed from sources listed.

B.1.1 Survey mining

Initially, we obtained bicycle ownership data from the surveys shown in Table B.1 conducted in various countries over 1970–2012. We used 1989 as the starting year for our analyses, as data for preceding years was only available for Chile, Indonesia,

Malaysia and Thailand. In these surveys, the relevant inquiry determined in a binary fashion if the households had one bicycle (or more) available. Many survey records were accessed using Stata and then compiled into a spreadsheet. Appendix A contains ownership data plots for all the countries, indicating the survey source of each point.

Table B.1 Survey sources for bicycle ownership data. *Sources 12, 13 and 14 were unused, as they were educational surveys conducted on school children and not nationally representative of households.

ID	Source	Acronym	Years conducted
1	World Health Surveys [145]	WHS	2002
2	Demographic and Health Surveys [40]	DHS	Multiple
3	Malaria Indicator Surveys [39]	MIS	2006-7, 2008-9
4	Integrated Public Use Microdata Services [119]	IPUMS	Multiple
5	International Crime Victim Surveys [67]	ICVS	1989-2002
6	India National Census [82]	INC	2001, 2011
7	Multiple Indicator Cluster Surveys 4 [86]	MICS4	2010-2011
8	Multiple Indicator Cluster Surveys 3 [85]	MICS3	2005-2009
9	Study on Global Ageing and Adult Health [144]	SAGE	2007-2011
10	Integrated Survey on the Welfare of the Population [84]	IBEP	2008-2009
11	Enquete Demographique et de Sante et a Indicateurs Multiples [83]	EDSM	2006
*12	Southern & Eastern Africa Consortium for Monitoring Educational Quality [174]	SACMEQ3	2005
*13	Southern & Eastern Africa Consortium for Monitoring Educational Quality [173]	SACMEQ2	1999
*14	Southern & Eastern Africa Consortium for Monitoring Educational Quality [173]	SACMEQ1	1995

The educational surveys conducted by the Southern and Eastern Africa Consortium for Monitoring Educational Quality (SACMEQ) were found to not be indicative of the national populations in comparison with data from other surveys, since the primary respondents were school pupils. The SACMEQ results were therefore not included in our analyses. For some countries, ownership data was available from multiple surveys within the same year. In initializing the data, we took the average value of the country-years where this was the case (for example, Vietnam had data available from both WHS and DHS in 2002). Also, data from any of the countries in the

United Kingdom (England, Northern Ireland, Scotland and Wales) was taken as representative of the UK. Finally, the International Crime Victim Surveys (ICVS) 1996 datapoint for Yugoslavia was considered valid for Macedonia. We therefore ended up with 150 countries after this pre-processing step.

There are a total of 452 data points. Table B.2 lists the initial countries in our dataset and their corresponding three-letter acronyms (ISO) before pre-processing.

Table B.2 Initial country names for which data was available. For analyses, Yugoslavia was considered as Macedonia, West Germany was taken as Germany, and England, Northern Ireland, Scotland and Wales were all considered as the United Kingdom. Data for Seychelles and Zanzibar was only available from the unused educational surveys, hence they do not appear in the final analyses.

Country	ISO	Country	ISO	Country	ISO
Afghanistan	AFG	Greece	GRC	Peru	PER
Albania	ALB	Guatemala	GTM	Philippines	PHL
Angola	AGO	Guinea	GIN	Poland	POL
Argentina	ARG	Guinea-Bissau	GNB	Portugal	PRT
Armenia	ARM	Guyana	GUY	Republic of Korea	KOR
Australia	AUS	Haiti	HTI	Republic of Moldova	MDA
Austria	AUT	Honduras	HND	Romania	ROM
Azerbaijan	AZE	Hungary	HUN	Russia	RUS
Bangladesh	BGD	India	IND	Rwanda	RWA
Belarus	BLR	Indonesia	IDN	Sao Tome and Principe	STP
Belgium	BEL	Iraq	IRQ	Scotland	XSC
Belize	BLZ	Ireland	IRL	Senegal	SEN
Benin	BEN	Israel	ISR	Serbia	ZZZX
Bhutan	BTN	Italy	ITA	Seychelles	SYC
Bolivia	BOL	Japan	JPN	Sierra Leone	SLE
Bosnia and Herzegovina	BIH	Jordan	JOR	Slovakia	SVK
Botswana	BWA	Kazakhstan	KAZ	Slovenia	SVN
Brazil	BRA	Kenya	KEN	Somalia	SOM
Bulgaria	BGR	Kyrgyzstan	KGZ	South Africa	ZAF
Burkina Faso	BFA	Laos	LAO	South Sudan	SSD
Burundi	BDI	Latvia	LVA	Spain	ESP
Cambodia	KHM	Lebanon	LBN	Sri Lanka	LKA
Cameroon	CMR	Lesotho	LSO	Sudan	SDN
Canada	CAN	Liberia	LBR	Suriname	SUR
Central African Republic	CAF	Lithuania	LTU	Swaziland	SWZ
Chad	TCD	Luxembourg	LUX	Sweden	SWE
Chile	CHL	Macedonia	MKD	Switzerland	CHE
China	CHN	Madagascar	MDG	Tajikistan	TJK
Colombia	COL	Malawi	MWI	Tanzania	TZA
Comoros	COM	Malaysia	MYS	Thailand	THA
Congo	COG	Maldives	MDV	Timor-Leste	TLS
Congo DRC	COD	Mali	MLI	Togo	TGO
Costa Rica	CRI	Malta	MLT	Trinidad and Tobago	TTO
Cote d'Ivoire	CIV	Mauritania	MRT	Tunisia	TUN
Croatia	HRV	Mauritius	MUS	Turkey	TUR
Czech Republic	CZE	Mexico	MEX	Turkmenistan	TKM
Denmark	DNK	Mongolia	MNG	Uganda	UGA
Djibouti	DJI	Montenegro	MNE	Ukraine	UKR
Dominican Republic	DOM	Morocco	MAR	United Arab Emirates	ARE
Ecuador	ECU	Mozambique	MOZ	United Kingdom England and Wales	XWA
Egypt	EGY	Myanmar	MMR	United Kingdom Northern Ireland	XNI
England	XWA	Namibia	NAM	United Kingdom Scotland	XSC
Eritrea	ERI	Nepal	NPL	United States	USA
Estonia	EST	Netherlands	NLD	Uruguay	URY
Ethiopia	ETH	New Zealand	NZL	Uzbekistan	UZB
Finland	FIN	Nicaragua	NIC	Vanuatu	VUT
France	FRA	Niger	NER	Venezuela	VEN
Gabon	GAB	Nigeria	NGA	Vietnam	VNM
Gambia	GMB	Northern Ireland	XNI	Yemen	YEM
Georgia	GEO	Norway	NOR	Yugoslavia	YUG
Germany	DEU	Pakistan	PAK	Zambia	ZMB
Germany West	ZZZY	Panama	PAN	Zanzibar	ZZZU
Ghana	GHA	Paraguay	PRY	Zimbabwe	ZWE

B.1.2 Household data

The Integrated Public Use Microdata Services [119] and World Health Surveys [145] records also contained estimates of the number of households in respondent countries, but for countries in other surveys we had to obtain these numbers from the United Nations [189], the United Nations Economic Commission for Europe (UNECE) [191] and other miscellaneous sources. We only searched for household populations in the years for which bicycle ownership data were available. In cases where household population numbers were not available, we estimated the number of households by multiplying the average household size by the population of the country (obtained from World Bank databases [206]). For countries where household numbers were not available in certain years, we used data for the closest earlier year.

The processing of household data is summarized in the following steps:

1. Search for number of households for countries by year.
2. If household data are not available for a country in a given year, use data for the closest earlier year.
3. If, for a certain year, step 2. is infeasible within a 20-year span, use the maximum household population available for that country in any year
4. If the number of households for a certain country is completely missing for a required year, take the average household size, and multiply by its population in that year to estimate the number of households.

B.2 Percentage bicycle ownership for each country

Figure B.1 shows individual bicycle ownership plots for each of the countries studied. The survey sources have also been labeled (refer to Table B.1). For all instances

in which more than one datapoint was available for a country-year (e.g. Dominican Republic-2002), we used an average in the pre-processing stage, but multiple country-years are shown in these plots to indicate survey diversity.

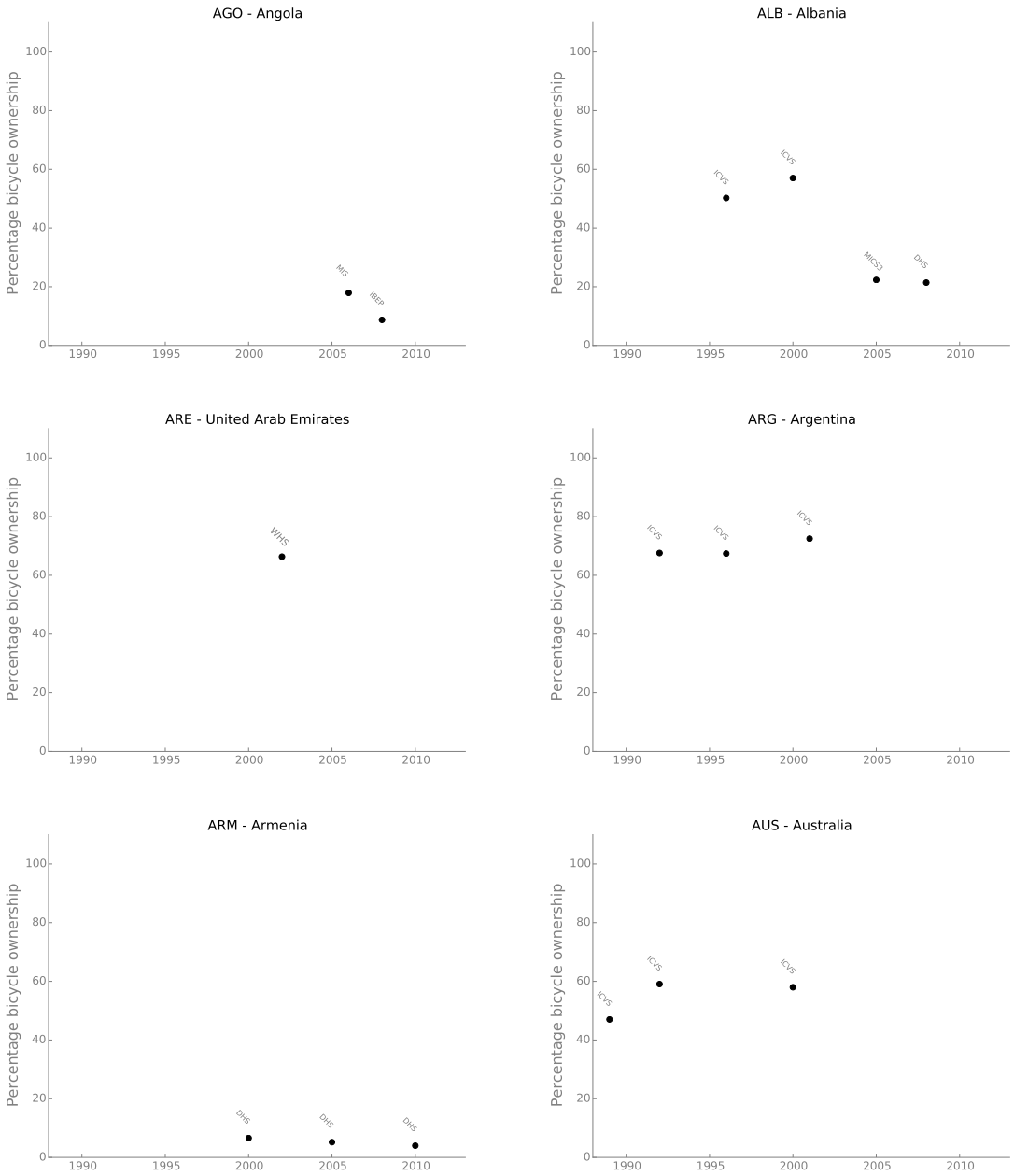

Figure B.1 Bicycle ownership trends by country

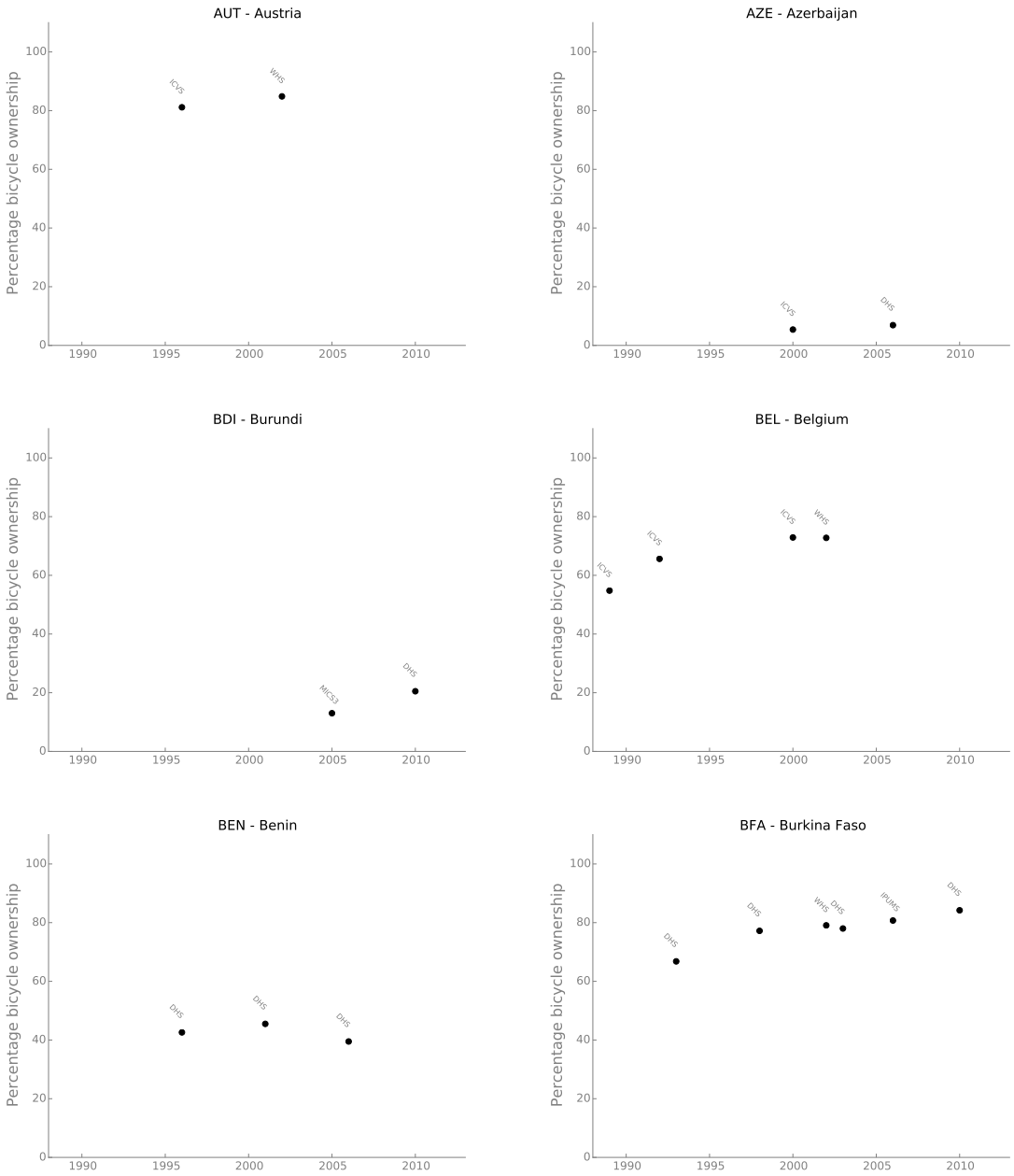

Figure B.1 Bicycle ownership trends by country (cont)

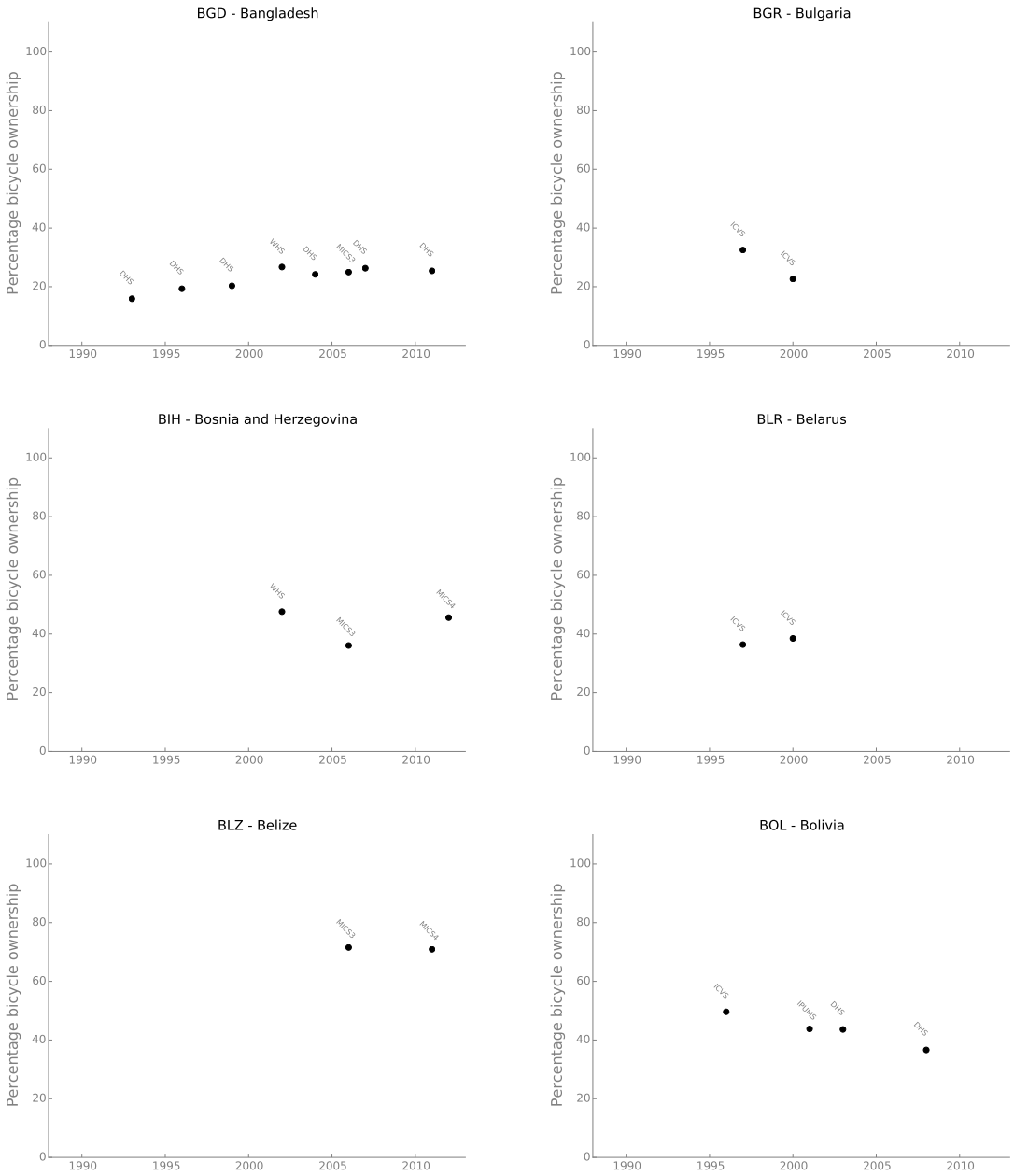

Figure B.1 Bicycle ownership trends by country (cont)

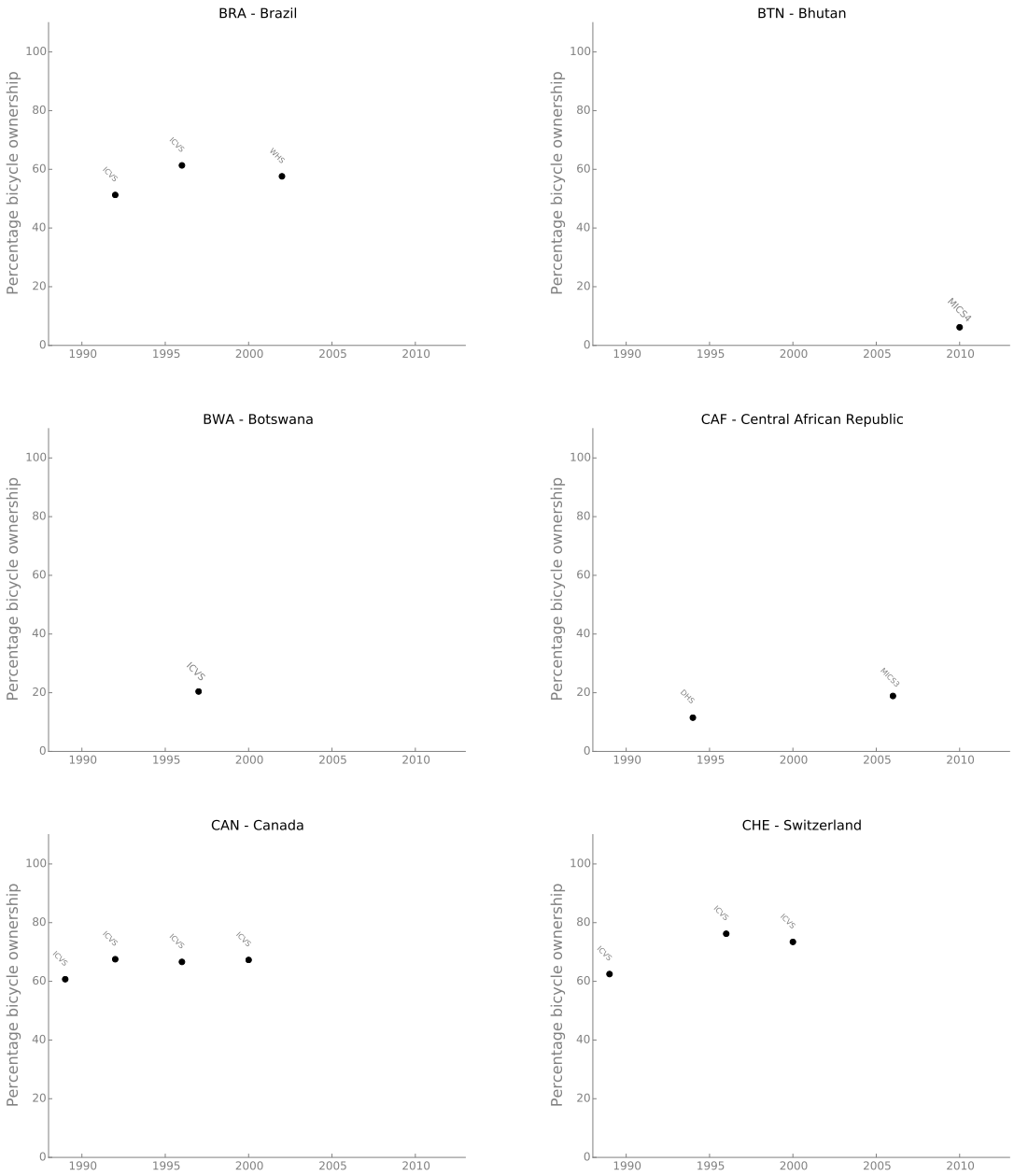

Figure B.1 Bicycle ownership trends by country (cont)

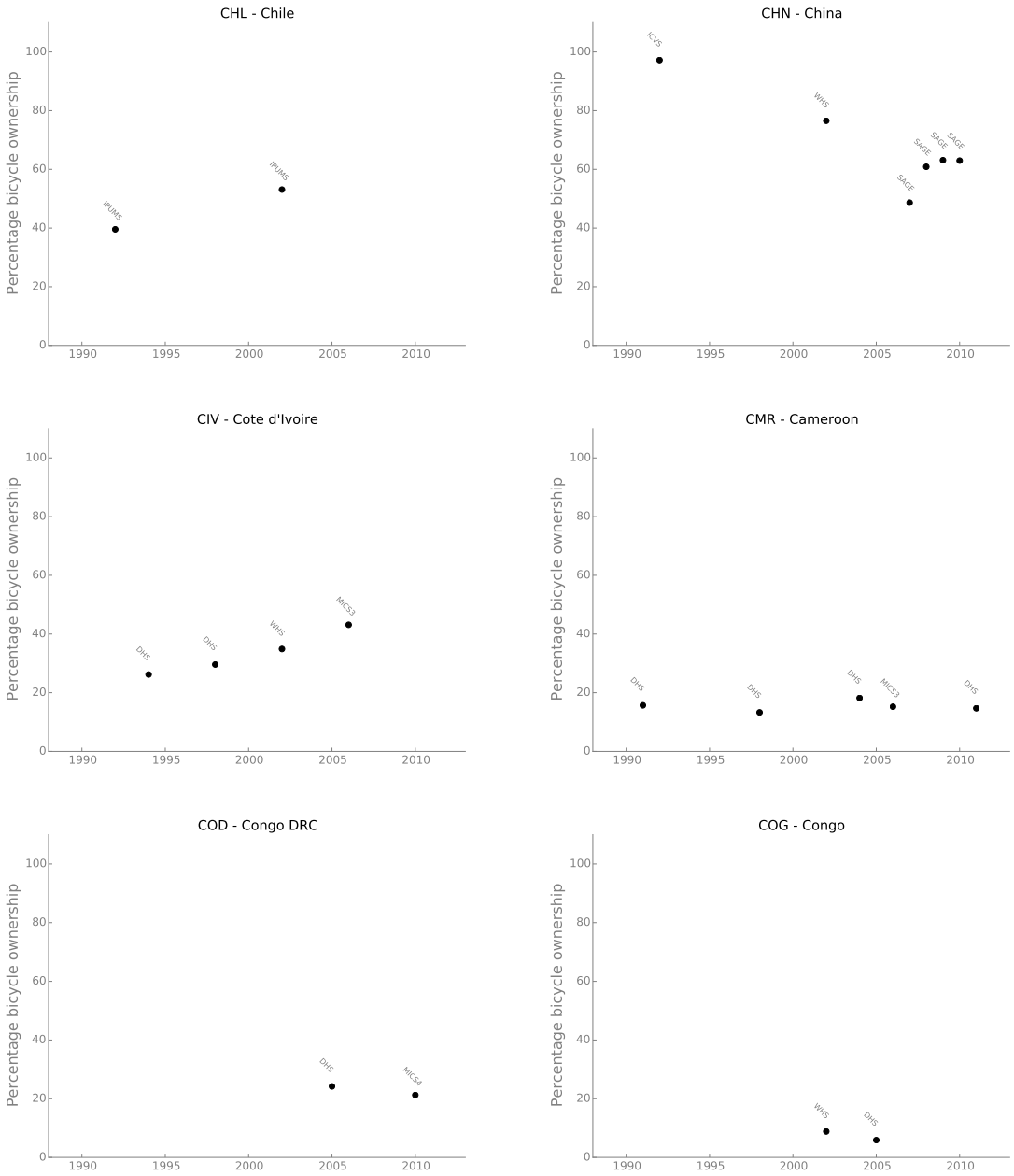

Figure B.1 Bicycle ownership trends by country (cont)

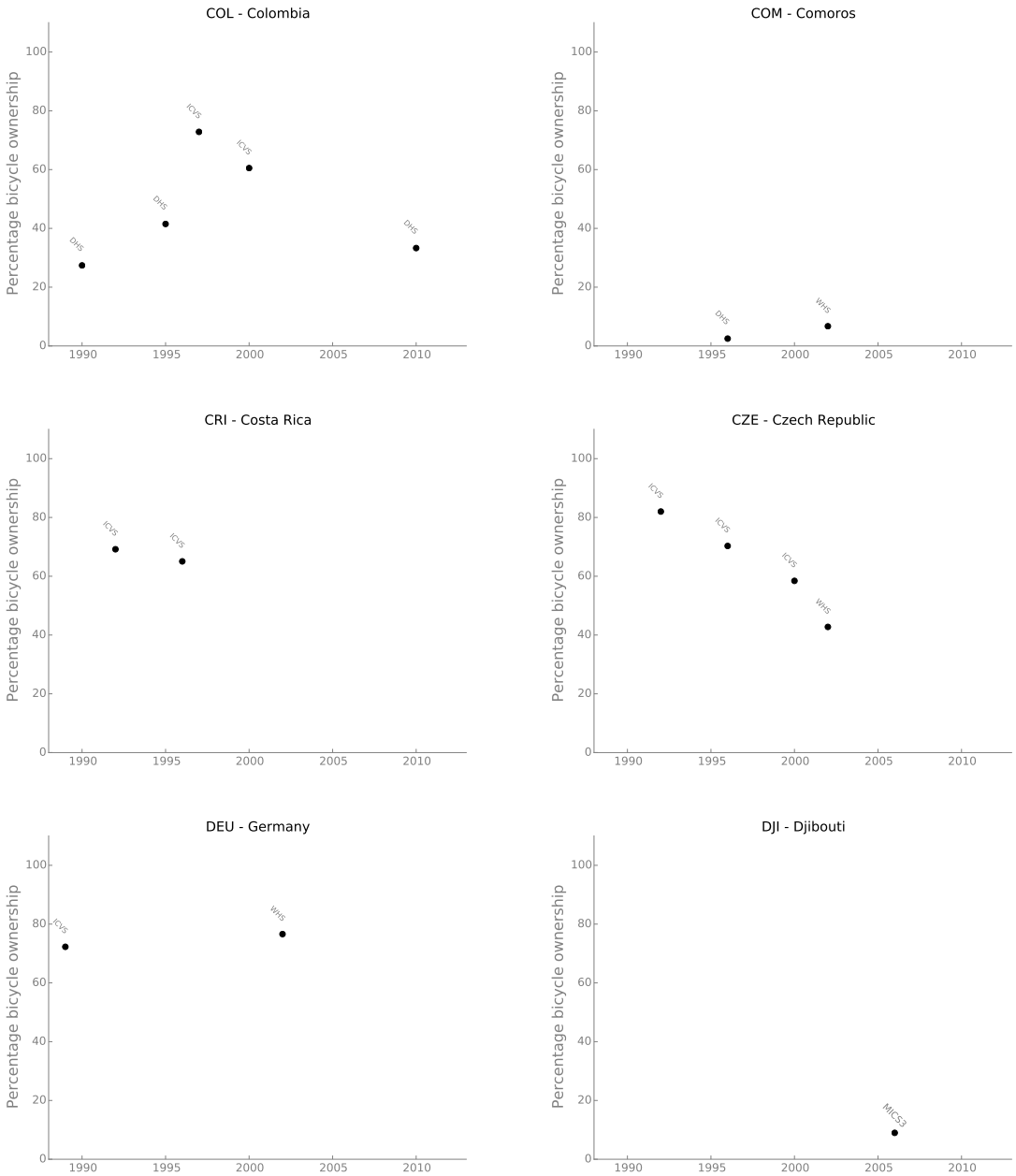

Figure B.1 Bicycle ownership trends by country (cont)

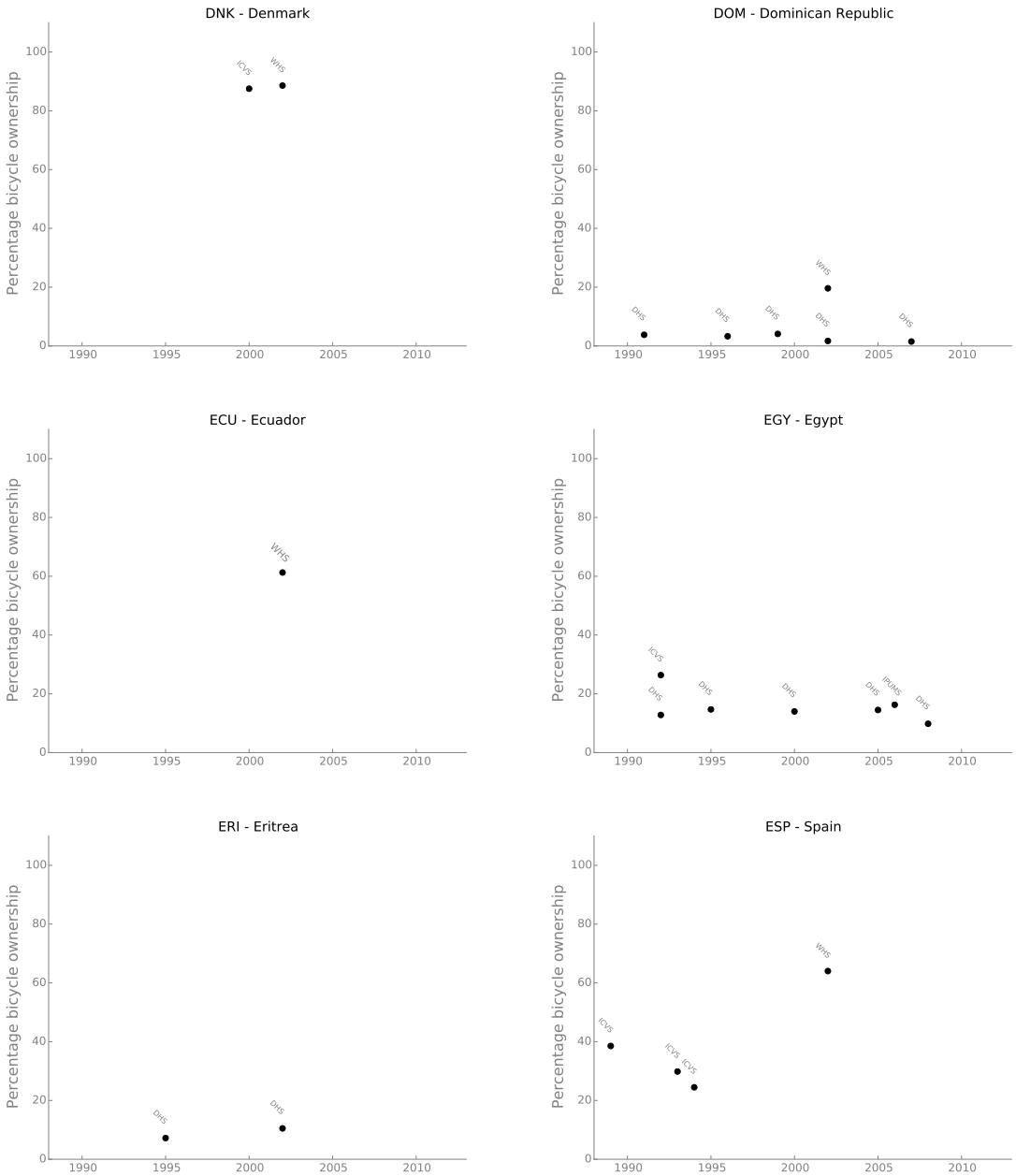

Figure B.1 Bicycle ownership trends by country (cont)

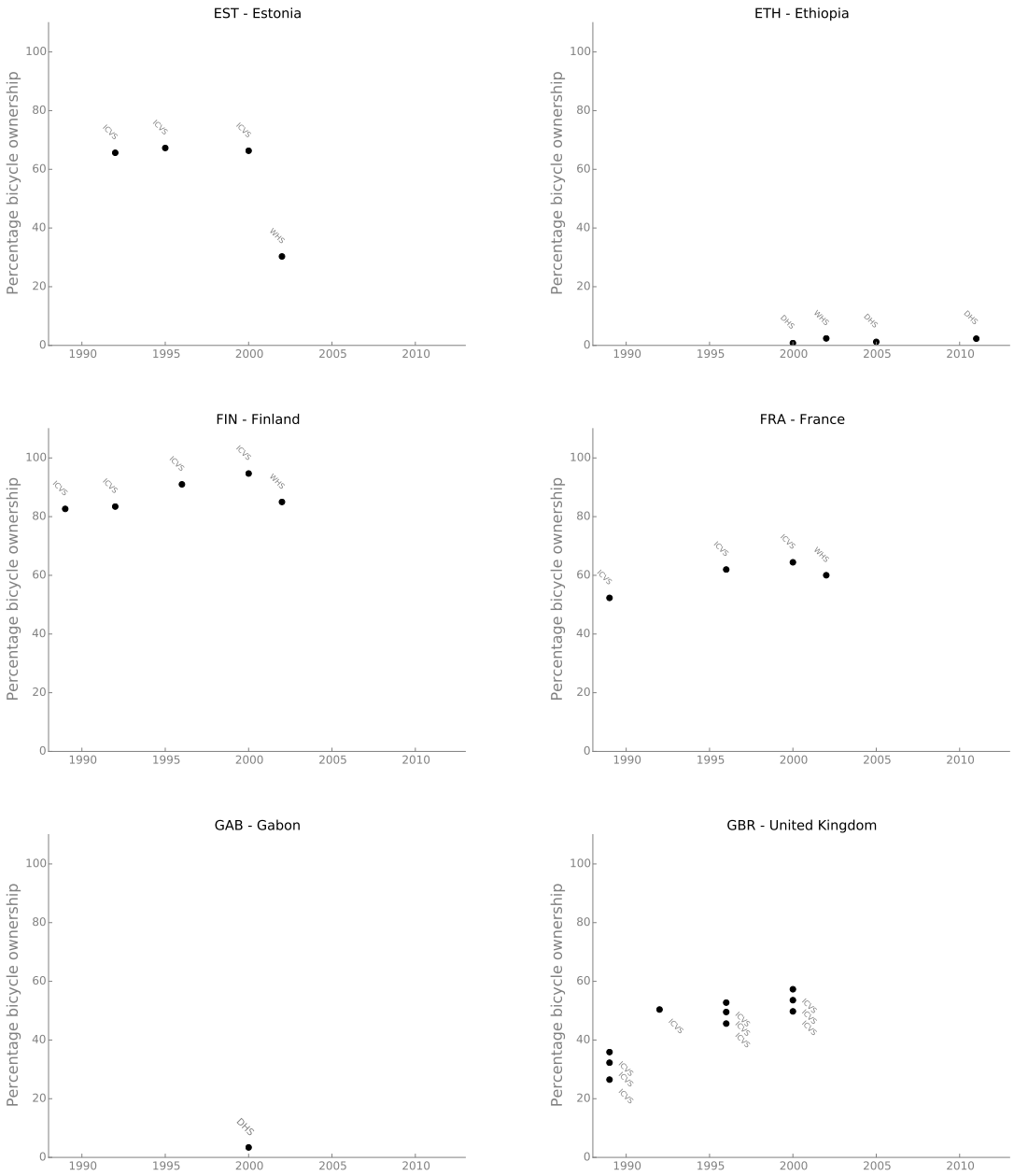

Figure B.1 Bicycle ownership trends by country (cont)

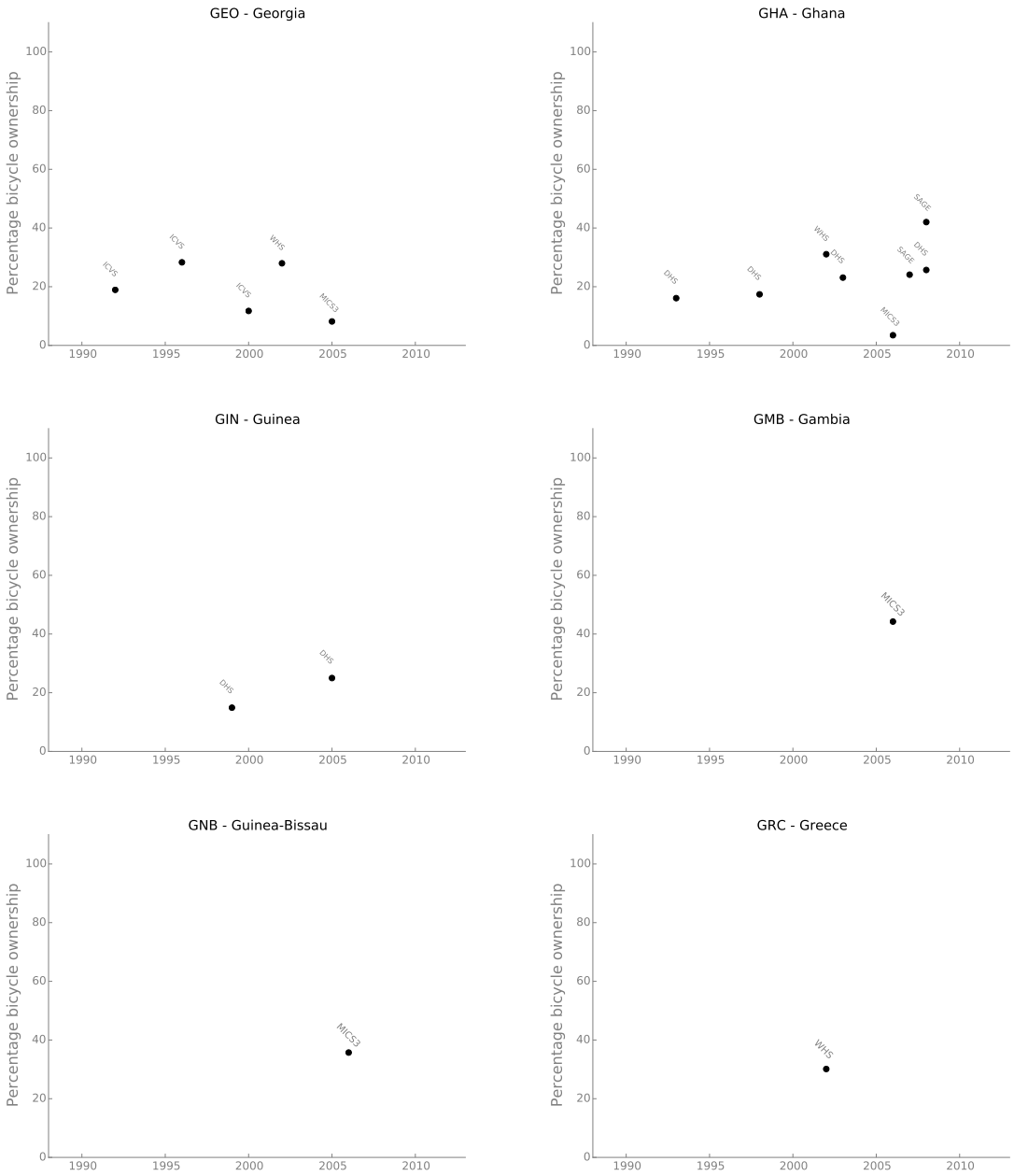

Figure B.1 Bicycle ownership trends by country (cont)

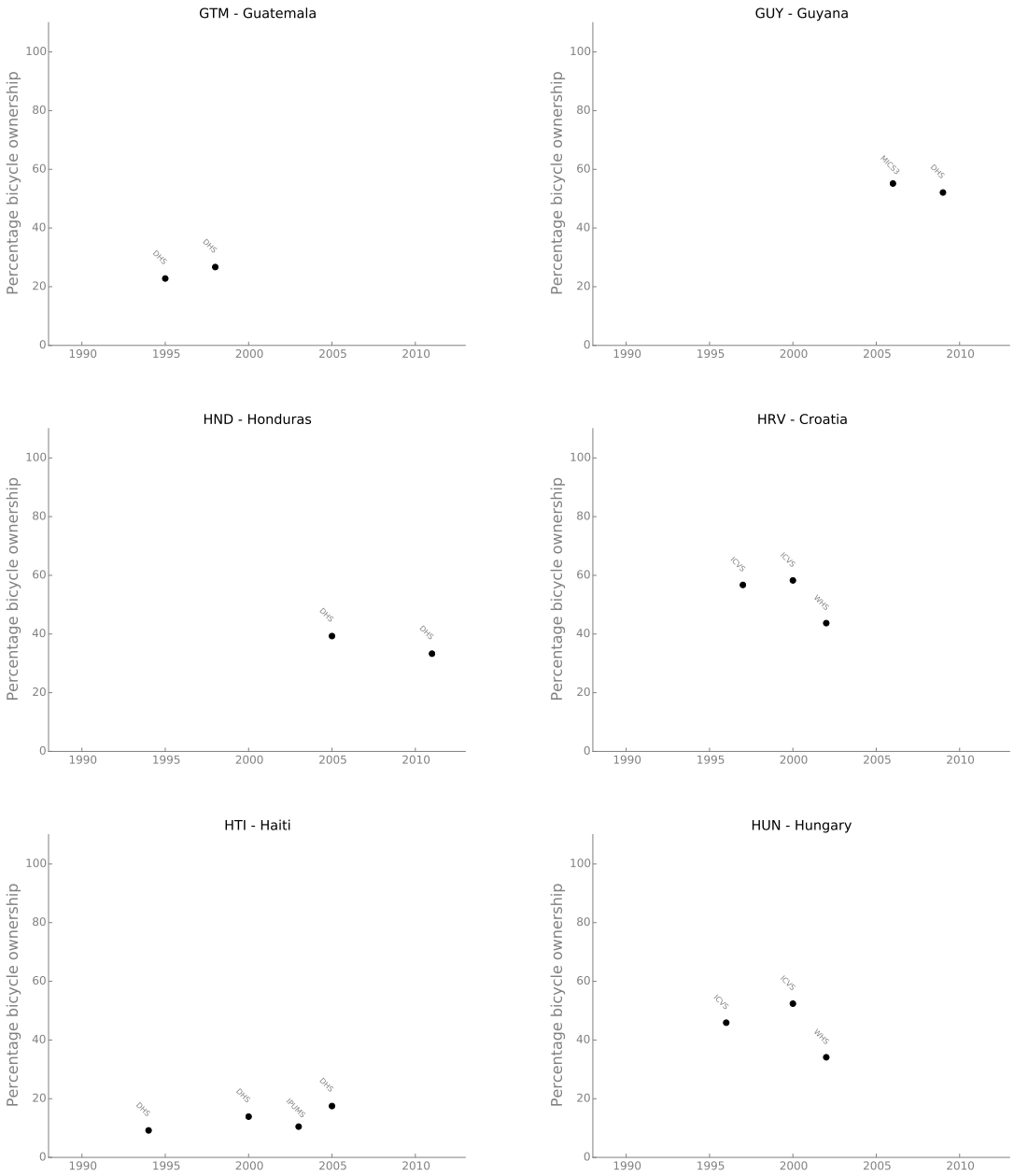

Figure B.1 Bicycle ownership trends by country (cont)

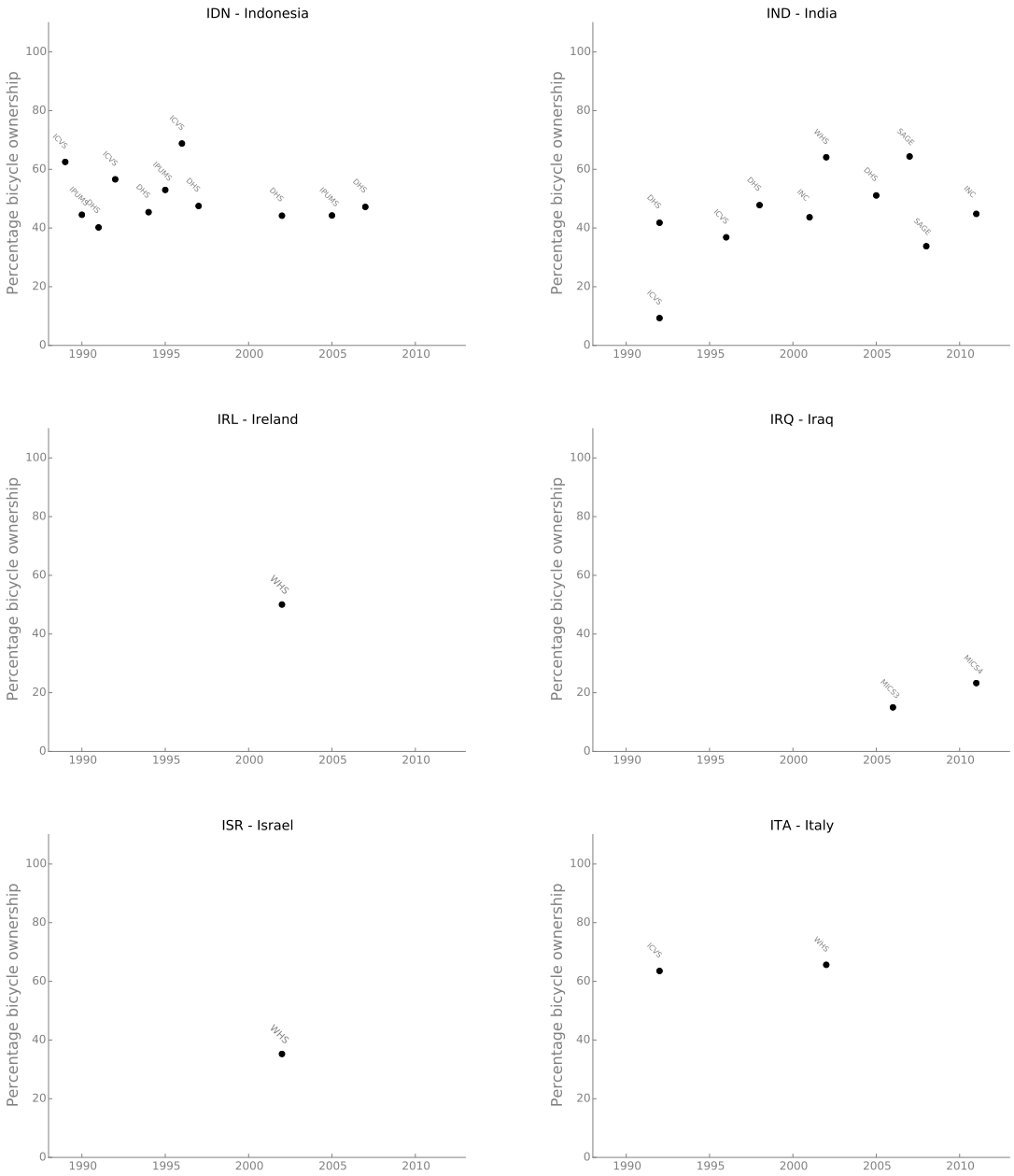

Figure B.1 Bicycle ownership trends by country (cont)

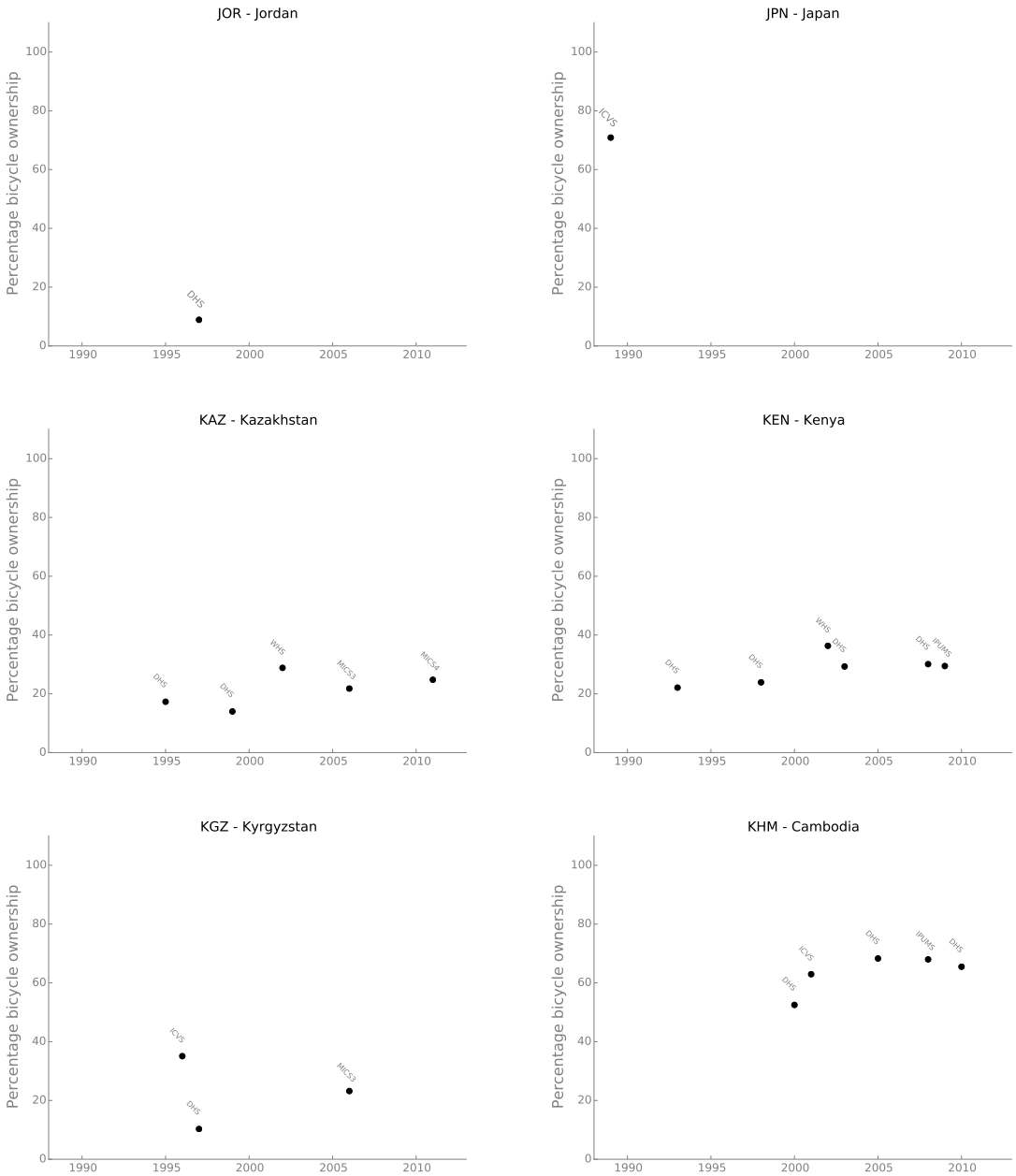

Figure B.1 Bicycle ownership trends by country (cont)

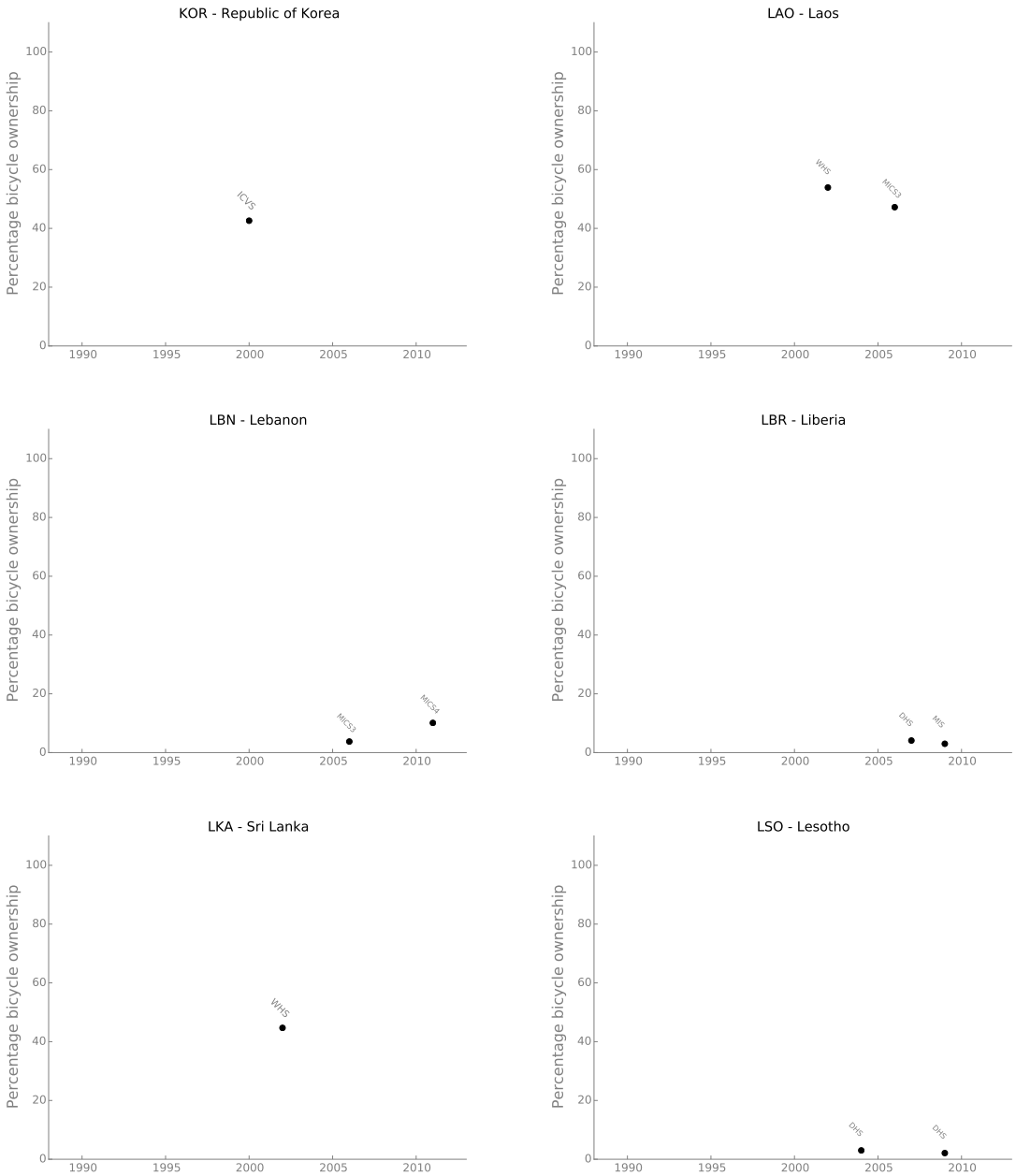

Figure B.1 Bicycle ownership trends by country (cont)

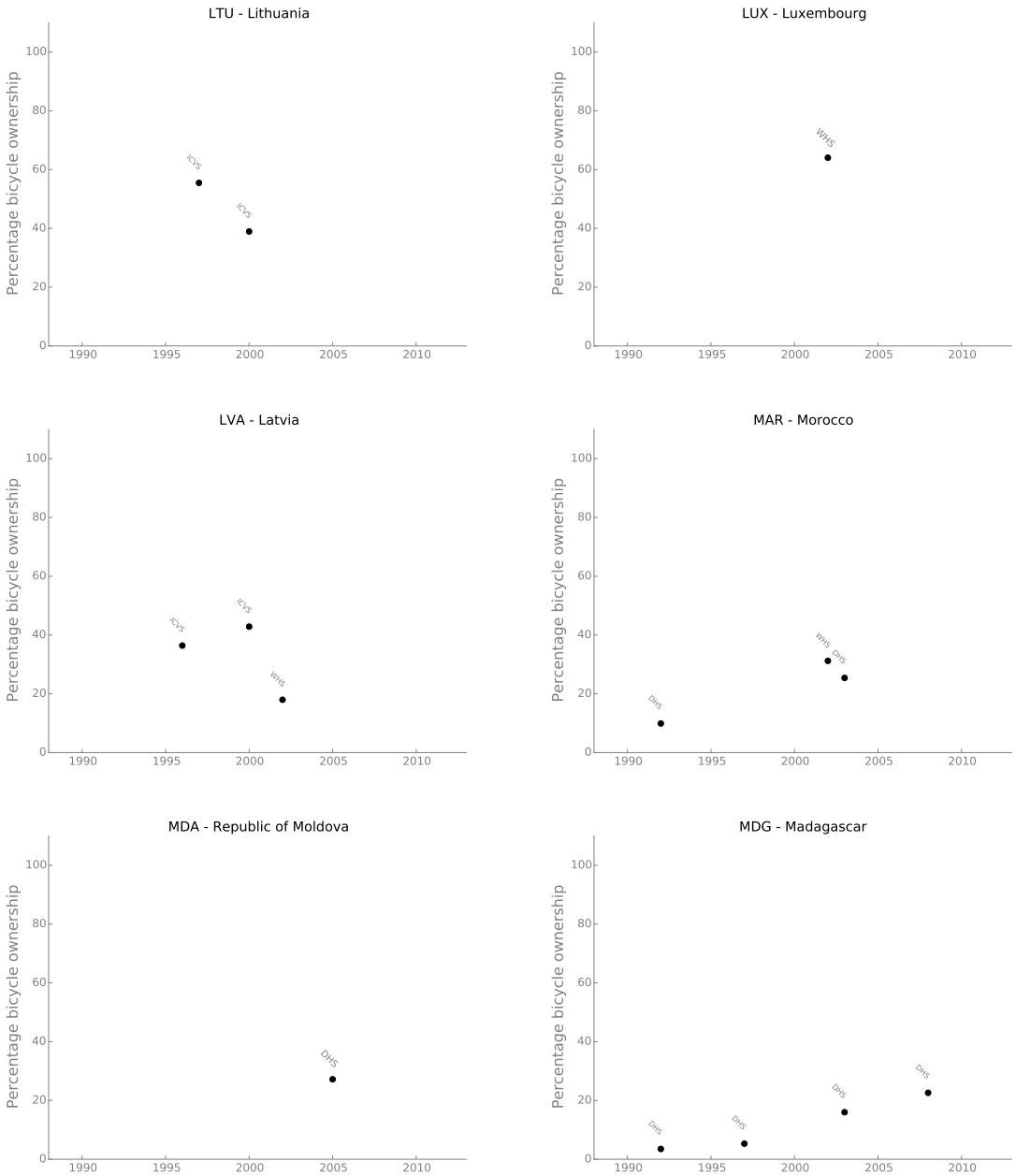

Figure B.1 Bicycle ownership trends by country (cont)

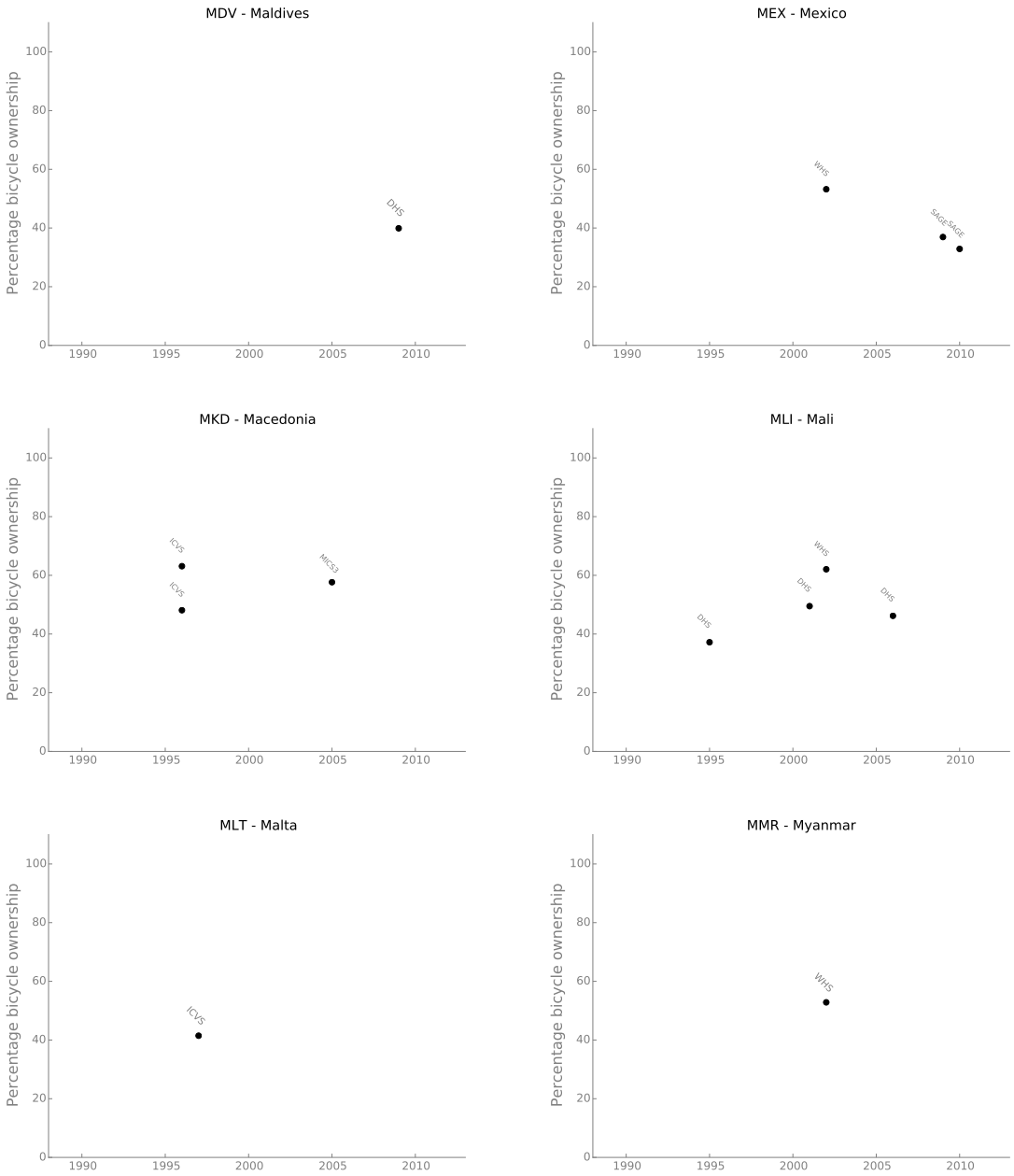

Figure B.1 Bicycle ownership trends by country (cont)

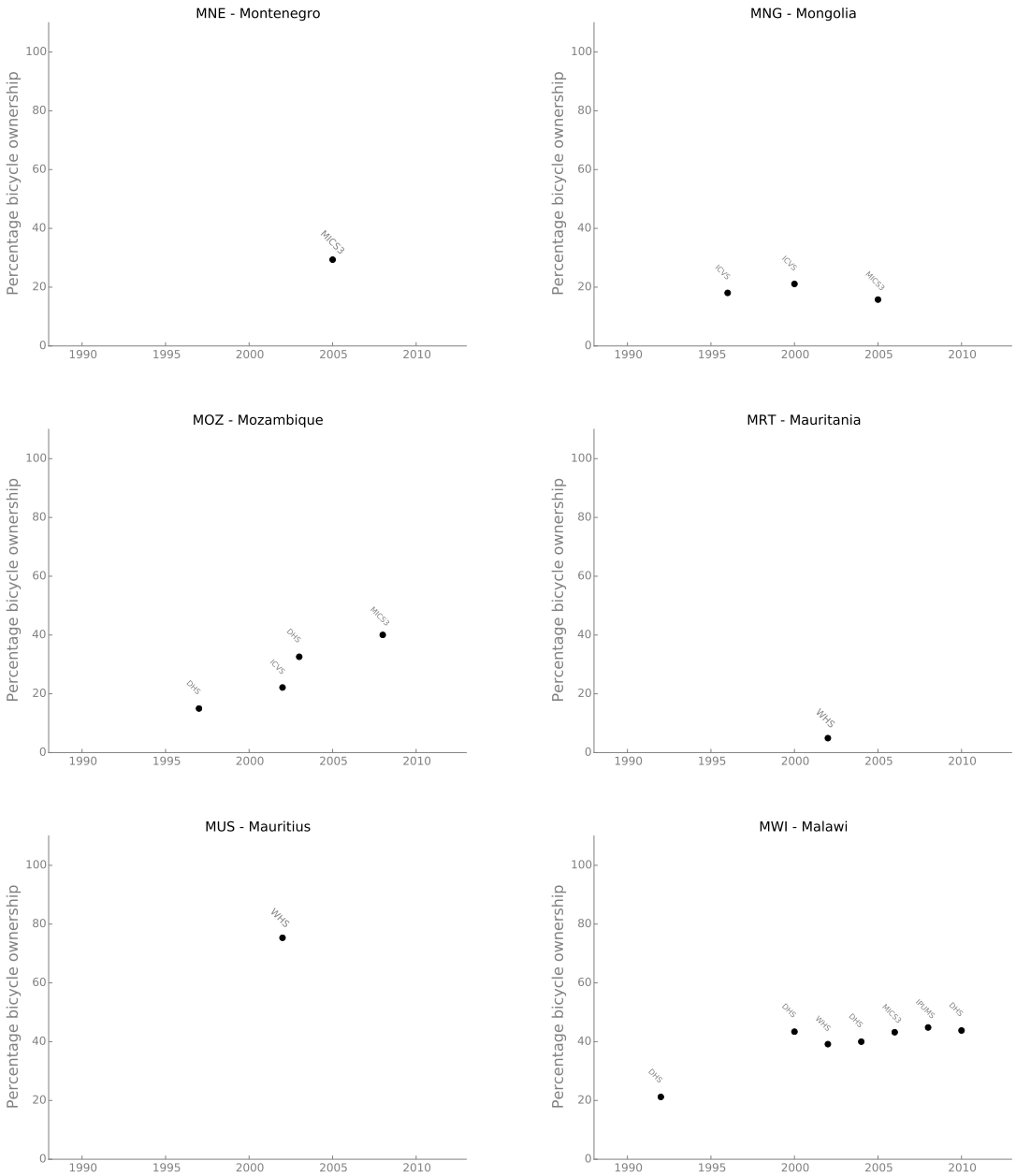

Figure B.1 Bicycle ownership trends by country (cont)

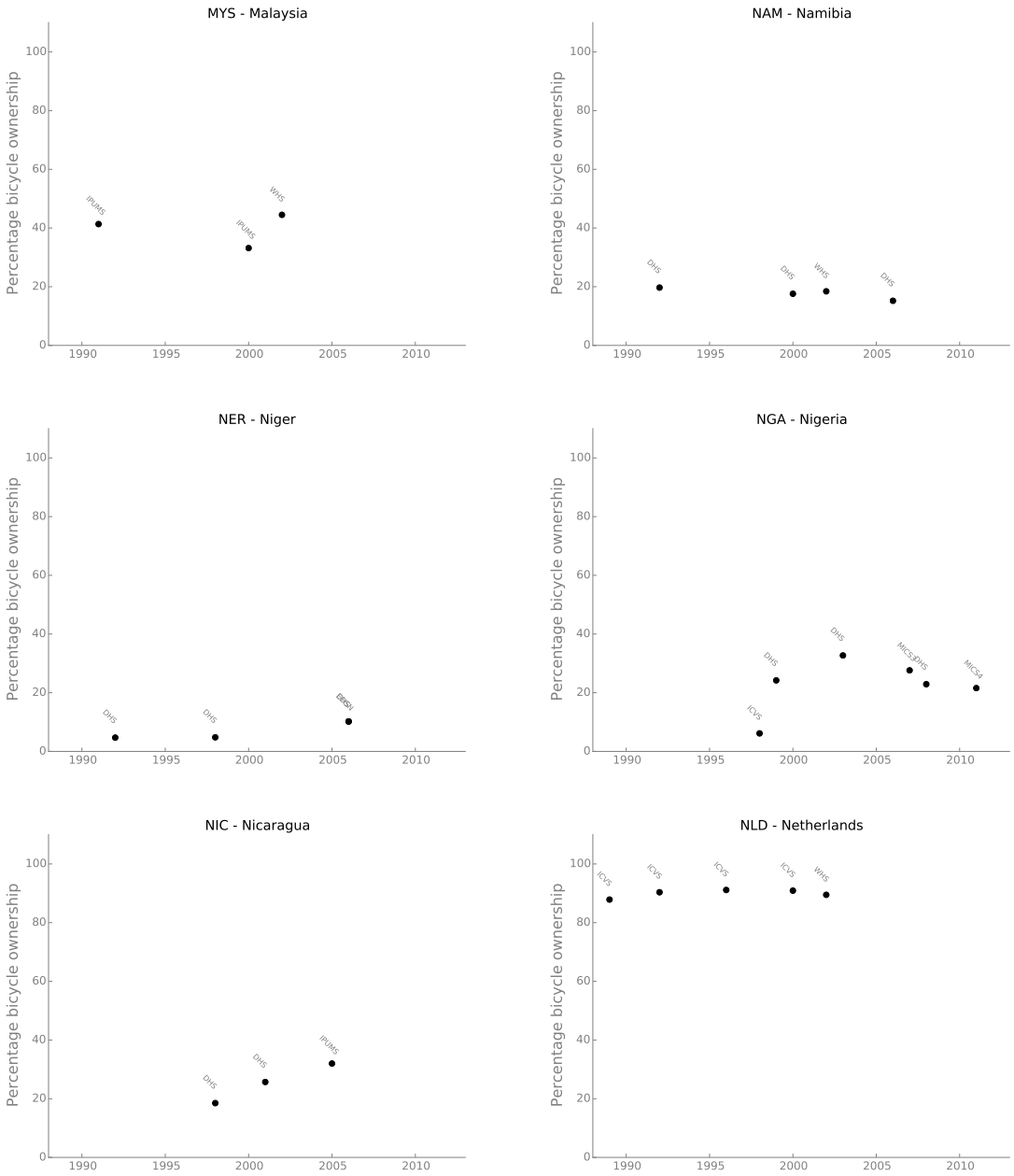

Figure B.1 Bicycle ownership trends by country (cont)

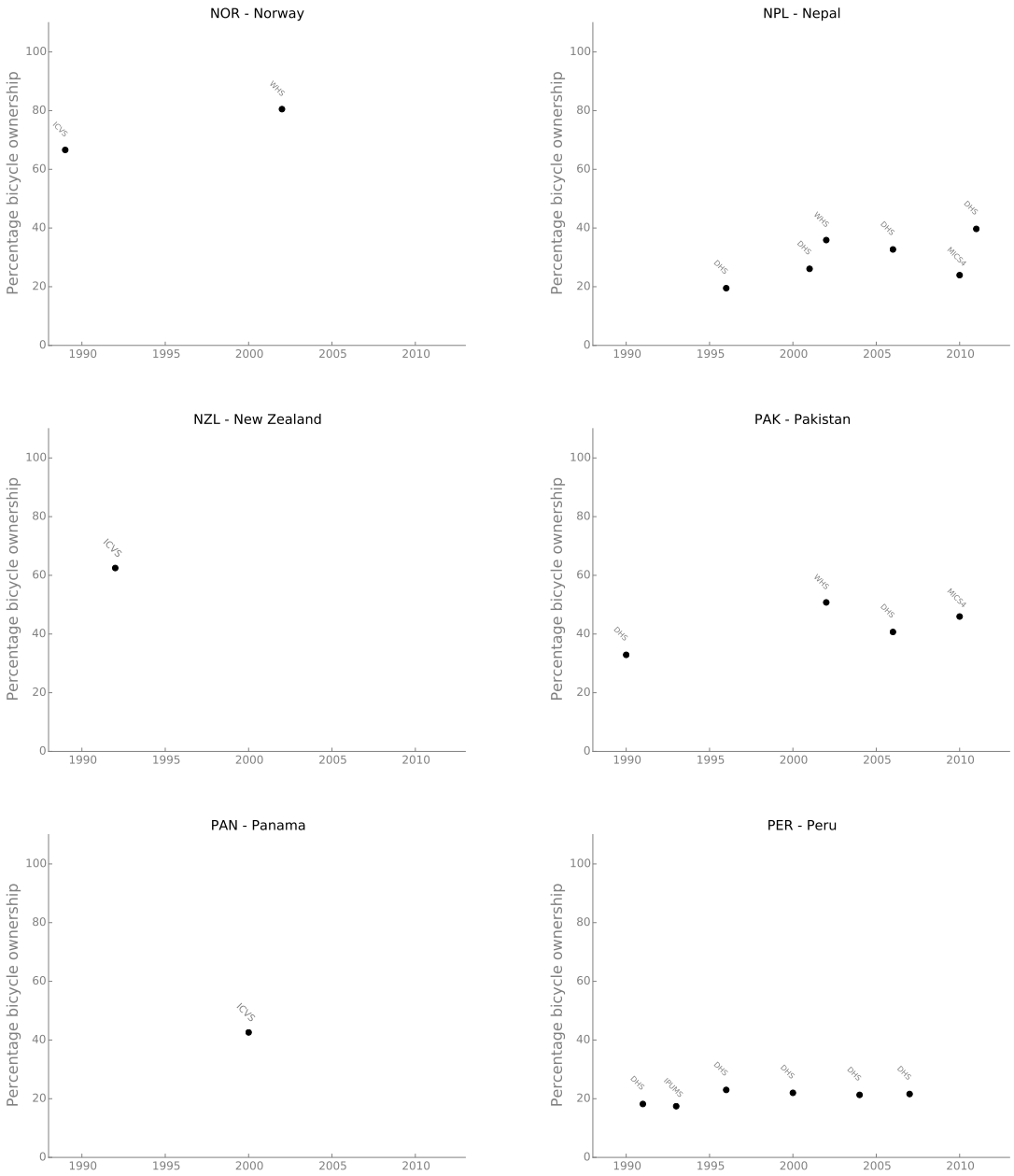

Figure B.1 Bicycle ownership trends by country (cont)

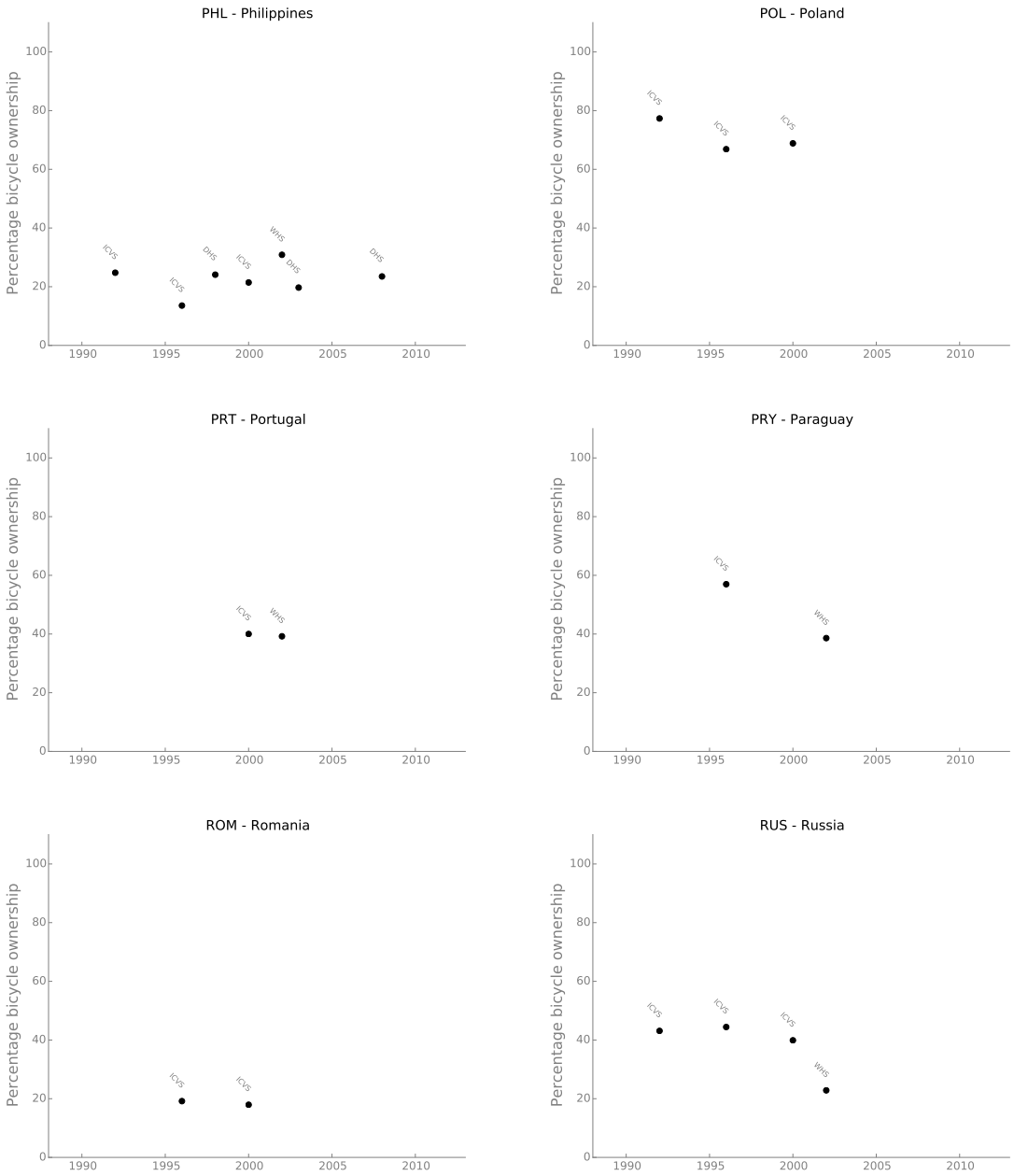

Figure B.1 Bicycle ownership trends by country (cont)

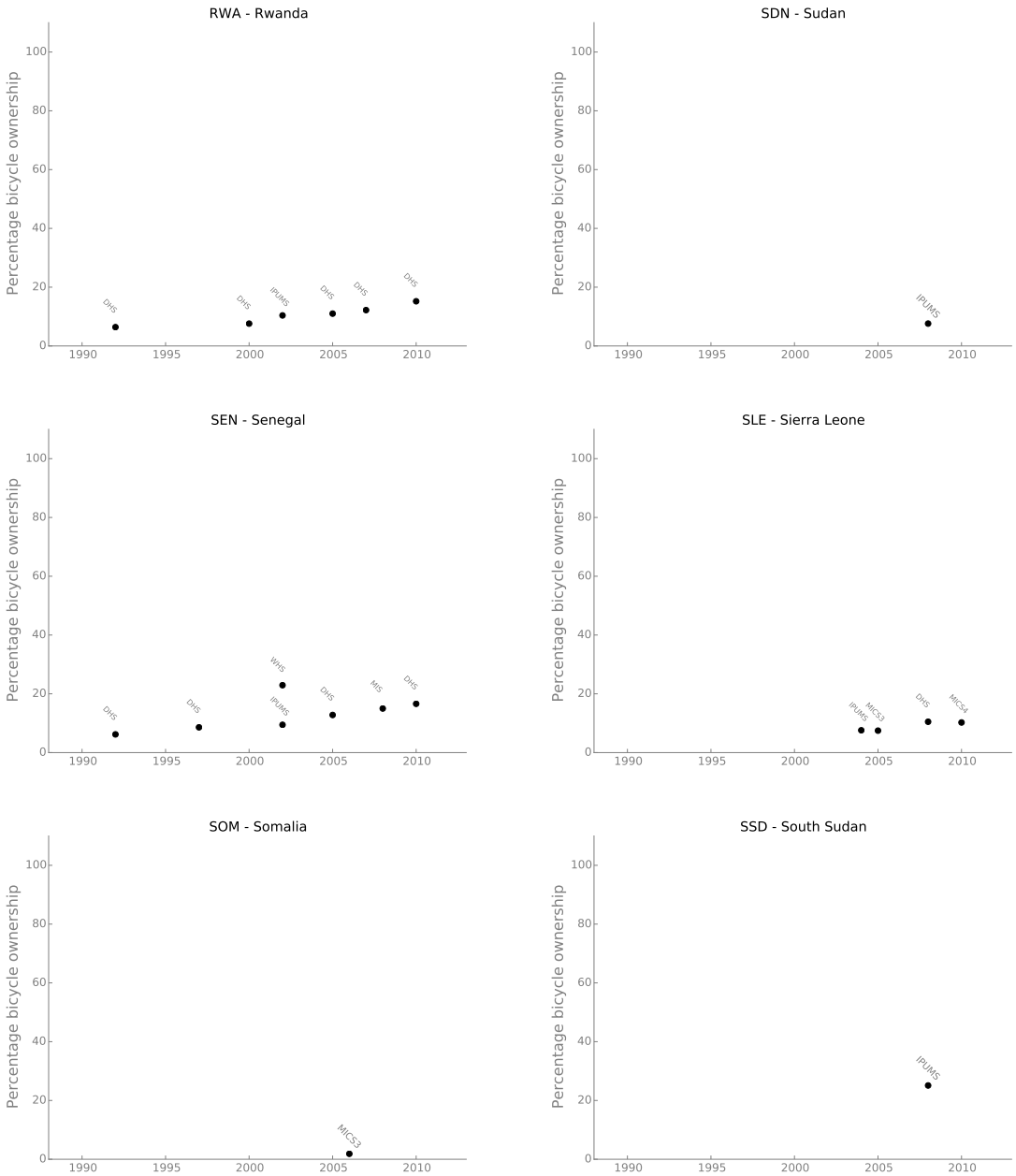

Figure B.1 Bicycle ownership trends by country (cont)

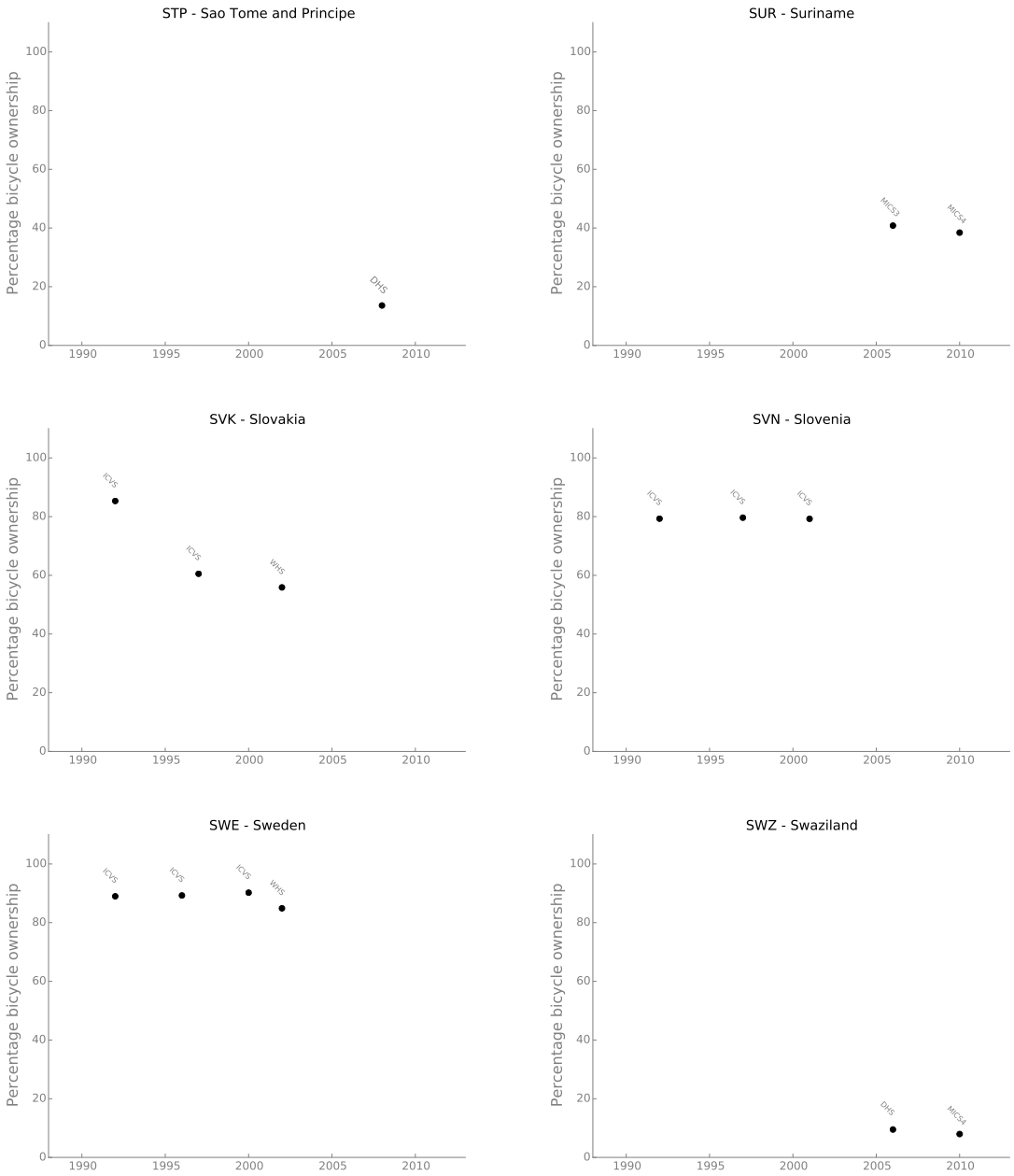

Figure B.1 Bicycle ownership trends by country (cont)

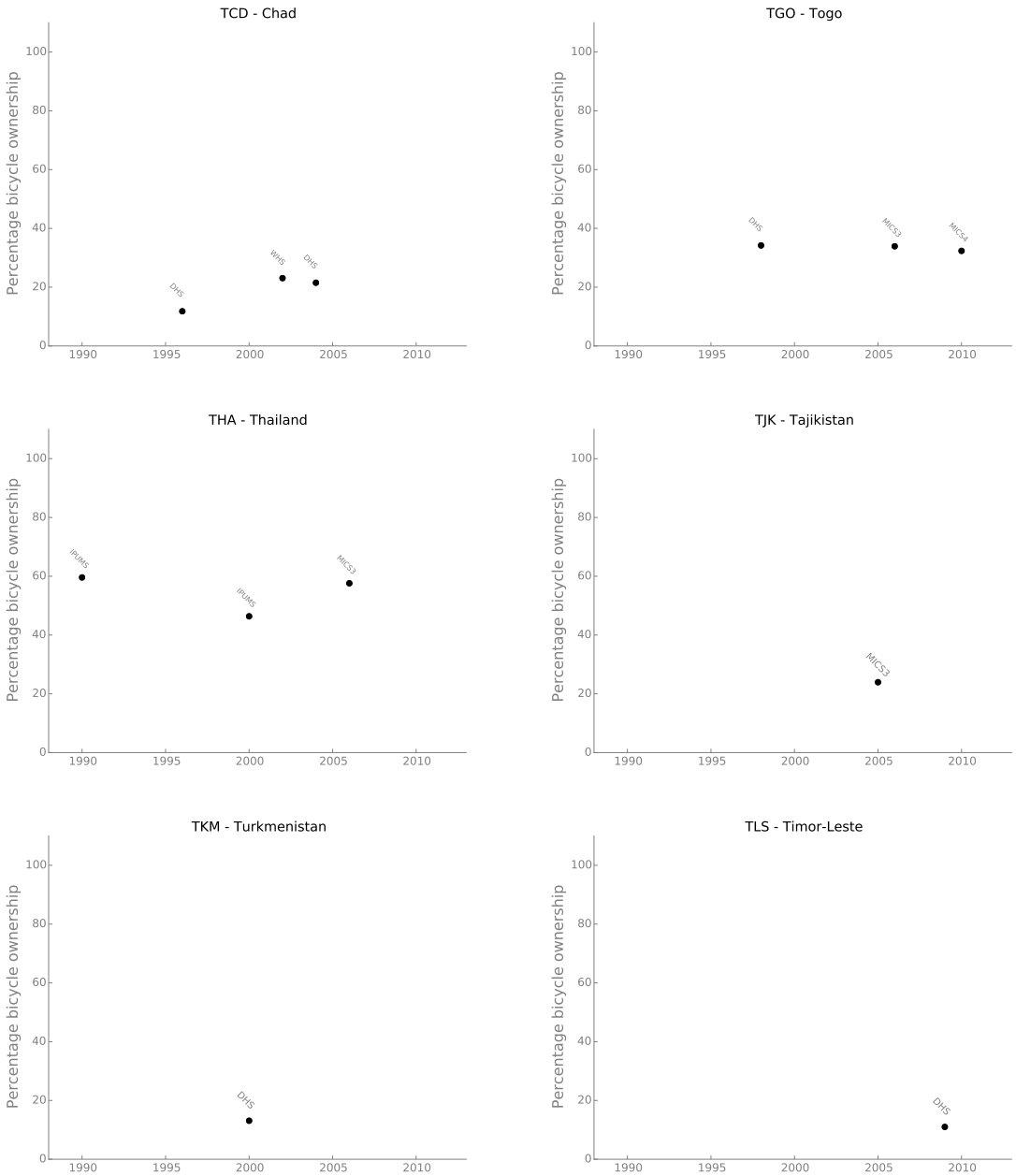

Figure B.1 Bicycle ownership trends by country (cont)

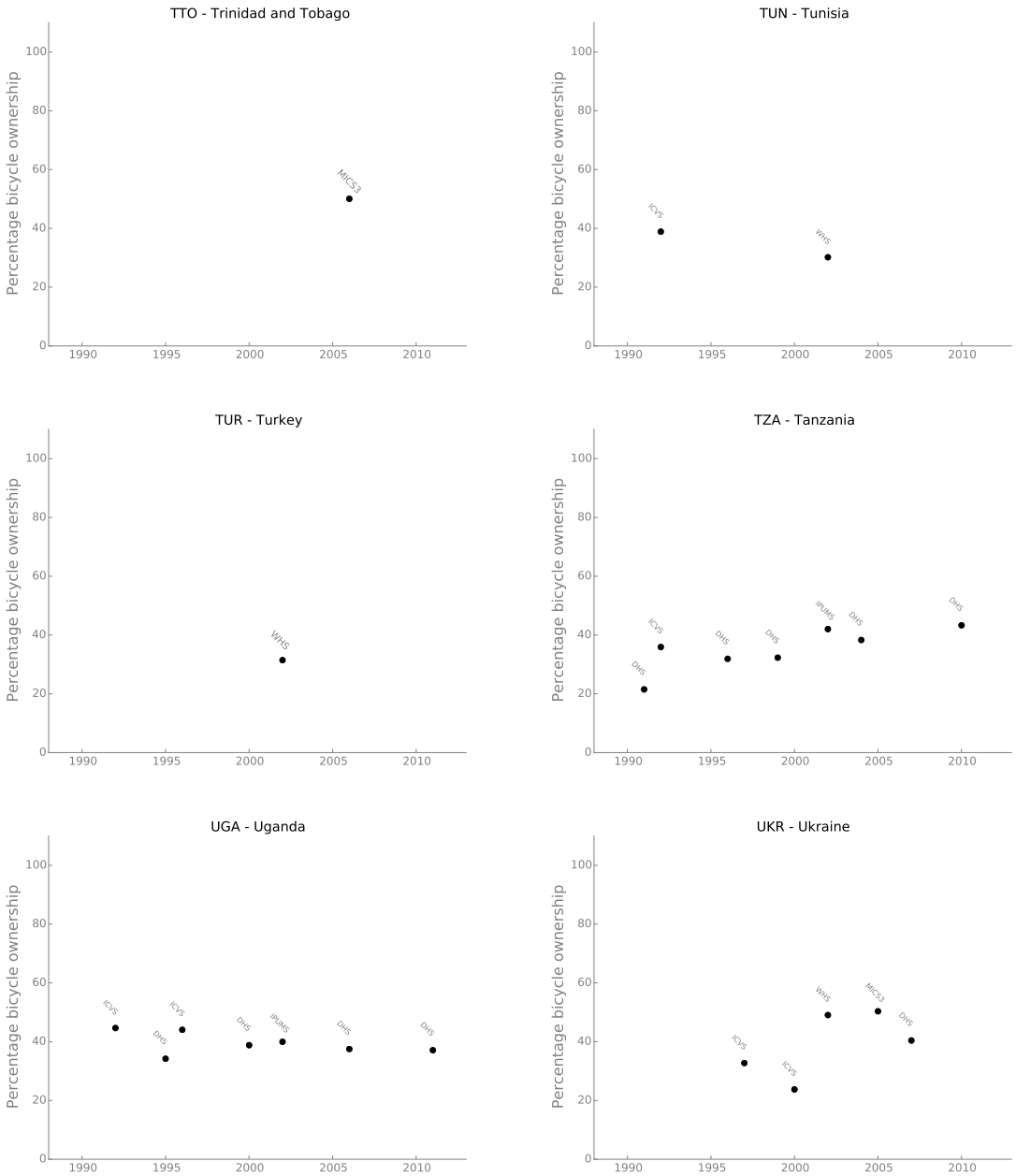

Figure B.1 Bicycle ownership trends by country (cont)

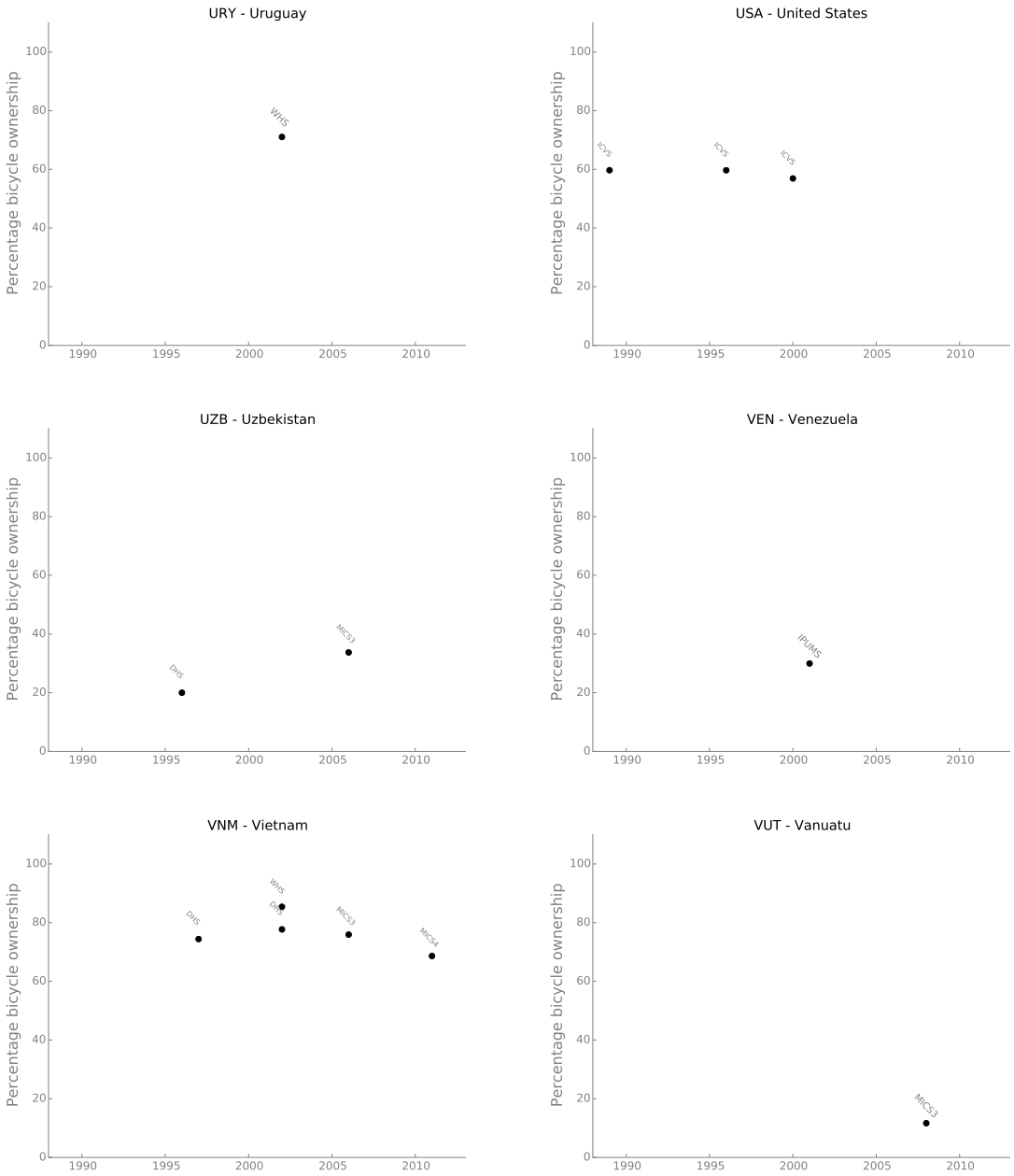

Figure B.1 Bicycle ownership trends by country (cont)

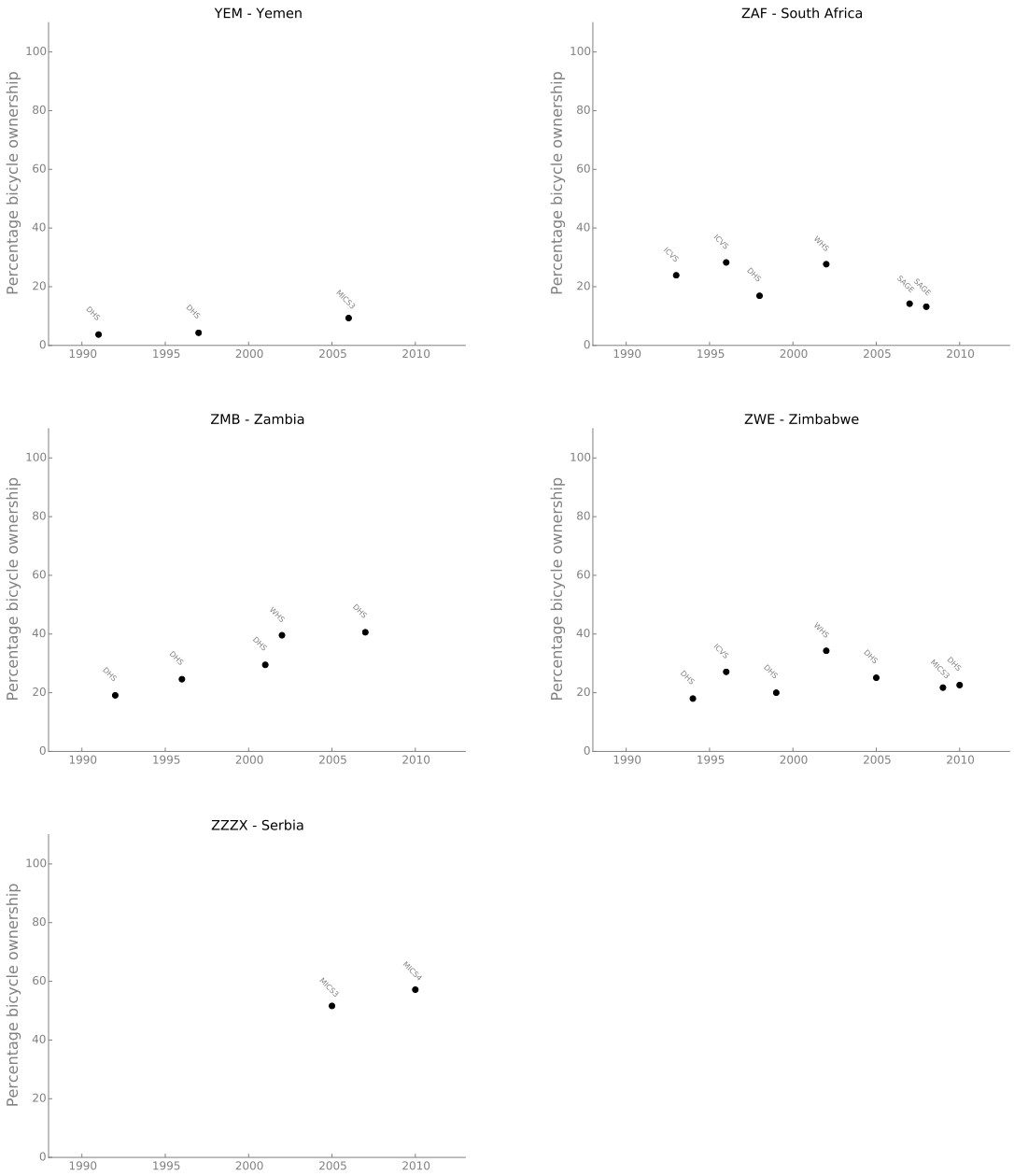

Figure B.1 Bicycle ownership trends by country (cont)

B.3 Reference data

B.3.1 Processed dataset

Table B.3 is the processed reference dataset, detailing the Year, country (ISO abbreviation), percentage bicycle ownership (PBO), estimated number of households and the corresponding cluster or group number.

Table B.3 Bicycle ownership data. ("PBO" represents "percentage bicycle ownership"

Year	ISO	PBO	Households	Group	Year	ISO	PBO	Households	Group
1989	AUS	47.00	7,760,322	2	2002	BRA	57.62	44,776,740	2
1989	BEL	54.79	3,608,178	2	2002	CHL	53.10	4,861,150	3
1989	CAN	60.72	8,281,530	2	2002	CHN	76.53	315,281,800	2
1989	CHE	62.48	2,543,540	2	2002	CIV	34.90	3,122,656	3
1989	DEU	72.27	26,977,920	1	2002	COG	8.85	575,082	4
1989	ESP	38.54	18,083,690	3	2002	COM	6.71	98,412	4
1989	FIN	82.64	1,781,771	1	2002	CZE	42.76	3,950,868	2
1989	FRA	52.31	19,392,640	2	2002	DEU	76.60	38,718,000	1
1989	GBR	31.56	20,200,000	3	2002	DNK	88.59	2,459,203	1
1989	IDN	62.52	34,315,135	2	2002	DOM	10.66	2,473,750	4
1989	JPN	70.88	51,842,307	2	2002	ECU	61.27	3,542,220	2
1989	NLD	87.86	5,111,000	1	2002	ERI	10.50	807,844	4
1989	NOR	66.61	1,523,508	1	2002	ESP	64.02	14,289,460	3
1989	USA	59.69	94,226,820	2	2002	EST	30.31	566,669	2
1990	COL	27.40	5,710,460	3	2002	ETH	2.39	15,239,290	4
1990	IDN	44.52	39,501,372	2	2002	FIN	85.00	2,354,082	1
1990	PAK	32.90	16,106,550	3	2002	FRA	60.03	23,808,072	2
1990	THA	59.59	11,813,400	2	2002	GEO	27.98	1,243,158	4
1991	CMR	15.70	1,756,460	4	2002	GHA	31.07	3,970,970	4
1991	DOM	3.80	1,222,400	4	2002	GRC	30.12	3,674,380	3
1991	IDN	40.20	39,501,372	2	2002	HRV	43.71	1,477,377	3
1991	MYS	41.34	3,909,600	3	2002	HUN	34.12	4,545,040	3
1991	PER	18.20	8,216,750	4	2002	IDN	44.20	51,249,710	2
1991	TZA	21.50	4,726,160	3	2002	IND	64.11	172,254,285	3
1991	YEM	3.70	1,845,684	4	2002	IRL	50.04	1,400,400	2
1992	ARG	67.60	11,996,510	2	2002	ISR	35.25	1,849,800	3
1992	AUS	59.07	7,760,322	2	2002	ITA	65.63	21,978,000	2
1992	BEL	65.61	3,953,125	2	2002	KAZ	28.83	4,160,216	4
1992	BRA	51.26	34,694,413	2	2002	KEN	36.33	6,342,120	4
1992	CAN	67.53	10,018,270	2	2002	LAO	53.90	1,023,107	2
1992	CHL	39.57	3,739,640	3	2002	LKA	44.69	407,065	3
1992	CHN	97.23	315,281,800	2	2002	LUX	64.04	171,953	2
1992	CRI	69.18	561,860	2	2002	LVA	17.98	802,848	3
1992	CZE	82.01	4,051,583	2	2002	MAR	31.21	4,459,460	4
1992	EGY	19.59	17,404,140	4	2002	MEX	53.21	22,268,196	3
1992	EST	65.64	597,100	2	2002	MLI	62.06	1,618,800	3
1992	FIN	83.44	2,036,732	1	2002	MMR	52.84	10,616,662	2
1992	GBR	50.39	21,576,100	3	2002	MOZ	22.15	4,655,396	4

Table B.3 Bicycle ownership data. ("PBO" represents "percentage bicycle ownership"

Year	ISO	PBO	Households	Group	Year	ISO	PBO	Households	Group
1992	GEO	18.93	1,243,158	4	2002	MRT	4.92	368,429	4
1992	IDN	56.59	39,501,372	2	2002	MUS	75.34	344,785	2
1992	IND	25.56	143,400,000	3	2002	MWI	39.16	2,290,050	3
1992	ITA	63.53	25,007,000	2	2002	MYS	44.49	4,778,200	3
1992	MAR	9.90	3,433,680	4	2002	NAM	18.43	16,839	4
1992	MDG	3.50	2,666,065	4	2002	NLD	89.48	6,934,263	1
1992	MWI	21.20	1,862,700	3	2002	NOR	80.51	1,961,548	1
1992	NAM	19.70	21,283	4	2002	NPL	35.89	4,586,995	4
1992	NER	4.70	1,134,000	4	2002	PAK	50.77	19,579,910	3
1992	NLD	90.35	6,061,000	1	2002	PHL	30.88	15,118,900	4
1992	NZL	62.49	1,443,636	2	2002	PRT	39.22	5,176,860	3
1992	PHL	24.77	11,561,260	4	2002	PRY	38.60	1,238,082	3
1992	POL	77.33	11,970,440	2	2002	RUS	22.85	52,711,375	3
1992	RUS	43.11	54,560,627	3	2002	RWA	10.39	1,917,190	4
1992	RWA	6.40	1,530,410	4	2002	SEN	16.20	1,079,990	4
1992	SEN	6.20	799,040	4	2002	SVK	55.89	2,071,743	2
1992	SVK	85.33	1,832,484	2	2002	SWE	84.88	4,448,746	1
1992	SVN	79.31	640,195	1	2002	TCD	23.07	1,118,597	4
1992	SWE	88.97	4,141,450	1	2002	TUN	30.17	1,458,100	3
1992	TUN	38.89	1,458,100	3	2002	TUR	31.45	16,446,644	3
1992	TZA	35.92	4,726,160	3	2002	TZA	42.02	8,417,680	3
1992	UGA	44.64	3,391,660	3	2002	UGA	39.96	5,292,710	3
1992	ZMB	19.10	1,295,010	3	2002	UKR	49.05	17,609,200	3
1993	BFA	66.80	1,452,690	1	2002	URY	71.03	1,180,670	2
1993	BGD	15.90	19,711,240	4	2002	VNM	81.55	17,804,633	2
1993	ESP	29.85	11,845,520	3	2002	ZAF	27.67	11,202,529	4
1993	GHA	16.10	5,702,340	4	2002	ZMB	39.58	1,862,250	3
1993	KEN	22.10	4,497,220	4	2002	ZWE	34.28	2,834,287	4
1993	PER	17.45	5,647,650	4	2003	BFA	78.00	1,631,770	1
1993	ZAF	23.89	17,258,500	4	2003	BOL	43.60	2,394,750	3
1994	CAF	11.50	802,163	4	2003	GHA	23.10	3,970,970	4
1994	CIV	26.20	2,584,056	3	2003	HTI	10.49	2,196,330	4
1994	ESP	24.48	11,845,520	3	2003	KEN	29.30	6,342,120	4
1994	HTI	9.20	1,147,920	4	2003	MAR	25.40	4,459,460	4
1994	IDN	45.40	39,501,372	2	2003	MDG	16.00	3,748,972	4
1994	ZWE	18.00	2,562,478	4	2003	MOZ	32.60	4,788,785	4
1995	COL	41.50	7,743,210	3	2003	NGA	32.70	43,404,000	4
1995	EGY	14.70	17,404,140	4	2003	PHL	19.70	15,118,900	4
1995	ERI	7.20	642,983	4	2004	BGD	24.20	26,259,590	4
1995	EST	67.27	597,100	2	2004	CMR	18.20	1,756,460	4
1995	GTM	22.80	1,980,924	4	2004	LSO	3.00	422,371	4
1995	IDN	52.98	38,612,325	2	2004	MWI	40.00	2,290,050	3
1995	KAZ	17.30	4,391,759	4	2004	PER	21.30	5,647,650	4
1995	MLI	37.20	1,365,150	3	2004	SLE	7.59	825,180	4
1995	UGA	34.20	3,391,660	3	2004	TCD	21.50	1,206,619	4
1996	ALB	50.22	791,830	3	2004	TZA	38.30	8,417,680	3
1996	ARG	67.41	11,996,510	2	2005	ALB	22.30	733,860	3
1996	AUT	81.14	3,093,200	1	2005	ARM	5.20	819,290	4
1996	BEN	42.60	764,000	3	2005	BDI	13.01	124,911	4
1996	BGD	19.30	19,711,240	4	2005	COD	24.20	7,945,294	4
1996	BOL	49.61	1,779,260	3	2005	COG	5.90	620,467	4
1996	BRA	61.34	34,694,413	2	2005	EGY	14.50	12,707,870	4

Table B.3 Bicycle ownership data. ("PBO" represents "percentage bicycle ownership"

Year	ISO	PBO	Households	Group	Year	ISO	PBO	Households	Group
1996	CAN	66.62	10,820,055	2	2005	ETH	1.20	16,594,169	4
1996	CHE	76.21	2,958,940	2	2005	GEO	8.16	1,173,675	4
1996	COM	2.50	84,521	4	2005	GIN	25.00	1,107,770	4
1996	CRI	65.06	561,860	2	2005	HND	39.30	1,444,000	3
1996	CZE	70.30	3,692,134	2	2005	HTI	17.50	2,196,330	4
1996	DOM	3.30	1,222,400	4	2005	IDN	44.28	52,300,392	2
1996	FIN	91.00	2,180,934	1	2005	IND	51.10	207,800,000	3
1996	FRA	61.97	22,616,500	2	2005	KHM	68.30	2,235,130	2
1996	GBR	49.30	21,576,100	3	2005	MDA	27.20	1,391,655	3
1996	GEO	28.31	1,243,158	4	2005	MKD	57.66	501,963	2
1996	HUN	45.90	4,387,780	3	2005	MNE	29.36	180,517	3
1996	IDN	68.80	38,612,325	2	2005	MNG	15.77	557,950	4
1996	IND	36.83	164,870,000	3	2005	NIC	31.99	1,193,390	4
1996	KGZ	35.08	2,493,770	4	2005	RWA	11.00	1,917,190	4
1996	LVA	36.41	859,823	3	2005	SEN	12.80	1,079,990	4
1996	MKD	63.11	501,963	2	2005	SLE	7.47	825,180	4
1996	MKD	48.11	501,963	2	2005	TJK	23.94	1,047,000	4
1996	MNG	18.05	427,830	4	2005	UKR	50.34	17,417,500	3
1996	NLD	91.13	6,468,682	1	2005	ZWE	25.10	2,849,907	4
1996	NPL	19.50	4,586,995	4	2005	ZZZX	51.62	2,521,190	2
1996	PER	23.00	5,647,650	4	2006	AGO	17.90	3,567,168	4
1996	PHL	13.57	13,621,900	4	2006	AZE	6.90	1,817,460	4
1996	POL	66.86	12,501,802	2	2006	BEN	39.50	936,000	3
1996	PRY	56.97	1,091,489	3	2006	BFA	80.72	2,362,060	1
1996	ROM	19.18	7,288,460	4	2006	BGD	24.98	28,716,961	4
1996	RUS	44.43	54,560,627	3	2006	BIH	36.10	1,067,120	3
1996	SWE	89.26	4,243,980	1	2006	BLZ	71.55	79,272	2
1996	TCD	11.80	900,913	4	2006	CAF	18.89	1,010,551	4
1996	TZA	31.90	4,726,160	3	2006	CIV	43.14	3,307,568	3
1996	UGA	44.04	3,391,660	3	2006	CMR	15.23	3,453,630	4
1996	USA	59.68	98,990,000	2	2006	DJI	8.98	125,006	4
1996	UZB	20.00	4,466,346	4	2006	EGY	16.28	17,404,140	4
1996	ZAF	28.27	9,938,010	4	2006	GHA	3.47	3,970,970	4
1996	ZMB	24.60	1,295,010	3	2006	GMB	44.24	158,032	3
1996	ZWE	27.11	2,656,078	4	2006	GNB	35.73	274,086	3
1997	BGR	32.50	2,964,577	4	2006	GUY	55.17	188,979	2
1997	BLR	36.40	3,873,139	3	2006	IRQ	15.01	2,654,020	4
1997	BWA	20.42	404,706	4	2006	KAZ	21.78	4,160,216	4
1997	COL	72.83	7,743,210	3	2006	KGZ	23.19	1,109,633	4
1997	HRV	56.72	1,544,250	3	2006	LAO	47.21	1,087,809	2
1997	IDN	47.50	38,612,325	2	2006	LBN	3.76	1,019,955	4
1997	JOR	8.90	973,430	4	2006	MLI	46.20	1,618,800	3
1997	KGZ	10.30	2,493,770	4	2006	MWI	43.21	2,290,050	3
1997	LTU	55.49	1,356,826	3	2006	NAM	15.20	16,839	4
1997	MDG	5.30	3,115,051	4	2006	NER	10.20	1,559,000	4
1997	MLT	41.47	119,479	3	2006	NPL	32.70	4,586,995	4
1997	MOZ	15.00	4,075,813	4	2006	PAK	40.70	19,579,910	3
1997	SEN	8.60	799,040	4	2006	SOM	1.85	1,860,314	4
1997	SVK	60.53	1,832,484	2	2006	SUR	40.82	134,001	3
1997	SVN	79.64	640,195	1	2006	SWZ	9.50	172,414	4
1997	UKR	32.73	36,235,710	3	2006	TGO	33.91	1,184,551	3
1997	VNM	74.40	10,684,460	2	2006	THA	57.60	16,541,700	2

Table B.3 Bicycle ownership data. ("PBO" represents "percentage bicycle ownership"

Year	ISO	PBO	Households	Group	Year	ISO	PBO	Households	Group
1997	YEM	4.30	2,397,618	4	2006	TTO	50.07	352,291	2
1998	BFA	77.20	1,631,770	1	2006	UGA	37.50	5,292,710	3
1998	CIV	29.60	2,890,724	3	2006	UZB	33.73	5,093,894	4
1998	CMR	13.30	1,756,460	4	2006	VNM	75.92	17,804,633	2
1998	GHA	17.40	5,702,340	4	2006	YEM	9.32	3,079,242	4
1998	GTM	26.70	2,121,248	4	2007	BGD	26.30	28,716,961	4
1998	IND	47.80	164,870,000	3	2007	CHN	48.65	2,226,546	2
1998	KEN	23.90	4,497,220	4	2007	DOM	1.50	2,473,750	4
1998	NER	4.80	1,246,000	4	2007	GHA	24.10	3,970,970	4
1998	NGA	6.14	43,404,000	4	2007	IDN	47.20	52,300,392	2
1998	NIC	18.50	828,150	4	2007	IND	64.38	207,800,000	3
1998	PHL	24.10	13,621,900	4	2007	LBR	4.10	688,360	4
1998	TGO	34.20	962,647	3	2007	NGA	27.62	36,840,000	4
1998	ZAF	16.90	9,938,010	4	2007	PER	21.60	8,216,750	4
1999	BGD	20.30	19,711,240	4	2007	RWA	12.20	1,917,190	4
1999	DOM	4.10	1,222,400	4	2007	UKR	40.40	17,341,100	3
1999	GIN	14.90	1,107,770	4	2007	ZAF	14.21	17,258,500	4
1999	KAZ	14.00	4,391,759	4	2007	ZMB	40.60	1,862,250	3
1999	NGA	24.20	43,404,000	4	2008	AGO	8.70	3,815,508	4
1999	TZA	32.30	4,726,160	3	2008	ALB	21.40	791,830	3
1999	ZWE	20.00	2,776,844	4	2008	BOL	36.60	2,394,750	3
2000	ALB	57.03	791,830	3	2008	CHN	60.87	2,226,546	2
2000	ARM	6.60	819,290	4	2008	EGY	9.80	17,404,140	4
2000	AUS	57.99	7,760,322	2	2008	GHA	33.86	3,970,970	4
2000	AZE	5.40	1,706,909	4	2008	IND	33.80	207,800,000	3
2000	BEL	72.90	4,237,775	2	2008	KEN	30.10	6,342,120	4
2000	BGR	22.62	2,964,577	4	2008	KHM	67.99	2,895,620	2
2000	BLR	38.49	3,855,016	3	2008	MDG	22.60	4,331,909	4
2000	CAN	67.28	10,820,055	2	2008	MOZ	40.05	5,484,945	4
2000	CHE	73.43	3,303,540	2	2008	MWI	44.83	2,998,640	3
2000	COL	60.51	7,743,210	3	2008	NGA	22.90	43,404,000	4
2000	CZE	58.43	3,854,791	2	2008	PHL	23.50	15,118,900	4
2000	DNK	87.52	2,438,307	1	2008	SDN	7.61	5,972,988	4
2000	EGY	14.00	12,707,870	4	2008	SEN	15.00	1,079,990	4
2000	EST	66.33	582,089	2	2008	SLE	10.50	825,180	4
2000	ETH	0.80	14,384,357	4	2008	SSD	25.10	1,322,742	4
2000	FIN	94.69	2,295,386	1	2008	STP	13.60	33,772	4
2000	FRA	64.44	23,808,072	2	2008	VUT	11.66	42,527	4
2000	GAB	3.40	194,000	4	2008	ZAF	13.19	1,322,742	4
2000	GBR	53.55	24,396,000	3	2009	CHN	63.12	2,226,546	2
2000	GEO	11.74	1,107,722	4	2009	GUY	52.10	192,853	2
2000	HRV	58.27	1,544,250	3	2009	KEN	29.45	8,952,300	4
2000	HTI	13.90	1,147,920	4	2009	LBR	3.00	688,360	4
2000	HUN	52.39	4,387,780	3	2009	LSO	2.10	422,371	4
2000	KHM	52.50	2,235,130	2	2009	MDV	39.90	43,197	3
2000	KOR	42.61	17,339,422	3	2009	MEX	36.93	25,469,850	3
2000	LTU	38.94	1,356,826	3	2009	TLS	11.00	194,962	4
2000	LVA	42.85	802,848	3	2009	ZWE	21.73	2,889,891	4
2000	MNG	21.10	557,950	4	2010	ARM	4.00	819,290	4
2000	MWI	43.40	2,290,050	3	2010	BDI	20.50	124,911	4
2000	MYS	33.17	4,778,200	3	2010	BFA	84.20	2,362,060	1
2000	NAM	17.60	21,283	4	2010	BTN	6.18	127,942	4

Table B.3 Bicycle ownership data. ("PBO" represents "percentage bicycle ownership"

Year	ISO	PBO	Households	Group	Year	ISO	PBO	Households	Group
2000	NLD	90.90	6,801,008	1	2010	CHN	62.97	2,226,546	2
2000	PAN	42.60	843,460	3	2010	COD	21.26	9,145,758	4
2000	PER	22.00	5,647,650	4	2010	COL	33.30	10,570,899	3
2000	PHL	21.44	15,118,900	4	2010	KHM	65.50	2,895,620	2
2000	POL	68.85	13,431,700	2	2010	MEX	32.88	29,036,410	3
2000	PRT	40.01	4,283,100	3	2010	MWI	43.80	2,998,640	3
2000	ROM	17.94	7,288,460	4	2010	NPL	23.94	4,586,995	4
2000	RUS	39.90	54,560,627	3	2010	PAK	45.96	19,579,910	3
2000	RWA	7.60	1,530,410	4	2010	RWA	15.20	1,917,190	4
2000	SWE	90.21	4,363,284	1	2010	SEN	16.60	1,079,990	4
2000	THA	46.37	16,541,700	2	2010	SLE	10.25	825,180	4
2000	TKM	13.10	882,631	4	2010	SUR	38.42	139,246	3
2000	UGA	38.80	3,391,660	3	2010	SWZ	7.96	172,414	4
2000	UKR	23.75	17,679,600	3	2010	TGO	32.34	1,313,752	3
2000	USA	56.89	123,688,760	2	2010	TZA	43.30	8,417,680	3
2001	ARG	72.49	10,408,520	2	2010	ZWE	22.60	2,932,057	4
2001	BEN	45.50	841,000	3	2010	ZZZX	57.16	2,521,190	2
2001	BOL	43.78	2,394,750	3	2011	AFG	31.82	3,933,172	3
2001	IND	43.67	172,254,285	3	2011	BGD	25.40	33,092,620	4
2001	KHM	62.95	2,235,130	2	2011	BLZ	70.92	79,272	2
2001	MLI	49.50	1,618,800	3	2011	CMR	14.70	3,453,630	4
2001	NIC	25.70	828,150	4	2011	ETH	2.30	19,475,612	4
2001	NPL	26.10	4,586,995	4	2011	HND	33.30	1,707,000	3
2001	SVN	79.25	640,195	1	2011	IND	44.82	207,800,000	3
2001	VEN	29.96	6,460,800	3	2011	IRQ	23.28	2,654,020	4
2001	ZMB	29.50	1,862,250	3	2011	KAZ	24.78	4,391,759	4
2002	ARE	66.35	642,224	2	2011	LBN	10.10	1,095,697	4
2002	AUT	84.85	3,314,200	1	2011	NGA	21.57	43,404,000	4
2002	BEL	72.77	4,319,040	2	2011	NPL	39.70	4,586,995	4
2002	BFA	79.07	1,631,770	1	2011	UGA	37.10	5,292,710	3
2002	BGD	26.71	26,259,590	4	2011	VNM	68.63	24,613,613	2
2002	BIH	47.61	1,206,791	3	2012	BIH	45.58	1,206,791	3

B.4 Code organization

The code for analyzing these data was written primarily in Python (using the IPython [148] system, along with the Pandas [113] and Matplotlib [77] packages), and it is available with other data resources at `ce.jhu.edu/sauleh/obls-gbu`.

Along with the main file (`main-v3.py`), supporting modules contain functions to carry out the tasks as listed below:

(1) `initialize.py`: Initialize data into dataframe

(2) `alignment.py`: Perform alignment using DTW algorithm and obtain separation matrix

(3) `clustering.py`: Hosts the functions that perform the goodness-of-fit and gap tests, and then perform the actual clustering to put the countries in groups

(4) `household.py`: Interpolation and data-reading functions to compute household statistics for each country

(5) `viz.py`: Visualization functions (maps, plots, etc) to make sense of data and results.

(6) `summaries.py`

An R script—`gaptest.R`—was also written to execute the gap test, but it is called from within the `gapTest` function in the `clustering` module.

The raw bicycle ownership data (organized into a spreadsheet) and other required elements (household data, shape files, etc) are stored in the `resources` directory. All tabular output is kept in `tables`, and visual output is stored in `Images`.

APPENDIX C

Mathematical formulation of North American crude oil model (NACOM)

Here, we provide a complete formulation of the equilibrium model for the North American crude oil market presented in Chapter 4. There are three optimization problems relating to the supply side, transportation and the demand sector, each with their own sets of constraints. These are detailed in the following three subsections. The MCP is formulated as a set of KKT conditions (not enumerated in this section) solved simultaneously. For further discussion on the basic model framework, please refer to Huppmann and Egging [79].

C.1 Acronyms used in Chapter 4

We describe the acronyms that appear frequently in Chapter 4 below in Table C.1.

Table C.1 Acronyms and abbreviations used with regard to the crude oil model

Acronym	Full meaning	Notes
API	American Petroleum Institute [gravity]	measure of crude oil quality
CAPP	Canadian Association of Petroleum Producers	
EIA	Energy Information Administration	United States
GAMS	General Algebraic Modeling System	
KKT	Karush-Kuhn-Tucker	in reference to first-order optimality conditions
MCP	Mixed Complementarity Problem	class of problems to which this model belongs
NACOM	North American crude oil model	
OPEC	Organization of the Petroleum Exporting Countries	
PADD	Petroleum Administration Defense District	
Pemex	Petróleos Mexicanos	Mexico state-run petroleum company

C.2 Further model nomenclature

A complete enumeration of the parameters and variables used in this model are given in Table C.2 and Table C.3, respectively.

Table C.2 Model parameters

Transportation (Arcs)	cap^A_{ya}	capacity, arc a in year y
	dep^A_{ya}	depreciation of arc capacity expansion
	exp^A_{ya}	capacity expansion limit, arc a year y
	inv^A_{ya}	unit investment costs, arc capacity expansion
	loss^A_{a}	loss rate, transit via arc a
	trf^A_{ya}	tariff, arc a in year y
Production	avl^P_{yne}	availability factor, production capacity
	gol^P_{yne}	logarithmic term, production cost function
	hor^P_{yne}	production horizon (reserves)
	lin^P_{yne}	linear term, production cost function
	loss^P_{sne}	loss rate, production, node n, fuel e
	qud^P_{yne}	quadratic term, production cost function
Demand	eff^D_{yne}	efficiency, demand satisfaction, fuel e
	ems^D_{ye}	GHG emission during fuel e consumption, node n
	eucc^D_{yne}	constant term, end use cost function
	eucl^D_{yne}	linear term, end use cost function
	int^D_{yn}	intercept, inverse demand function, node n
	slp^D_{yn}	slope, inverse demand function, node n

Table C.3 Variables

Production	α^P_{ysne}	production capacity constraint dual
	γ^P_{ysne}	production horizon constraint dual
	q^P_{ysne}	quantity produced
	z^P_{ysne}	production capacity expansion
Transportation (Arcs)	f^A_{ya}	operator arc flow
	p^A_{ya}	arc capacity market clearing price
	q^A_{ysa}	quantity transported, arc a
	τ^A_{ya}	arc capacity constraint dual
	z^A_{ya}	arc capacity expansion dual
	ζ^A_{ya}	arc capacity expansion limit dual
Demand	p^D_{yne}	final demand price of fuel e
	q^D_{ysne}	quantity sold to refinery sector
Other	f^G_{yn}	quantity of GHG emissions at node g
	ϕ^A_{ya}	mass balance constraint dual

C.3 List of nodes

Table C.4 lists the nodes in the model, their abbreviations and their regions.

Table C.4 List of nodes, their abbreviations and regions in the model.

Node	Abbreviation	Region	Producer	Consumer
Alabama	AL	PADD3	0	0
Alaska	AK	PADD5	1	1
Arizona	AZ	PADD5	0	0
Arkansas	AR	PADD3	0	0
California	CA	PADD5	1	1
Colorado	CO	PADD4	1	1
Connecticut	CT	PADD1	0	0
Delaware	DE	PADD1	0	1
District of Columbia	DC	PADD1	0	0
Eastern Canada	EC	CAN	1	1
Florida	FL	PADD1	0	0
Georgia	GA	PADD1	0	0
Hawaii	HI	PADD5	0	0
Idaho	ID	PADD4	0	0
Illinois	IL	PADD2	0	1
Indiana	IN	PADD2	0	1
Iowa	IA	PADD2	0	0
Kansas	KS	PADD2	1	1
Kentucky	KY	PADD2	0	1

Table C.4 List of nodes, their abbreviations and regions in the model.

Node	Abbreviation	Region	Producer	Consumer
Louisiana	LA	PADD3	1	1
Maine	ME	PADD1	0	0
Maryland	MD	PADD1	0	0
Massachusetts	MA	PADD1	0	0
Mexico	MX	MEX	1	1
Michigan	MI	PADD2	0	0
Minnesota	MN	PADD2	0	1
Mississippi	MS	PADD3	0	1
Missouri	MO	PADD2	0	0
Montana	MT	PADD4	0	1
Nebraska	NE	PADD2	0	0
Nevada	NV	PADD5	0	0
New Hampshire	NH	PADD1	0	0
New Jersey	NJ	PADD1	0	1
New Mexico	NM	PADD3	1	1
New York	NY	PADD1	0	0
North Carolina	NC	PADD1	0	0
North Dakota	ND	PADD2	1	1
Ohio	OH	PADD2	0	1
Oklahoma	OK	PADD2	1	1
Oregon	OR	PADD5	0	0
Pennsylvania	PA	PADD1	0	1
Rest of World	RW	ONA	1	1
Rhode Island	RI	PADD1	0	0
South Carolina	SC	PADD1	0	0
South Dakota	SD	PADD2	0	0
Tennessee	TN	PADD2	0	1
Texas	TX	PADD3	1	1
Utah	UT	PADD4	0	0
Vermont	VT	PADD1	0	0
Virginia	VA	PADD1	0	0
Washington	WA	PADD5	0	1
West Virginia	WV	PADD1	0	0
Western Canada	WC	CAN	1	1
Wisconsin	WI	PADD2	0	0
Wyoming	WY	PADD4	1	1
Alabama Rail Terminal	AL_R	PADD3		
Alaska Rail Terminal	AK_R	PADD5		
Arizona Rail Terminal	AZ_R	PADD5		
Arkansas Rail Terminal	AR_R	PADD3		
California Rail Terminal	CA_R	PADD5		
Colorado Rail Terminal	CO_R	PADD4		
Connecticut Rail Terminal	CT_R	PADD1		
Delaware Rail Terminal	DE_R	PADD1		
District of Columbia Rail Terminal	DC_R	PADD1		
Eastern Canada Rail Terminal	EC_R	CAN		
Florida Rail Terminal	FL_R	PADD1		
Georgia Rail Terminal	GA_R	PADD1		
Hawaii Rail Terminal	HI_R	PADD5		
Idaho Rail Terminal	ID_R	PADD4		
Illinois Rail Terminal	IL_R	PADD2		
Indiana Rail Terminal	IN_R	PADD2		

Table C.4 List of nodes, their abbreviations and regions in the model.

Node	Abbreviation	Region	Producer	Consumer
Iowa Rail Terminal	IA_R	PADD2		
Kansas Rail Terminal	KS_R	PADD2		
Kentucky Rail Terminal	KY_R	PADD2		
Louisiana Rail Terminal	LA_R	PADD3		
Maine Rail Terminal	ME_R	PADD1		
Maryland Rail Terminal	MD_R	PADD1		
Massachusetts Rail Terminal	MA_R	PADD1		
Michigan Rail Terminal	MI_R	PADD2		
Minnesota Rail Terminal	MN_R	PADD2		
Mississippi Rail Terminal	MS_R	PADD3		
Missouri Rail Terminal	MO_R	PADD2		
Montana Rail Terminal	MT_R	PADD4		
Nebraska Rail Terminal	NE_R	PADD2		
Nevada Rail Terminal	NV_R	PADD5		
New Hampshire Rail Terminal	NH_R	PADD1		
New Jersey Rail Terminal	NJ_R	PADD1		
New Mexico Rail Terminal	NM_R	PADD3		
New York Rail Terminal	NY_R	PADD1		
North Carolina Rail Terminal	NC_R	PADD1		
North Dakota Rail Terminal	ND_R	PADD2		
Ohio Rail Terminal	OH_R	PADD2		
Oklahoma Rail Terminal	OK_R	PADD2		
Oregon Rail Terminal	OR_R	PADD5		
Pennsylvania Rail Terminal	PA_R	PADD1		
Rhode Island Rail Terminal	RI_R	PADD1		
South Carolina Rail Terminal	SC_R	PADD1		
South Dakota Rail Terminal	SD_R	PADD2		
Tennessee Rail Terminal	TN_R	PADD2		
Texas Rail Terminal	TX_R	PADD3		
Utah Rail Terminal	UT_R	PADD4		
Vermont Rail Terminal	VT_R	PADD1		
Virginia Rail Terminal	VA_R	PADD1		
Washington Rail Terminal	WA_R	PADD5		
West Virginia Rail Terminal	WV_R	PADD1		
Western Canada Rail Terminal	WC_R	CAN		
Wisconsin Rail Terminal	WI_R	PADD2		
Wyoming Rail Terminal	WY_R	PADD4		

C.4 Transportation arcs in the model and their initial parameter values

The arc data gathered for the model are shown in Table C.5. Some parameters were later adjusted for calibration purposes.

Table C.5 Transportation arcs for crude oil included in the model.

Outgoing Node	Incoming Node	Type	Tariff	Capacity	Capacity Constrained
AK	CA	Ship	6	0	0
AK	RW	Ship	2	0	1
AK	WA	Ship	6	0	0
AL_R	FL_R	Rail	2.15	0	0
AL_R	GA_R	Rail	1.4	0	0
AL_R	MS_R	Rail	1.35	0	0
AL_R	TN_R	Rail	1.45	0	0
AR	MS	BargeR	5.5	0	0
AR_R	LA_R	Rail	1.61	0	0
AR_R	MO_R	Rail	1.56	0	0
AR_R	MS_R	Rail	1.49	0	0
AR_R	OK_R	Rail	1.61	0	0
AR_R	TN_R	Rail	1.78	0	0
AR_R	TX_R	Rail	2	0	0
AZ_R	CA_R	Rail	2.27	0	0
AZ_R	NM_R	Rail	1.72	0	0
AZ_R	NV_R	Rail	2.14	0	0
AZ_R	UT_R	Rail	2.1	0	0
CA	CA_R	Load	1	40	1
CA	RW	Ship	2	0	1
CA_R	AZ_R	Rail	2.27	0	0
CA_R	CA	UnLoad	1	215.76	1
CA_R	NV_R	Rail	1.48	0	0
CA_R	OR_R	Rail	2.52	0	0
CO	CO_R	Load	1	140.99	1
CO	OK	Pipeline	4.86	75	1
CO_R	CO	UnLoad	1	6	1
CO_R	KS_R	Rail	1.96	0	0
CO_R	NE_R	Rail	1.99	0	0
CO_R	NM_R	Rail	1.71	0	0
CO_R	OK_R	Rail	2.12	0	0
CO_R	UT_R	Rail	1.87	0	0
CO_R	WY_R	Rail	1.64	0	0
CT_R	NY_R	Rail	1.22	0	0
DE	DE_R	Load	1	0	1
DE_R	DE	UnLoad	1	145	1
DE_R	MD_R	Rail	1.09	0	0
DE_R	PA_R	Rail	1.24	0	0
EC	DE	Ship	1.5	0	0

Table C.5 Transportation arcs for crude oil included in the model.

Outgoing Node	Incoming Node	Type	Tariff	Capacity	Capacity Constrained
EC	EC_R	Load	1	0	1
EC	NJ	Ship	1.5	0	0
EC	NY	Ship	1.5	0	0
EC	PA	Ship	1.5	0	0
EC	RW	Ship	4	0	0
EC_R	EC	UnLoad	1	240	1
EC_R	MI_R	Rail	7.88	0	0
EC_R	MN_R	Rail	9.01	0	0
EC_R	NY_R	Rail	3.35	0	0
EC_R	VT_R	Rail	2.88	0	0
EC_R	WC_R	Rail	6	0	0
FL_R	AL_R	Rail	2.15	0	0
FL_R	GA_R	Rail	1.92	0	0
GA	NC	Pipeline	4.81	860	1
GA_R	AL_R	Rail	1.4	0	0
GA_R	FL_R	Rail	1.92	0	0
GA_R	SC_R	Rail	1.36	0	0
GA_R	TN_R	Rail	1.36	0	0
IA_R	IL_R	Rail	1.57	0	0
IA_R	MN_R	Rail	1.61	0	0
IA_R	MO_R	Rail	1.58	0	0
IA_R	NE_R	Rail	1.63	0	0
IA_R	SD_R	Rail	1.86	0	0
IA_R	WI_R	Rail	1.55	0	0
ID_R	MT_R	Rail	1.64	0	0
ID_R	NV_R	Rail	2.06	0	0
ID_R	OR_R	Rail	12.93	0	0
ID_R	UT_R	Rail	1.76	0	0
ID_R	WA_R	Rail	13	0	0
ID_R	WC_R	Rail	10.39	0	0
ID_R	WY_R	Rail	1.94	0	0
IL	IL_R	Load	1	0	1
IL	IN	Pipeline	4.8	2,620	1
IL	KY	Pipeline	4.82	256	1
IL	MS	BargeR	5.5	0	0
IL	OH	Pipeline	4.78	290	1
IL_R	IA_R	Rail	1.57	0	0
IL_R	IL	UnLoad	1	312.04	1
IL_R	IN_R	Rail	1.3	0	0
IL_R	KY_R	Rail	1.71	0	0
IL_R	MO_R	Rail	1.49	0	0
IL_R	WI_R	Rail	1.64	0	0
IN	IN_R	Load	1	0	1
IN	MI	Pipeline	4.85	2,620	1
IN_R	IL_R	Rail	1.3	0	0
IN_R	IN	UnLoad	1	0	1
IN_R	KY_R	Rail	1.37	0	0
IN_R	MI_R	Rail	1.6	0	0
IN_R	OH_R	Rail	1.41	0	0
KS	KS_R	Load	1	0	1
KS	OK	Pipeline	4.78	230	1
KS_R	CO_R	Rail	1.96	0	0

Table C.5 Transportation arcs for crude oil included in the model.

Outgoing Node	Incoming Node	Type	Tariff	Capacity	Capacity Constrained
KS_R	KS	UnLoad	1	32	1
KS_R	MO_R	Rail	1.56	0	0
KS_R	NE_R	Rail	1.43	0	0
KS_R	OK_R	Rail	1.26	0	0
KY	KY_R	Load	1	0	1
KY_R	IL_R	Rail	1.71	0	0
KY_R	IN_R	Rail	1.37	0	0
KY_R	KY	UnLoad	1	0	1
KY_R	MO_R	Rail	2.04	0	0
KY_R	OH_R	Rail	1.48	0	0
KY_R	TN_R	Rail	1.13	0	0
KY_R	VA_R	Rail	1.61	0	0
KY_R	WV_R	Rail	1.21	0	0
LA	LA_R	Load	1	10	1
LA	MS	BargeS	5.5	0	0
LA	RW	Ship	2	0	1
LA	TN	BargeR	6.8	0	0
LA	TN	Pipeline	4.84	1,200	1
LA	TX	Pipeline	4.8	325	1
LA_R	AR_R	Rail	1.61	0	0
LA_R	LA	UnLoad	1	687.23	1
LA_R	MS_R	Rail	1.36	0	0
LA_R	TX_R	Rail	1.83	0	0
MA_R	NY_R	Rail	1.37	0	0
MA_R	RI_R	Rail	1	0	0
MD_R	DE_R	Rail	1.09	0	0
MD_R	PA_R	Rail	1.19	0	0
MD_R	VA_R	Rail	1.22	0	0
MD_R	WV_R	Rail	1.52	0	0
ME	EC	Pipeline	4.78	300	1
MI	EC	Pipeline	4.85	40	1
MI	NJ	Pipeline	4.86	0	1
MI_R	EC_R	Rail	4.88	0	0
MI_R	IN_R	Rail	1.6	0	0
MI_R	OH_R	Rail	1.51	0	0
MI_R	WI_R	Rail	1.61	0	0
MN	MN_R	Load	1	0	1
MN_R	EC_R	Rail	5.01	0	0
MN_R	IA_R	Rail	1.61	0	0
MN_R	MN	UnLoad	1	0	1
MN_R	ND_R	Rail	1.73	0	0
MN_R	SD_R	Rail	1.68	0	0
MN_R	WC_R	Rail	11.2	0	0
MN_R	WI_R	Rail	1.53	0	0
MO	MS	BargeR	5.5	0	0
MO_R	AR_R	Rail	1.56	0	0
MO_R	IA_R	Rail	1.58	0	0
MO_R	IL_R	Rail	1.49	0	0
MO_R	KS_R	Rail	1.56	0	0
MO_R	KY_R	Rail	2.04	0	0
MO_R	NE_R	Rail	1.9	0	0
MO_R	OK_R	Rail	1.79	0	0

Table C.5 Transportation arcs for crude oil included in the model.

Outgoing Node	Incoming Node	Type	Tariff	Capacity	Capacity Constrained
MO_R	TN_R	Rail	1.88	0	0
MS	MS_R	Load	1	0	1
MS	PA	BargeS	5	0	0
MS_R	AL_R	Rail	1.35	0	0
MS_R	AR_R	Rail	1.49	0	0
MS_R	LA_R	Rail	1.36	0	0
MS_R	MS	UnLoad	1	50	1
MS_R	TN_R	Rail	1.62	0	0
MT	MT_R	Load	1	0	1
MT	WA	Pipeline	4.86	0	1
MT	WY	Pipeline	4.81	145	1
MT_R	ID_R	Rail	1.64	0	0
MT_R	MT	UnLoad	1	0	1
MT_R	ND_R	Rail	2.25	0	0
MT_R	SD_R	Rail	2.41	0	0
MT_R	WA_R	Rail	20.43	0	0
MT_R	WC_R	Rail	9.82	0	0
MT_R	WY_R	Rail	1.79	0	0
MX	AL	Ship	0.4	0	0
MX	LA	Ship	0.4	0	0
MX	MS	Ship	0.4	0	0
MX	NJ	Ship	4	0	0
MX	RW	Ship	1.5	0	0
MX	TX	Ship	0.4	0	0
NC	NJ	Pipeline	4.86	860	1
NC_R	SC_R	Rail	1.28	0	0
NC_R	TN_R	Rail	1.66	0	0
NC_R	VA_R	Rail	1.37	0	0
ND	IL	Pipeline	4.91	2,620	1
ND	MT	Pipeline	4.75	145	1
ND	ND_R	Load	1	1,262.99	1
ND_R	EC_R	Rail	2	17	1
ND_R	MN_R	Rail	1.73	0	0
ND_R	MT_R	Rail	2.25	0	0
ND_R	ND	UnLoad	1	0	1
ND_R	SD_R	Rail	1.51	0	0
ND_R	WC_R	Rail	10.39	0	0
NE	OK	Pipeline	4.8	591	1
NE_R	CO_R	Rail	1.99	0	0
NE_R	IA_R	Rail	1.63	0	0
NE_R	KS_R	Rail	1.43	0	0
NE_R	MO_R	Rail	1.9	0	0
NE_R	SD_R	Rail	1.51	0	0
NE_R	WY_R	Rail	2.19	0	0
NJ	NJ_R	Load	1	0	1
NJ	RW	Ship	2	0	1
NJ_R	NJ	UnLoad	1	101.47	1
NJ_R	NY_R	Rail	1.25	0	0
NJ_R	PA_R	Rail	1.29	0	0
NM	NM_R	Load	1	173.98	1
NM	TX	Pipeline	4.9	400	1
NM_R	AZ_R	Rail	1.72	0	0

Table C.5 Transportation arcs for crude oil included in the model.

Outgoing Node	Incoming Node	Type	Tariff	Capacity	Capacity Constrained
NM_R	CO_R	Rail	1.71	0	0
NM_R	NM	UnLoad	1	0	1
NM_R	OK_R	Rail	2.14	0	0
NM_R	TX_R	Rail	2.43	0	0
NV_R	AZ_R	Rail	2.14	0	0
NV_R	CA_R	Rail	1.48	0	0
NV_R	ID_R	Rail	2.06	0	0
NV_R	OR_R	Rail	2.26	0	0
NV_R	UT_R	Rail	1.73	0	0
NY_R	CT_R	Rail	1.22	0	0
NY_R	EC_R	Rail	4.85	0	0
NY_R	MA_R	Rail	1.37	0	0
NY_R	NJ_R	Rail	1.25	0	0
NY_R	PA_R	Rail	1.34	0	0
OH	LA	BargeR	5.5	0	0
OH	OH_R	Load	1	24	1
OH	TX	BargeR	5.5	0	0
OH_R	IN_R	Rail	1.41	0	0
OH_R	KY_R	Rail	1.48	0	0
OH_R	MI_R	Rail	1.51	0	0
OH_R	OH	UnLoad	1	56.76	1
OH_R	PA_R	Rail	1.44	0	0
OH_R	WV_R	Rail	1.09	0	0
OK	IL	Pipeline	4.91	913	1
OK	LA	BargeR	5	0	0
OK	OK_R	Load	1	722.97	1
OK	TX	Pipeline	3.11	850	1
OK_R	AR_R	Rail	1.61	0	0
OK_R	CO_R	Rail	2.12	0	0
OK_R	KS_R	Rail	1.26	0	0
OK_R	MO_R	Rail	1.79	0	0
OK_R	NM_R	Rail	2.14	0	0
OK_R	OK	UnLoad	1	176.76	1
OK_R	TX_R	Rail	0.99	0	0
OR	CA	BargeS	5	0	0
OR	WA	BargeS	5	0	0
OR_R	CA_R	Rail	2.52	0	0
OR_R	ID_R	Rail	5.93	0	0
OR_R	NV_R	Rail	2.26	0	0
OR_R	OR	UnLoad	1	200	1
OR_R	WA_R	Rail	1.43	0	0
PA	KY	BargeR	5.5	0	0
PA	LA	BargeR	5.5	0	0
PA	MS	BargeS	4	5.3	1
PA	PA_R	Load	1	0	1
PA_R	DE_R	Rail	1.24	0	0
PA_R	MD_R	Rail	1.19	0	0
PA_R	NJ_R	Rail	1.29	0	0
PA_R	NY_R	Rail	1.34	0	0
PA_R	OH_R	Rail	1.69	0	0
PA_R	PA	UnLoad	1	275	1
PA_R	WV_R	Rail	1.57	0	0

Table C.5 Transportation arcs for crude oil included in the model.

Outgoing Node	Incoming Node	Type	Tariff	Capacity	Capacity Constrained
RI_R	MA_R	Rail	1	0	0
RW	AK	Ship	2	0	0
RW	AL	Ship	2	0	0
RW	CA	Ship	1.5	0	0
RW	DE	Ship	2	0	0
RW	EC	Ship	4	0	0
RW	LA	Ship	2	0	0
RW	MS	Ship	2	0	0
RW	MX	Ship	2	0	0
RW	NJ	Ship	2	0	0
RW	NY	Ship	2	0	0
RW	PA	Ship	2	0	0
RW	TX	Ship	2	0	0
RW	WA	Ship	2	0	0
SC_R	GA_R	Rail	1.36	0	0
SC_R	NC_R	Rail	1.28	0	0
SD_R	IA_R	Rail	1.86	0	0
SD_R	MN_R	Rail	1.68	0	0
SD_R	MT_R	Rail	2.41	0	0
SD_R	ND_R	Rail	1.51	0	0
SD_R	NE_R	Rail	1.51	0	0
SD_R	WY_R	Rail	2	0	0
TN	IL	Pipeline	4.78	1,200	1
TN	TN_R	Load	1	0	1
TN_R	AL_R	Rail	1.45	0	0
TN_R	AR_R	Rail	1.78	0	0
TN_R	GA_R	Rail	1.36	0	0
TN_R	KY_R	Rail	1.13	0	0
TN_R	MO_R	Rail	1.88	0	0
TN_R	MS_R	Rail	1.62	0	0
TN_R	NC_R	Rail	1.66	0	0
TN_R	TN	UnLoad	1	0	1
TN_R	VA_R	Rail	1.85	0	0
TX	EC	Ship	2	0	0
TX	GA	Pipeline	4.93	860	1
TX	LA	BargeR	5	0	0
TX	MS	BargeR	5	0	0
TX	NJ	Ship	5	0	0
TX	NY	BargeS	5	0	0
TX	OH	Pipeline	5	300	1
TX	OK	Pipeline	4.85	720	1
TX	PA	BargeS	6	0	0
TX	RW	Ship	2	0	1
TX	TX_R	Load	1	741.95	1
TX_R	AR_R	Rail	2	0	0
TX_R	LA_R	Rail	1.83	0	0
TX_R	NM_R	Rail	2.43	0	0
TX_R	OK_R	Rail	1.74	0	0
TX_R	TX	UnLoad	1	752.51	1
UT_R	AZ_R	Rail	2.1	0	0
UT_R	CO_R	Rail	1.87	0	0
UT_R	ID_R	Rail	1.76	0	0

Table C.5 Transportation arcs for crude oil included in the model.

Outgoing Node	Incoming Node	Type	Tariff	Capacity	Capacity Constrained
UT_R	NV_R	Rail	1.73	0	0
UT_R	WY_R	Rail	1.72	0	0
VA_R	KY_R	Rail	1.61	0	0
VA_R	MD_R	Rail	1.22	0	0
VA_R	NC_R	Rail	1.37	0	0
VA_R	TN_R	Rail	1.85	0	0
VA_R	WV_R	Rail	1.08	0	0
VT_R	EC_R	Rail	4.38	0	0
WA	OR	Pipeline	4.81	295	1
WA	RW	Ship	2	0	1
WA	WA_R	Load	1	0	1
WA_R	ID_R	Rail	2.5	0	0
WA_R	OR_R	Rail	1.43	0	0
WA_R	WA	UnLoad	1	163	1
WA_R	WC_R	Rail	10.38	0	0
WC	MN	Pipeline	4.96	880	1
WC	MT	Pipeline	4.99	145	1
WC	ND	Pipeline	4.93	2,620	1
WC	NE	Pipeline	4.92	591	1
WC	WC_R	Load	1	990.46	1
WC	WY	Pipeline	4.93	280	1
WC_R	EC_R	Rail	6	0	0
WC_R	ID_R	Rail	10.39	0	0
WC_R	MN_R	Rail	11.2	0	0
WC_R	MT_R	Rail	9.82	0	0
WC_R	ND_R	Rail	10.39	0	0
WC_R	WA_R	Rail	10.38	0	0
WC_R	WC	UnLoad	1	7	1
WI_R	IA_R	Rail	1.55	0	0
WI_R	IL_R	Rail	1.64	0	0
WI_R	MI_R	Rail	1.61	0	0
WI_R	MN_R	Rail	1.53	0	0
WV	KY	BargeR	5.5	0	0
WV	LA	BargeR	5.5	0	0
WV	TX	BargeR	5.5	0	0
WV_R	KY_R	Rail	1.21	0	0
WV_R	MD_R	Rail	1.52	0	0
WV_R	OH_R	Rail	1.09	0	0
WV_R	PA_R	Rail	1.57	0	0
WV_R	VA_R	Rail	1.08	0	0
WY	IL	Pipeline	4.99	280	1
WY	KS	Pipeline	4.84	230	1
WY	WY_R	Load	1	555	1
WY_R	CO_R	Rail	1.64	0	0
WY_R	ID_R	Rail	1.94	0	0
WY_R	MT_R	Rail	1.79	0	0
WY_R	NE_R	Rail	2.19	0	0
WY_R	SD_R	Rail	2	0	0
WY_R	UT_R	Rail	1.72	0	0
WY_R	WY	UnLoad	1	0	1

C.5 The Petroleum Administration for Defense Districts

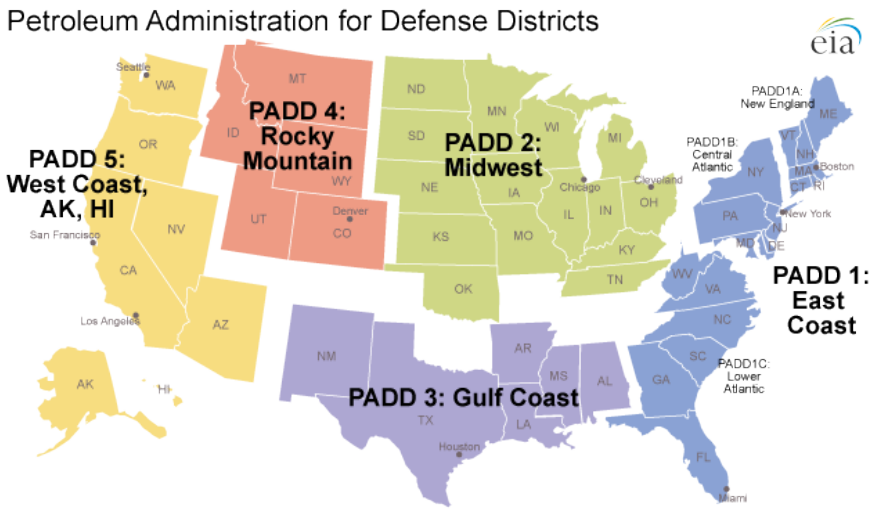

Figure C.1 Petroleum Administration for Defense Districts (Source: EIA [193])

The Petroleum Administration Defense Districts (PADDs) were historically drawn up to organize gasoline distribution during wartime rationing [193], but they have now been established as the baseline for recording and analyzing crude oil movements in the U.S. (Figure C.1), especially by the Energy Information Administration. As described in Subsection 4.4.4, we use the PADD regional crude oil movement data as the basis for calibrating base case flows through the U.S. We also occasionally use them in highlighting regional changes at various points in Chapter 4.

C.6 Model and reference flow comparisons

To validate our model, we compare flows to reference data at the regional level, which is the best resolution available. The interregional flows in the base year 2012 for each of the modes are shown in Figure C.2, Figure C.3 and Figure C.4.

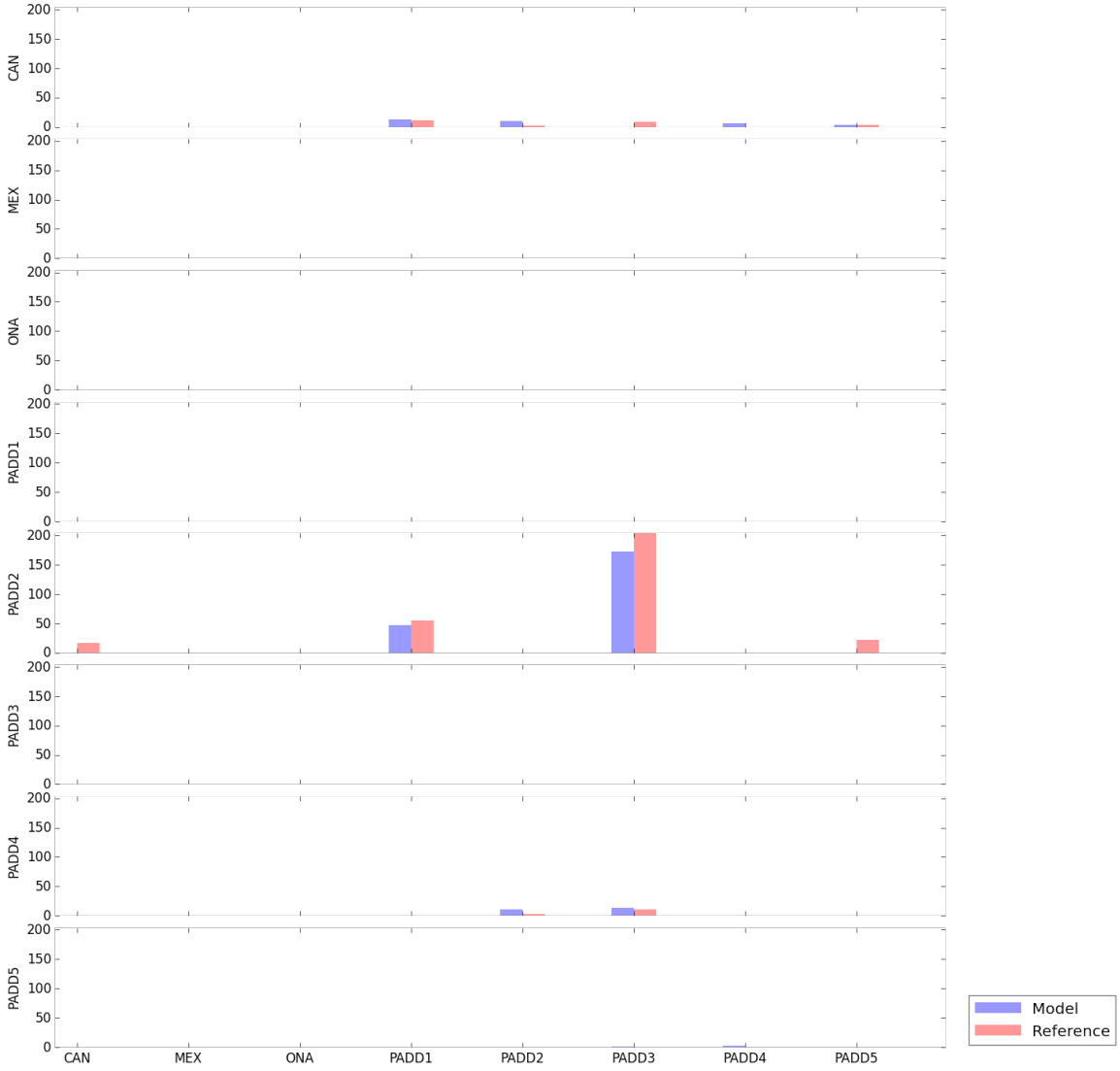

Figure C.2 Comparison of model and reference interregional flows via rail in 2012

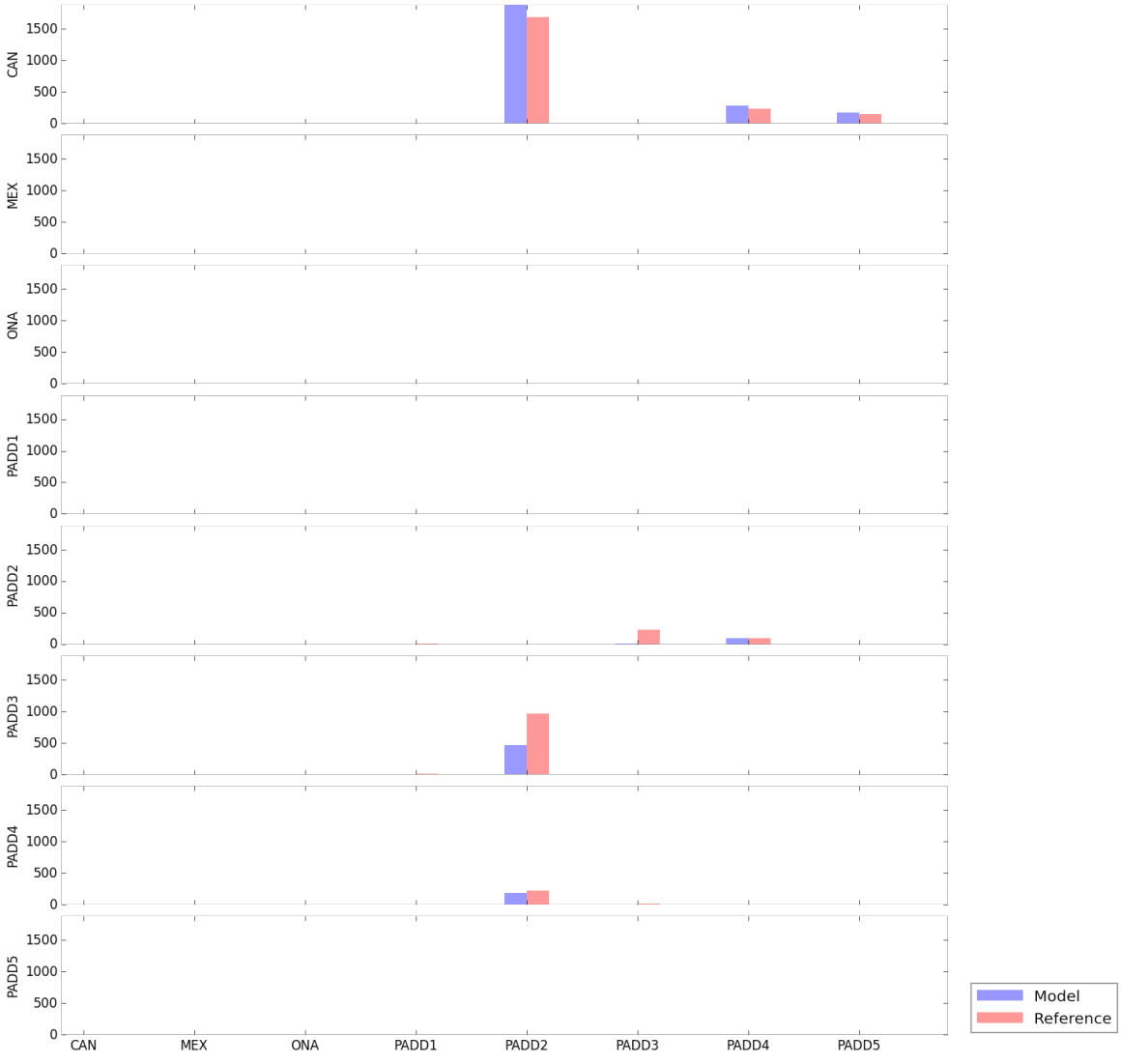

Figure C.3 Comparison of model and reference interregional flows via pipeline in 2012

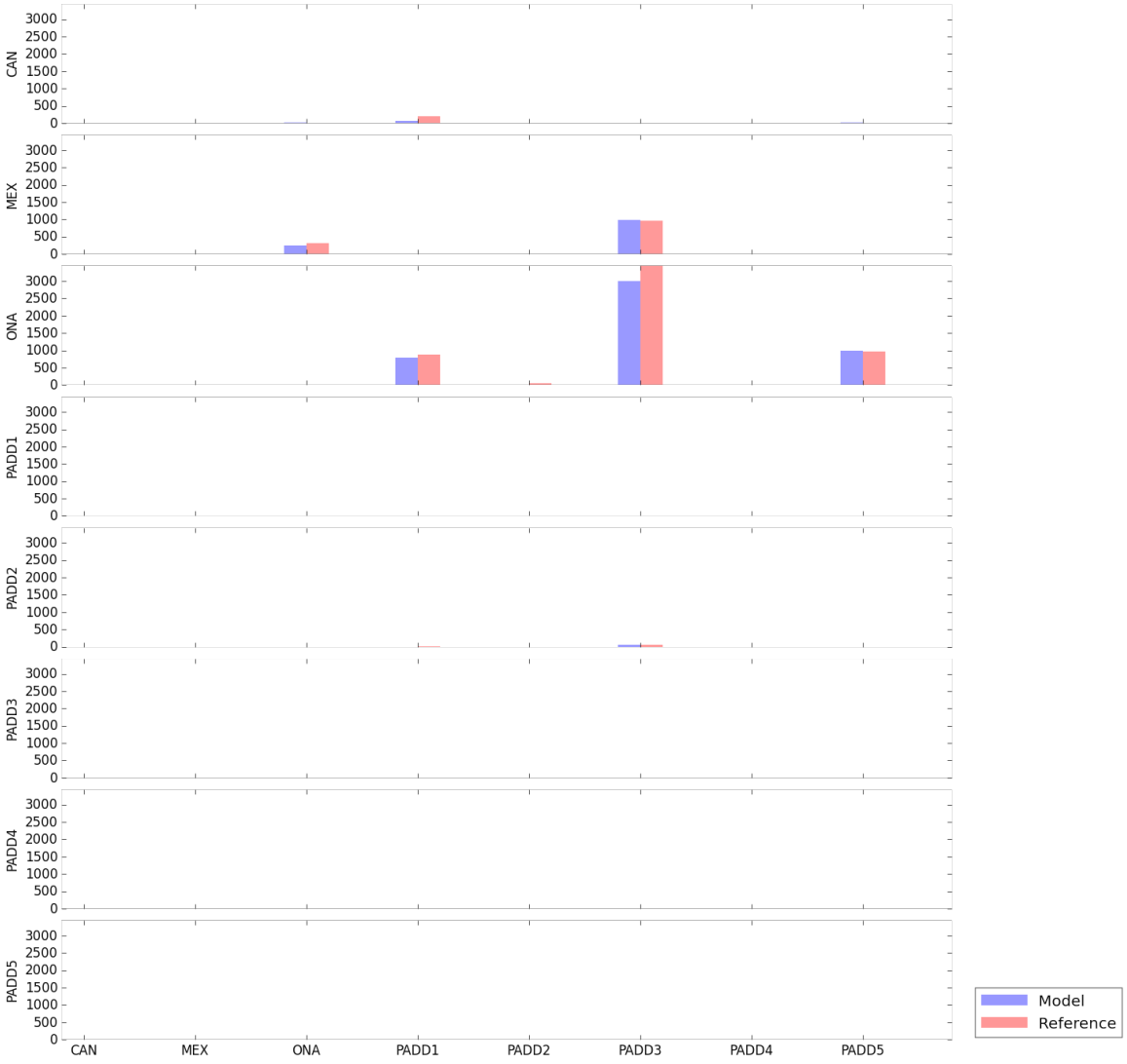

Figure C.4 Comparison of model and reference interregional flows via tanker/barge in 2012

Bibliography

[1] Nader Alkathiri, Yazeed Al-Rashed, Tilak K. Doshi, and Frederic Murphy. Asian premium or North Atlantic discount: Does geographical diversification in oil trade always impose costs? Discussion Paper KS-1522-DP016A, King Abdullah Petroleum Studies and Research Center (KAPSARC), August 2015.

[2] Tom Allan. Edinburgh's hidden cycle paths. http://www.guardian.co.uk/environment/bike-blog/2011/jun/17/interactive-map-edinburgh-cycle-paths, June 2011. Accessed on: May 14, 2013.

[3] American Fuel & Petrochemical Manufacturers. Refining U.S. petroleum: A survey of U.S. refinery use of growing U.S. crude oil production. Report, AFPM, Washington, DC, March 2015. URL https://www.afpm.org/uploadedFiles/Refining-US-Capacity.pdf. Survey Conducted by: Veris Consulting, Charles LeRoy.

[4] Aris Anagnostopoulos, Ravi Kumar, and Mohammad Mahdian. Influence and correlation in social networks. In *Proceedings of the 14th ACM SIGKDD International Conference on Knowledge Discovery and Data Mining*, KDD '08, pages 7–15, New York, NY, USA, 2008. ACM. ISBN 978-1-60558-193-4.

doi: 10.1145/1401890.1401897. URL http://doi.acm.org/10.1145/1401890.1401897.

[5] K. J. Arrow, E. W. Barankin, and D. Blackwell. Admissible points of convex sets. In H.W. Kuhn and A.W. Tucker, editors, *Contributions to the Theory of Games,*, volume 2, pages 87–91. Princeton University Press, Princeton, 1953.

[6] Canadian Fuels Association. Canada's refining sector, 2014. URL http://canadianfuels.ca/en/refining-sites-and-capacity.

[7] Association of Oil Pipe Lines. U.S. liquids pipeline usage & mileage report. Technical report, American Petroleum Institute, October 2014.

[8] Association of Oil Pipe Lines. U.S. liquids pipeline usage & mileage report. Technical report, American Petroleum Institute, November 2015.

[9] augenschein Filmproduktion GmbH. Tour du faso: Synopsis, 2016. URL http://www.tourdufaso-film.com/en/. A documentary by Wilm Huygen.

[10] Silvania Avelar and Lorenz Hurni. On the design of schematic transport maps. *Cartographica*, 41(3):217–228, 2006.

[11] Silvania Avelar and Matthias Müller. Generating topologically correct schematic maps. *Proceedings Ninth International Symposium on Spatial Data Handling*, 2000.

[12] Chris Baerveldt, de Gerhard G. van Bunt, and M. Marjolijn Vermande. Selection patterns, gender and friendship aim in classroom networks. *Zeitschrift für Erziehungswissenschaft*, 17(5):171–188, 2014.

[13] D. Bannister. Cities, mobility and climate change. *Journal of Transport Geography*, pages 1538–1546, 2011.

[14] Michael A. Bekos, Michael Kaufmann, Katerina Potika, and Antonios Symvonis. Line crossing minimization on metro maps. In Seok-Hee Hong, Takao Nishizeki, and Wu Quan, editors, *Graph Drawing*, volume 4875 of *Lecture Notes in Computer Science*, pages 231–242. Springer Berlin Heidelberg, 2008. ISBN 978-3-540-77536-2. URL http://dx.doi.org/10.1007/978-3-540-77537-9_24.

[15] Richard Bellman and R. Kalaba. On adaptive control processes. *Automatic Control, IRE Transactions on*, 4(2):1–9, Nov 1959.

[16] Beyond DC. Us bikesharing annual reports, 2014. URL http://beyonddc.com/log/?page_id=6319.

[17] Kavi Bhalla, Marc Shotten, Aaron Cohen, Michael Brauer, Saeid Shahraz, Richard Burnett, Katherine Leach-Kemon, Greg Freedman, Christopher J.L. Murray, Rita Van Dingenen, Frank Dentener, Theo Vos, Mohsen Naghavi, Jerry Abraham, David Bartels, and Pon-Hsiu Weh. Transport for health: the global burden of disease due to injuries and air pollution from motorized road transport. Report, Global Road Safety Facility, The World Bank; Institute for Health Metrics and Evaluation, Seattle, WA: IHME; Washington, DC: The World Bank, 2014.

[18] National Energy Board. Energy East Project, December 2015. URL https://www.neb-one.gc.ca/pplctnflng/mjrpp/nrgyst/index-eng.html. Canada.

[19] Jason Bordoff. U.S. crude oil export policy. Columbia SIPA, Center on Global Energy Policy, July 2014. URL https://www.eia.gov/conference/2014/pdf/presentations/bordoff.pdf. EIA Energy Conference.

[20] Barry Bosworth and Susan M. Collins. Accounting for growth: Comparing China and India. *J. Econ. Perspect.*, 22(1):45–66, 2008.

[21] Aaron Brady, Steve Kelly, Kevin Birn, James Fallon, Clarke Lind, Juan Osuna, and Dominik Rozwadowski. North america's heavy crude future: Western canadian access, the us refining system, and offshore supply. Strategic report, IHS Energy, February 2015. URL http://www.eenews.net/assets/2015/02/23/document_pm_02.pdf.

[22] Hannah Breul and Bill Brown. Crude oil swaps with mexico could provide economic and environmental benefits. U.S. Energy Information Administration, September 2015. URL https://www.eia.gov/todayinenergy/detail.cfm?id=22872.

[23] Sergio Cabello, Mark de Berg, and Marc van Kreveld. Schematization of networks. *Computational Geometry: Theory and Algorithms*, 30:223–238, 2005.

[24] Canada's Oil and Natural Gas Producers. Crude oil: Forecast, markets & transportation. Report, Canadian Association of Petroleum Producers (CAPP), June 2014.

[25] Rafael G. Cano, Guilherme Kunigami, Cid C. de Souza, and Pedro J. de Rezende. A hybrid GRASP heuristic to construct effective drawings of proportional symbol maps. *Computers & Operations Research*, 40(5): 1435–1447, 2013. ISSN 0305-0548. URL http://dx.doi.org/10.1016/j.cor.2012.09.007.

[26] Andrea Capocci, Vito DP Servedio, Francesca Colaiori, Luciana S Buriol, Debora Donato, Stefano Leonardi, and Guido Caldarelli. Preferential

attachment in the growth of social networks: The internet encyclopedia Wikipedia. *Physical Review E*, 74(3):036116, 2006.

[27] A. Charnes, W. W. Cooper, and R. O. Ferguson. Optimal estimation of executive compensation by linear programming. *Management Science*, 1(2): 138–151, 1955.

[28] T. Donna Chen and Kara M. Kockelman. Management of a shared, autonomous, electric vehicle fleet: Implications of pricing schemes. In *Proceedings of the 95th Annual Meeting of the Transportation Research Board*, January 2016. URL http://www.caee.utexas.edu/prof/kockelman/public_html/TRB16SAEVsModeChoice.pdf.

[29] T. Donna Chen, Kara M. Kockelman, and Josiah P. Hanna. Operations of a shared, autonomous, electric vehicle fleet: Implications of vehicle and charging infrastructure decisions. In *Proceedings of the 95th Annual Meeting of the Transportation Research Board*, January 2016. URL http://www.caee.utexas.edu/prof/kockelman/public_html/TRB16SAEVsModeChoice.pdf.

[30] Adam Christensen and Sauleh Siddiqui. A complementarity model of the US biofuels market. *Biofuels, Bioproducts, and Biorefineries*, 9(4):397 – 411, July 2014.

[31] Blake Clayton. The case for allowing U.S. crude oil exports. Policy Innovation Memorandum 34, Council on Foreign Relations, July 2013. Renewing America.

[32] Gabriel Collins. California crude trains: How much oil is actually coming in and where is it coming from? North America Shale Blog, March 2015. URL http://goo.gl/J1U89U.

[33] Photius Coutsoukis. North America pipelines map: Crude oil (petroleum) pipelines, natural gas pipelines, products pipelines. Information Technology Associates, http://www.theodora.com/pipelines/north_america_oil_gas_and_products_pipelines.html, May 2008.

[34] John Dales and Phil Jones. International cycling infrastructure best practice study. Report for transport for london, Urban Movement, Phil Jones Associates, December 2014. URL http://content.tfl.gov.uk/international-cycling-infrastructure-best-practice-study.pdf.

[35] Indraneel Das and J. E. Dennis. Normal-boundary intersection: A new method for generating the pareto surface in nonlinear multicriteria optimization problems. *SIAM J. on Optimization*, 8(3):631–657, March 1998. ISSN 1052-6234. doi: 10.1137/S1052623496307510. URL http://dx.doi.org/10.1137/S1052623496307510.

[36] Coral Davenport. Citing climate change, Obama rejects construction of Keystone XL oil pipeline, November 2015. URL http://nyti.ms/1MN5hpL.

[37] Lisa Davison and Angela Curl. A transport and health geography perspective on walking and cycling. *J. Transp. Health*, 1(4):341 – 345, 2014.

[38] Jeroen Johan de Hartog, Hanna Boogaard, Hans Nijland, and Gerard Hoek. Do the health benefits of cycling outweigh the risks? *Environ. Health Persp.*, 118(8):1109–1116, 2010.

[39] The Demographic and Health Surveys Program. Malaria Indicator Surveys. http://www.dhsprogram.com/What-We-Do/Survey-Types/MIS.cfm, June 2014. accessed on May 27, 2013.

[40] DHS. The Demographic and Health Surveys Program. http://www.statcompiler.com, June 2014. Accessed on May 27, 2013.

[41] Jennifer A. Dlouhy. Rare Alaskan crude shipment heads to South Korea. Fuelfix, September 2014. URL http://fuelfix.com/blog/2014/09/29/rare-alaskan-crude-shipment-heads-to-south-korea/.

[42] Thomas J. Duesterberg, Donald A. Norman, and Jeffrey F. Werling. Lifting the crude oil export ban: The impact on U.S. manufacturing. Report 14/014, The Aspen Institute, Washington, DC, October 2014.

[43] Tim Dwyer, Nathan Hurst, and Damian Merrick. A fast and simple heuristic for metro map path simplification. In *Advances in Visual Computing*, volume 5359 of *Lecture Notes in Computer Science*, pages 22–30. Springer Berlin Heidelberg, 2008. ISBN 978-3-540-89645-6. URL http://dx.doi.org/10.1007/978-3-540-89646-3_3.

[44] Matthias Ehrgott. Vilfredo pareto and multi-objective optimization. *Optimization Stories, Journal der Deutschen Mathematiker-Vereiningung, Extra*, 21:447–453, 2012.

[45] Linn Engvall and Alexandra Stojanoska. Mexico's oil industry: A paradigm shift in the making? Bachelor thesis, University of Gothenburg School of Business, Economics and Law, 2014. URL https://gupea.ub.gu.se/bitstream/2077/36949/1/gupea_2077_36949_1.pdf. Department of Business Administration.

[46] ESCAP. Combatting congestion. *Transport and Communications Bulletin for Asia and the Pacific*, 82, December 2013. Transport Division (TD) of the United Nations Economic and Social Commission for Asia and the Pacific (ESCAP).

[47] Augusto Eusébio and José Rui Figuiera. Finding non-dominated solutions in

bi-objective integer network flow problems. *Computers & Operations Research*, 36(9):2554–2564, 2009.

[48] Felipe Feijoo, Daniel Huppmann, Larissa Sakiyama, and Sauleh Siddiqui. North American natural gas model impact of cross-border trade with Mexico. Discussion Paper 1553, German Institute for Economic Research (DIW Berlin), 2016.

[49] M. C. Ferris and J. S. Pang. Engineering and economic applications of complementarity problems. *SIAM Review*, 39(4):669 – 713, December 1997.

[50] Michael C. Ferris and Todd S. Munson. Complementarity problems in GAMS and the PATH solver. *Journal of Economic Dynamics and Control*, 24(2):165 – 188, 2000.

[51] Fietsberaad. Continuous and integral: The cycling policies of Groningen and other European cycling cities. Publication Number 7, Dutch Bicycle Council, Utrecht, The Netherlands, 2006.

[52] Martin Fink, Herman Haverkort, Martin Nöllenburg, Maxwell Roberts, Julian Schuhmann, and Alexander Wolff. Drawing metro maps using bézier curves. In *Graph Drawing*, volume 7704 of *Lecture Notes in Computer Science*, pages 463–474. Springer Berlin Heidelberg, 2013. ISBN 978-3-642-36762-5. URL http://dx.doi.org/10.1007/978-3-642-36763-2_41.

[53] John Fritelli. Shipping U.S. crude oil by water: Vessel flag requirements and safety issues. Technical Report R43653, Congressional Research Service, July 2014.

[54] John Fritelli, Anthony Andrews, Paul W. Parfomak, Robert Pirog, Jonathan L. Ramseur, and Michael Ratner. U.S. rail transportation of crude

oil: Background and issues for congress. Technical Report R43390, Congressional Research Service, December 2014.

[55] Diana Furchtgott-Roth. Pipelines are safest for transportation of oil and gas. Issue Brief 23, Manhattan Institute for Policy Research, 2013.

[56] Steven A. Gabriel, Antonio J. Conejo, Carlos Ruiz, and Sauleh Siddiqui. Solving discretely constrained, mixed linear complementarity problems with applications in energy. *Computers & Operations Research*, 40(5):1339–1350, 2013. ISSN 0305-0548. URL http://dx.doi.org/10.1016/j.cor.2012.10.017.

[57] Steven A. Gabriel, Antonio J. Conejo J. David Fuller, and Benjamin F. Hobbs Carlos Ruiz. *Complementarity Modeling in Energy Markets*, volume 180 of *International Series in Operations Research & Management Science*. Springer Science+Business Media, New York, 2013.

[58] Bernat Gacias and Frédéric Meunier. Design and operation for an electric taxi fleet. *OR Spectrum*, 37(1):171–194, 2014.

[59] GAMS Development Corporation. General algebraic modeling system (gams), 2012. URL https://www.gams.com/. Release 23.9.5.

[60] Ken Garland. *Mr. Beck's Underground Map*. Capital Transport Publishing, 1994.

[61] Alyson L. Geller. Smart growth: A prescription for livable cities. *American Journal of Public Health*, 93(9):1410–1415, September 2003.

[62] Toni Giorgino. Computing and visualizing dynamic time warping alignments in R: The dtw package. *Journal of Statistical Software*, 31(7), 2009.

[63] Rolf Golombek, Eystein Gjelsvik, and Knut Einar Rosendahl. Effects of liberalizing the natural gas markets in Western Europe. *Energy Journal,*, 16 (1):85–112, 1995.

[64] Deborah Gordon, Adam Brandt, Joule Bergerson, and Jonathan Koomey. *Know Your Oil: Creating a Global Oil-Climate Index*. Carnegie Endowment for International Peace, Washington, DC, 2015.

[65] Brian C. Gozun and Marie Danielle V. Guillen. Towards a sustainable transportation environment: The case of "pedicabs" and cycling in the philippines. In *CODATU XIII*, Challenges and Solutions for a Sustainable Development, Ho Chi Minh City, Vietnam, 2008. CODATU. http://goo.gl/IQyNbp.

[66] Elspeth Graham. What is a mental map? *Area*, 8(4):259–262, 1976. URL http://www.jstor.org/stable/20001137.

[67] ICVS International Working Group, Anna Alvazzi del Frate, Jan J.M. van Dijk, John van Kesteren, Pat Mayhew, Ugi Svekic, United Nations Interregional Crime, Italy Justice Research Institute (UNICRI), Turin, United Nations Office of Drugs, and Austria Crime, Vienna. International Crime Victimization Survey (ICVS) 1989-2000. http://www.unicri.it/services/library_documentation/publications/icvs/data/, 1998.

[68] Zhan Guo. Mind the map! The impact of transit maps on travel decisions in public transit. *Transportation Research Part A: Policy and Practice*, 45(7): 625639, 2011.

[69] William C. Hahn and Robert A. Weinberg. A subway map of cancer pathways.

http://www.nature.com/nrc/poster/subpathways/index.html, May 2002. Subway map designed by Claudia Bentley. Web design by Nick Allin.

[70] Y. V. Haimes, L. S. Lasdon, and D. A. Wismer. On a bicriterion formation of the problems of integrated system identification and system optimization. *IEEE Transactions on Systems, Man and Cybernetics*, SMC-1(3):296–297, 1971.

[71] Lucas Harms, Luca Bertolini, and Marco te Brömmelstroet. Spatial and social variations in cycling patterns in a mature cycling country exploring differences and trends. *J. Transp. Health*, 1(4):232 – 242, 2014.

[72] Niel Hens, Nele Goeyvaerts, Marc Aerts, Ziv Shkedy, Pierre Van Damme, and Philippe Beutels. Mining social mixing patterns for infectious disease models based on a two-day population survey in belgium. *BMC Infectious Diseases*, 9 (1):1–18, 2009. ISSN 1471-2334. doi: 10.1186/1471-2334-9-5. URL http://dx.doi.org/10.1186/1471-2334-9-5.

[73] David V. Herlihy. *Bicycle: The History*. Yale University Press, Taunton, Mass., 2006.

[74] Karen Hofman and Xianguo Li. Canada's energy perspectives and policies for sustainable development. *Applied Energy*, 86(4):407 – 415, 2009.

[75] Seok-Hee Hong, Damian Merrick, and Hugo A. D. do Nascimento. The metro map layout problem. *Conferences in Research and Practice in Information Technology*, 35:91–100, 2004.

[76] Billy House, Kathleen Miller, and Erik Wasson. Pelosi, White House support plan allowing U.S. crude oil exports. Bloomberg Politics, December 2015. URL http://bloom.bg/1P69q61.

[77] J. D. Hunter. Matplotlib: A 2d graphics environment. *Computing In Science & Engineering*, 9(3):90–95, 2007.

[78] Daniel Huppmann. Endogenous investment decisions in natural gas equilibrium models with logarithmic cost functions. *European Journal of Operational Research*, 231(2):503–506, 2012.

[79] Daniel Huppmann and Ruud Egging. Market power, fuel substitution and infrastructure—a large-scale equilibrium model of global energy markets. *Energy*, 75:483–500, October 2014.

[80] Daniel Huppmann and Franziska Holz. Crude oil market power—a shift in recent years? *The Energy Journal*, 33(4), 2012.

[81] Christophe Hurter, Mathieu Serrurier, Roland Alonso, Gilles Tabart, and Jean-Luc Vinot. An automatic generation of schematic maps to display flight routes for air traffic controllers: structure and color optimization. In *Proceedings of the International Conference on Advanced Visual Interfaces*, AVI '10, pages 233–240, New York, NY, USA, 2010. ACM Press.

[82] IndiaStat. India National Census. http://www.indiastat.com, June 2014. accessed on June 10, 2013.

[83] UNICEF Child Info. Enquête Démographique et de Santé et à Indicateurs Multiples. http://www.childinfo.org/mics3_surveys.html, April 2013. accessed on June 14, 2013.

[84] UNICEF Child Info. Inquérito Integrado Sobre o Bem-Estar da População. http://www.childinfo.org/mics3_surveys.html, April 2013. accessed on June 14, 2013.

[85] UNICEF Child Info. Multiple Indicator Cluster Surveys/MICS3. http://www.childinfo.org/mics3_surveys.html, April 2013. accessed on June 14, 2013.

[86] UNICEF Child Info. Multiple Indicator Cluster Surveys/MICS4. http://www.childinfo.org/mics4_surveys.html, April 2013. accessed on June 14, 2013.

[87] P. L. Jacobsen. Safety in numbers: more walkers and bicyclists, safer walking and bicycling. *Injury Prevention*, 9:205–209, 2003.

[88] A. K. Jain, Jianchang Mao, and K. M. Mohiuddin. Artificial neural networks: a tutorial. *Computer*, 29(3):31–44, Mar 1996.

[89] A. K. Jain, M. N. Murty, and P. J. Flynn. Data clustering: A review. *ACM Computing Surveys*, 31(3):264–323, September 1999.

[90] Dilwyn Jenkins and Rough Guides. *The Rough Guide to Peru*. Rough Guides. Penguin, 2009. ISBN 9781405384322. URL https://books.google.com/books?id=BFZsW8seJ54C. p. 48.

[91] J. Kallrath, editor. *Algebraic Modeling Systems*, volume 104 of *Applied Optimization*, chapter GUSS: Solving Collections of Data Related Models Within GAMS, pages 35–56. Springer-Verlag Berlin Heidelberg, 2012.

[92] Michael Kennedy. An economic model of the world oil market. *The Bell Journal of Economics and Management Science*, 5(2):540–577, 1974. ISSN 00058556. URL http://www.jstor.org/stable/3003120.

[93] Archana Khurana, Arul Sundaramoorthy, and I. A. Karimi. Improving mixed integer linear programming formulations. *Proc of AIChE*, 2005.

[94] Lutz Kilian. The impact of the shale oil revolution on U.S. oil and gasoline prices. CFS Working Paper 499, Center for Financial Studies (CFS), Goethe University Frankfurt, 2014.

[95] Tinne Hoff Kjeldsen. A contextualized historical analysis of the kuhntucker theorem in nonlinear programming: The impact of world war ii. *Historia Mathematica*, 27:331 – 361, 2000.

[96] Till Koglin and Tom Rye. The marginalisation of bicycling in modernist urban transport planning. *J. Transp. Health*, 1(4):214–222, 12 2014.

[97] T. C. Koopmans. Analysis of production as an efficient combination of activities. In T.C. Koopmans, editor, *Activity Analysis of Production and Allocation*, volume 13, pages 33–97. Cowles Commission for Research in Economics Monograph, John Wiley & Sons, 1951.

[98] Noureddine Krichene. World crude oil and natural gas: a demand and supply model. *Energy Economics*, 24(6):557 – 576, 2002. ISSN 0140-9883. doi: http://dx.doi.org/10.1016/S0140-9883(02)00061-0. URL http://www.sciencedirect.com/science/article/pii/S0140988302000610.

[99] Kevin J. Krizek. Estimating the economic benefits of bicycling and bicycle facilities: an interpretive review and proposed methods. In Pablo Coto-Milln and Vicente Inglada, editors, *Essays on Transport Economics*, Contributions to Economics, pages 219–248. Physica-Verlag HD, 2007. ISBN 978-3-7908-1764-5. doi: 10.1007/978-3-7908-1765-2_14. URL http://dx.doi.org/10.1007/978-3-7908-1765-2_14.

[100] H. W. Kuhn and A. W. Tucker. Nonlinear programming. In J. Neyman, editor, *Proceedings of the Second Berkeley Symposium on Mathematical*

Statistics and Probability, pages 481–492, Berkeley, 1951. University of California Press.

[101] Lissy Langer, Daniel Huppmann, and Franziska Holz. Lifting the US crude oil export ban: A numerical partial-equilibrium analysis. Discussion Paper 1548, German Institute for Economic Research (DIW Berlin), 2016.

[102] Kate Lanier and Adam El Nakhal. U.S. Energy: From the oil crisis to the White House roof & beyond. MintPress News, July 2015. URL http://www.mintpressnews.com/MyMPN/u-s-energy-from-the-oil-crisis-to-the-white-house-roof-beyond/.

[103] Steven Levine, Gary Taylor, Daniel Arthur, and Michael Tolleth. Understanding crude oil and product markets. Technical report, American Petroleum Institute, September 2014.

[104] J. T. Linderoth and M. W. P. Savelsbergh. A computational study of search strategies for mixed integer programming. *INFORMS Journal on Computing*, 11(2):173–187, 1999. doi: 10.1287/ijoc.11.2.173. URL http://dx.doi.org/10.1287/ijoc.11.2.173.

[105] Todd Alexander Litman. Economic value of walkability. Paper, Victoria Transport Policy Institute, March 2014. Presented at the Transportation Research Board, 82nd Annual Meeting.

[106] Rafael Lozano, Mohsen Naghavi, Kyle Foreman, Stephen Lim, Kenji Shibuya, Victor Aboyans, Jerry Abraham, Timothy Adair, et al. Global and regional mortality from 235 causes of death for 20 age groups in 1990 and 2010: a systematic analysis for the global burden of disease study 2010. *Lancet*, 380 (9859):2095 – 2128, 2013. ISSN 0140-6736. doi:

http://dx.doi.org/10.1016/S0140-6736(12)61728-0. URL http://www.sciencedirect.com/science/article/pii/S0140673612617280.

[107] R. T. Marler and J. S. Arora. Survey of multi-objective optimization methods for engineering. *Structural and Multidisciplinary Optimization*, 26(6):369–395, 2004.

[108] Rafael Martí and Vicente Estruch. Incremental bipartite drawing problem. *Computers & Operations Research*, 28(13):1287–1298, 2001. ISSN 0305-0548. URL http://dx.doi.org/10.1016/S0305-0548(00)00040-X.

[109] George Mavrotas. Effective implementation of the ε-constraint method in multi-objective mathematical programming problems. *Applied Mathematics and Computation*, 213:455–465, 2009.

[110] George Mavrotas and Kostas Florios. An improved version of the augmented epsilon-constraint method (AUGMECON2) for finding the exact pareto set in multi-objective integer programming problems. *Applied Mathematics and Computation*, 219:9652–9669, 2013.

[111] S. Mavrotas and D. Diakoulaki. A branch and bound algorithm for mixed zero-one multiple objective linear programming. *European Journal of Operational Research*, 107(3):530–541, 1998.

[112] Allen McFarland and Tom Doggett. Five states and the Gulf of Mexico produce more than 80% of U.S. crude oil. U.S. Energy Information Administration, March 2014. URL https://www.eia.gov/todayinenergy/detail.cfm?id=15631.

[113] Wes McKinney. Data structures for statistical computing in python. In Stéfan van der Walt and Jarrod Millman, editors, *Proceedings of the 9th Python in Science Conference*, pages 51–56, 2010.

[114] Kenneth B. Medlock, Amy Myers Jaffe, and Meghan O'Sullivan. The global gas market, LNG exports and the shifting US geopolitical presence. *Energy Strategy Reviews*, 5:14 – 25, 2014.

[115] Kenneth Barry Medlock III. Modeling the implications of expanded US shale gas production. *Energy Strategy Reviews*, 1(1):33 – 41, 2012.

[116] Bastien Mérigot, Jean-Pierre Durbec, and Jean-Claude Gaertner. On goodness-of-fit measure for dendrogram-based analyses. *Ecology*, 91(6): 1850–1859, 2010.

[117] Peter Midgley. Bicycle-sharing schemes: Enhancing sustainable mobility in urban areas. Background Paper 8, GLobal Transport Knowledge Partnership, International Road Federation, New York, May 2011. United Nations Department of Economic and Social Affairs.

[118] Stanley Milgram. The small-world problem. *Pyschology Today*, 1(1):61 – 67, May 1967.

[119] University of Minnesota Minnesota Population Center. Integrated Public Use Microdata Series, International: Version 6.2 [Machine Readable Database]. https://international.ipums.org/international/, 2013. accessed on June 13, 2013.

[120] L. Moreira-Matias, J. Gama, M. Ferreira, J. Mendes-Moreira, and L. Damas. Predicting taxi passenger demand using streaming data. *IEEE Transactions on Intelligent Transportation Systems*, 14(3):1393–1402, Sept 2013.

[121] Jad Mouawad. Oil industry asks court to block rail transport safety rules. The New York Times, May 2015. URL http://nyti.ms/1AVFv7V.

[122] Jad Mouawad. New oil train rules are hit from all sides. The New York Times, May 2015. URL http://nyti.ms/1bmdr6G.

[123] Christopher J L Murray, Theo Vos, Rafael Lozano, Mohsen Naghavi, Abraham D Flaxman, et al. Disability-adjusted life years (DALYs) for 291 diseases and injuries in 21 regions, 1990–2010: a systematic analysis for the global burden of disease study 2010. *Lancet*, 380(9859):2197–2223, 2013. ISSN 0140-6736. doi: http://dx.doi.org/10.1016/S0140-6736(12)61689-4. URL http://www.sciencedirect.com/science/article/pii/S0140673612616894.

[124] Dan Murtaugh. Shale seen shifting flows at Americas biggest oil port. Bloomberg Business, July 2014. URL http://bloom.bg/1zUyB7q.

[125] Michael Muskal. Alaska oil, exported for first time in a decade, heads to South Korea. Los Angeles Times, September 2014. URL http://www.latimes.com/nation/nationnow/la-na-alaska-oil-export-south-korea-20140930-story.html.

[126] National Energy Board. Crude oil and petroleum products. https://www.neb-one.gc.ca/nrg/sttstc/crdlndptrlmprdct/index-eng.html, 2015. Canada.

[127] National Energy Board. Canadian crude oil exports by rail - quarterly data. https://www.neb-one.gc.ca/nrg/sttstc/crdlndptrlmprdct/stt/cndncrdlxprtsrl-eng.html, November 2015.

[128] M. E. J. Newman. Assortative patterns in networks. *Physical Review Letters*, 89(20), 2002.

[129] M. E. J. Newman. Mixing patterns in networks. *Physical Review E*, 67(2), 2003.

[130] M. E. J. Newman. Detecting community structure in networks. *Eur. Phys. J. B*, 38:321–330, 2004.

[131] CBC News. Hydro-Québec raises concerns about Energy East pipeline, March 2015. URL http://www.cbc.ca/news/canada/montreal/hydro-qu%C3%A9bec-raises-concerns-about-energy-east-pipeline-1.2982723.

[132] Blake Nicholson and James MacPherson. TransCanada to seek U.S. approval for $600m Upland pipeline. CBC News, February 2015. URL http://www.cbc.ca/news/canada/calgary/transcanada-to-seek-u-s-approval-for-600m-upland-pipeline-1.2964374.

[133] Jorge Nocedal and Stephen J. Wright. *Numerical Optimization*. Springer Series in Operations Research and Financial Engineering. Springer, New York, NY, second edition, 2006.

[134] Martin Nöllenburg and Alexander Wolff. Drawing and labeling high-quality metro maps by mixed-integer programming. *IEEE Transactions on Visualization and Computer Graphics*, 17(5), May 2011.

[135] United States. Dept. of Health and Human Services. *Physical Activity and Health: A Report of the Surgeon General*. DIANE Publishing, 1996. ISBN 9781428927940. URL http://books.google.com/books?id=WZZPc1FmL7QC.

[136] Oil and Gas Policy and Regulatory Affairs Division (Oil and Gas Division). Canadian crude oil, natural gas and petroleum products: Review of 2009 & outlook to 2030. Annual working paper, Natural Resources Canada (NRCan), 2011. URL http://www.nrcan.gc.ca/sites/www.nrcan.gc.ca/files/energy/pdf/eneene/sources/crubru/revrev/pdf/revrev-09-eng.pdf.

[137] Oil Change International. North American crude by rail. http://priceofoil.org/rail-map/, 2015.

[138] P. Oja, S. Titze, A. Bauman, B. de Geus, P. Krenn, B. Reger-Nash, and T. Kohlberger. Health benefits of cycling: a systematic review. *Scand. J. Med. Sci. Spor.*, 21(4):496–509, 2011. ISSN 1600-0838. doi: 10.1111/j.1600-0838.2011.01299.x. URL http://dx.doi.org/10.1111/j.1600-0838.2011.01299.x.

[139] Olufolajimi Oke and Sauleh Siddiqui. Efficient automated schematic map drawing using multiobjective mixed integer programming. *Computers & Operations Research*, 61:1 – 17, 2015.

[140] Olufolajimi Oke, Kavi Bhalla, David C. Love, and Sauleh Siddiqui. Tracking global bicycle ownership patterns. *Journal of Transport and Health*, 2(4): 490–501, 2015.

[141] Olufolajimi Oke, Kavi Bhalla, David C. Love, and Sauleh Siddiqui. Spatial associations in household global bicycle ownership. *Annals of Operations Research*, 2016. In review.

[142] Olufolajimi Oke, Daniel Huppmann, Max Marshall, Ricky Poulton, and Sauleh Siddiqui. Mitigating environmental and public-safety risks of united states crude-by-rail transport. *Energy Strategy Reviews*, 2016. In review.

[143] Ontario Energy Board (OEB). Giving a voice to Ontarians on Energy East: Report to the Minister. Report, Ontario Energy Board, August 2015. URL http://www.ontarioenergyboard.ca/html/oebenergyeast/documents/report_to_minister/energyeast_report_to_minister_EN.pdf.

[144] World Health Organization. Study on global ageing and adult health.

http://apps.who.int/healthinfo/systems/surveydata/index.php/catalog/sage, February 2012. accessed on July 1, 2013.

[145] World Health Organization. World Health Survey. http://apps.who.int/healthinfo/systems/surveydata/index.php/catalog/whs, June 2013. accessed on May 27, 2013.

[146] Mark Ovenden. *Transit Maps of the World*. Penguin Books, 2007.

[147] V. Pareto. *Manual of Political Economy*. Augustus M. Kelley Publishers, New York, 1971.

[148] Fernando Pérez and Brian E. Granger. IPython: A system for interactive scientific computing. *Computing in Science & Engineering*, 9:21–29, 2007. doi:10.1109/MCSE.2007.53.

[149] Kristina Peterson. Congress passes $1.15 trillion spending bill. The Wall Street Journal, December 2015. URL http://www.wsj.com/articles/house-passes-1-15-trillion-spending-bill-1450450381.

[150] Pipeline and Hazardous Materials Safety Administration (PHMSA), Department of Transportation (DOT). Hazardous materials: Enhanced tank car standards and operational controls for high-hazard flammable trains; final rule. In *Federal Register*, volume 80. National Records and Archives Administration, May 2015.

[151] M. Piraveenan, M. Prokopenko, and A. Zomaya. Assortative mixing in directed biological networks. *IEEE/ACM Transactions on Computational Biology and Bioinformatics*, 9(1):66–78, 2012. ISSN 1545-5963.

[152] Michael Pratt, Olga L Sarmiento, Felipe Montes, David Ogilvie, Bess H Marcus, Lilian G Perez, Ross C Brownson, Lancet Physical Activity Series

Working Group, and Lars Bo Andersen. The implications of megatrends in information and communication technology and transportation for changes in global physical activity. *Lancet*, 380(9838):282–93, 2012. ISSN 0140-6736. doi: 10.1016/S0140-6736(12)60736-3.

[153] H. Prillinger. U-bahn in Wien. http://homepage.univie.ac.at/horst.prillinger/metro/m/largemap.html, October 2013.

[154] Helen C. Purchase, Robert F. Cohen, and Murray James. Validating graph drawing aesthetics. *Lecture Notes in Computer Science*, 1027:435–446, 1996.

[155] Mohan S. Rana, S. K. Maity, and Jorge Ancheyta. *Hydroprocessing of Heavy Oils and Residua*, chapter Maya Heavy Crude Oil Hydroprocessing Catalysts, pages 191–238. CRC Press, Boca Raton, May 2007. Eds. Jorge Ancheyta and James G. Speight.

[156] Carlton Reid. The petition that paved america. Roads Were Not Built For Cars, March 2012. URL http://www.roadswerenotbuiltforcars.com/the-petition-that-paved-america/.

[157] Joao Tiago Ribeiro, Rui Rijo, and Antonio Leal. Fast automatic schematics for public transport spider maps. *Procedia Technology*, 5:659–669, 2012.

[158] David Rojas-Rueda, Audrey de Nazelle, Marko Tainio, and Mark J Nieuwenhuijsen. The health risks and benefits of cycling in urban environments compared with car use: health impact assessment study. *BMJ*, 343, 2011. ISSN 0959-8138. doi: 10.1136/bmj.d4521.

[159] Mark Roseland. *Toward Sustainable Communities: Solutions for Citizens and Their Governments*. New Society Publishers, Gabriola Island, BC, Canada, fourth edition, July 2012.

[160] Hiroaki Sakoe and Seibi Chiba. Dynamic programming algorithm optimization for spoken word recognition. *IEEE Transactions on Acoustics, Speech and Signal Processing*, ASSP-26(1):43–49, February 1978.

[161] Mamdouh G. Salameh. The new frontiers for the United States energy security in the 21st century. *Applied Energy*, 76(1–3):135 – 144, 2003.

[162] Maria P. Scaparra and Richard L. Church. A bilevel mixed-integer program for critical infrastructure protection planning. *Computers & Operations Research*, 35(6):1905–1923, 2008. ISSN 0305-0548. URL http://dx.doi.org/10.1016/j.cor.2006.09.019. Part Special Issue: OR Applications in the Military and in Counter-Terrorism.

[163] Andreas Schäfer, John B. Heywood, Henry D. Jacoby, and Ian A. Waitz. *Transportation in a Climate-Constrained World*. MIT Press, April 2009.

[164] Clare Ribando Seelke, Michael Ratner, M. Angeles Villarreal, and Phillip Brown. Mexico's oil and gas sector: Background, reform efforts, and implications for the United States. Technical Report R43313, Congressional Research Service, September 2015.

[165] D. C. Sheppard. Social solutions for climate change mitigation and adaptation: Cross cultural lessons from Denmark to the United States. *Intersect*, 4(1):67–91, 2011.

[166] Henrietta Sherwin and Steve Melia. Cycle mapping in the UK and the London Cycle Map. Project report, University of the West of England, Bristol, 2012. Ideas in Transit.

[167] S. Siddiqui, S. Azarm, and S. A. Gabriel. On improving normal boundary intersection method for generation of pareto frontier. *Struct. Multidiscip.*

Optim., 46(6):839–852, 2012. ISSN 1615-147X. URL http://dx.doi.org/10.1007/s00158-012-0797-1.

[168] Sauleh Siddiqui and Adam Christensen. Determining energy and climate market policy using multiobjective programs with equilibrium constraints. *Energy*, 94:316 – 325, 2016. doi: http://dx.doi.org/10.1016/j.energy.2015.11.002. URL http://www.sciencedirect.com/science/article/pii/S0360544215015194.

[169] Sauleh Siddiqui and S. A. Gabriel. An SOS1-based approach for solving MPECs with a natural gas market application. *Netw Spat Econ*, 13(2): 205–227, July 2013.

[170] Henry Small. Co-citation in the scientific literature: A new measure of the relationship between two documents. *Journal of the American Society for Information Science*, 24(4):265–269, 1973.

[171] Nick Smith. New oil pipeline to move 100,000 barrels per day, October 2015. URL http://bismarcktribune.com/news/local/govt-and-politics/new-oil-pipeline-to-move-barrels-per-day/article_2e8ba30a-06ea-565d-a93c-c98f0a5e3d9b.html.

[172] Rajendra Solanki. Generating the noninferior set in mixed integer biobjective linear programs: An application to a location problem. *Computers & Operations Research*, 18(1):1–15, 1991. ISSN 0305-0548. URL http://dx.doi.org/10.1016/0305-0548(91)90037-R.

[173] Southern and Eastern Africa Consortium for Monitoring Educational Quality. Data archive for the SACMEQ I and SACMEQ II projects (v.6.0). Compact Disc, October 2009. Compiled by: Kenneth N. Ross, Mioko Saito, Stephanie Dolata, Miyako Ikeda and Linda Zuze.

[174] Southern and Eastern Africa Consortium for Monitoring Educational Quality. Data archive for the SACMEQ III project (v.6.0). Compact Disc, 2012. Compiled by: Demus Makuwa, Njora Hungi, Kenneth N. Ross, Mioko Saito, Stephanie Dolata, Frank van Capelle, Laura Paviot, Jocelyne Vellien, Jan Maarse.

[175] Ivan P. Stanimirovic. Compendious lexicographic method for multi-objective optimization. *Ser. Math. Inform.*, 2012.

[176] S. Steffensen and M. Ulbrich. A new relaxation scheme for mathematical programs with equilibrium constraints. *SIAM Journal on Optimization*, 20(5): 2504–2539, 2010.

[177] Christian Steglich, Tom A. B. Snijders, and Michael Pearson. Dynamic networks and behavior: separating selection from influence. *Sociological Methodology*, 40(1):329–393, 2010.

[178] J.M. Stott, P. Rodgers, R.A. Burkhard, M. Meier, and M.T.J. Smis. Automatic layout of project plans using a metro map metaphor. In *Proceedings of the Ninth International Conference on Information Visualisation*, pages 203–206, 2005.

[179] Jonathan Stott, Peter Rodgers, Juan Carlos Martinez-Ovando, and Stephen G. Walker. Automatic metro map layout using multicriteria optimization. *IEEE Transactions on Visualization and Computer Graphics*, 17 (1), January 2011.

[180] Mark Sydenham, Martin Baillie, and Tom Allan. Edinburgh innertube map. http://www.innertubemap.com/, 2011. First accessed on: May 14, 2013.

[181] Richard J. A. Talbert. *Rome's World: The Peutinger Map Reconsidered*. Cambridge University Press, 2010.

[182] Roberto Tamassia. On embedding a graph in the grid with the minimum number of bends. *Siam Journal of Computing*, 16(3):421–444, 1987.

[183] Sarah A Teichmann and M Madan Babu. Gene regulatory network growth by duplication. *Nat Genet*, 36(5):492–496, 05 2004.

[184] The Bakken Magazine Staff. Dakota Access pipeline receives approvals from SD, Illinois, January 2016. URL http://thebakken.com/articles/1427/dakota-access-pipeline-receives-approvals-from-sd-illinois.

[185] Robert Tibshirani, Guenther Walther, and Trevor Hastie. Estimating the number of clusters in a data set via the gap statistic. *J. R. Statist. Soc. B*, 63 (2):411–423, 2001.

[186] TransCanada. Proposed project: Upland Pipeline Project, December 2015. URL http://www.transcanada.com/docs/Key_Projects/TransCanada-Proposed-Upland-Pipeline-Project-Canada-December-2015.pdf.

[187] Jeffrey Travers and Stanley Milgram. An experimental study of the small world problem. *Sociometry*, 32(4):425 – 443, December 1969.

[188] UN. Political declaration of the high-level meeting of the general assembly on the prevention and control of non-communicable diseases., 2011. United Nations Item 117: 1–13.

[189] UN. Demographic yearbook. http://unstats.un.org/unsd/demographic/products/dyb/dyb_Household/dyb_household.htm, 2013. United Nations Statistics Division.

[190] UN-Habitat. *Enhancing urban safety and security: Global report on human*

settlements 2007. United Nations Human Settlements Programme, Earthscan, London and Sterling, VA, 2007.

[191] UNECE. Private households by household type. http://w3.unece.org/pxweb/dialog/varval.asp?ma=08_GEFHPrivHouse_r&path=../database/STAT/30-GE/02-Families_households/&lang=1&ti=Private+households+by+household+type, 2014. United Nations Economic Commission for Europe Statistical Division Database.

[192] Noel D. Uri and Roy Boyd. Crude oil imports into the united states. *Applied Energy*, 31(2):101 – 118, 1988.

[193] U.S. Energy Information Administration. PADD regions enable regional analysis of petroleum product supply and movements. https://www.eia.gov/todayinenergy/detail.cfm?id=4890, February 2012.

[194] U.S. Energy Information Administration. Annual energy outlook 2015 with projections to 2040. Report DOE/EIA-0383, U.S. Energy Information Administration, Washington, DC, April 2015.

[195] U.S. Energy Information Administration. International energy statistics. http://tinyurl.com/gp3tb6b, 2015.

[196] U.S. Energy Information Administration. Petroleum & other liquids. http://www.eia.gov/petroleum/data.cfm, 2015.

[197] U.S. Energy Information Administration. Weekly petroleum status report: Highlights. Petroleum & Other Liquids, January 2016. URL https://www.eia.gov/petroleum/supply/weekly/pdf/highlights.pdf. Data for week ending Jan. 22, 2016.

[198] U.S.C. Energy Policy and Conservation Act. Public Law 94-163, 94th Congress, December 1975. URL https://www.gpo.gov/fdsys/pkg/STATUTE-89/pdf/STATUTE-89-Pg871.pdf. Statute 89, S. 622.

[199] Thomas Vincent, Florian Seipp, Stefan Ruzika, Anthony Przybylski, and Xavier Gandibleux. Multiple objective branch and bound for mixed 0-1 linear programming: Corrections and improvements for the biobjective case. *Computers and Operations Research*, 40(1):498–509, 2013. ISSN 0305-0548. URL http://dx.doi.org/10.1016/j.cor.2012.08.003.

[200] Voice of America. Two wheels a way of life in Burkina Faso. http://www.voanews.com/content/a-13-2008-05-19-voa51/406615.html, 2009.

[201] Malcolm J. Wardlaw. History, risk, infrastructure: perspectives on bicycling in the Netherlands and the UK. *J. Transp. Health*, 1(4):243 – 250, 2014.

[202] John Glen Wardrop. Some theoretical aspects of road traffic research. *Proceedings of the Institution of Civil Engineers*, 1(3):325–362, 1952.

[203] Alexander Wolff. Drawing subway maps: A survey. *Informatik—Forschung und Entwicklung*, 22(1):23–44, 2007.

[204] J. Woodcock. Public health benefits of strategies to reduce greenhouse-gas emissions: urban land transport. *Lancet*, 374(9705):1930–1943, 2009.

[205] World Bank. GDP per capita, PPP (current international $). http://data.worldbank.org/indicator/NY.GDP.PCAP.PP.CD, 2015.

[206] World Bank. Population, total. http://data.worldbank.org/indicator/SP.POP.TOTL, 2015.

[207] L. A. Zadeh. Optimality and non-scalar-valued performance criteria. *IEEE Transactions on Automatic Control*, 8:59–60, 1963.

Vita

Olufolajimi (Jimi) Oke was born in Ibadan, Nigeria, on the 19th of November 1987. He obtained his Bachelor of Arts in 2010 from Williams College, Massachusetts, with majors in Physics and Music. As an undergraduate, he pursued research interests in quantum entanglement and fiber optics. In recognition of his contributions to teaching and research, he was awarded the Physics Department's Howard P. Stabler prize upon graduation. He also received Sigma Xi honors in the same year.

After teaching mathematics for two years at The Pennington School, New Jersey, Jimi enrolled in the doctoral program in Civil Engineering at The Johns Hopkins University in 2012. Since then, he has studied energy and transportation systems and applied network and optimization theories toward solving related problems. Jimi received a traineeship in 2013 from the Global Obesity Prevention Center to support research on an agent-based model to study obesity in the Baltimore adolescent population. In 2015, he was awarded the Gordon Croft Fellowship in partial support of research on the U.S. crude oil market to address current oil transportation infrastructure concerns.

During his time at Johns Hopkins, Jimi has devoted significant effort to education. Besides teaching assistantships, he obtained a fellowship to develop higher-impact assessments for the Probability and Statistics course in the Civil Engineering department. He also designed a short course based on his work in schematic mapping to introduce mathematical programming and modeling concepts to sophomores.

Jimi's papers have been published in *Computers & Operations Research*, *Journal of Transport & Health* and *Physical Review Letters*. He also has forthcoming manuscripts in *Annals of Operations Research* and *Energy Strategy Reviews*. In June 2016, Jimi will begin work as a postdoctoral research associate at the Singapore-MIT Alliance for Research and Technology, where he will be applying machine learning and optimization methods to developing sustainable urban mobility systems for the future.

Colophon

This document was created in LaTeX (developed by Donald Knuth and Leslie Lamport) and BibTeX, and edited on the AUCTeX system in Aquamacs. The body text is set 12pt with Computer Modern Roman. Other fonts include Computer Modern Sans Serif. Some of the figures are typeset using the TikZ/PGF packages by Till Tantau.